The University of Nottingham

Division of Advanced Drug Delivery and Tissue engineering

Folate-mediated Macromolecule Delivery across the Epithelium

Emilia Moradi

Thesis submitted to the University of Nottingham
for the degree of Doctor of Philosophy

November 2011

BEST COPY AVAILABLE.

TEXT IN ORIGINAL IS BOUND INTO THE SPINE

'Knowledge is as wings to man's life, and a ladder for his ascent. Its acquisition is incumbent upon everyone. The knowledge of such sciences, however, should be acquired as can profit the peoples of the earth, and not those which begin with words and end with words'

Baha'u'llah

Abstract

Folate uses the natural endocytosis pathway *via* the folate receptor (FR) to enter the cells. Folate conjugation to small or macromolecular therapeutics has hence been exploited for intracellular delivery to, particularly, cancerous cells. This work reports on the expression and functionality of FR in polarised cell monolayer models of respiratory and gastrointestinal mucosa with the view to assess its potential for delivery of folate-modified macromolecular therapeutics either intracellularly or across the epithelium. Four cell lines representing bronchial and intestinal epithelium; cancer-derived intestinal Caco-2 and bronchial cell line Calu-3, and non-cancerous intestinal and bronchial cell lines IEC-6 and HBEC were cultured on permeable membranes to produce polarised monolayers. Expression of FR was confirmed by RT-PCR and Western blot analysis for all the tested cell types and shown to be dependent on culturing time. The functionality of the receptor for endocytosis was demonstrated by a model macromolecular folate conjugate (fluorescent ovalbumin-folate (OVA-FA)), whereby significantly higher cellular uptake of the folate-conjugate, relative to non-folate control, was clearly demonstrated. Importantly the data showed that the expressed folate receptor was capable of mediating transport of the macromolecular folate conjugate across (transcytosis) the cells in the polarised monolayers.

Preliminary studies led to investigation of the folate mediated uptake and transport of folate modified nanoparticles (NPs). It was shown that folate modified NPs traversed the Calu-3 layers and studies characterizing this transport indicated folate involvement in this process. Adsorption of OVA-FA on the surface of NPs was seen to promote their cellular uptake and transport across the cell layers.

To examine the mechanism of cellular uptake and transport of folate modified nanoparticles, various endocytic inhibitors were employed. The study demonstrated an involvement of the caveolar pathway in internalization of folate modified nanoparticles; as judged from a significant reduction of internalization in filipin (inhibitor of caveolar pathway) treated cells. Moreover, the work also showed evidence of transport of folate-modified nanoparticles via the caveolar pathway, since translocation of nanoparticles across the cell monolayer was absent when this path was inhibited.

Disruption of actin filament and microtubules caused no difference in cellular uptake of NPs but increased the transcytosis of folate modified NPs.

Confocal microscopy, Transmission Electron Microscopy (TEM), Total Internal Reflection Microscopy (TIRM) and Total Internal Reflection Florescence microscopy (TIRFM) were used to confirm and visualize quantitative data.

This study also investigated the effects of surface ligand distribution pattern (ligand clustering and density) on the internalization of nanoparticles by Calu-3 cells cultured as polarised layers. The density of the displayed ligand was manipulated by controlling the conjugation level of folate-ovalbumin, while ligand clustering was achieved by co-adsorption of varying mixtures of folate-ovalbumin conjugate (at different ligand density levels) and unconjugated ovalbumin. Increasing ligand density on the nanoparticle surface resulted in increased internalization of modified nanoparticles by the cells, up to a saturation level. Surface ligand density also affected the cellular uptake pathway; from predominantly clathrin to predominantly caveolae-mediated as the ligand density was increased. It was further demonstrated that surface clustering of the folate ligand enhanced cellular internalization of nanoparticles, relative to its dispersed surface distribution.

Acknowledgements

I would like to send my highest gratitude to my supervisor Dr Snow Stolnik for her supervision, advice, and guidance since the days I began my work as well as giving me extraordinary experiences throughout the work. Above all and the most needed, she provided me unflinching encouragement and support in various ways. Her truly scientist intuition has made her as a constant oasis of ideas and passions in science, which exceptionally inspire and enrich my growth as a student, a researcher and a scientist want to be. I am indebted to her more than she knows.

I am heartily thankful to my co-supervisor, Dr Martin Garnett, for his encouragement, guidance and detailed and constructive comments throughout this work. I gratefully acknowledge Dr Franco Falcone and Dr Cynthia Bosquillon for their advice during my PhD time.

I also benefited by outstanding help from Dr Gerard Byrne with his particular skill in microscopy. The live imaging of this work would not have been existed without him. I recollect with affection the help and emotional support rendered by him as well. Many thanks go to my dearest friend, Dr Driton Vllasaliu for science discussion and the pleasure working together during these years. Furthermore, I would like to express a special thank you to Dr Sarir Sarmad for her support, trust and friendship.

Collective and individual acknowledgments are also owed to my colleagues Dimitra, Robyne, Mathiue, Manali, Lizzy, Paulina, Kelly and Dr Kevin Webb whose present somehow perpetually refreshed, helpful, and memorable.

I was extraordinarily fortunate in having Dr Parviz Javid as my professor in Bahai Institute of Higher Education (BIHE). I could never have embarked and started all of

this without his prior teachings in Pharmacy and thus opened up unknown areas to me. Although he is no longer with us, he is forever remembered. I am sure he shares our joy and happiness in the heaven.

I finish with Iran, where the most basic source of my life energy resides: my family. This thesis is simply impossible without them.

I am indebted to my father, for his care and love. My father, is the person who established and natured my fundamental learning character, showing me the joy of intellectual pursuit ever since I was a child. As a typical father, he worked industriously and spares no effort to provide the best possible environment for me. He had never complained in spite of all the hardships in his life..

I cannot ask for more from my mother as she is simply perfect. I have no suitable word that can fully describe her unflagging love and support throughout my life.

Words fail me to express my appreciation to my sister Mozhgan whose dedication, love and persistent confidence in me has taken the load off my shoulder. Last but not least, my gratitude goes to my brother Erfan, who passed away 20 years ago, but I still feel his endless love and support in every second of my life.

Table of Contents

Abstract III

Acknowledgements V

List of Figures XIII

List of Tables XVIII

Abbreviations XIX

Chapter 1 Folate-Mediated Drug Delivery 1

1.1 Non-invasive drug delivery 2

1.2 Mucosal administration of protein drugs 3

1.2.1 Oral rout 3

1.2.2 Nasal rout 3

1.2.3 Buccal rout 3

1.2.4 Pulmonary rout 4

1.3 Barriers to mucosal drug delivery 5

1.4 Crossing the mucosal barriers: possible pathways 6

1.4.1 Paracellular pathway 7

1.4.2 Transcellular pathway 8

1.4.2.1 Small molecules 8

1.4.2.2 Macromolecules 8

1.5 Endocytosis pathways 9

1.5.1 Phagocytosis 9

1.5.2 Pinocytosis 9

1.5.3 Receptor-mediated endocytosis 10

1.6 Transcytosis 11

1.7 Receptor-mediated drug delivery 11

1.8 Receptors involved in macromolecular transports across the respiratory epithelial layer 13

1.8.1FcRn receptor 13

1.8.2 gp 60 receptor, Albondin 14

1.8.3 Polymeric immunoglobulin receptor (pIgR) for basal- apical transport of IgA 15

1.8.4 Folate receptor (FR) 15

1.9 Folate-mediated drug delivery 15

1.9.1 Folates 16

1.9.2 Folate carriers 16

1.9.2.1 Reduced folate carrier 17

1.9.2.2 Proton coupled folate transporter (PCFT) 17

1.9.2.3 Folate receptor 18

1.9.3 Tissue distribution of FRs 19

1.9.4 Expression of FRs in malignant tissue 20

1.9.5 Folic acid; an ideal ligand for FR 20

1.9.6 Folate decorated carriers for FR mediated drug targeting 21

1.10 Aims and objectives 22

1.11 References 24

Chapter 2 Materials & General Methods 33

2.1 Materials 34

2.1.1 Cell lines and routine cell culture materials 34

2.1.2 Labware 35

2.1.3 Cell staining reagents 35

2.1.4 Chemicals 36

2.2 General Methods 37

2.2.1 Cell Maintenance 37

2.2.1.1 Cell revival 37

2.2.1.2 Cell maintenance 37

2.2.1.3 Preparation of Frozen Stock 38

2.2.1.4 Seeding cells on transwells-Conventional 38

2.2.1.5 Seeding cells on transwells-Inverted 39

2.2.2 TEER Measurement 40

2.2.3 FITC-dextran (FD) permeability experiments 42

2.2.4 MTS cell toxicity assay 44

2.2.5 Cell imaging and labelling 45

2.2.5.1 Coverslip preparation 45

2.2.5.2 Zonula Occludense (ZO-1) TJ staining 46

2.2.5.3 Caveolin-1 and Clathrin staining 46

2.2.5.4. Folate receptor (FR) staining 47

2.2.6 Statistical analysis 47

2.3 References 48

Chapter 3 Folate receptor expression in bronchial and intestinal epithelial cell lines: Potential for uptake and transport of macromolecules 49

3.1. Introduction 50

3.1.1 Calu-3 51

3.1.2 HBEC 52

3.1.3 Caco-2 52

3.1.4 IEC-6 52

3.2 Material and Methods 53

3.2.1 Polymerase Chain Reaction (PCR) 53

3.2.1.1 PCR primer design 53

3.2.1.2 Total RNA isolation 53

3.2.1.3 Reverse Transcriptase (RT)-PCR 54

3.2.2 Western Blot 54

3.2.3 Preparation of Ovalbumin-Folic Acid-FITC Conjugate 55

3.2.4 Preparation of Ovalbumin-Folic Acid-TRITC Conjugate 57

3.2.5 Preparation of membrane-cultured Calu-3 cells 58

3.2.6 TEER profiles of cell monolayers 58

3.2.7 Permeability study of FD4 across cell layers 58

3.2.8 FA-OVA-TRITC uptake by cell layers 59

3.2.9 FA-OVA -FITC translocation across cell layers 60

3.2.10 Receptor competition 60

3.2.11 Zonula Occludens (ZO-1) TJ staining 61

3.2.12 Confocal Fluorescence imaging 61

3.3 Results 62

3.3.1 Synthesis of folate conjugates 62

3.3.1.1 Preparation of FA-OVA-FITC 62

3.3.1.2 Preparation of FA-OVA-TRITC 63

3.3.2. Formation of electrically tight cell monolayer 66

3.3.3. FD4 permeability across cell layers 67

3.3.4. Expression of folate binding protein on cell layers 68

3.3.5. Expression of folate binding protein on cell layers 69

3.3.6. Cell uptake of folate and non-folate conjugates 69

3.3.6.1 Confocal microscopy analysis of cellular uptake of folate and non-folate conjugates 71

3.3.7. OVA-FA-FITC transport across cell layers 78

3.4 Discussion 82

3.5 Conclusion 90

3.6 References 91

Chapter 4 Intracellular Trafficking Study of Folate-modified Nanoparticles across Epithelium via Transcytosis 96

4.1 Introduction 96

4.1.1 Endocytosis 98

4.1.1.1 Clathrin-mediated endocytosis (CME) 98

4.1.1.2 Caveolae-mediated endocytosis 100

4.1.2 Involvement of actin filament in endocytosis 102

4.1.3 Involvement of actin microtubules in endocytosis 102

4.2 Material and Methods 104

4.2.1 Preparation of Folate and non-Folate modified nanoparticles 104

4.2.2 Light-Scattering Measurements 104

4.2.3 Calu-3 Cell monolayer 105

4.2.4 Immunostaining for FRs in Calu-3 monolayer 105

4.2.5 Cellular uptake and transport experiments 105

4.2.6 Cytotoxicity of Endocytosis Inhibitors and folate and non folate modified nanoparticles 106

4.2.7 Basolateral medium analysis: Transmission Electron Microscope (TEM) 106

4.2.8 Confocal Microscopy 107

4.3 Results 108

4.3.1 Synthesis of NPs 108

4.3.1.1 NPs synthesis 108

4.3.2 MTS cell toxicity assay 110

4.3.2.1 Effect of NPs on Calu-3 metabolic activity: MTS Assay 110

4.3.2.2Effect of endocytic inhibitors on Calu-3 metabolic activity: MTS Assay ... 111

4.3.3 Filipin and chlorpromazine effect on Cholera toxin B and transferrin uptake 115

4.3.4 Imunostaining for FRs 117

4.3.5 Cell uptake of folate and non-folate at 37°C and 4°C 119

4.3.6 Cell uptake of folate and non-folate in the presence of different inhibitors... 120

4.3.7 Confocal microscopy analysis 123

4.3.7.1 Cell uptake of folate-modified NPs at 37°C and 4°C 123

4.3.7.2 Cell uptake of folate-modified NPs in the presence of inhibitors 126

4.3.8 Transport study of folate and non-folate modified NPs at 37°C and 4°C 129

4.3.9 Basolateral medium analysis: TEM 130

4.3.10 Transport study of folate modified NPs in the presence of inhibitors..... 135

4.4 Discussion 137

4.4.1 Uptake study of folate-modified NPs 140

4.4.2 Transport study of folate-modified NPs 141

4.4.3 Uptake and transport study of folate-modified NPs in the presence of endocytic inhibitors 142

4.5 Conclusion 150

4.6 Refrences 151

Chapter 5 Ligand Density and Clustering Effects on Endocytosis of Folate-modified Nanoparticles 160

5.1 Introduction 161

5.2 Material and Methods 164

5.2.1 Preparation of Folate and non-Folate modified nanoparticles 162

5.2.2 Light-Scattering Measurements 162

5.2.3 Cell culture 165

5.2.4 Cell uptake studies 165

5.3 Results 166

5.3.1 Nanoparticle preparation and characterization 166

5.3.2 Nanoparticle characterization 167

5.3.3 Effect of ligand density on cellular internalization of nanoparticles 169

5.3.4 Effect of surface ligand density on cellular internalization pathway (endocytosis) 171

5.3.5 Effect of ligand clustering on cellular internalization 173

5.4 Discussion 177

5.5 Conclusions 180

5.6 References 181

Chapter 6 Applications of Total Internal Reflection Microscopy and Total Internal Reflection Fluorescence Microscopy (TIRM/TIRF) for live cell imaging 184

6.1 Introduction 185

6.1.1 Total internal reflection microscopy (TIRM) 185

6.1.2 Total internal reflection fluorescence (TIRF) microscopy 186

6.1.3 Combined TIR/TIRF microscope 186

6.2 Material and methods 189

6.2.1 Plasmids 189

6.2.2 Oligonucleotide primers 189

6.2.3 Antibiotics 190

6.2.4 Luria Bertani medium 190

6.2.5 Molecular Biology Techniques 190

6.2.5.1 cDNA 190

6.2.5.2 Sample preparation 190

6.2.5.3 DNA Agarose gel electrophoresis 191

6.2.5.4 DNA molecular weight markers 191

6.2.6 DNA manipulation 191

6.2.6.1 Extraction of PCR amplified DNA from agarose gel 191

6.2.6.2 DNA restriction enzymes 192

6.2.6.3 Ligation of insert DNA and plasmid DNA 192

6.2.7 Introduction of DNA into bacterial cells 192

6.2.7.1 Electroporation of electrocompetent E. coli cells 192

6.2.8 Isolation of plasmid DNA 193

6.2.9 DNA sequence analysis 193

6.2.10 Transfection 193

6.2.11 Folate modified Nanoparticles 194

6.2.12 Zonula Occludens (ZO-1) TJ staining 194

6.2.13 TIRM/TIRF Microscopy 194

6.2.14 Image analysis 195

6.2.15 Confocal Microscopy 196

6.3 Result 197

6.3.1 Calu-3 cell layer cultured on the underside of permeable membrane 197

6.3.2 TIRM imaging of Calu-3 cells 197

6.3.2 Clathrin and caveolin1 expression in Calu-3 cells 201

6.3.4 TIRM/TIRF imaging of clathrin and caveolae mediated endocytosis of folate modified NPs 205

6.4 Discussion 206

6.5 Conclusion 211

6.6 References 212

Chapter 7 Summary and Future Directions 215

7.1 Overall summary 216

7.2 Future view of folate targeted delivery 219

7.3 References 221

List of Figures

Chapter 1

Figure 1.1 Barriers to pulmonary drug delivery.....6

Figure 1.2 Transport pathways across the epithelial layer.....7

Figure 1.3 Structure of folic acid 16

Figure 1.4 Receptor-mediated endocytosis of folate conjugates 19

Chapter 2

Figure 2.1 Schematic diagram of cells grown inside (conventional) and on the underside (inverted) of a filter insert.....40

Figure 2.2 Schematic representation of the Epithelial Voltohmmeter system used to measure TEER of the cell layers.....42

Chapter3

Figure 3.1 Epifluorescence images of Calu-3, HBEC, Caco-2 and IEC-6.....51

Figure 3.2 Synthesis of FA-OVA-TRITC.....64

Figure 3.3 Synthesis of FA-OVA-FITC.....65

Figure 3.4 TEER profiles of HBEC, IEC-6, Caco-2 and Calu-3 cells cultured on membrane.....66

Figure 3.5 The expression of FOLR1 mRNA by RT-PCR.....68

Figure 3.6 Western blot analysis of folate binding protein.....69

Figure 3.7 Uptake study of OVA-folic acid-TRITC and OVA-TRITC in four epithelial layers.....70

Figure 3.8 Confocal images for cellular uptake study of FA-OVA-TRITC and OVA-TRITC in Caco-2 cell layers.....72

Figure 3.9 Confocal images for cellular uptake study of FA-OVA-TRITC and OVA-TRITC in Calu-3 cell layers.....73

Figure 3.10 Confocal images for cellular uptake study of FA-OVA-TRITC and OVA-TRITC in IEC-6 cell layers.....74

Figure 3.11 Confocal images for cellular uptake study of FA-OVA-TRITC and OVA-TRITC in HBE cell layers.....75

Figure 3.12 Gallery of cross sections images of cellular uptake of FA-OVA-TRITC conjugates in Caco-2 cell layers.....76

Figure 3.13 Gallery of cross sections images of cellular uptake of FA-OVA-TRITC conjugates in Calu-3 cell layers.....77

Figure 3.14 Transport study across Calu-3 and HBE cell layers.....79

Figure 3.15 Transport study across Caco-2 and IEC-6 cell layers.....80

Chapter 4

Figure 4.1 Pathway of entry to the cells, adopted from.....98

Figure 4.2 Overview of the steps involved in clathrin-mediated endocytosis.....99

Figure 4.3 Size characterisation of unmodified, OVA-FA-adsorbed and OVA-adsorbed NPs (c) by DLS.....109

Figure 4.4 Effect of NPs on Calu-3 metabolic activity, MTS assay.....110

Figure 4.5 Effect of different inhibitors on Calu-3 metabolic activity, as determined by the MTS assay.....113

Figure 4.6 Effect of chlorpromazine and filipin on internalization of transferrin and cholera toxin B into Calu-3 cells.....116

Figure 4.7 Immunostaining for FRs 118

Figure 4.8 Effect of temperature on cell uptake of OVA-FA-NPs and OVA-NPs.....119

Figure 4.9 Uptake study of OVA-FA-NPs and OVA-NPs in the presence of different inhibitor.....121

Figure 4.10 Uptake study of OVA-FA-NPs at 37°C and 4°C.....124

Figure 4.11 Gallery image of cellular uptake of OVA-FA NPs.....125

Figure 4.12 Three dimensional images of endocytosis of OVA-FA-NPs in untreated and filipin-treated Calu-3 cell layers.....127

Figure 4.13 Three dimensional images of endocytosis of OVA-FA-NPs in dynasore-treated and cytochalasin D-treated Calu-3 cell layers.....128

Figure 4.14 Effect of temperature on cell transport of OVA-FA-NPs and OVA-NPs.....130

Figure 4.15 Transport study 132

Figure 4.16 Transport study of OVA-FA-NPs versus time in the presence of endocytosis inhibitors 134

Figure 4.17 Transmission electronic microscopy images of apical and basolateral media of Calu-3 cells 136

Chapter 5

Figure 5.1 Preparation of folate decorated polystyrene nanoparticles.....166

Figure 5.2 Particle size and distribution of unmodified and modified with either unconjugated OVA or folate-conjugated OVA.....169

Figure 5.3 Effect of ligand density on cellular internalization of nanoparticles in Calu-3 layers.....170

Figure 5.4 Cellular internalization of folate-modified NPS in the presence of endocytosis inhibitors 172

Figure 5.5 Effect of the surface ligand distribution on cellular internalisation of NPs at corresponding ligand amount.....176

Chapter 6

Figure 6.1 Schematic picture of TIRM/TIRF microscope.....188

Figure 6.2 Confocal images of ZO-1 of immunostaining of Calu-3 cell layer grown in conventional and inverted configurations.....197

Figure 6.3 TIRM image of a Calu-3 cell.....198

Figure 6.4 TIRM image of apical surface of Calu-3 cell layer cultured on the underside of permeable membranes.....199

Figure 6.5 Series of images from a TIRM time-lapse sequence of unlabelled Calu-3 cell layer cultured on permeable filter for 21 days.....200

Figure 6.6 TIRM/TIRF image of a Calu-3 cell transfected with DsRed-caveolin1.....201

Figure 6.7 TIRM/TIRF image of a Calu-3 cell transfected with EGFP-clathrin.....201

Figure 6.8 Twelve sequential TIRF images are demonstrating the presence of numerous DsRed-caveolae vesicles.....203

Figure 6.9 Six sequential TIRF images are demonstrating the presence of numerous EGFP-clathrin puncta.....203

Figure 6.10 Schematic picture of live cell imaging of Calu-3 cell layer grown on the underside of permeable membrane.....209

List of Tables

Chapter 1

Table.1.1 Endocytosis pathways.....9

Table 1.2 Ligands normally used for receptor-mediated drug delivery.....13

Chapter 3

Table 3.1 Transepithelial Permeability Coefficient (Papp) of dextran-FITC (4kDa).....67

Chapter 4

Table 4.1 Selected concentrations of inhibitors.....114

Chapter 5

Table 5.1 Cellular internalization of folate surface modified nanoparticles.....175

Abbreviations

%	Percentage
°	Degree
°C	Degree Celsius
AP	Assembly protein
ATCC	American Type Culture Collection
BSA	Bovine serum albumin
CADs	Cationic amphiphilic drugs
CAV1	Caveolin 1
Clathrin Lca	Clathrin light chain
CME	Clathrin-mediated endocytosis
CO2	Carbon dioxide
Da	Dalton
DABCO	1,4-Diazabicyclo-octane
DAPI	4'-6-Diamidino-2-phenylindole
dH2O	Distilled Water
DLS	Dynamic Light Scattering
DMEM	Dulbeco's modified eagles medium
DMSO	Dimethylsulphoxide
ECDI	1-Ethyl-3-(3-dimethylaminopropyl)carbodimide
EDTA	Ethylene diamine tetraacetic acid
Em	Emission
EMEM	Essential Minimum Eagle's Medium
Exc	Excitation
FCS	Foetal calf serum
FA	Folic acid
FBS	Foetal Bovine Serum
FCS	Foetal Calf Serum
FD4	Fluorescein Isothiocyanate-dextran 4 kilodalton
FITC	Fluorescenein isothiocyanates
FR	Folate receptor
gDNA	Genomic DNA

GEECs	GPI-AP enriched endosomal compartments
GI	Gastrointestinal
GPI	Glycosylphosphatidylinositol
GTP	Guanosine triphosphate
HBEC	Human bronchial epithelial cells
HBSS	Hanks balanced salt solution
HCG	Human chorionic gonadotropin
HEPES	4-(2-hydroxyethyl)-1-piperazineethanesulfonic
HRP	Horseradish Peroxidase
Hs-GAPDH	Homo sapiens glyceraldehyde-3-phosphate dehydrogenase
ICAM-1	intercellular cell adhesion molecule-1
IEC-6	Intestinal epithelial cells
IgG	Immunoglobulin G
kDa	Kilodalton
KSFM	Keratinocyte serum-free medium
IL-4	Intrleukin-4
IN	Intranasal
M	Molar
MDCK	Madin-Darby canine kidney
MEM	Minimum Essential Medium
Min	Minute
ml	Millilitre
MSR	Molar substitution ratio
MTS	3-(4,5-dimethylthiazol-2-yl)-5(3-carboxymethonyphenol)-2-(4-sulfophenyl)-2H-tetrazolium
MW	Molecular weight
NP	Nanoparticle
OVA	Ovalbumin
Papp	Apparent permeability coefficient
PBS	Phosphate buffered saline
PCR	Polymerase Chain Reaction
PDL	Poly- D lysine

PM	Plasma membrane
RME	Receptor mediated endocytosis
Rpm	round per minute
RT	Reverse Transcriptase
Sec	Second
SL	Sublingual
TD	Transdermal
TEER	Trans epithelial electrical resistance
TJ	Tight junction
TRITC	Tetramethylrodamine isothiocyanate
TEM	Transmission Electron Microscopy
TIRF	Total internal reflection fluorescence
TIRM	Total internal reflection microscopy
µl	Microlitre
µm	Micrometer
v/v	Volume per unit Volume
w/v	Weight per unit Volume
ZO-1	Zonula occludens-1

Chapter 1

Folate-Mediated Drug Delivery

1.1 Non-invasive drug delivery

The development of drugs based on biotechnology products is a rapidly expanding area within the pharmaceutical industry. These products are increasingly proteins; peptide or nucleic acid based molecules. However delivery of such molecules and their translation to clinic requires new drug delivery systems. The growth in protein drugs is unfortunately not matched by developments of effective and convenient delivery systems for this class of therapeutics. Currently, protein drugs are predominantly administered parenterally. This is due to their high molar mass, hydrophilicity and their inability to withstand the environment in the gastrointestinal tract, resulting in an inadequate absorption and hence poor bioavailability following oral administration. However, disadvantages associated with the parenteral route, including patient discomfort and high cost, necessitate research into non-invasive ways of administering this class of therapeutics [1].

So the need for non-invasive drug delivery arises for many reasons such as:

- Possibility of proteins and peptides delivery without injection
- Less side effect
- More efficient delivery of active components
- No need for constant medical supervision
- More patient convenience
- Painless administration

This is why non-invasive methods of drug delivery are recently receiving a lot of attention and great efforts have been devoted to investigate feasibility of new non-invasive routes [2].

1.2 Mucosal administration of protein drugs: potential routes

The research in potential routes for non-invasive drug delivery has led to discoveries in the potential exploitation of mucosal routes including oral rout, pulmonary route, nasal route, buccal route, rectal route, vaginal route and ocular route [3, 4].

1.2.1Oral route

The oral mucosal drug delivery is the preferred and alternative method of drug administration that offers many advantages such as ease of self-administration, convenience and lower costs. However, the gastrointestinal tract is a complicated system of organs designed primarily to break down food and absorb nutrient molecules. Following their oral administration, many peptides and proteins will be destroyed before absorption can take place in the small intestine. This is because of the presence of proteolytic enzymes and an unfavorable acidic environment [5, 6].

1.2.2 Nasal route

Some of the characteristics of the nasal cavity that make the delivery of therapeutics through the nasal mucosa attractive, include the relatively large surface area available for absorption (approximately 150 cm^2), the highly vascularised submucosa, and the avoidance of both gastric and first pass metabolism. Furthermore, the nasal mucosa exhibits a lower enzymatic activity when compared to the gastrointestinal tract.

Potential problems associated with the use of the nasal route for drug delivery include filtration of foreign particles and rapid mucociliary clearance, which may affect the absorption of macromolecules [7, 8].

1.2.3 Buccal route

Delivery through the buccal cavity offers avoidance of first pass metabolism as the blood vessels of the oral mucosa drain directly into the jugular vein. Furthermore, the oral cavity is highly vascularized and provides an environment almost free from the acidity and protease activity encountered elsewhere in the mucosa [9].

1.2.4 Pulmonary route

It is believed that the pulmonary route has many potential benefits as a portal of entry for systemic drugs.

- Pulmonary epithelium provides a higher bioavailability than other non-invasive routes of drug delivery. The lungs are more permeable to macromolecules than any other routes. Some of the most promising therapeutic agents are peptides and proteins, which could be inhaled instead of injected; thereby improving compliance (The bioavailability of peptides and proteins is 10 to 200 times greater by the pulmonary route as compared with other non-invasive routes).
- The lungs are even more permeable to small molecules than the gastrointestinal (GI) tract. Evidence also suggests that the lungs display high bioavailabilities and rapid absorption of small lipophilic compounds, indicating that there is high permeability and low metabolising activity.
- The lungs have a small portion of the drug-metabolizing and efflux transporter activity compared to the gut and liver. Thus, small molecules can be delivered efficiently into the body through the lungs without the production of a complex array of metabolites.
- Inhalation provides a greater speed of response. For example inhaled Insulin is more rapidly absorbed than subcutaneously injected insulin and provides more physiological response to a meal [3].

- The large surface area of approximately 70 – 140 m^2 in adult human lungs can be efficiently used for the administration of a large variety of drugs [1, 3, 10].

So Lung drug delivery has gained the most attention and it is considered that mucosal surfaces of respiratory system can be the most common and convenient route for delivering drugs to the body.

1.3 Barriers to mucosal drug delivery

Successful delivery and systemic absorption of protein therapeutics following mucosal administration requires several biological barriers to be overcome. Using the airway mucosa as an example, these barriers are presented schematically in Figure 1.1. The epithelial cells (Figure 1.1), which are covered by a layer of mucus, are the major barrier to drug transport. The epithelial barrier has intercellular tight junctions (TJ) and is organised as a tightly connected continuous layer of cells characterised by distinct apical and basolateral surfaces with specific structural modifications. Although the mucosal layer is permeable to water, gases, and lipophilic substances, the permeability to large, hydrophilic proteins is limited. The non-absorptive clearance processes are another hurdle to systemic delivery and can have a major impact on the amount of active drug available for transport across the mucosa. The role of mucociliary clearance is to remove unwanted and potentially irritable particles. For example, insoluble drugs and/or insoluble delivery systems deposited in the upper airways are rapidly cleared [11]. The presence of proteases that may degrade the administered protein drug is also an important barrier limiting the availability of peptides and proteins at the mucosal surface and hence their absorption [12].

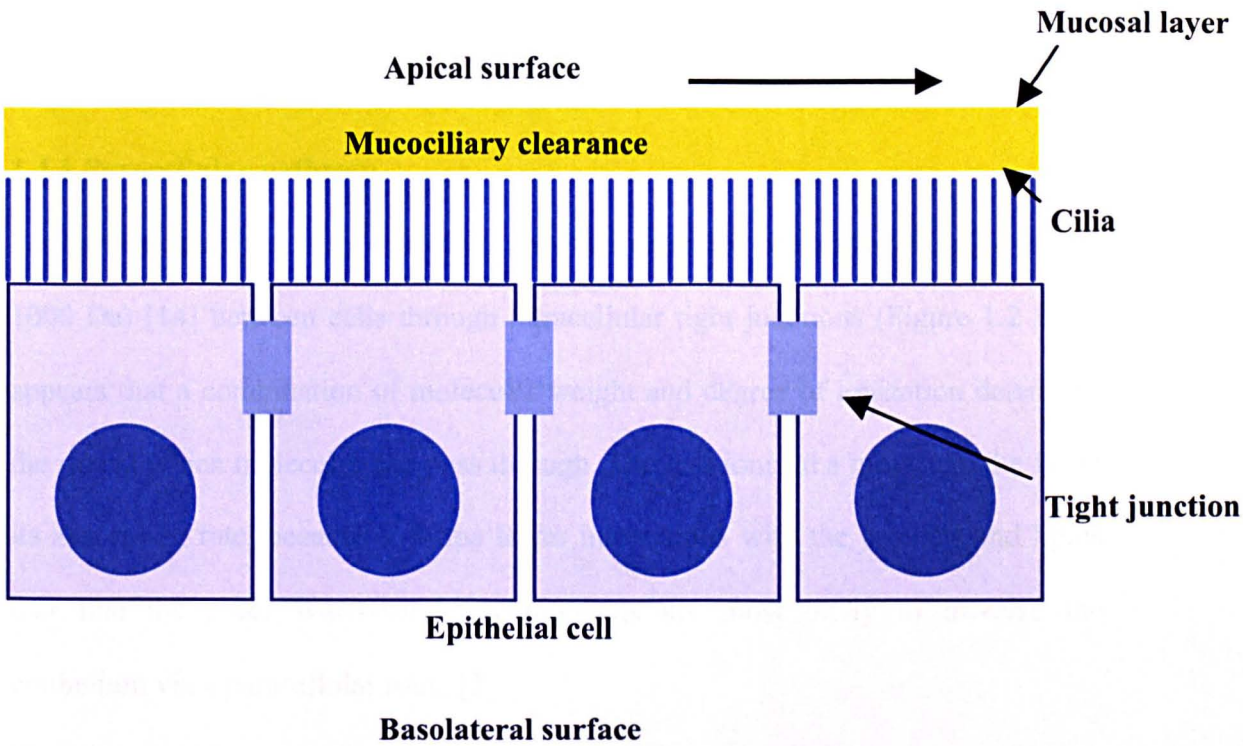

Figure 1.1 *Barriers to mucosal drug delivery. The epithelial layer, which is composed of tightly clustered ciliated cells connected by tight junction, forms a virtually impermeable barrier. The cilia are surrounded by a thin fluid film of mucus which is secreted by goblet cells. Cilia beat resulting in a unidirectional upwards movement of mucus which is an integral part of lung defence mechanisms, enabling efficient clearance of inhaled particles.*

1.4 Crossing the mucosal barriers: possible pathways

While some small, amphipathic molecules have the ability to partition into and out of lipid bilayer membranes (apical and basolateral) allowing them to readily enter and leave the epithelial cells without a specific transport system (Figure 1.2A), the transport of smaller hydrophilic macromolecules is limited to the paracellular route (i.e. between adjacent cells; Figure 1.2B). Larger macromolecules and nano-sized particles can also be transported across the cells via transcytosis route through a series of vesicular structures (Figure 1.2C). However, the organization and

movement of these vesicles is highly regulated to minimize the non-selective transport of macromolecules into and out of the body [13].

1.4.1 Paracellular pathway

Paracellular transport is the selective, passive movement of small molecules (below 1000 Da) [14] between cells through intracellular tight junctions (Figure 1.2 B). It appears that a combination of molecular weight and degree of ionization determine the rate at which molecules can pass through. The less ionized a molecule, the faster its absorption rate, because it forms fewer interactions with the proteins and lipids that line the pore. Water-soluble compounds are most likely to traverse the epithelium via a paracellular route [3].

Tight junctions comprise a major barrier towards the paracellular transport of larger solutes. The dimensions of the paracellular space lie between 10 and 30–50 Å, suggesting that solutes having a molecular radius exceeding 15 Å (3.5 kDa) will be excluded from this route [15, 16]: this includes most therapeutic proteins.

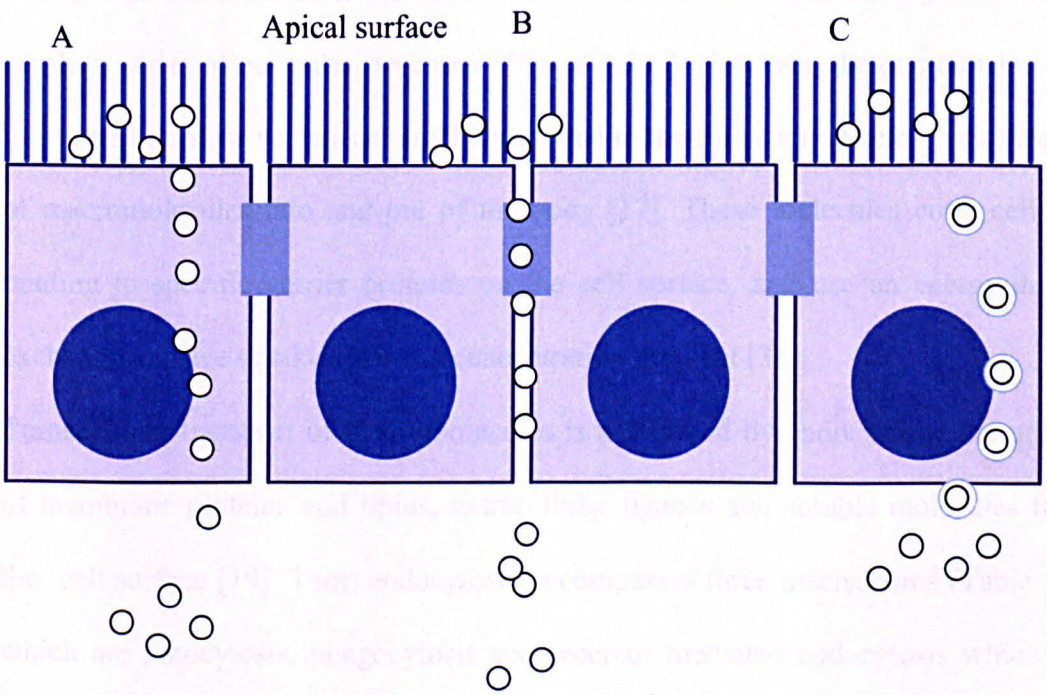

Figure 1.2 *Transport pathways across the epithelial layer. a) Transcellular route, applicable to small, lipophilic molecules, b) Paracellular (between cells) route, relevant to relatively small, hydrophilic macromolecules, and c) Transcytosis (which may be receptor mediated), through which large macromolecules and nanoparticles can potentially traverse the mucosal surfaces.*

1.4.2 Transcellular pathway

1.4.2.1 Small molecules

Small lipid-soluble compounds are rapidly absorbed and transported without a specific transport system presumably because they can integrate into the lipid bilayer of the epithelial cell membrane (Figure 1.2 A). This constitutes the "transcellular pathway" in which compounds pass from the apical to basolateral side by traveling through the cellular membrane [17, 18].

1.4.2.2 Macromolecules

Transport of larger macromolecules and nano-sized particles can be transported through the epithelial layer *via* active transcellular mechanism (transcytosis) which employs series of vesicular structures (Figure 1.2 C). However, the organization and movement of these vesicles is highly regulated to minimize a non-selective transport of macromolecules into and out of the body [17]. These molecules enter cells by binding to specific carrier proteins on the cell surface, and use an energy-driven exchange to drive uptake against a concentration gradient [3].

Transcellular transport of macromolecules is performed by endocytosis; the uptake of membrane proteins and lipids, extracellular ligands and soluble molecules from the cell surface [19]. Term endocytosis encompasses three mechanisms (Table 1.1) which are pinocytosis, phagocytosis and receptor mediated endocytosis which are known to play a role in the uptake of macromolecules [20, 21].

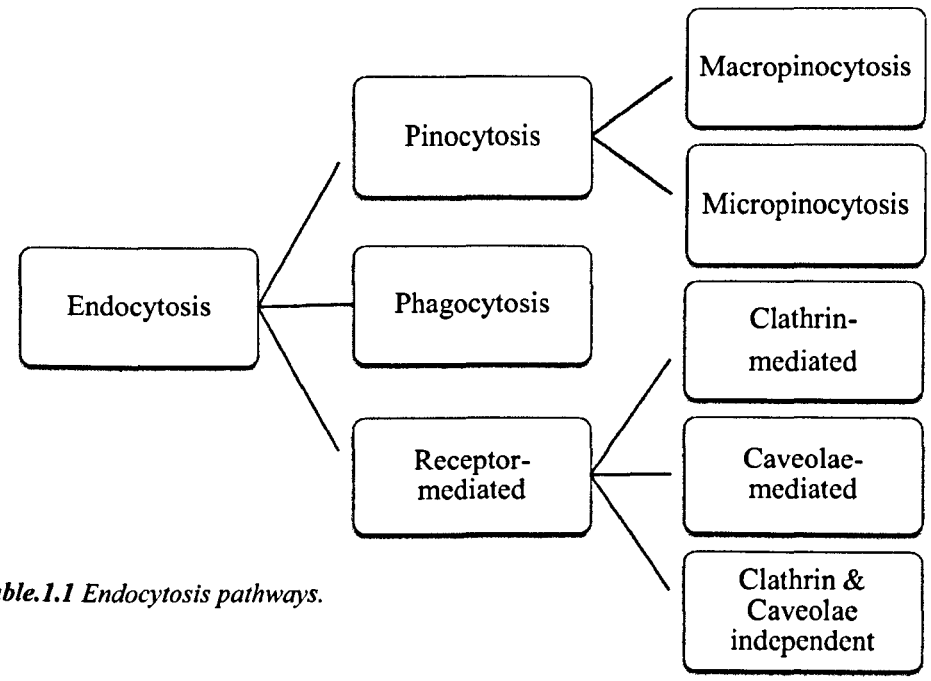

Table.1.1 Endocytosis pathways.

1.5 Endocytosis pathways

1.5.1 Phagocytosis

Phagocytosis is a process in which a cell imports outside material to form an internal phagosome structure. The phagosome usually merges with the lysosome, and then the material is subsequently degraded and released extracellularly via exocytosis, or released intracellularly to undergo further processing [22]. In most multicellular animals phagocytic cells play a major role in immune system rather than as a means to gain nourishment [23].

1.5.2 Pinocytosis

Pincytosis or 'fluid phase' endocytosis is a less specific mechanism which enables cell to ingest droplets of liquid from extracellular environment by vesicles that invaginate from the cell membrane. Consequently the amount internalized by the cell by this route is proportional to the component's concentration in the

extracellular environment. Pinocytic vesicles tend to be smaller than vesicles produced by other endocytic processes [19].

1.5.3 Receptor-mediated endocytosis

Receptor -mediated endocytosis (RME), potentially the most important endocytosis type for drug targeting (see 1.7), utilizes a special class of cell membrane receptors to initiate the process (see chapter 4, section 4.1.1). Initially, extracellular material (ligand) binds to receptors on the cell membrane. This is typically a highly specific event. Following the receptor-ligand binding, the plasma membrane surrounding the ligand-receptor complex starts to invaginate until a distinct internal vesicle, called an "early endosome" forms and separates for the membrane into the cytosol.

Formed endosomal vesicles are transported inside the cell cytosol to different intracellular destinations. They may eventually interact with the Trans Golgi reticulum, where they are believed to fuse with membranous compartments prior to converting into late endosomes. At this stage, there are four possible fates of the ligand and receptor:

- Ligand and its receptor can be fused to the lysosomes for destruction (e.g. various receptor-hormones complexes)
- The ligand can be directed to a lysosome for destruction, and its receptor is recycled back to the plasma membrane for another endocytosis (e.g. asialoglycoprotein receptor)
- The ligand can be directed into the cytosol, while its receptor is recycled back to the plasma membrane to for another round of endocytosis (e.g. folic acid)

- ❖ Both the ligand and its receptor can be recycled back to the plasma membrane (e.g. transferrin, folic acid)

Noticeably, the destination of many receptor-ligand complexes can change from one of the above categories to another, depending on the percentage of occupancy of the cell surface receptor [24].

1.6 Transcytosis

Transcytosis is a vesicular transport of macromolecules from one side to the other side of the cell and it is a strategy utilised by multicellular organisms to move material between two specific environments without changing the compositions of those environments [25]. Transcytosis can occur in both apical to basal and basal to apical directions. It is mostly recognised as a dominant way of transport in polarised epithelial cells, in addition it is widely adopted by most endothelial tissue of the body. Transcytosis can generally be categorised into receptor mediated (see section 1.5.3) and receptor independent. The latter includes fluid phase and adsorptive uptake into cells. Adsorptive uptake involves electrostatic interaction between receptor and ligand [14, 26].

1.7 Receptor-mediated drug delivery

Most current drugs distribute non-specifically and randomly throughout the body, entering both healthy and pathological cells with roughly equal efficiency so it is not surprising the health of normal cells can be compromised as they are sensitive to such drugs.

In the case of drugs designed to have only small changes in cell behaviour (e.g., aspirin), such side effects are usually acceptable. However, when the drug is

designed to induce cell death or a major change in cell behaviour, toxicity to normal cells can limit its use. The development of receptor-targeted drug delivery has been initiated primarily to limit the distribution of drugs to only the pathological cells and to minimize side effects to normal cells. Furthermore, receptor-mediated drug delivery can also enable membrane-impermeant drugs to enter target cells by receptor mediated endocytosis [27-29]. Targeted drug delivery systems aims to expand the therapeutic window of drugs by increasing their delivery to the target tissue and improving target–non-target tissue ratio. This will in turn lead to a reduction in the minimum effective dose of the drug and an improvement in therapeutic efficacy at equivalent plasma concentrations. Given the often limited number of targeted receptor sites on any given target tissue, targeted delivery is a particularly attractive approach for agents with narrow therapeutic windows and/or which are active at very low concentrations [30].

Three factors should be considered for receptor mediated drug delivery:

- High affinity of the receptor for the ligand
- The attached drug should have no competing affinity of its own
- The delivery system does not become trapped in non-targeted pathways

Different biological ligands have been utilized to deliver drugs to target cell. Most of these have been linked to functionally active peptides or proteins, and in some cases to small molecular weight chemotherapeutic medicines.

Table 1.2 lists some of the most common ligand-receptor systems used for the delivery of therapeutic molecules.

Ligand	Drug Payload	References
Insulin	enzymes, particle	[31, 32]
Epidermal growth factor	Protein toxins, micelles,	[33-35]
Transferrin	Drugs, Protein toxins, vectors	[28, 36]
IgG	Proteins, DNA	[37, 38]
Vitamin B_{12}	NPs, peptides, imaging agents	[36, 39, 40]
Folate	All pharmaceutical classes	[41-44]

Table 1.2 Ligands normally used for receptor-mediated drug delivery

1.8 Receptors involved in macromolecular transports across mucosal layer

1.8.1FcRn receptor

The transport of IgG across cellular barriers plays a central role in mediating effective humoral immunity. The Fc receptor for IgG (FcRn) has been well characterized in the transfer of passive humoral immunity from a mother to her fetus [45]. In addition, throughout life, FcRn is involved in transepithelial transcytosis of IgG in both apical-to-basolateral and basolateral-to-apical directions in lung [46, 47], recent studies have investigated its potential for pulmonary absorption of therapeutic proteins [48].

The apical-to-basolateral transcytosis pathway of IgG/FcRn has been explored in various cell types [49-51] to investigate the possibility of delivering biotherapeutics through the epithelium of airways and whether coupling biological agents with Fc

fragments could be used to exploit FcRn mediated transport for systemic drug delivery [51, 52].

By using fluorescence imaging techniques, it has been shown that following cellular internalization FcRn sorts IgGs in the sorting endosome [53]. The transport vesicles containing IgG bound to FcRn do not fuse with the degradative lysosomes, but rather pass through the epithelial cell in the apical to basolateral direction with eventual release of intact IgG to the interstitial space [53].

1.8.2 gp 60 receptor, Albondin

Human serum albumin (HSA) is thought to facilitate transcytosis of unbound and albumin-bound plasma constituents into the basal space. It is believed that the distal respiratory epithelial tract allows slow but finite translocation of albumin into the interstitial and vascular spaces from the air spaces of the lung [54]. This process is initiated by binding of albumin to a cell membane, 60 kDa glycoprotein (gp60) receptor (albondin) [55].

Studies using radiolabelled bovine serum albumin ([^{3}H]- methylated BSA) across rat alveolar epithelial monolayers show that the flux of BSA from the apical to basolateral membrane was greater than from the basolateral to the apical direction [56].

The review by Kim et al suggests that passive diffusion and non-specific adsorptive endocytosis of albumin is unlikely. The latter is thought to be true since the net negative charge owing to cationic molecules on cellular membranes would prevent adsorption of albumin since it is also negatively charged at physiological pH. From the presentation of their findings it may be assumed that albumin is largely taken up by epithelial cells through transcytotic mechanisms. They demonstrated in cultured

type II alveolar epithelial cells that albumin transcytosis is regulated by Albondin [57].

Hence it is potentially possible to utilise albumin uptake/ transport mechanism for targeted delivery of macromolecules. In recent years, Albondin has been utilised for delivery of anti-cancer drugs and peptides [58, 59].

1.8.3 Polymeric immunoglobulin receptor (pIgR) for basal- apical transport of IgA

Immunoglobulin A (IgA) is also transported across the epithelial barrier; however it is transcytosed in the basal to apical direction. Its delivery across the cell has been clearly defined. It binds to its complementary pIgR at the basolateral surface; binding stimulates endocytosis of the IgA-pIgR complex into clathrin coated pits (see section 4.1.1). The endosome containing this complex moves away from the plasma membrane and is trafficked into the common endosome and to the apical recycling endosome. The vesicle containing the complex fuses with the apical plasma membrane. PIgR undergoes proteolytic cleavage by a serine protease localised in the apical membrane. Cleavage releases 'secretory' IgA from the mucosal surface. The function of these pIg receptors is to contribute to mucosal defence of the upper airways by apical secretion of IgA [60, 61].

1.8.4 Folate receptor (FR)

There are few reports on the presence of folate receptor at the apical membrane of epithelial cells of some human tissues [62, 63]. The expression of FR in lung epithelium (type I and type II alveolar epithelial cells) is still an open question, and no specific function has been defined for this tissue [64]. The expression and potential of this receptor for mucosal delivery of macromolecules and nanoparticles

has been studied in this work and the results will be presented/discussed in following chapters.

1.9 Folate-mediated drug delivery

1.9.1 Folates

Folate is the generic name for folic acid (Figure 1.3) and other structurally related compounds (known as vitamin B_9) which are an important constituent of the human diet. They play several metabolic roles, including DNA synthesis, cell division, growth and survival. Folate is needed to carry one-carbon groups for methylation reactions and nucleic acid synthesis [35]. Folic acid is the non-physiological, synthetic, oxidized form of the vitamin. Tetrahydrofolate (THF) and dihydrofolate, in their biologically active form, act as carriers/donors of methyl groups and function as important cofactors in the synthesis of purines and pyrimidines . The total body content of folate is estimated to be 38–96 mg.

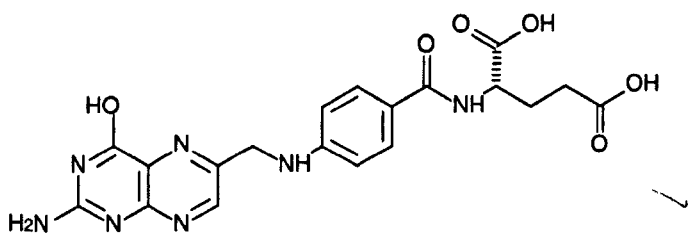

Figure 1.3 Structure of folic acid

1.9.2 Folate carriers

Because animal cells lack enzymes of the folate biosynthetic pathway, their survival and growth are dependent on their ability to acquire and utilize this vitamin. Thus, effective mechanisms for uptaking exogenous folates are needed.

Folate is a hydrophilic molecule due to the two carboxylate moieties positioned at the distal end of the folate molecule, so passive membrane permeability at

physiological temperature and pH is not possible [65]. To overcome this obstacle, there are three mechanisms for the cellular internalization of the vitamin including (i) reduced folate carrier (RFC), (ii) folate receptors (FRs) and (iii) the recently identified proton coupled folate transporter (PCFT) [66].

1.9.2.1 Reduced folate carrier

Reduced folate carrier is the first cloned transporter that was found to transport folates [67]. RFC which is an anionic carrier for transporting reduced folate to cytoplasm [68] is the major route of folate delivery. It's a typical facilitative trans-membrane protein with 12 predicted trans-membrane domains [69] which appears to be expressed ubiquitously in the body [70]. RFC is characterized by a relatively high affinity for N5-substituted reduced folates and folate analogs, such as methotrexate (MTX) (K_m 5 1–5 μM), but has a much lower affinity for folic acid (K_m 5 100–200 μM) [71]. The human RFC gene has been cloned, and its predicted amino acidic sequence seems to indicate a 60-kDa glycoprotein, which belongs to the super-family of trans-membrane spanning transporters [72]. This transporter functions optimally at around neutral pH [67].

1.9.2.2 Proton coupled folate transporter (PCFT)

PCFT is recently discovered in intestine (predominantly expressed in duodenum) and it is involved in folate uptake in epithelial layer. It is responsible for transport of folate at an acidic pH of 5.5, but its transport activity was absent at near-neutral pH [66, 67]. A report by Low et al has showed that PCFT is critical to intestinal folate absorption and transport into the central nervous system because there are loss-of-function mutations in this gene in the autosomal recessive disorder, hereditary folate malabsorption [73]. PCFT is also expressed in the brain, where it might export folates from acidified endosomes after FRα-mediated endocytosis [74].

1.9.2.3 Folate receptor

Folate receptors belongs to a family of high affinity folate binding proteins which are encoded by three different genes α, β,and γ located on chromosome 11 . The mature FRs are similar (68-79% identical in amino acid sequence) proteins which contain 229-236 amino acids and 2(β,γ) or 3(α) N-glycosylation sites with a 38-40 kDa molecular weight [42]. FRα and FRβ are attached to the cell membrane by glycosylphosphatidylinositol (GPI) anchor and internalize their cargo by active receptor mediated endocytosis, whereas FRγ ,which is a soluble folate binding protein, is secreted because of lack of an efficient signal sequence for GPI modification [75, 76].

FRs bind folic acid (an oxidized form of folate) with high affinity. FR α-isoform has a dissociation constant (K_d) for folic acid of 0.1 nM, which is approximately 10-fold lower than its K_d for reduced folates (e.g., 5-methyltetrahydrofolate) [77] whereas FRβ curiously lack affinity for folic acid and various folate derivatives [30].

Receptor-mediated uptake of folate or folate conjugates proceeds through a series of distinct steps, beginning with conjugate binding to a cell surface FR and terminating with release of cargo into the cytoplasm (Figure 1.4). Thus, after membrane invagination and internalization to form an endocytic vesicle, acidification of the endosomal compartment to pH ~5 results in release of some (but not all) folate or folate conjugates from their receptor. Trafficking of the acidic endosome to a recycling centre then allows separation of membrane-bound FR from released cargo. Released folate or folate conjugates are seen to escape the endosome through an unknown mechanism, resulting in drug deposition in the cytoplasm. In contrast, membrane bound FR largely recycle back to the cell surface, allowing for delivery of additional folate-linked drugs into the cell. In different cells, the recycling rate *in*

vivo varies from one cycle every 4 h to one cycle every 12 h. In other FR positive (FR+) cells, the recycling rate may be faster.

Importantly, it has been observed that folate conjugates mostly do not enter lysosomes for destruction, thus enabling the delivery of different therapeutic materials in to the cells [78-81].

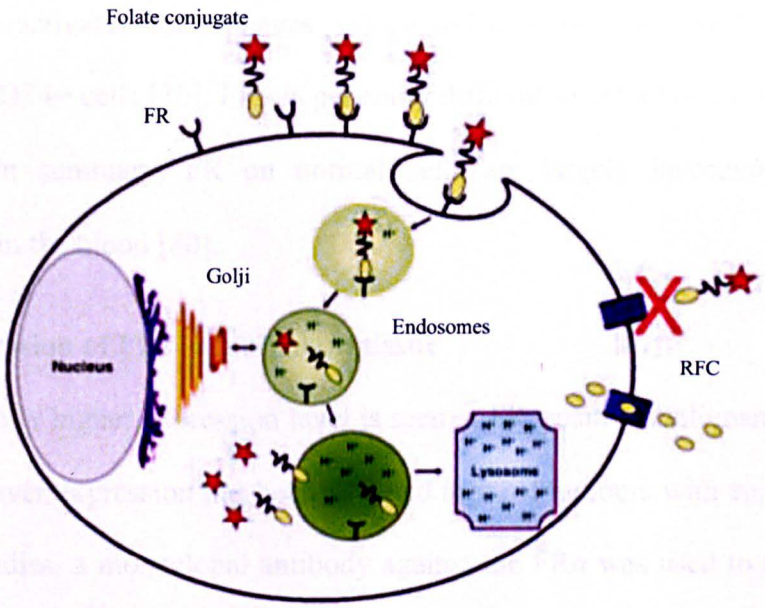

Figure 1.4 *Receptor-mediated endocytosis of folate conjugates. Folate conjugates bind to FRs. Then cell membrane invaginates and pinches off to form an endosome. As the endosomal compartment acidifies, the folate conjugate releases from the receptor into the cytosol. Although the reduced folate carrier is present in virtually all cells, oxidised folates are not substrates, and therefore, are taken up only by folate receptor. Adopted from [80]*

1.9.3 Tissue distribution of FRs

Expression of FRs in humans is restricted to certain normal tissues. Significant FRα abundance has been detected in epithelial cells, kidney (proximal tubules), lungs, choroid plexus, intestine and thyroid. In all these tissues these receptors are expressed on the apical membrane surface [30, 82, 83]. For example, in the choroid

plexus, receptor is localized to the brain side of the blood-brain barrier, where it is inaccessible to blood-borne folates or folate-drug conjugates. Or there is high expression of FRα in proximal tubules of the kidney where it is believed to capture folates prior to their urinary excretion and then return them back into circulation *via* a transcellular reabsorption process [84, 85].

FRβ is absent in most normal tissue, but it has been observed with a low expression in placenta, activated macrophages, spleen and thymus. FR type β has been also found on CD34+ cells [30]. FRγ is generally difficult to detect in any normal tissue. [62, 86]. In summary, FR on normal cells are largely inaccessible to folate conjugates in the blood [80].

1.9.4 Expression of FRs in malignant tissue

A significantly higher expression level is seen in FR-positive malignant tissues [30]. FR type α over expression has been detected in most tumours with epithelial origin. In some studies, a monoclonal antibody against the FRα was used to determine the frequency of FRα overexpression in human tumour by indirect immunohistochemical staining. High receptor overexpression were seen in many types of tumours including ovarian, endometrial, colorectal, breast, lung, renal cell brain metastases derived from epithelial cancers and neuroendocrine carcinoma [62].

FR type β is mostly overexpressed in non-epithelial tumours such as sarcomas, acute myeloid leukaemia, and FR type γ is mainly restricted to malignancies of hematopoietic origin including lymphoid cells [84].

1.9.5 Folic acid; an ideal ligand for FR

Folic acid, as well as its high binding affinity to FR, has many attractive properties as a targeting ligand for internalisation of conjugated therapeutics. Due to its ability

to target not only FR cancers, but also many inflammatory diseases, applications of folate targeting to drug delivery will become more diverse than other targeting ligands. Folic acid is soluble in water, it has low immunogenicity and a relatively low MW (MW=441.4gmol-1), it is easily available and has a good storage stability in addition to simple conjugation chemistry [87].

Simple covalent attachment of folic acid to different macromolecules has been shown to lead to conjugate internalization by folate receptor-positive cells in an identical fashion to that of free folic acid [84]. Also the apparent lack of toxicity of folate conjugates, tested to date, is added to this list of attributes enhancing its chance of more success than most other ligands under investigation (e.g., monoclonal IgGs, peptide, hormones, etc.) [80].

These properties have allowed drug delivery experts to conjugate various materials on to folic acid for folate mediated delivery (see section 1.9.6).

1.9.6 Folate decorated carriers for FR mediated drug targeting

Folate targeting was invented after Bart Kamen's group at the University of Texas reported that folate is entered into the cells via a receptor-mediated endocytic process in 1986 [88]. After that many researchers started working on folate targeted drug delivery. The prevalence of FR overexpression among human tumors makes it a good marker for targeted drug delivery to these tumors.

Hence up to the present time, folate has been covalently attached to a wide range of drug delivery carriers such as liposomes, imaging complexes [89-91], polymer conjugates [92], protein toxins, plasmid DNA [64, 93], chemotherapeutic and immunotherapeutic agents [81, 94], nano-particulates [95-97], proteins [98] and radiopharmaceutical agents [99].

Among them, anti-cancer liposomes with having surface exposed folate moieties have been extensively studied for passively targeting cancer cells [100]. In particular various anti-cancer agents have been considered and can be exploited for targeted drug delivery. However, the sub-cellular transport mechanism of folate-conjugate is only partly characterised hence further research is required to determine the pathways and the effects of ligands on the pathway [88].

1.10 Aims and objectives

The majority of studies have described folate mediated drug delivery to cancerous cells, whilst data on targeted drug delivery via folate receptor to non-cancerous cells or tissues are scarce.

Also reports on the possible role of folate receptor in transport in epithelial cells are rare. These studies mostly deal with the transport of folate molecule in apical to basolateral direction for translocation of folate in proximal tubule cells of kidney [101, 102], basolateral to apical transport of folate in retinal pigment epithelium [103] and folate transport in choroid plexus [104]. To the best of our knowledge, there is no published data on folate mediated transport of macromolecules.

So the main aims of this thesis are first to exploit the expression of FR in different epithelial cell lines (cancerous and non-cancerous cell lines) and secondly to discover the potential of this receptor in uptake and transport of folate-decorated proteins and nanoparticles across epithelial cell monolayers. To this end, polarised epithelial cell layers (Calu-3, HBEC, Caco-2 and IEC-6) will be adopted to serve as an *in vitro* model of epithelia. Furthermore, endocytic mechanism involved in folate-mediated nanoparticle internalization and translocation across cell layers will be investigated by using different endocytic-pathway inhibitors.

And lastly, in order to improve uptake and transport of nanoparticles across the cell layers, the effect of different concentration of ligand on nanoparticle surface will be explored.

1.11 References

1. Bansal, S.S., et al., *Advanced drug delivery systems of curcumin for cancer chemoprevention.* Cancer Prev Res (Phila), 2011. **4**(8): p. 1158-71.
2. Rotello, V.M., *Advanced drug delivery reviews theme issue. Preface.* Adv Drug Deliv Rev, 2008. **60**(11): p. 1225.
3. Patton, J.S., C.S. Fishburn, and J.G. Weers, *The lungs as a portal of entry for systemic drug delivery.* Proc Am Thorac Soc, 2004. **1**(4): p. 338-44.
4. Needleman, I.G., F.C. Smales, and G.P. Martin, *An investigation of bioadhesion for periodontal and oral mucosal drug delivery.* J Clin Periodontol, 1997. **24**(6): p. 394-400.
5. Zhang, H., J. Zhang, and J.B. Streisand, *Oral mucosal drug delivery: clinical pharmacokinetics and therapeutic applications.* Clin Pharmacokinet, 2002. **41**(9): p. 661-80.
6. Hearnden, V., et al., *New developments and opportunities in oral mucosal drug delivery for local and systemic disease.* Adv Drug Deliv Rev, 2011.
7. Bitter, C., K. Suter-Zimmermann, and C. Surber, *Nasal drug delivery in humans.* Curr Probl Dermatol, 2011. **40**: p. 20-35.
8. Graff, C.L. and G.M. Pollack, *Nasal drug administration: potential for targeted central nervous system delivery.* J Pharm Sci, 2005. **94**(6): p. 1187-95.
9. Mehuys, E. and C. Vervaet, *[Buccal drug delivery systems].* J Pharm Belg, 2009(4): p. 109-14.
10. Groneberg, D.A., et al., *Fundamentals of pulmonary drug delivery.* Respir Med, 2003. **97**(4): p. 382-7.
11. Cryan, S.A., N. Sivadas, and L. Garcia-Contreras, *In vivo animal models for drug delivery across the lung mucosal barrier.* Adv Drug Deliv Rev, 2007. **59**(11): p. 1133-51.
12. Zhang, J.Y., Y. Wang, and C. Prakash, *Xenobiotic-metabolizing enzymes in human lung.* Curr Drug Metab, 2006. **7**(8): p. 939-48.
13. Di Colo, G., Y. Zambito, and C. Zaino, *Polymeric enhancers of mucosal epithelia permeability: Synthesis, transepithelial penetration-enhancing properties, mechanism of action, safety issues.* Journal of Pharmaceutical Sciences, 2008. **97**(5): p. 1652-1680.

14. Hubbard, A.L. and P.L. Tuma, *Transcytosis: Crossing cellular barriers.* Physiological Reviews, 2003. **83**(3): p. 871-932.

15. Roger, E., et al., *Lipid nanocarriers improve paclitaxel transport throughout human intestinal epithelial cells by using vesicle-mediated transcytosis.* J Control Release, 2009. **140**(2): p. 174-81.

16. Madara, J.L., *Regulation of the movement of solutes across tight junctions.* Annual Review of Physiology, 1998. **60**: p. 143-159.

17. Folsch, H., P.E. Mattila, and O.A. Weisz, *Taking the Scenic Route: Biosynthetic Traffic to the Plasma Membrane in Polarized Epithelial Cells.* Traffic, 2009. **10**(8): p. 972-981.

18. Mostov, K., T. Su, and M. ter Beest, *Polarized epithelial membrane traffic: conservation and plasticity.* Nature Cell Biology, 2003. **5**(4): p. 287-293.

19. Nichols, B.J. and J. Lippincott-Schwartz, *Endocytosis without clathrin coats.* Trends Cell Biol, 2001. **11**(10): p. 406-12.

20. Wrana, J.L. and C. Le Roy, *Clathrin- and non-clathrin-mediated endocytic regulation of cell signalling.* Nature Reviews Molecular Cell Biology, 2005. **6**(2): p. 112-126.

21. Doherty, G.J. and H.T. McMahon, *Mechanisms of Endocytosis.* Annual Review of Biochemistry, 2009. **78**: p. 857-902.

22. Tse, S.M., et al., *Differential role of actin, clathrin, and dynamin in Fc gamma receptor-mediated endocytosis and phagocytosis.* J Biol Chem, 2003. **278**(5): p. 3331-8.

23. Stuart, L.M. and R.A. Ezekowitz, *Phagocytosis: elegant complexity.* Immunity, 2005. **22**(5): p. 539-50.

24. Christopher Leamon, P.S.L., *Receptor–Mediated Drug Delivery.* 9 ed2005.

25. Tuma, P.L. and A.L. Hubbard, *Transcytosis: crossing cellular barriers.* Physiol Rev, 2003. **83**(3): p. 871-932.

26. Mostov, K., et al., *Membrane Traffic and Transcytosis in Polarized Epithelial-Cells - Signals, Mechanisms, and Regulation.* Journal of Cellular Biochemistry, 1993: p. 49-49.

27. Zhao, X., H. Li, and R.J. Lee, *Targeted drug delivery via folate receptors.* Expert Opin Drug Deliv, 2008. **5**(3): p. 309-19.

28. Qian, Z.M., et al., *Targeted drug delivery via the transferrin receptor-mediated endocytosis pathway.* Pharmacological Reviews, 2002. **54**(4): p. 561-87.

29. Vyas, S.P., A. Singh, and V. Sihorkar, *Ligand-receptor-mediated drug delivery: an emerging paradigm in cellular drug targeting.* Crit Rev Ther Drug Carrier Syst, 2001. **18**(1): p. 1-76.

30. Sudimack, J. and R.J. Lee, *Targeted drug delivery via the folate receptor.* Adv Drug Deliv Rev, 2000. **41**(2): p. 147-62.

31. Fukuta, M., et al., *Delivery of peptides across the blood-brain barrier using a silent ligand.* Stp Pharma Sciences, 1997. **7**(1): p. 85-91.

32. Gupta, A.K., et al., *Receptor-mediated targeting of magnetic nanoparticles using insulin as a surface ligand to prevent endocytosis.* Ieee Transactions on Nanobioscience, 2003. **2**(4): p. 255-261.

33. Li, W.P., et al., *Receptor-binding, biodistribution, and metabolism studies of (64)Cu-DOTA-cetuximab, a PET-imaging agent for epidermal growth-factor receptor-positive tumors.* Cancer Biotherapy and Radiopharmaceuticals, 2008. **23**(2): p. 158-171.

34. Zeng, F.Q., H. Lee, and C. Allen, *Epidermal growth factor-conjugated poly(ethylene glycol)-block-poly(delta-valerolactone) copolymer micelles for targeted delivery of chemotherapeutics.* Bioconjug Chem, 2006. **17**(2): p. 399-409.

35. Song, S.X., et al., *Peptide ligand targeted delivery to EGFR expressing cancer cells in vitro and in vivo.* 2006 International Conference on Biomedical and Pharmaceutical Engineering, Vols 1 and 2, 2006: p. 487-490.

36. Li, H. and Z.M. Qian, *Transferrin/transferrin receptor-mediated drug delivery.* Med Res Rev, 2002. **22**(3): p. 225-50.

37. Dumont, J.A., et al., *Delivery of an erythropoietin-Fc fusion protein by inhalation in humans through an immunoglobulin transport pathway.* Journal of Aerosol Medicine-Deposition Clearance and Effects in the Lung, 2005. **18**(3): p. 294-303.

38. Rojanasakul, Y., et al., *Targeted Gene Delivery to Alveolar Macrophages Via Fc Receptor-Mediated Endocytosis.* Pharm Res, 1994. **11**(12): p. 1731-1736.

39. Gupta, Y., D.V. Kohli, and S.K. Jain, *Vitamin B12-mediated transport: a potential tool for tumor targeting of antineoplastic drugs and imaging agents.* Crit Rev Ther Drug Carrier Syst, 2008. **25**(4): p. 347-79.

40. Chalasani, K.B., et al., *A novel vitamin B12-nanosphere conjugate carrier system for peroral delivery of insulin.* J Control Release, 2007. **117**(3): p. 421-9.

41. Dixit, V., et al., *Synthesis and grafting of thioctic acid-PEG-folate conjugates onto Au nanoparticles for selective targeting of folate receptor-positive tumor cells.* Bioconjugate Chemistry, 2006. **17**(3): p. 603-609.

42. Hilgenbrink, A.R. and P.S. Low, *Folate receptor-mediated drug targeting: From therapeutics to diagnostics.* Journal of Pharmaceutical Sciences, 2005. **94**(10): p. 2135-2146.

43. Kim, S.H., et al., *Target-specific cellular uptake of PLGA nanoparticles coated with poly(L-lysine)-poly(ethylene glycol)-folate conjugate.* Langmuir, 2005. **21**(19): p. 8852-7.

44. Low, P.S. and S.A. Kularatne, *Folate-targeted therapeutic and imaging agents for cancer.* Current Opinion in Chemical Biology, 2009. **13**(3): p. 256-262.

45. Tillinger, W., W. Ulrich, and G. Oberhuber, *Expression of the neonatal Fc receptor, FcRn, in the adult upper GI tract - Influence of mucosal inflammation.* Gastroenterology, 2002. **122**(4): p. A530-A531.

46. Lencer, W.I., et al., *Bidirectional FcRn-dependent IgG transport in a polarized human intestinal epithelial cell Line.* Journal of Clinical Investigation, 1999. **104**(7): p. 903-911.

47. Israel, E.J., et al., *Expression of the neonatal Fc receptor, FcRn, on human intestinal epithelial cells.* Immunology, 1997. **92**(1): p. 69-74.

48. Bitonti, A.J. and J.A. Dumont, *Pulmonary administration of therapeutic proteins using an immunoglobulin transport pathway.* Advanced Drug Delivery Reviews, 2006. **58**(9-10): p. 1106-1118.

49. Crow, A.R., S.J. Suppa, and A.H. Lazarus, *Expression of the Neonatal Fc Receptor FcRn Is Not Required for the Amelioration of Murine ITP by IVIg or a Monoclonal Antibody.* Blood, 2010. **116**(21): p. 1048-1048.

50. Fuchs, R., et al., *Functional Expression of the Human Neonatal Fc-receptor, hFcRn, in Isolated Cultured Human Syncytiotrophoblasts.* Placenta, 2009. **30**(6): p. 507-515.

51. Roopenian, D.C. and S. Akilesh, *FcRn: the neonatal Fc receptor comes of age.* Nature Reviews Immunology, 2007. **7**(9): p. 715-725.

52. Ward, E.S., et al., *Exocytosis of IgG as mediated by the receptor, FcRn: An analysis at the single-molecule level.* Proceedings of the National Academy of Sciences of the United States of America, 2004. **101**(30): p. 11076-11081.

53. Ward, E.S., et al., *Evidence to support the cellular mechanism involved in serum IgG homeostasis in humans.* International Immunology, 2003. **15**(2): p. 187-195.

54. Kim, K.J., et al., *Absorption of intact albumin across rat alveolar epithelial cell monolayers.* American Journal of Physiology-Lung Cellular and Molecular Physiology, 2003. **284**(3): p. L458-L465.

55. Malik, A.B., et al., *Evidence for the role of alveolar epithelial gp60 in active transalveolar albumin transport in the rat lung.* Journal of Physiology-London, 2001. **533**(2): p. 547-559.

56. Matsukawa, Y., et al., *Size dependent dextran transport across rat alveolar epithelial cell monolayers.* Journal of Pharmaceutical Sciences, 1997. **86**(3): p. 305-309.

57. Kim, K.J. and A.B. Malik, *Protein transport across the lung epithelial barrier.* American Journal of Physiology-Lung Cellular and Molecular Physiology, 2003. **284**(2): p. L247-L259.

58. Swaan, P.W. and L.A. Bareford, *Endocytic mechanisms for targeted drug delivery.* Advanced Drug Delivery Reviews, 2007. **59**(8): p. 748-758.

59. Shin, D.M., et al., *Therapeutic nanoparticles for drug delivery in cancer.* Clinical Cancer Research, 2008. **14**(5): p. 1310-1316.

60. Brandtzaeg, P., *Mucosal Immunity: Induction, Dissemination, and Effector Functions.* Scandinavian Journal of Immunology, 2009. **70**(6): p. 505-515.

61. van Egmond, M., et al., *IgA and the IgA Fc receptor.* Trends Immunol, 2001. **22**(4): p. 205-11.

62. Parker, N., et al., *Folate receptor expression in carcinomas and normal tissues determined by a quantitative radioligand binding assay.* Analytical Biochemistry, 2005. **338**(2): p. 284-293.

63. Lu, Y. and P.S. Low, *Folate-mediated delivery of macromolecular anticancer therapeutic agents.* Adv Drug Deliv Rev, 2002. **54**(5): p. 675-93.

64. Kelemen, L.E., *The role of folate receptor alpha in cancer development, progression and treatment: cause, consequence or innocent bystander?* Int J Cancer, 2006. **119**(2): p. 243-50.

65. Leamon, C.P. and P.S. Low, *Folate-mediated targeting: from diagnostics to drug and gene delivery.* Drug Discovery Today, 2001. **6**(1): p. 44-51.

66. Subramanian, V.S., J.S. Marchant, and H.M. Said, *Apical membrane targeting and trafficking of the human proton-coupled transporter in polarized epithelia.* Am J Physiol Cell Physiol, 2008. **294**(1): p. C233-40.

67. Nakai, Y., et al., *Functional characterization of human proton-coupled folate transporter/heme carrier protein 1 heterologously expressed in mammalian cells as a folate transporter.* J Pharmacol Exp Ther, 2007. **322**(2): p. 469-76.

68. Kaufman, Y., et al., *Reduced folate carrier mutations are not the mechanism underlying methotrexate resistance in childhood acute lymphoblastic leukemia.* Cancer, 2004. **100**(4): p. 773-782.

69. Zhao, R., Y.G. Assaraf, and I.D. Goldman, *A mutated murine reduced folate carrier (RFC1) with increased affinity for folic acid, decreased affinity for methotrexate, and an obligatory anion requirement for transport function.* J Biol Chem, 1998. **273**(30): p. 19065-71.

70. Wong, S.C., et al., *Isolation of Human Cdnas That Restore Methotrexate Sensitivity and Reduced Folate Carrier Activity in Methotrexate Transport-Defective Chinese-Hamster Ovary Cells.* Journal of Biological Chemistry, 1995. **270**(29): p. 17468-17475.

71. Matherly, L.H., *Molecular and cellular biology of the human reduced folate carrier.* Prog Nucleic Acid Res Mol Biol, 2001. **67**: p. 131-62.

72. Corona, G., et al., *Role of folate receptor and reduced folate carrier in the transport of 5-methyltetrahydrofolic acid in human ovarian carcinoma cells.* Int J Cancer, 1998. **75**(1): p. 125-33.

73. Zhao, R., et al., *A role for the proton-coupled folate transporter (PCFT-SLC46A1) in folate receptor-mediated endocytosis.* J Biol Chem, 2009. **284**(7): p. 4267-74.

74. Steinfeld, R., et al., *Folate receptor alpha defect causes cerebral folate transport deficiency: a treatable neurodegenerative disorder associated with disturbed myelin metabolism.* Am J Hum Genet, 2009. **85**(3): p. 354-63.

75. Razak, A.R.A., et al., *Expression of folate receptor alpha (FRa) in malignant pleural mesothelioma patients by immunohistochemistry: a clinico-pathological analysis.* Lung Cancer, 2009. **63**: p. S27-S27.

76. Matherly, L.H. and D. Goldman, *Membrane transport of folates.* Vitamins and Hormones - Advances in Research and Applications, Vol 66, 2003. **66**: p. 403-456.

77. Rijnboutt, S., et al., *Endocytosis of GPI-linked membrane folate receptor-alpha.* Journal of Cell Biology, 1996. **132**(1-2): p. 35-47.

78. Low, P.S., et al., *Ligand binding and kinetics of folate receptor recycling in vivo: Impact on receptor-mediated drug delivery.* Molecular Pharmacology, 2004. **66**(6): p. 1406-1414.

79. Lee, R.J., S. Wang, and P.S. Low, *Measurement of endosome pH following folate receptor-mediated endocytosis.* Biochimica Et Biophysica Acta-Molecular Cell Research, 1996. **1312**(3): p. 237-242.

80. Low, P.S. and A.R. Hilgenbrink, *Folate receptor-mediated drug targeting: From therapeutics to diagnostics.* Journal of Pharmaceutical Sciences, 2005. **94**(10): p. 2135-2146.

81. Low, P.S. and S.A. Kularatne, *Folate-targeted therapeutic and imaging agents for cancer.* Curr Opin Chem Biol, 2009. **13**(3): p. 256-62.

82. Leamon, C.P., et al., *Folate receptor expression in carcinomas and normal tissues determined by a quantitative radioligand binding assay.* Analytical Biochemistry, 2005. **338**(2): p. 284-293.

83. Kamen, B.A. and A.K. Smith, *A review of folate receptor alpha cycling and 5-methyltetrahydrofolate accumulation with an emphasis on cell models in vitro.* Advanced Drug Delivery Reviews, 2004. **56**(8): p. 1085-1097.

84. Hilgenbrink, A.R. and P.S. Low, *Folate receptor-mediated drug targeting: from therapeutics to diagnostics.* J Pharm Sci, 2005. **94**(10): p. 2135-46.

85. Kalli, K.R., et al., *Folate receptor alpha as a tumor target in epithelial ovarian cancer.* Gynecologic Oncology, 2008. **108**(3): p. 619-626.

86. Salbaum, J.M., R.H. Finnell, and C. Kappen, *Regulation of folate receptor 1 gene expression in the visceral endoderm.* Birth Defects Res A Clin Mol Teratol, 2009. **85**(4): p. 303-13.

87. Shia, J., et al., *Immunohistochemical Expression of Folate Receptor-alpha in Ovarian Epithelial Neoplasms Bears Clinical and Pathological Significance.* Modern Pathology, 2009. **22**: p. 237a-237a.

88. Leamon, C.P. and J.A. Reddy, *Folate-targeted chemotherapy.* Adv Drug Deliv Rev, 2004. **56**(8): p. 1127-41.

89. Kamaly, N., et al., *Folate receptor targeted bimodal liposomes for tumor magnetic resonance imaging.* Bioconjug Chem, 2009. **20**(4): p. 648-55.

90. Lee, R.J., J. Wu, and Q. Liu, *A folate receptor-targeted liposomal formulation for paclitaxel.* International Journal of Pharmaceutics, 2006. **316**(1-2): p. 148-153.

91. Lee, R.J. and P.S. Low, *Delivery of Liposomes into Cultured Kb Cells Via Folate Receptor-Mediated Endocytosis.* Journal of Biological Chemistry, 1994. **269**(5): p. 3198-3204.

92. Jing, X.B., et al., *Folate-Conjugated Micelles and Their Folate-Receptor-Mediated Endocytosis.* Macromolecular Bioscience, 2009. **9**(11): p. 1059-1068.

93. Lam, J.K., et al., *Folate conjugated phosphorylcholine-based polycations for specific targeting in nucleic acids delivery.* J Drug Target, 2009. **17**(7): p. 512-23.

94. Koyakutty, M., et al., *Folate receptor targeted, rare-earth oxide nanocrystals for bi-modal fluorescence and magnetic imaging of cancer cells.* Biomaterials, 2010. **31**(4): p. 714-729.

95. Choi, H., et al., *Iron oxide nanoparticles as magnetic resonance contrast agent for tumor imaging via folate receptor-targeted delivery.* Academic Radiology, 2004. **11**(9): p. 996-1004.

96. Dixit, V., et al., *Synthesis and grafting of thioctic acid-PEG-folate conjugates onto Au nanoparticles for selective targeting of folate receptor-positive tumor cells.* Bioconjug Chem, 2006. **17**(3): p. 603-9.

97. Oyewumi, M.O. and R.J. Mumper, *Influence of formulation parameters on gadolinium entrapment and tumor cell uptake using folate-coated*

nanoparticles. International Journal of Pharmaceutics, 2003. **251**(1-2): p. 85-97.

98. Low, P.S. and A.C. Antony, *Folate receptor-targeted drugs for cancer and inflammatory diseases - Preface.* Advanced Drug Delivery Reviews, 2004. **56**(8): p. 1055-1058.

99. Linder, K.E., et al., *In vitro & in vivo studies with alpha-and gamma-isomers of Tc-99m-oxa-folate show uptake of both isomers in folate-receptor (+) KB cell lines.* Journal of Nuclear Medicine, 2000. **41**(5): p. 119p-119p.

100. Park, T.G. and H.S. Yoo, *Folate receptor targeted biodegradable polymeric doxorubicin micelles.* Journal of Controlled Release, 2004. **96**(2): p. 273-283.

101. Sikka, P.K. and K.E. McMartin, *Determination of folate transport pathways in cultured rat proximal tubule cells.* Chemico-Biological Interactions, 1998. **114**(1-2): p. 15-31.

102. Birn, H., J. Selhub, and E.I. Christensen, *Internalization and Intracellular-Transport of Folate-Binding Protein in Rat-Kidney Proximal Tubule.* American Journal of Physiology, 1993. **264**(2): p. C302-C310.

103. Chancy, C.D., et al., *Expression and differential polarization of the reduced-folate transporter-1 and the folate receptor alpha in mammalian retinal pigment epitheliu.* Journal of Biological Chemistry, 2000. **275**(27): p. 20676-20684.

104. Kennedy, M.D., et al., *Evaluation of folate conjugate uptake and transport by the choroid plexus of mice.* Pharm Res, 2003. **20**(5): p. 714-9.

Chapter 2

General materials & methods

2.1 Materials

2.1.1 Cell lines and routine cell culture materials

Caco-2 cells (passage 30) were obtained from the European Collection of Cell Cultures (ECACC)(used up to passage50), Calu-3 cells passage 25) were obtained from the American Type Culture Collection (ATCC) (and used up to passage 40). HBEC and IEC-6 cells were a generous gift from the City Hospital (Nottingham , UK) and used at passages 2-4 and 11-20 respectively. Dulbecco's Modified Eagles Medium (DMEM), RPMI 1640 (free folate medium), Hanks Balanced Salt Solution (HBSS), 2.5% Trypsin/EDTA, Antibiotic/Antimycotic solution (containing penicillin, streptomycin and amphotericin), L-glutamine, Foetal Calf Serum (FCS), Hydrocortisone solution (50 μM, sterile-filtered), Human Transferrin, Triiodothyronine (sodium salt), Epidermal growth factor (recombinant, lyophilised powder), Non-essential amino acids 100X (NEM), Insulin solution (10 mg/mL insulin in 25 mM HEPES), Interleukin-4 (IL-4) (recombinant, lyophilized powder), Trypan Blue (0.4% w/v), NaOH and Triton–X 100, were all obtained from Sigma Aldrich, UK. Ham's F12 and Keratinocyte serum-free medium (KSFM), bovine pituitary extract, and G418 were obtained from Invitrogen.

All cell media were supplemented with penicillin, streptomycin and amphotericin B at final concentrations of 100 units/ml, 0.1 mg/ml and 0.25 μg/ml, respectively and also with FCS (except KSFM) and L-glutamine at final media concentrations of 10% v/v and 2 mM, respectively. DMEM was further supplemented with 5% NEM for Caco-2, with Ham's F12 for Calu-3 and with 5ml NEM, IL-4 (50 ng/ml) and Insulin (0.1 units/ml) for IEC-6.

KSFM was also supplemented with Bovine pituitary extract (25 μg/ml), recombinant epidermal growth factor (0.2 ng/ml), G418 (15 mg/ml), Hydrocortisone (0.5 mg/ml), Transferrin (10 mg/ml) and Triiodothyronine (6.5 mg/ml).

Dimethylsulphoxide (DMSO) and 4-(2-hydroxyethyl)-1-piperazineethanesulfonic acid (HEPES), used as cryopreservant, were purchased from Sigma Aldrich.

Phosphate buffered saline (PBS) containing 0.14M NaCl, 0.01M phosphate at pH 7.4 was prepared from tablets obtained from Oxoid (Basingstoke, UK). All water used was obtained from an ELGA purification system (resistivity 18.2 MV-cm, Maxima USF ELGA, High Wycombe, UK), and sterilized by being autoclaved. 3-(4, 5-dimethylthiazol-2-yl)-5-(3-carboxymethoxyphenyl)-2-(4-sulfophenyl)-2H-tetrazolium (MTS) reagent was purchased from Promega (USA).

2.1.2 Labware

Permeable supports - Transwells® (12 mm diameter, 0.4 μm pore size, and polyester membrane), Tissue culture flasks (75 cm^2, 250 ml, 0.2 μm vented plug seal cap) and 96-well polystyrene microplates were obtained from Corning Life Sciences (Holland). 6, 12, 24-well plates (Tissue culture treated, flat bottom with low evaporation lid) were purchased from Becton Dickinson Labware (Becton Dickinson and company, NJ, USA). Minisart filters (non-pyrogenic, 0.2 μm) were purchased from Sartorius (UK). Glass cover slips with 15 mm diameter and glass-bottom petri culture dish with 10 cm diameter were purchased from Sigma Aldrich. Sterile universals (5 ml and 30 ml volume capacity) were obtained from Sterilin (UK). Sterile cryovials (1 ml capacity) were supplied by NUNC.

2.1.3 Cell staining reagents

Mouse, Anti-human Zonula Occludens-1 (ZO-1, TJ protein) antibody was purchased from Zymed, (part of Invitrogen). Goat Anti-Human Caveolin 1 (CAV1) antibody

was obtained from Abcam plc, Mouse Anti- Human Clathrin Monoclonal Antibody was obtained from United States Biological.

Mouse Anti-Human FOLR1 Purified MaxPab Polyclonal Antibody was purchased from Abnova Corporation.

Goat, Anti-Mouse FITC and TRITC labelled, Goat, Anti-Mouse horseradish peroxidase (HRP)-conjugated and Mouse Anti-Goat TRITC labelled secondary antibodies were all purchased from Sigma Aldrich.

DAPI (4',6-diamidino-2-phenylindole) with antifade mounting media (commercially known as SlowfadeGold®) and CellTrackerTM Green were obtained from Invitrogen. 1, 4-Diazabicyclo-octane (DABCO, UV mountant) was obtained from Sigma Aldrich.

2.1.4 Chemicals

FITC-labelled dextran (FD) of approximate average Molecular weight (MW) of 4 kDa (FD4), 1-Ethyl-3-(3-dimethylaminopropyl)-carbodimide (ECDI), Tetramethylrodamine isothiocyanate (TRITC) Paraformaldehyde, Triton X-100, Bovine Serum Albumin (BSA), Tween 20, Folic acid (FA) calcium salt, Bradford reagent, Poly-D lysine (PDL) were all obtained from Sigma Aldrich. Fluorescein isothiocyanate (FITC) was purchased from Molecular Probes (Paisley, UK). Red fluorescent polystyrene nanoparticles, Sulphate-modified of 30 nm nominal diameter were obtained from Sigma Aldrich. PD-10 desalting columns (Sephadex G-25 Medium) were purchased from GE Healthcare (UK Limited Little Chalfont). Ethanol and acetone used in the project were HPLC grade.

All other chemicals were obtained from Sigma Aldrich.

2.2 General Methods

2.2.1 Cell Maintenance

2.2.1.1 Cell revival

Cryovials containing cells from the liquid nitrogen bank were thawed by swirling in a water bath at 37°C. Then the entire contents of the cryovial (storage medium+cells) were transferred into a 75 cm^2 flask containing warmed appropriate supplemented medium as described in section 2.1.1 and incubated at 37°C for approximately 2-4 hours. After that, the cell suspension was transferred into a microcentrifuge tube and centrifuged (Eppendorf 5417 R centrifuge, AG 22331 Hamburg) at 250g for 5 minutes. The supernatant was removed and the cells were cultured as usual in fresh media.

2.2.1.2 Cell maintenance

All cell lines were routinely cultured in 75 cm^2 flasks at 5% CO_2, 95% relative humidity and 37°C until confluence. Cell culture media was replaced every other day by removing the old culture media from the flasks, followed by the addition of 12-15 ml of fresh media, pre-warmed to 37°C. Cell growth was checked under microscope to determine confluence. Once 90%-100% confluent, cells were passaged by removing medium from the flask and cells were washed by adding 10 ml warmed PBS to the flask. Then PBS was aspirated and replaced by 4 mL of pre-warmed 2.5% trypsin/EDTA to the flask. Then flask was placed in incubator for 10-15 min, or until detached. Following cell detachment, they were checked under microscope to confirm that cells are detached from the surface, and then 6 mL of media was added to dilute and deactivate trypsin. The mixture was pipetted out of the flask into a 15 mL centrifuge tube to centrifuge at 250g for 5 min. After

centrifugation, supernatant was aspirated and cell pellet was re-suspended in pre-warmed culture medium.

An appropriate volume of cell suspension was then aliquotted in to a new flask (containing pre-warmed culture medium appropriate for the cell line) for further culturing. Split ratios between 1:3 and 1:5 were normally used for Calu-3 and HBEC cells, while ratios between 1:4 and 1:8 were typically used for both IEC-6 and Caco-2 cells.

2.2.1.3 Preparation of Frozen Stock

Cells were trypsinized to detach from the flask as mentioned in the sub-culturing protocol in 2.2.1.2. After centrifugation of the cell suspension, supernatant was removed by gently pipetting out without disturbing the cell pellet, and then cell pellet was re-suspended in 1 ml of supplemented medium with 10% sterile DMSO. Cell suspension was transferred into sterile cryovial which was placed into a freezing container (Mr Frosty) in a -80°C freezer for a gradual, controlled temperature decrease. Cells were stored at -80°C for up to 4 weeks. Thereafter, they were transferred into a liquid nitrogen cell storage tank.

2.2.1.4 Seeding cells on transwells-Conventional (Inside transwell, see figure 2.1)

Although the membrane is treated for cell culture, it is important to properly prepare the transwell membrane for cell attachment. Most cells will respond to a simple pre-soak of the membrane in serum containing medium. So Transwell® filters were incubated with folate free RPMI 1640 medium (250 µl and 1.5 ml of folate free RPMI 1640 medium (containing appropriate mentioned supplements for each cell line) on the apical and basolateral chambers, respectively) at 37°C for approximately 15 min prior to the addition of cells.

After detaching cells using the method described in 2.2.1.2, cells were counted using a haemocytometer and the volume of the cell suspension containing the required number of cells was calculated. These volumes were subsequently added to the apical chamber of the transwells. The number of cells added (seeding density) was 10^5 per 1 cm^2 of the Transwell® filter area. The apical chamber volume was made up to 500 µl by adding warmed RPMI. After seeding, the cells were maintained at 5% CO_2, 37°C and media were changed every other day until used in experiments. All cell lines were typically cultured on filters for different period prior to their use in experiments as confluent and polarised cell layers.

2.2.1.5 Seeding cells on transwells-Inverted (Underside of transwell, see figure 2.1)

To culture cells on the underside of a Transwell® insert, the permeable filter was placed upside-down inside the chamber of a 6-well tissue culture plate. 10^5 cells were seeded on top of the filter with the same method described in 2.2.1.4 and the 6-well plate cover was placed against the top of the filter to prevent evaporation. Cells were allowed to adhere for 5 h prior to re-inversion of the Transwell® permeable insert, and subsequently cultured as described above (section 2.2.1.4).

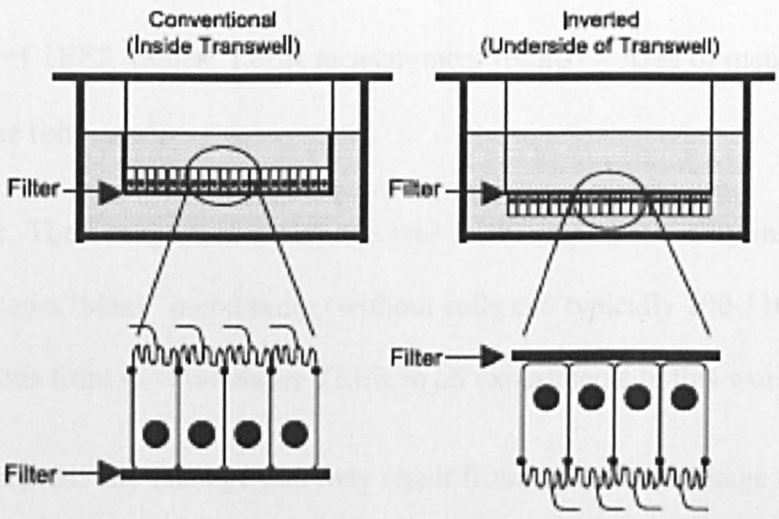

Figure 2.1 *Schematic diagram of cells grown inside (conventional) and on the underside (inverted) of a filter insert. Adopted from [1]*

2.2.2 TEER Measurement

Transepithelial Electrical Resistance (TEER) measures the resistance resulting from passing a current across a cell monolayer. TEER is affected by the pore size and the density of the membranes. The TEER value is considered a good measure of the integrity of cell monolayers formed on transwell membranes and reflects the degree of confluence of the cells. It's the most convenient, reliable and non-destructive method to monitor the growth of epithelial tissue cultures in vitro and determine the presence and the tightness of the cellular tight junctions (TJs) [2]. Measurements of TEER are determined using a special probe attached to a voltmeter (EVOM Voltammeter, World Precision Instruments, Aston, and Stevenage, UK). As shown in figure 2.2, the sterile TEER meter probes were placed into each well (short probe was submerged in the medium bathing the cells on the apical side, while the long probe was placed in medium present on the basolateral chamber).

TEER values reported in this work take into account the area of the cell layer (assumed to amount to the area of the Transwell® filter) and are expressed as $\Omega.cm^2$.

Calculation of TEER values: TEER measurement (ohms) × Area of membrane (cm^2) =TEER value ($ohm.cm^2$)

Furthermore, The background resistance was taken into account by measuring the resistance across 'blank' membranes (without cells and typically 100-110 Ωcm^2) and subtracting this from the monolayer TEER in all experiments in this work.

In order to prevent any damage that may result from a possible leakage of ions from the probes, the culture medium was replaced after TEER measurements. TEER was measured every other day starting from day 7 post seeding. All measurements were conducted in triplicate or quadruplicate.

Note as an additional control of integrity of cell monolayers used in all experiments, TEER for each transwell was checked at the end of experiment. For this purpose, medium was added to the upper and lower chambers. Severe reduction seldom occurred (<3% of wells); the data from these wells were not included in the final analysis.

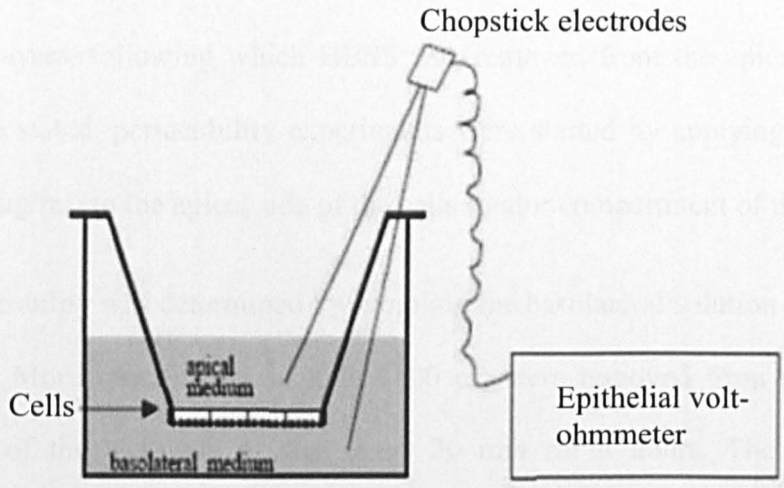

Figure 2.2 *Schematic representation of the Epithelial Voltohmmeter system used to measure TEER of the cell layers.*

2.2.3 FITC-dextran (FD) permeability experiments

Filter cultured cell layers exhibiting TEER ≥500 $\Omega.cm^2$ were considered adequate for FD permeability experiments. TEER measurements were conducted prior to the permeability experiments in order to ensure that the cell layers were confluent and intact. TEER was also recorded after the permeability experiment in order to confirm intactness of the cell layers throughout the experimental period. The permeability of monolayers was tested by fluorescein isothiocyanate (FITC)-labelled dextran of molecular weight 4400 (FD4). HBSS was used as medium transport in the experiments and in order to maintain a desired pH (7.4) it was supplemented with 25 mM HEPES buffer. Permeability experiments were performed in the following way. Culture medium was removed from the cell layers and cells washed with warm (37°C) PBS. HBSS supplemented with HEPES was then added to the apical (0.5 ml) and basolateral (1.5 ml) chambers of the Transwell® system. Cells were incubated at 37°C/5% CO_2 with HBSS for approximately 45 min for the purpose of equilibration.

TEER was then measured in order to confirm the 'confluence' and the intactness of the cell layers, following which HBSS was removed from the apical side. Unless otherwise stated, permeability experiments were started by applying 0.5 ml of the FD (500 μg/ml) to the apical side of the cells (donor compartment of the transwells).

FD permeability was determined by sampling the basolateral solution at regular time intervals. More specifically, samples (100 μl) were removed from the basolateral chamber of the transwell system every 30 min for 4 hours. The samples were immediately replaced with equal volumes of HBSS. Between sampling times, cells were incubated at 37°C/5% CO2. To ensure that the cell layer integrity remained intact during the permeability experiment, TEER was measured following the final sampling point. Samples were transferred into a black 96-well plate, which was then covered with aluminium foil to protect from light. FD fluorescence (485 nm excitation, 535 nm emission) was then determined using an MFX microtiter plate fluorometer (Dynex Technologies, USA). FD in the basolateral solutions was quantified by converting the fluorescence readings into FD concentrations and amounts, through construction of calibration curves. Briefly, this involved measuring the fluorescence intensity of progressively diluted FD solutions of known concentrations. At least three such calibration curves were established; the mean values were then calculated and used for FD quantitation in each experiment. FD permeability is expressed as the apparent permeability coefficient (P_{app}), calculated using the following equation

$$P_{app} = \frac{dQ}{dt}\frac{1}{ACo}$$

Where:

dQ/dt is the permeability rate [amount FD (μg) traversing the cell layers over time (s)]. This was determined by plotting the amount of transported solute over time and calculating the gradient of the straight-line (i.e. steady state) portion (typically transport over time points 30 min – 3 h) of the resulting curve

A is the surface area across which transport studies were measured (1.1 cm^2), and

C_o is the initial FD concentration.

2.2.4 MTS cell toxicity assay

A number of studies reported that the MTS in vitro cytotoxicity assay is a convenient method for assessing cell viability containing a novel tetrazolium compound, 3-(4,5-dimethylthiazol-2-yl)-5-(3-carboxymethoxyphenyl)- 2-(4-sulfophenyl)-2H-tetrazolium (inner salt), and an electron coupling reagent (phenazine ethosulfate; PES).The main features of this assay are its ease of use, accuracy and rapid indication of toxicity [3]. The MTS assay is based on the conversion of a tetrazolium salt into a coloured, aqueous soluble formazan product by mitochondrial activity of viable cells at 37°C. The amount of formazan produced by dehydrogenase enzymes is directly proportional to the number of living cells in culture and can be measured at 492 nm [4].

This assay was conducted in the following way. Cells were cultured in a 96-well plate at a density of 10^4 cells per well and incubated at 37°C, 5% CO_2 for 24 hours. This seeding density was chosen as it produced an absorbance value within the linear range of the assay, as recommended by the manufacturer. After 24 hours, the medium was replaced with 100 μl of test compounds dissolved in HBSS and then cells were incubated for 4 hours. HBSS and Triton X-100 (0.1% v/v in HBSS) were used as the negative and positive controls respectively. Sample solutions (and controls) were then aspirated and cells washed with PBS. Then culture medium (100

µl at 37°C) plus MTS reagent (20 µl) were added onto each well and cells were incubated for 1-4 hours (typically 2 hours). Absorbance at 492 was measured using a Dynex absorbance microplate reader (Dynex Technologies, USA).

The relative cell metabolic activity (%) was calculated using the following equation:

$$\text{Relative metabolic activity} = \frac{(S-T)}{(H-T)} \times 100$$

Where:

S is the absorbance with the tested samples

T is the absorbance with Triton X-100

H is the absorbance with HBSS

2.2.5 Cell imaging and labelling

2.2.5.1 Coverslip preparation

Coverslips were immersed in 70% ethanol for 20 min and then rinsed with Ultra-Pure Water four times. Then HCl (10 ml 1M) was added and they were sonicated (DECON, Ultrasonic Ltd, Conway, UK) for 20 min. After that HCL was aspirated and cover slips were put under running Ultra-Pure Water for 30 minutes. Then they were transferred onto a clean filter paperin a glass petridish to be autoclaved. In order to be dried, they were placed in the oven at 40°C. After drying, under the fume hood, they were treated with PDL (1 ml) overnight.

Then PDL was aspirated and coverslips were washed with PBS 3-5 times and left immersed in PBS overnight under the fume hood. The following day, they were ready to be used in the cell culture experiments for cell imaging.

2.2.5.2 Zonula Occludens (ZO-1) TJ staining

Confluent cell monolayers were washed with PBS and fixed in 4% paraformaldehyde in PBS for approximately 10 min at room temperature. Cells were then washed 3 times with PBS and permeabilised by incubating with Triton X-100 (0.1% v/v in PBS) for approximately 10 min. Cells were then washed with PBS, followed by the application of 1% BSA/PBS for approximately 1 hour. Thereafter, BSA/PBS solution was aspirated and replaced with mouse, anti-human ZO-1 (primary) antibody, diluted in 1% BSA/PBS to a final concentration of 10 μg/ml. Cell samples were incubated with the primary antibody for 1 hour. The primary antibody solution was then removed and cells washed with PBS (5 times). FITC- or Cy5-labelled goat, anti-mouse (secondary) antibody, diluted according to manufacturer's instructions in 1% BSA/PBS was then applied to the cells for 1 hour. The secondary antibody solution was then aspirated and cells washed with PBS extensively. The Transwell® filter membrane was excised and mounted on glass slides (using DAPI-containing, ProLong® Gold antifade/mounting medium). Samples were mounted on glass slides with DABCO and covered with glass cover slips for confocal imaging, which was performed using the confocal system using Leica TCS SP2 system mounted on a Leica DMIRE2 inverted microscope.

2.2.5.3 Caveolin-1 and Clathrin staining

Confluent cell monolayers cultured on filters were fixed, permeabilised and treated with 1% BSA/PBS as described in 2.2.5.2

Then cells were rinsed with PBS and incubated with Mouse anti-human Clathrin or goat anti-human Caveolin 1 (CAV1) primary antibodies diluted in 1% BSA/PBS to the final concentration provided by manufacturer for 1 hour. After removing the primary antibodies, cells were washed three times with PBS, then they were

incubated with the secondary antibodies (Goat anti-mouse FITC labelled or mouse anti-goat cy5 labelled) for 1 h. Secondary antibodies were aspirated and cells were washed three times with PBS extensively (10 min for each wash). Samples were prepared for examination by confocal microscopy as described in 2.2.5.2

2.2.5.4. Folate receptor (FR) staining

Folate receptor immunostaining was performed on cell monolayers in the same fashion described (2.2.5.2 and 2.2.5.3) using mouse anti-human FOLR1 primary antibody and goat anti-mouse TRITC labelled secondary antibody.

2.2.6 Statistical analysis

All experiments were carried out three times using triplicate samples. One way analysis of variance (ANOVA) followed by Bonferroni post-hoc test was applied for comparison of group means at a p value of 0.05.

2.3 References

1. Wakabayashi, Y., et al., *Four-dimensional imaging of filter-grown polarized epithelial cells.* Histochem Cell Biol, 2007. 127(5): p. 463-72.
2. Klingberg, T.D., et al., *Application of measurements of transepithelial electrical resistance of intestinal epithelial cell monolayers to evaluate probiotic activity.* Appl Environ Microbiol, 2005. 71(11): p. 7528-30.
3. Malich, G., B. Markovic, and C. Winder, *The sensitivity and specificity of the MTS tetrazolium assay for detecting the in vitro cytotoxicity of 20 chemicals using human cell lines.* Toxicology, 1997. 124(3): p. 179-92.
4. O'Toole, S.A., et al., *The MTS assay as an indicator of chemosensitivity/resistance in malignant gynaecological tumours.* Cancer Detect Prev, 2003. 27(1): p. 47-54.

Chapter 3

Folate receptor expression in bronchial and intestinal epithelial cell lines: Potential for uptake and transport of macromolecules

3.1. Introduction

Folate uses the natural endocytosis pathway *via* folate receptor (FR) to enter cells. As mentioned in chapter one (1.9.5.) simple covalent attachment of folic acid to different macromolecules has been shown to lead to conjugate internalization by folate receptor-positive cells in an identical fashion to that of free folic acid [1]. Folate conjugation to small or macromolecular therapeutics has hence been exploited for intracellular delivery to, particularly, cancerous cells. The majority of studies have described folate mediated drug delivery to cancerous cells, typically using the folate receptor expressing KB cell line [2], whilst data on targeted drug delivery *via* folate receptor to non-cancerous cells or tissues are scarce as FR is not expressed on most normal cell types. There are few reports on the presence of folate receptor at the apical membrane of epithelial cells of some human tissues [3] although the expression of FR in lung epithelium is still an open question and no specific function has been defined in such a case [4].

Present work attempts first to assess the presence of FRs on the apical membrane of four different epithelial cell lines: Caco-2 (intestinal) and Calu-3 (bronchial), both cancerous in origin, and the non-cancerous HBEC (Human Bronchial Epithelial Cells) and IEC-6 (Intestinal Epithelial Cells). Secondly, as endocytosis pathways are closely linked to the pathways for transport, we investigated if folate mediated uptake can result in transport across the epithelium in apical to basolateral direction of a model macromolecular compound. To the best of our knowledge there are no published reports on the transport of macromolecules, or macromolecular therapeutics, which are mediated by the folate receptor as investigated here. If folate mediated transepithelial transport is indeed possible, this would open up potential applications in mucosal delivery of biologicals.

3.1.1 Calu-3

Calu-3 cells (Figure 3.1 A) are a human bronchial epithelial cell line derived from human bronchial sub-mucosal glands of a patient with adenocarcinoma of the lung. It is a well-differentiated and characterized cell line which demonstrates many characteristics of the respiratory epithelium when grown on permeable membranes [5]. In the human lung, the sub-mucosal glands are a major source of airway surface liquid, mucins, and other immunologically active substances, and Calu-3 cells can reflect all these properties [5, 6].

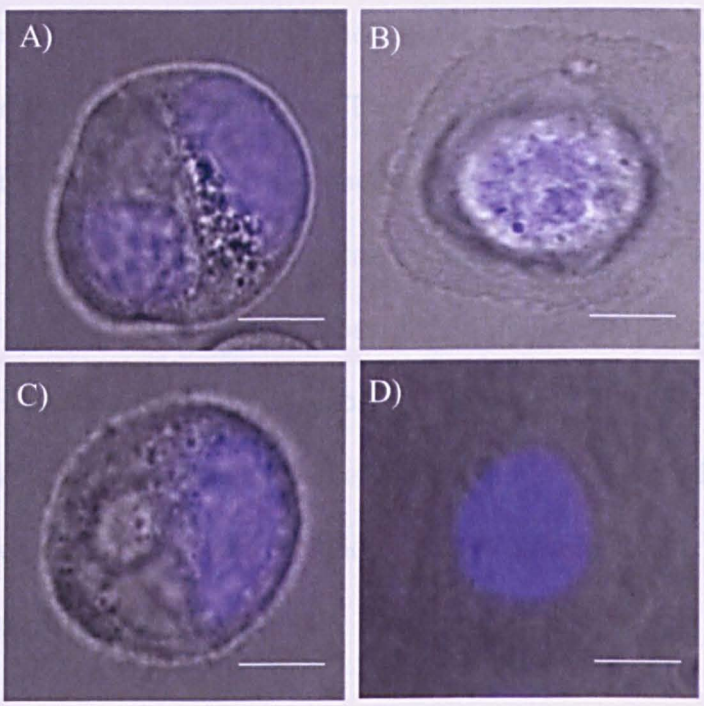

Figure 3.1 *Epifluorescence images of Calu-3 (A), HBEC (B), Caco-2 (C) and IEC-6 (D). Blue colour represents cell nuclei stained with DAPI (Scale bar: 5μm).*

3.1.2 HBEC

HBE cell line (Figure 3.1 B) has been developed as a model of the airway epithelium which forms polarised cell layers *in vitro* [7]. According to recent studies, it is shown that the HBE cell line could be a suitable candidate for an *in vitro* model for mechanistic studies of drug transport processes involved in the smaller airways. HBE Cell layers express drug transport systems that are also present in the human bronchus *in vivo* [8].

3.1.3 Caco-2

Caco-2 (Figure 3.1 C) is a human epithelial colorectal adenocarcinoma cell line which is derived from a colon carcinoma. They are able to become differentiated and polarised such that their phenotype, morphologically and functionally, resembles the enterocytes (absorptive cells) lining the small intestine [9]. Caco-2 cell monolayers have been widely used in studies of absorptive mechanisms for drugs, such as passive transcellular and paracellular transport, carrier-mediated influx and efflux mechanisms. Since Caco-2 cells express certain transporters and metabolic enzymes, Caco-2 cell monolayers are used to study drug–drug interaction and metabolic stability of drugs, respectively [10].

3.1.4 IEC-6

IEC-6 (Figure 3.1 D) is a small intestinal cell line which is derived from native rat ileal crypts. It is used as an *in vitro* model of intestinal epithelium mostly for the study of epithelial permeability as it forms confluent epithelial layer when grown on permeable membranes [11].

3.2 Material and Methods

All chemicals were purchased from Sigma-Aldrich (UK) unless otherwise specified.

3.2.1 Polymerase Chain Reaction (PCR)

3.2.1.1 PCR primer design

Primers were designed using Primer3 software (version 0.4.0) with default setting. Primers were designed to be intron-spanning to discriminate cDNA from genomic DNA (gDNA). Gene specificity was confirmed using Primer BLAST on the NCBI website. The following primers were purchased from Sigma-Aldrich:

For human cell lines (Calu-3, HBEC and Caco-2):

HsFOR1 forward primer: 5'-GAGGAAGAATGCCTGCTGTT-3

HsFOR1 reverse primer: 5'-AGTCCAGTTCCAGCCCTTGT-3

For rat cell line (IEC-6):

RnFOLR1 forward primer: 5-'CACAAGCCAGGAAGCACATA-3

RnFOLR1 reverse primer 5'-GTCCAGTTCCATCCCTTGTG-3

3.2.1.2 Total RNA isolation

Total RNA (1 μg) was isolated by the μMACSTM mRNA Isolation Kit (Miltenyi Biotech, Bergisch Gladbach, Germany) according to the manufacturer's protocol for adherent cells from Calu-3, HBEC, Caco-2 and IEC-6 monolayers on different days post-seeding on the Transwell support (12 mm diameter, 0.4 μm pore size, Corning Costar, Holland).

3.2.1.3 Reverse Transcriptase (RT)-PCR

1 μg of total RNA was reverse transcribed in a volume of 20 μl with GeneAmp RNA PCR kit (Applied Bio, UK). For PCR amplification, RT reaction (1 μl) was added to 10 μl REDTaq ReadyMixTM PCR Reaction Mix with MgCl2 and made up to 20 μl with water and forward and reverse primers (0.25 μM final concentration each). Cycling conditions were as follows: 94°C for 5 min, followed by 35 cycles of 94°C for 30s, 58°C for 45 s and 72°C for 90s followed by 72°C for 5 min final extension. PCR products were then subjected to electrophoresis on 1% (w/v) agarose gels in 0.5x TBE buffer (1 M Tris-HCl; 1M Boric acid; 0.05 M EDTA; pH 8.0) with the addition of ethidium bromide to a final concentration of 10 μg/m. The gels were run in 0.5 × TBE buffer and electrophoresis was performed at 90-110 V. DNA fragments were visualised on a UV transilluminator with Gene Genius Bio imaging software (UVP, USA). Rn-β-actin and Hs-GAPDH (Homo sapiens glyceraldehyde-3-phosphate dehydrogenase) were used as positive controls for reverse transcription and genomic DNA obtained from human or rat cells was used as a control to demonstrate ability of intron-spanning primers to discriminate between cDNA and gDNA.

3.2.2 Western Blot

Expression of FR protein was determined by Western blotting using mouse anti-Human FOLR1 for human cell lines and anti–rat alpha-FR. Cell monolayers were washed with ice-cold PBS and lysed in a buffer consisting of 150 mM NaCl, 50 mM Tris HCl, pH 7.5, 0.5% Nonidet 40, 50 mM NaF, 1 mM sodium orthovanadate (Na_3VO_4), 1 mM phenylmethanesulphonylfluoride (PMSF), and 1% aprotinin at 4°C for 30 minutes. Cell lysates were cleared of cell debris by centrifugation (25,000g; 30 minutes) (Eppendorf 5417R centrifuge-AG 22331 Hamburg). Protein

concentration was determined using Bradford assay. Samples containing protein (20 μg) were mixed with non-reducing buffer and separated on an SDS–12% polyacrylamide gel. They were then transferred to Nitrocellulose membranes (Whatman, Protran, USA) and blocked with 5% (w/v) nonfat dry milk in PBS containing 0.05% (v/v) Tween- 20 for 2 hours. Membranes were washed with PBS–0.01%Tween 20, and then incubated with primary antibody (diluted as appropriate in blocker) at room temperature for 2 hours. After intensive washing (3 × 20 min) with PBS 0.5 % (v/v) Tween 20, membranes were incubated with horseradish peroxidase conjugated secondary antibody at 1:1000 dilutions in blocker at room temperature with rocking for 2 hours. To eliminate excess secondary antibody, the membranes were washed as before.

Blots were developed by using chemiluminescent substrate following manufacturer's instructions (Invitrogen Western Breeze kit, UK). Blots were corded using Luminescent Image Analyzer (LAS-4000, Fujifilm, UK).

3.2.3 Preparation of Ovalbumin-Folic Acid-FITC (FA -OVA-FITC) Conjugate

The FA-OVA-FITC conjugate with a low level of FITC labelling was used for transport experiments.

The first step was to prepare OVA-FITC conjugate with the following method. OVA (40mg) was dissolved into 0.1M sodium carbonate buffer (pH 9.5). A 2-3 fold molar excess of fluorescein FITC, dissolved in acetone (0.5 ml) was slowly added to the OVA solution. The mixture was stirred for 20 minutes and left at room temperature for 4 hours in complete darkness. Excess FITC was separated on PD10 column and UV measurements (Beckman DU-640 Spectrophotometer) were taken at λ_{495} for FITC and at λ_{280} for OVA (λ_{495}=7.97 x 10^4). The eluted fractions 3 to 11 were

collected and pooled together and the UV measurements were repeated on the pooled fractions at the above-mentioned wavelengths.

OVA concentration was measured by Bradford assay at 595 nm ($\lambda_{595}=2.4 \times 10^4$).

FITC concentration was achieved by using equation 3.1

$C_{FITC} = A_{495}/ \varepsilon$ equation 3.1

A is absorbance at the given wavelength, and ε is extinction coefficient of FITC at 495 nm. The molar ratio was the number of moles of FITC to OVA.

One-half of the OVA-FITC conjugate was further conjugated to folic acid, and the other half was left unmodified as a control.

The second step is the formation of OVA-FA-FITC. The following molar ratios of starting materials were needed for conjugate formation,

Number of moles of folic acid: number of moles of BSA=40/1

Number of moles of ECDI: number of moles of folic acid=1.5/1

This was expected to give a conjugate with a final Molar Substitution Ratio (MSR) of 7-15 moles of folic acid per mole of OVA.

Folic acid and ECDI were added to 1 ml of OVA-FITC solution while stirring. The pH was controlled during the first 15 minutes (pH 6.6), and then the reaction was left with stirring overnight in darkness. The reaction mixture contained OVA, folic acid, and 1-ethyl-3-(3-dimethylaminopropyl)-carbodimide (ECDI) in a molar ratio of 1:40:60 respectively.

The resulting conjugate was desalted and purified with PD10 column (Sephadex G-25 Medium) eluted with PBS and molar ratio of folic acid to OVA was determined by spectrophotometer for FITC and folic acid at λ_{495} and λ_{364} respectively. Then

fractions 4 to 12 were collected and pooled together and again measured at the previously mentioned wavelength.

OVA concentration was measured by Bradford reagent by UV at 595 nm. The calibration curve was constructed using OVA standards in a concentration range of 0.0625 mg/ml to 1 mg/ml.

Folic acid concentration was determined using equation 3.2 in below;

$C_{\text{folic acid}} = A_{364} / \varepsilon$ where $\varepsilon=6.5 \times 10^3$ equation 3.2

3.2.4 Preparation of Ovalbumin-Folic Acid-TRITC (FA-OVA-TRITC) Conjugate

TRITC is preferable as a label for acidic compartments, because FITC has a reduced fluorescence at acidic pH, whereas TRITC fluorescence is slightly increased in acidic conditions [12]. OVA (40mg) was dissolved in 0.1 M sodium carbonate buffer (pH 9.5). In another vial, TRITC (5 mg) was dissolved in ethanol (1 ml) and added to OVA solution and the reaction stirred in a cold room overnight. The reaction mixture was purified by PD10 column. TRITC and OVA were quantitated spectrophotometrically at λ_{555} and λ_{280} respectively. Then fractions 3 to 8 were collected and pooled together and again measured at the previously mentioned wavelength. TRITC concentration was obtained with equation 3.3 and OVA concentration was measured by Bradford assay

$C_{\text{TRITC}} = A_{555} / \varepsilon$ while $\varepsilon_{555}=2.4 \times 10^4$ equation 3.3

One-half of the OVA-TRITC conjugate was further conjugated to folic acid, and the other half was left unmodified as a control. Folic acid in 40 fold molar excess and ECDI in 60 fold molar excess to OVA were added to OVA-TRITC (1ml) solution at

pH 6.6. The reaction was stirred overnight. The conjugate then was purified using a PD10 column with PBS elution buffer and the molar ratio of folic acid to OVA determined as above.

OVA concentration was calculated with Bradford assay and TRITC concentration was measured at λ_{555}, by equation 3.3 while the folic acid content was measured at λ_{364} (equation 3.2).

Note that in order to prevent light degradation of FITC and TRITC, all experiments were conducted under low lighting and all containers covered with aluminium foil. All conjugates were divided into 0.5 ml aliquots and stored at -20 °C.

3.2.5 Preparation of membrane-cultured Calu-3 cells

Calu-3, HBEC, Caco-2 and IEC-6 cells were cultured on flasks until confluence. Thereafter cells were detached from the flasks, seeded and cultured on membranes (10^5 cells per well) according to the methods detailed previously (section 2.2.1.2 and 2.2.1.4).

3.2.6 TEER profiles of cell monolayers

TEER measurements were conducted (in the manner described in section 2.2.2) every 2 days starting from day 7 post seeding.

3.2.7 Permeability study of FD4 across cell layers

All cell layers were used for FD4 permeability experiment when TEER reached $\geq$500 $\Omega.cm^2$ (see section 2.2.3). Culture medium was initially replaced with warmed (37°C) HBSS (transport medium). Cells were allowed to equilibrate in HBSS for approximately 30 min, following which TEER measurements were conducted in order to confirm cell layer intactness. HBSS was then removed from the apical side

of the cells and replaced with a solution of FD4 dissolved in HBSS (500 μg/ml). The rest of the experiment was conducted in the manner described previously (section 2.2.3).

3.2.8 FA-OVA-TRITC uptake by cell layers

Cell uptake of FA-OVA -TRITC was assessed on the confluent Calu-3 layers. Before each experiment, the culture medium was removed and the cell layers were rinsed with PBS and allowed to equilibrate for 1h at 37°C in HBSS supplemented with 15 mM 4-(2-hydroxyethyl)-1-piperazine-ethane sulfonic acid (HEPES). TRITC labelled folate (FA-OVA-TRITC) - or non-folate (OVA-TRITC) conjugate (0.5 mg/ml) solutions in HBSS were added to the apical side of the cell layers. The uptake study was performed for a period of four hours. The conjugate samples were then aspirated and cell layers washed with PBS extensively (5x) and followed with washing with 0.4% (w/v) Trypan Blue solution to quench extracellular fluorescence. The cells were then digested with 0.2 M NaOH in 0.5% Triton X-100 which also produced cell detachment from the membranes. The cells were centrifuged (25,000g) for 30 sec. The fluorescence intensity of the supernatant was measured by Fluorescence Spectrophotometer (Varian Cary Eclipse Fluorescence Spectrometer, UK). TRITC was quantitated using a standard curve at E_x 529 nm and E_m 596 nm to determine amount of TRITC. The amount of OVA taken up into cells was calculated from the molar ratio of TRITC to OVA determined after conjugate synthesis described in 3.2.4.

3.2.9 FA-OVA -FITC translocation across cell layers

All cell lines were cultured on membrane as before (section 2.2.1.4) and used as confluent layers. Transport experiments were commenced after replacement of the culture medium with HBSS buffer and equilibration for approximately 1 hour.

FA- OVA-FITC and OVA-FITC were applied to the apical side of the cells at a final concentration of 0.5 mg/ml (in HBSS) and its transport across the cell layers was determined by sampling the basolateral solution (100 µl volumes) at regular time intervals (every hour for four hours). The volumes sampled from the basolateral chamber were replaced with fresh HBSS.

The donor (apical) solution was also sampled at the start of the experiment and at 240 minutes, in order to determine the apical concentration of conjugates at the beginning and the end of the transport experiment. The entire sample were transferred into a 96-well plate and their fluorescence intensities determined by a fluorescence plate reader (MFX Microtiter, Dynex Technologies Ltd., Worthing). Cell monolayer integrity during and at the end of the experiment was monitored by TEER measurements.

Note that the calibration curve used to quantify FA-OVA-FITC and FA-OVA-TRITC was in these instances constructed by measuring the fluorescence of known concentrations of FA-OVA-FITC and FA-OVA-TRITC progressively diluted in a solution of Triton X-100, 0.1% v/v in HBSS.

3.2.10 Receptor competition

In the inhibition experiments, free folate (1mM) was added to the apical side of confluent cell layers prior to folate conjugate application.

3.2.11 Zonula Occludens (ZO-1) TJ staining

Samples for confocal imaging of TJ were immunostained with ZO-1 as described in section 2.2.5.2.

3.2.12 Confocal Fluorescence imaging

Samples were prepared for confocal scanning microscopy as described in section 2.2.5.2. Images were taken with a 63×1.4 NA Apochromat oil immersion objective lens.

3.3 Results

3.3.1 Synthesis of folate conjugates

All conjugates (FA-OVA-FITC and FA-OVA -TRITC) were synthesised by the coupling of carboxyl group of folic acid with the ε amino group of lysine in the OVA. They were all synthesised successfully with a high Molar Substitution Ratio (MSR) of folic acid to OVA.

3.3.1.1 Preparation of FA-OVA-FITC

The first step of FA-OVA-FITC (Figure 3.3) synthesis was preparation of OVA-FITC, which is the reaction of isothiocyanate group of FITC with the free amino residue (ε-amino group of lysine). FITC concentration was calculated by equation 3.1 at 495 nm and OVA concentration was assayed using Bradford reagent. The MSR of FITC to OVA was calculated to be 1.5 ± 0.3 (means ±S.D, n=6) mole of FITC per mole OVA. A low MSR was obtained as required to ensure that minimum fluorescence quenching occurred to maximise the brightness of the signal from the label.

The conjugation of FA to OVA-FITC was performed using EDCI, a water soluble coupling agent. These syntheses were done at pH 6.4-6.6 because it was reported by Garnett that at this pH the efficiency of coupling would be better than at higher pH [12].

Folic acid concentration was calculated by equation 3.2. The MSR was calculated to be 13.09 ± 1.04 (means ±S.D, n=6) mole folic acid per mole OVA.

3.3.1.2 Preparation of FA-OVA-TRITC

FA-OVA -TRITC conjugate was prepared (Figure 3.2) as described in section 3.2.4. The MSR of this conjugation was 34.1 ± 1.0 (means ±S.D, n=6) mole of TRITC per mole OVA. The concentration of folic acid was calculated by equation 3.2. The molar substitution was calculated 12.4 ±1.6 (means ±S.D, n=6) moles of folic acid per mole of OVA.

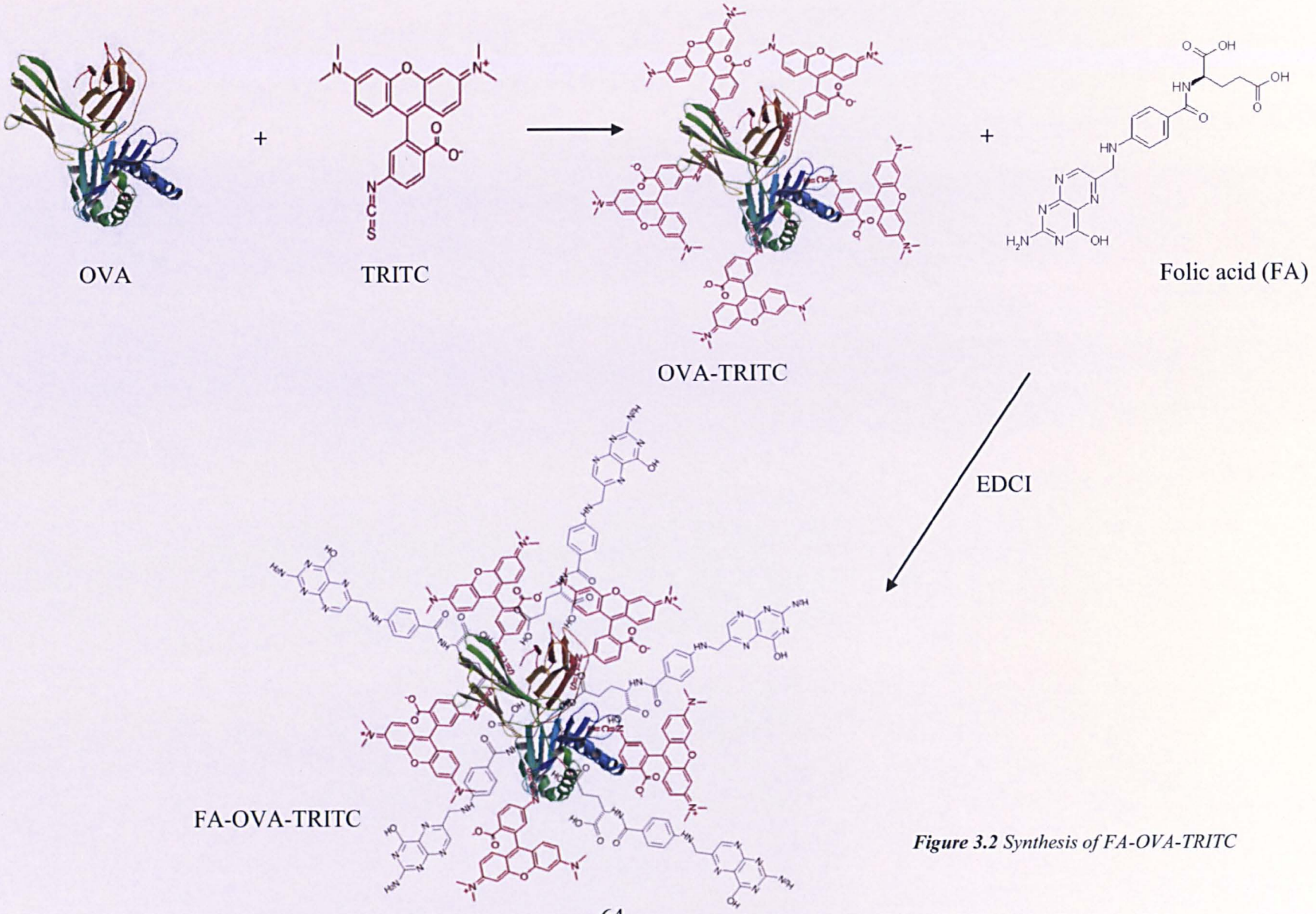

Figure 3.2 *Synthesis of FA-OVA-TRITC*

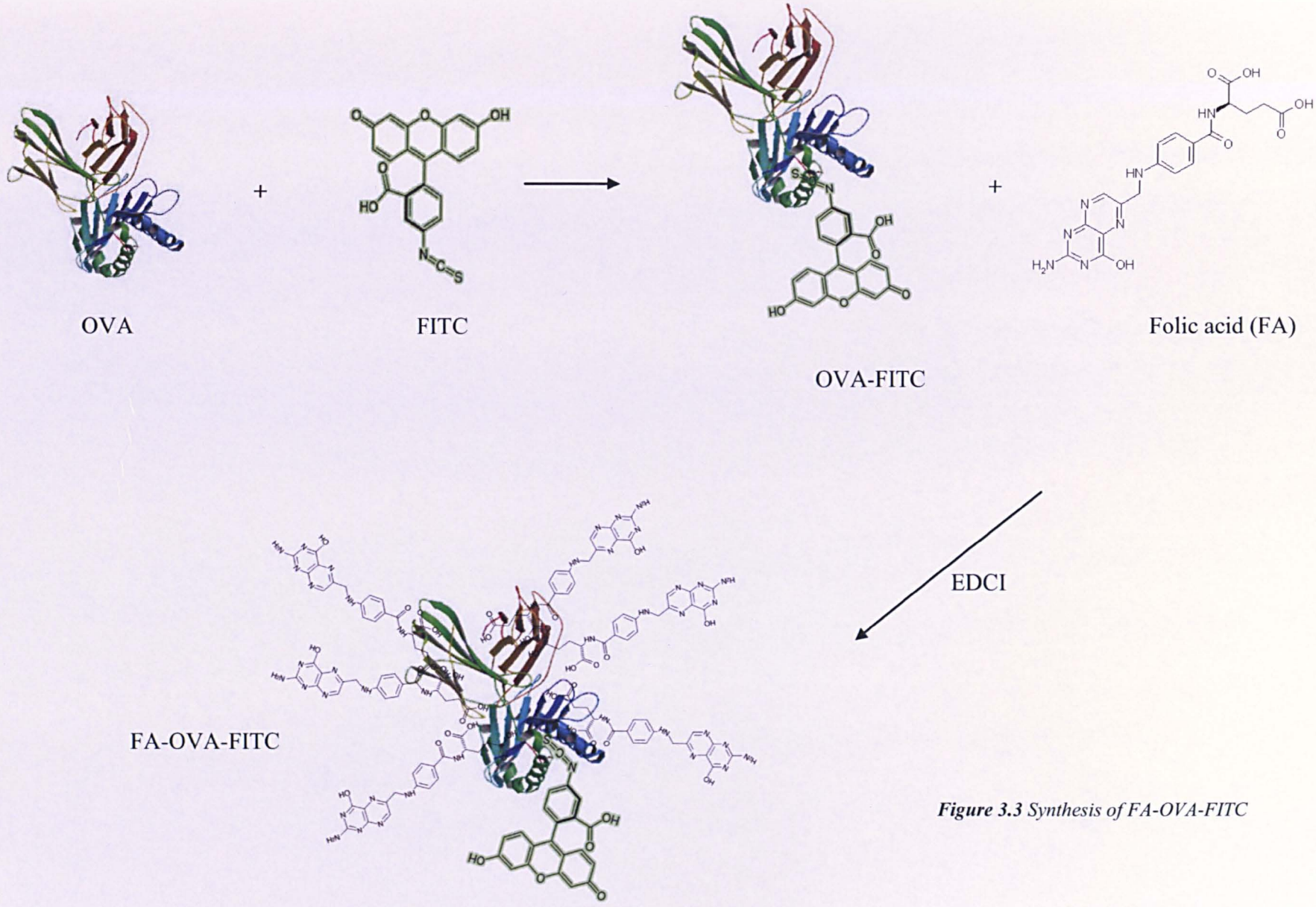

Figure 3.3 *Synthesis of FA-OVA-FITC*

3.3.2. Formation of electrically tight cell monolayer

The formation of monolayers by cells cultured on permeable membranes was monitored by measuring TEER (Figure 3.4). The profiles indicated that all the cell types tested were capable of forming electrically tight monolayers, although there were significant differences in their behaviour regarding both the timing and extent of TEER plateau values. No meaningful increase in TEER was observed until day 6-7 of culture for the cell layers cultured. TEER for non-cancerous cell lines (IEC-6 and HBEC) reached lower plateau values compared to cancerous cell lines (Caco-2 and Calu-3). TEER for Caco-2, Calu-3 and IEC-6 plateaued between days 16-25 before decreasing, while HBEC monolayer reached a plateau at later approximately day 30.

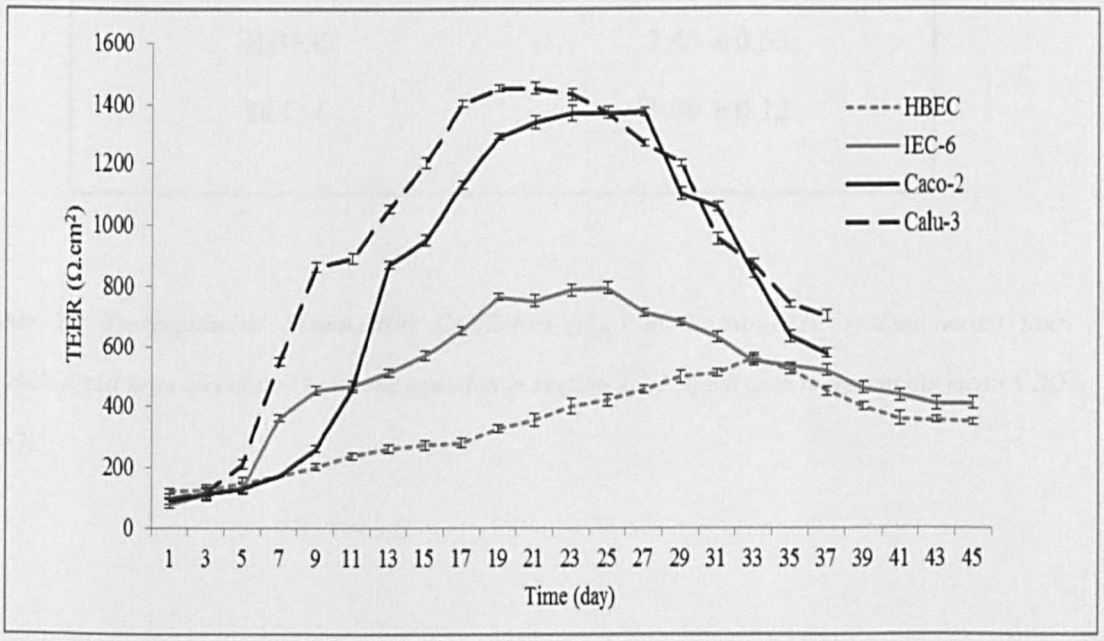

Figure 3.4 *TEER profiles of HBEC, IEC-6, Caco-2 and Calu-3 cells cultured on membrane. TEER is expressed as the measured resistance per area (cm^2) of the cell layer. Background TEER due to the membrane was subtracted from the reported TEER values. Data presented as the mean ± SD (n=3).*

3.3.3. FD4 permeability across cell layers

In order to investigate the barrier properties of the cell layers, permeability of FITC labelled Dextran (4400Da) was performed and obtained P_{app} values are presented in Table 3.1. Confluent cell layers grown on filters presented an efficient barrier to FD4 translocation all showing low P_{app} values integrating the integrity of cell layers and their suitability for transport study.

Cell lines	P_{app} ($\times 10^{-7}$ cm/s)
Calu-3	4.76 ± 0.34
Caco-2	3.91 ± 0.02
HBEC	2.45 ± 0.53
IEC-6	3.06 ± 0.12

Table 3.1 *Transepithelial Permeability Coefficient (P_{app}) of dextran-FITC (4kDa) across four epithelial cell lines calculated using the equation in section 2.2.3. Each data represent the mean ± SD (n=3).*

3.3.4. Expression of folate binding protein on cell layers

Expression of the FOLR1 mRNA in cultured cell layers was assessed by reverse transcription polymerase chain reaction (RT-PCR)(as described in methods in section 3.2.1). Rn-β-actin, Hs-GAPDH and gDNA were used as positive controls as described in 3.2.1.3 section. The analysis was performed at different time points post cell seeding onto permeable membrane. As shown in Figure 3.5, expression of FOLR1 mRNA (310 bp for human cell lines and 325 bp for rat IEC-6 cell line) was confirmed for all the cell layers investigated, although at different time points of culturing.

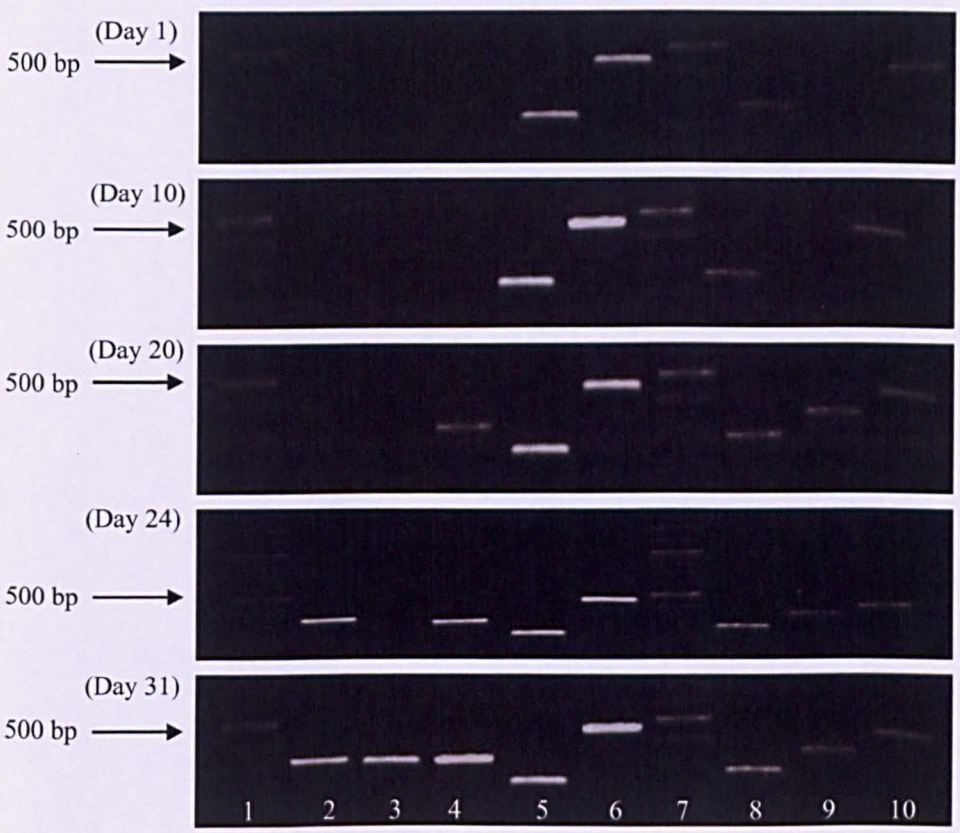

Figure 3.5 *The expression of FOLR1 mRNA by RT-PCR at different days post seeding of Calu-3, HBEC, Caco-2 and IEC-6 cells on permeable membrane. gDNA obtained from human or rat cells was used as a control to demonstrate ability of intron-spanning primers to discriminate between cDNA and genomic DNA; Hs-GAP-DH and Rn-β-actin were included as a positive control for RT.*

The lanes are as follows: 1) 100 bp DNA ladder, 2) FOLR1 cDNA from Calu-3 (310bp), 3) FOLR1 cDNA in HBEC (310bp), 4) FOLR1 cDNA in CaCo-2 (310bp), 5) Hs-GAPDH (240 bp), 6) Hs gDNA (462bp), 7) 100 bp DNA ladder, 8) Rn-β-actin (278bp), 9) FOLR1 mRNA in IEC-6 (325bp), 10) Rn gDNA (418bp)

3.3.5. Expression of folate binding protein on cell layers

To confirm expression of FR at the protein level, Western blotting analysis was conducted after mRNA detection. The data (Figure 3.6) demonstrate that folate receptor is eventually expressed in all epithelial cell lines cultured, but at different and specific time points of the culture.

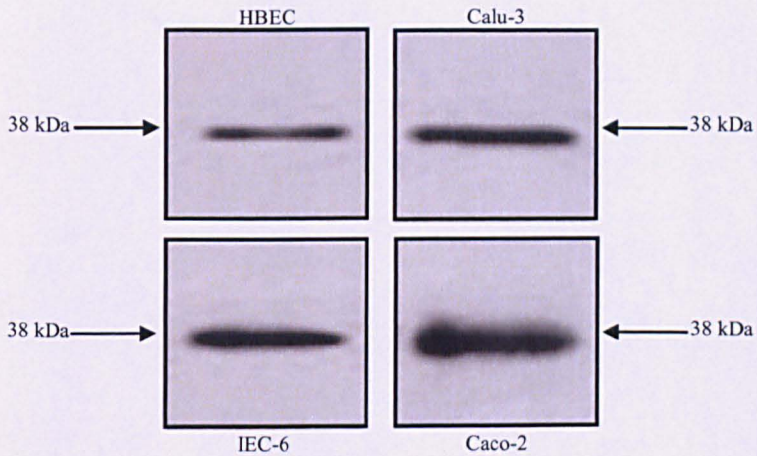

Figure 3.6 *Western blot analysis of folate binding protein (38kD) expression by HBEC, Calu-3, IEC-6 and Caco-2 cells cultured on permeable membrane. Samples (with total protein content, 20 μg/ml) were taken at day 31 for HBEC, 24 for Calu-3, 20 for IEC-6 and 20 day post seeding for Caco-2 cells. Bands obtained by chemiluminescent detection.*

3.3.6. Cell uptake of folate and non-folate conjugates

Uptake studies of FA-OVA-TRITC and OVA-TRITC (control) conjugates were performed at time point in the cell culture when expression of FR was confirmed (section 3.3.4 and 3.3.5). The high molar ratio of TRITC in the conjugates was used because previous study shows that TRITC undergoes quenching at high SMR, and

consequently is not very visible when in solution outside of the cells. However following cellular internalization and subsequent degradation of the OVA inside the lysosome, the fluorescence of TRITC is increased considerably, as the quenching no longer occurs, which improves its intracellular visualisation [12].

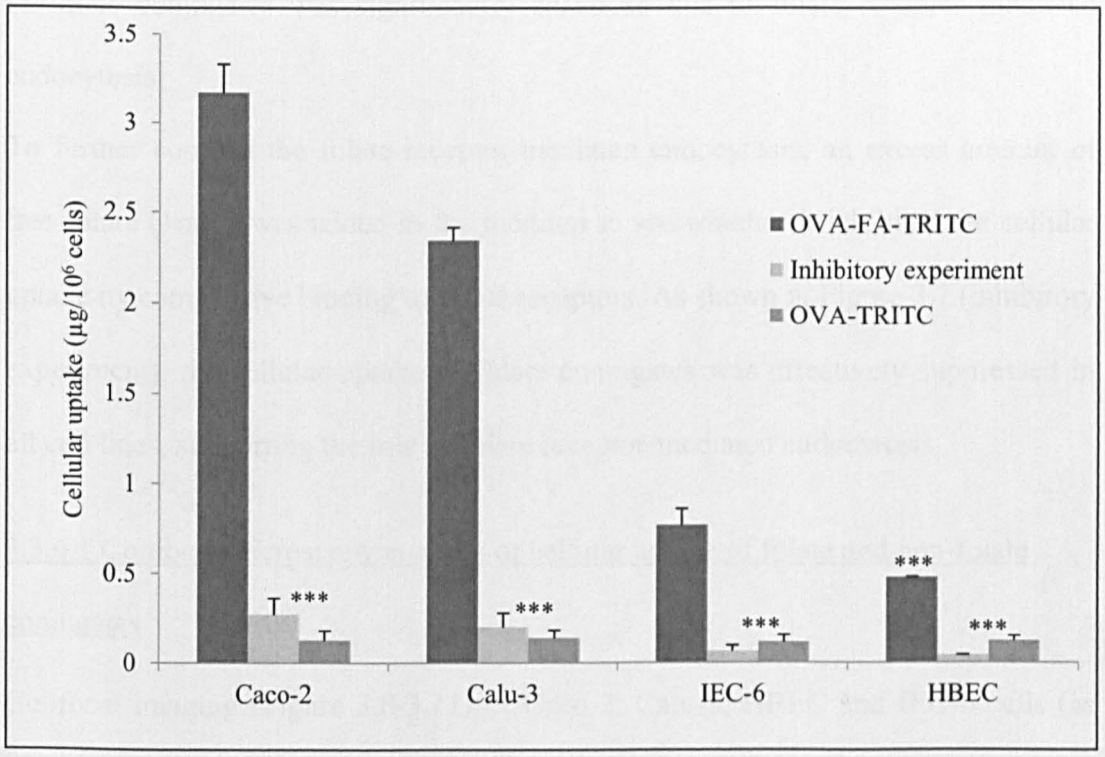

Figure 3.7 *Uptake study of FA-OVA-TRITC and OVA-TRITC in four epithelial layers. TRITC labelled folate- or non-folate conjugate (0.5 mg/ml) solution was added to the apical side of the cell layer. In the inhibitory experiments, 1 mmol free folate was added prior to folate conjugate application. The data represent the composite of three experiments, each performed in triplicate including folate and non-folate conjugate up-take for 4 hours, and folate conjugate uptake in the presence of unlabelled folic acid. One way analysis of variance (ANOVA) with Bonferroni post-hoc test was used. Uptake amount of folate conjugate was significantly different from controls (P<0.001). Error bar represents mean ± standard deviation (n=3).*

Quantitative analysis of cellular internalization is shown in Figure 3.7. It should be noted that extracellular fluorescence was quenched by washing the cell layers with Trypan Blue solution, as described in section 3.2.8.

Internalization of folate conjugates was significantly higher ($P<0.001$) relative to non-folate conjugates for all the cell types tested indicating that the cellular uptake of folate conjugates was significantly enhanced due to folate receptor mediated endocytosis.

To further confirm the folate receptor-mediated endocytosis, an excess amount of free folate (1mM) was added in the medium to see whether it inhibited the cellular uptake by competitive binding to folate receptors. As shown in Figure 3.7 (inhibitory experiment), the cellular uptake of folate conjugates was effectively suppressed in all cell lines, supporting the role of folate receptor-mediated endocytosis

3.3.6.1 Confocal microscopy analysis of cellular uptake of folate and non-folate conjugates

Confocal imaging (Figure 3.8-3.11) of Caco-2, Calu-3, HBEC and IEC-6 cells (as confluent membrane-cultured layers) incubated with FA-OVA-TRITC and OVA-TRITC conjugates revealed the presence of FA-OVA-TRITC (A) and OVA-TRITC (B) inside cells. The cell nucleus was counter-stained using DAPI (Section 2.2.5.2).

It is apparent from the images that red fluorescence of folate conjugates was greater than that of non-folate conjugates in all cell layers indicating the higher internalization and distribution of folate conjugates compared to non-folate conjugates. Three dimensional images showing vertical axis ('z-axis') of cell layers presented on the sides of overlay images exhibited punctuate cytoplasmic distribution of folate conjugates from apical to basolateral.

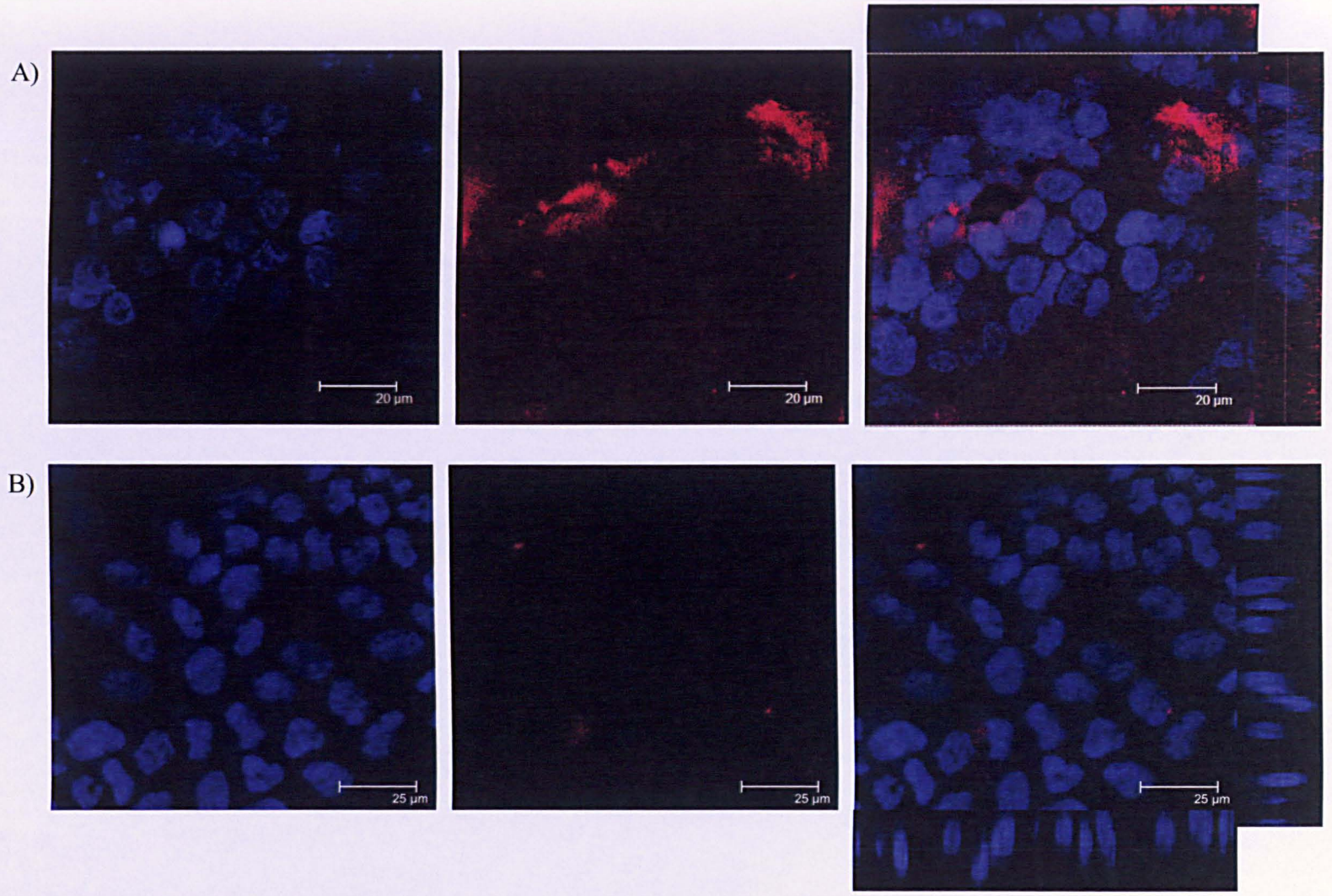

Figure 3.8 *Confocal images for cellular uptake study of FA-OVA-TRITC conjugates (A) (0.5 mg/ml) and OVA-TRITC conjugates (B) (0.5 mg/ml) in Caco-2 cell layers . Blue channel (left): cell nuclei stained with DAPI, Red channel (middle): TRITC fluorescence and Overlay image (right). Vertical (z-) axis shown on the overlay image.*

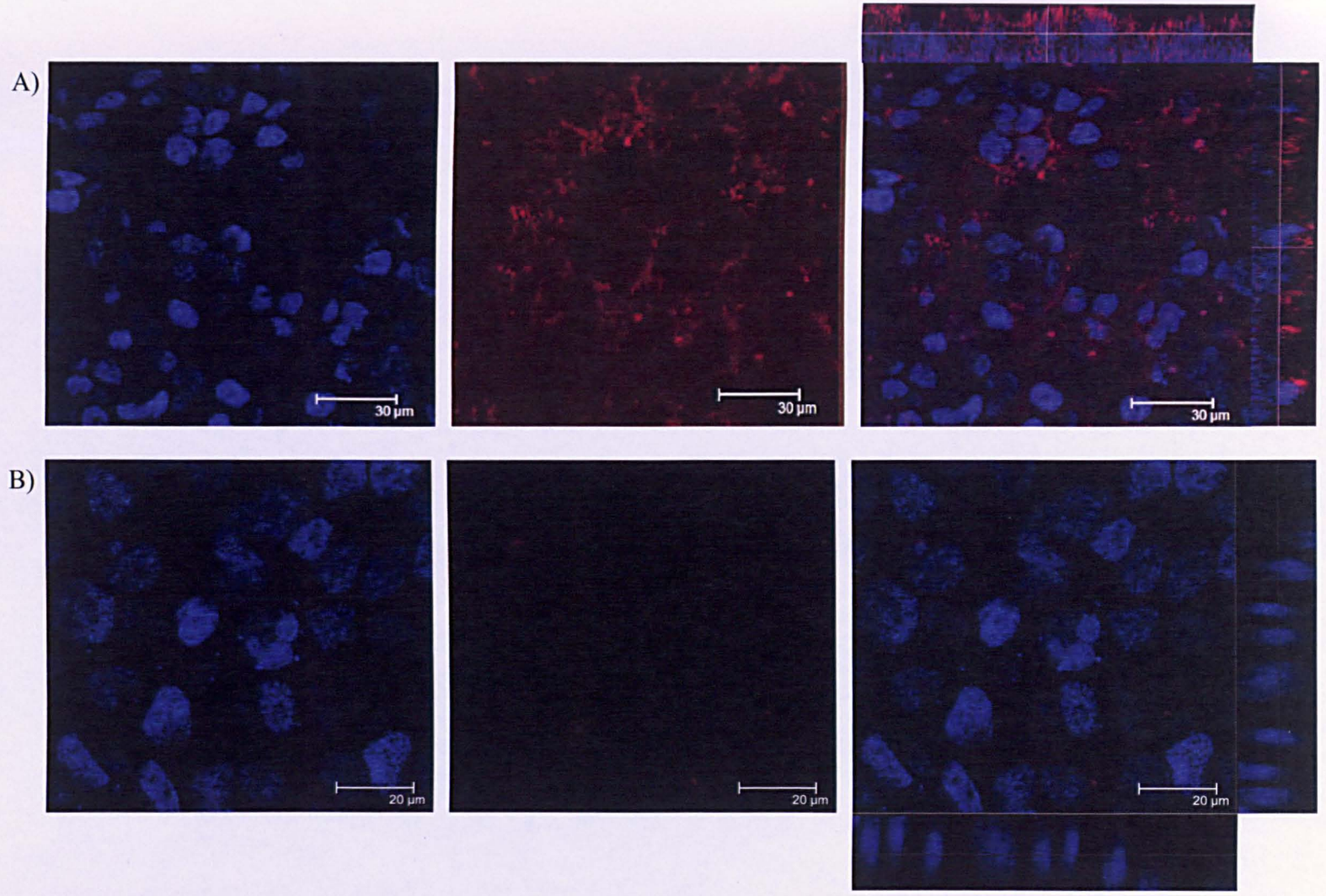

Figure 3.9 *Confocal images for cellular uptake study of FA-OVA-TRITC conjugates (A) (0.5 mg/ml) and OVA-TRITC conjugates (B) (0.5 mg/ml) in Calu-3 cell layers . Blue channel (left): cell nuclei stained with DAPI, Red channel (middle): TRITC fluorescence and Overlay image (right). Vertical (z-) axis shown on the overlay image.*

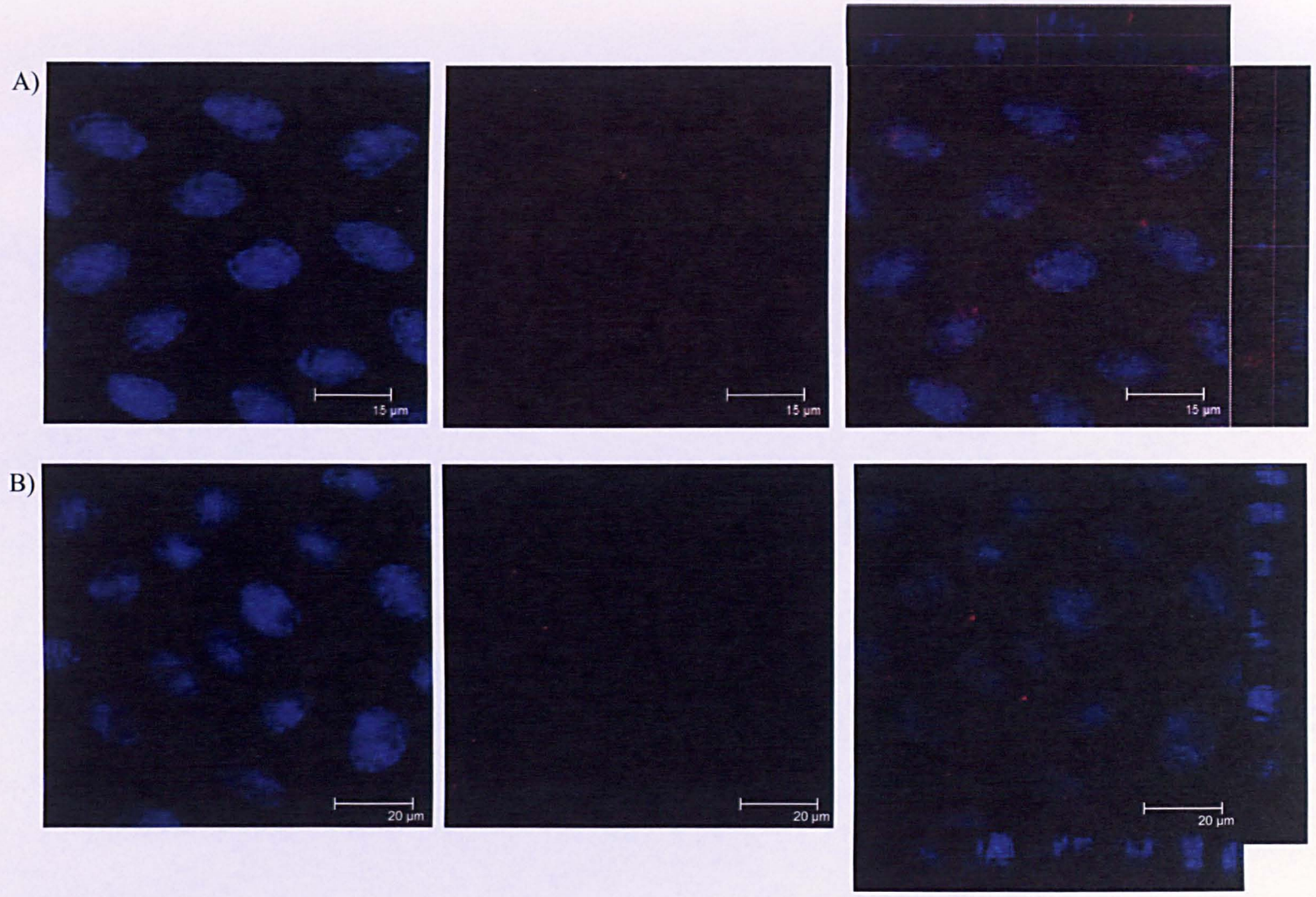

Figure 3.10 *Confocal images for cellular uptake study of FA-OVA-TRITC conjugates (A) (0.5 mg/ml) and OVA-TRITC conjugates (B) (0.5 mg/ml) in HBEC cell layers . Blue channel (left): cell nuclei stained with DAPI, Red channel (middle): TRITC fluorescence and Overlay image (right). Vertical (z-) axis shown on the overlay image.*

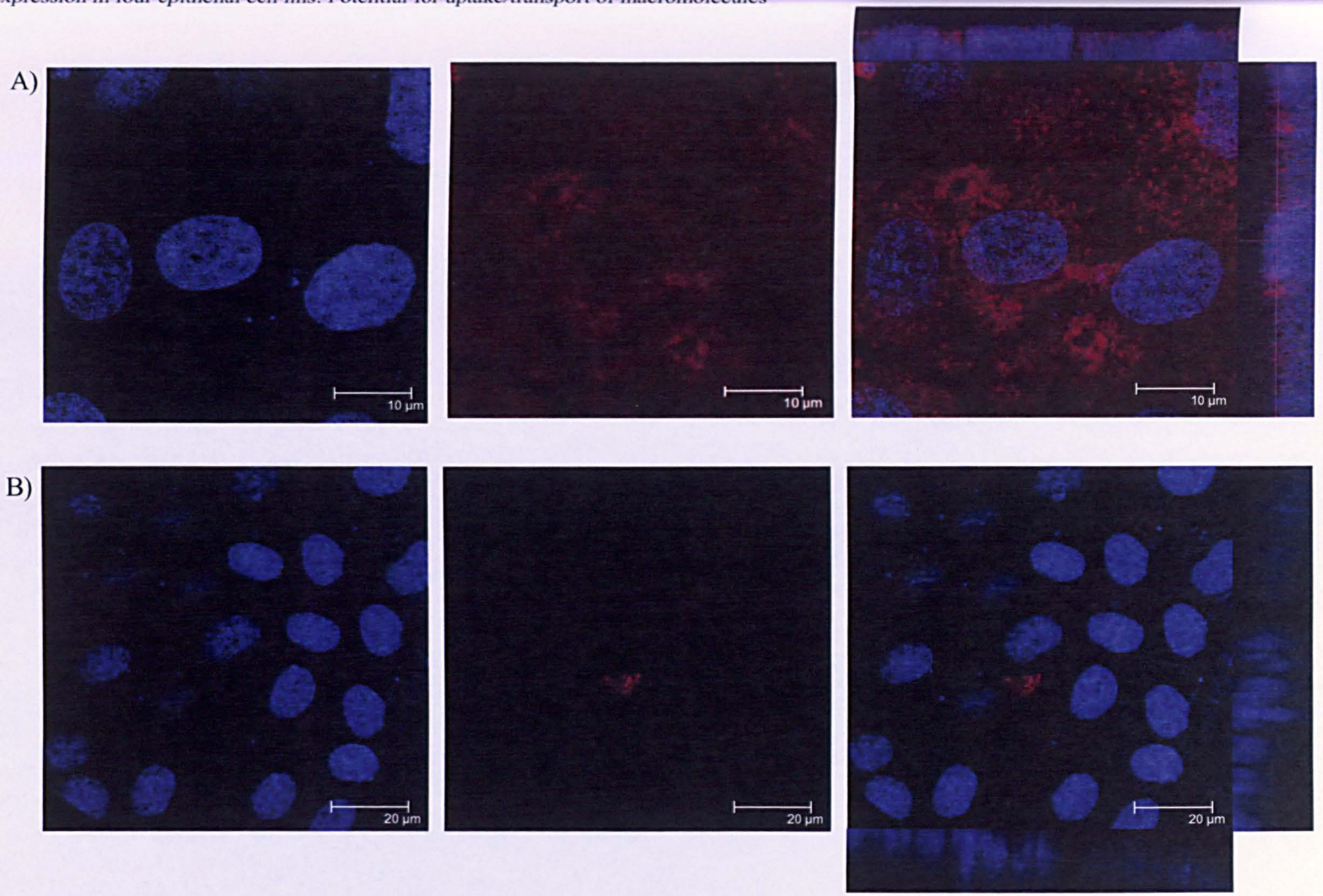

Figure 3.11 *Confocal images for cellular uptake study of FA-OVA-TRITC conjugates (A) (0.5 mg/ml) and OVA-TRITC conjugates (B) (0.5 mg/ml) in IEC-6 cell layers . Blue channel (left): cell nuclei stained with DAPI, Red channel (middle): TRITC fluorescence and Overlay image (right). Vertical (z-) axis shown on the overlay image.*

The gallery of images in Figure 3.12 depicts the internalization of FA-OVA-TRITC cojugates in Caco-2 cell layer as cross sections through the cell layer ('z-axes'). It demonstrates the presence of the conjugates throughout the cell cytoplasm from apical to basolateral side

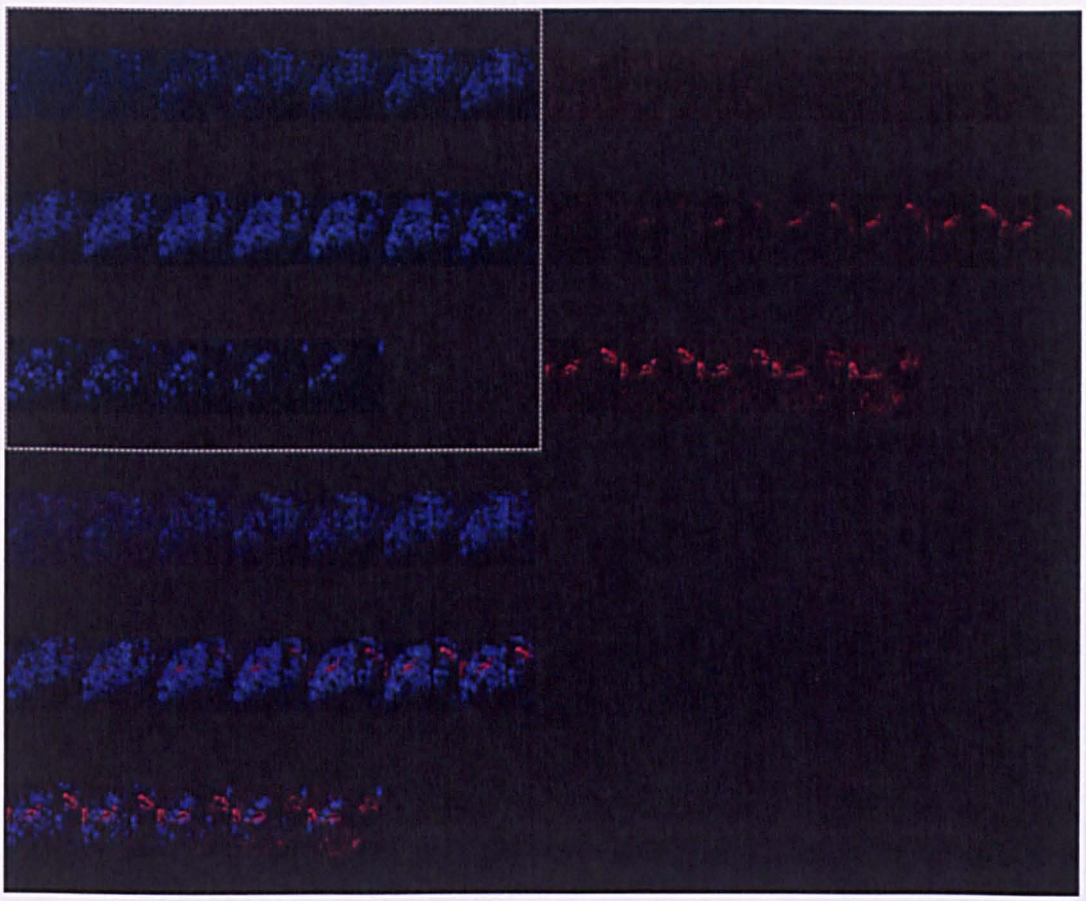

Figure 3.12 *Figure represents a gallery of cross sections images from confocal microscopy (from the apical to basolateral side of cell layer) for cellular uptake of FA-OVA-TRITC conjugates (0.5 mg/ml) in Caco-2 cell layers. Blue channel (top left): cell nuclei stained with DAPI, Red channel (top right): TRITC fluorescence and Overlay image (bottom right).*

Figure 3.13 depicts a continuous ring of immunostaining of confluent, membrane-cultured Calu-3 cells with an antibody to ZO-1 protein, a structural and functional component of TJs. It revealed the distribution of this protein as continuous 'rings' circling the cells at cell-cell contacts. In combination with the measured TEER, this

strongly suggests that the cell layers have functional intercellular TJs and are similar to epithelial cell layers *in vivo* with respect to permeability.

This gallery image also shows that endocytosed TRITC-folate conjugate is present throughout the cell profile from apical to basolateral membrane, with a significant amount of TRITC label appearing below the level of the ZO-1.

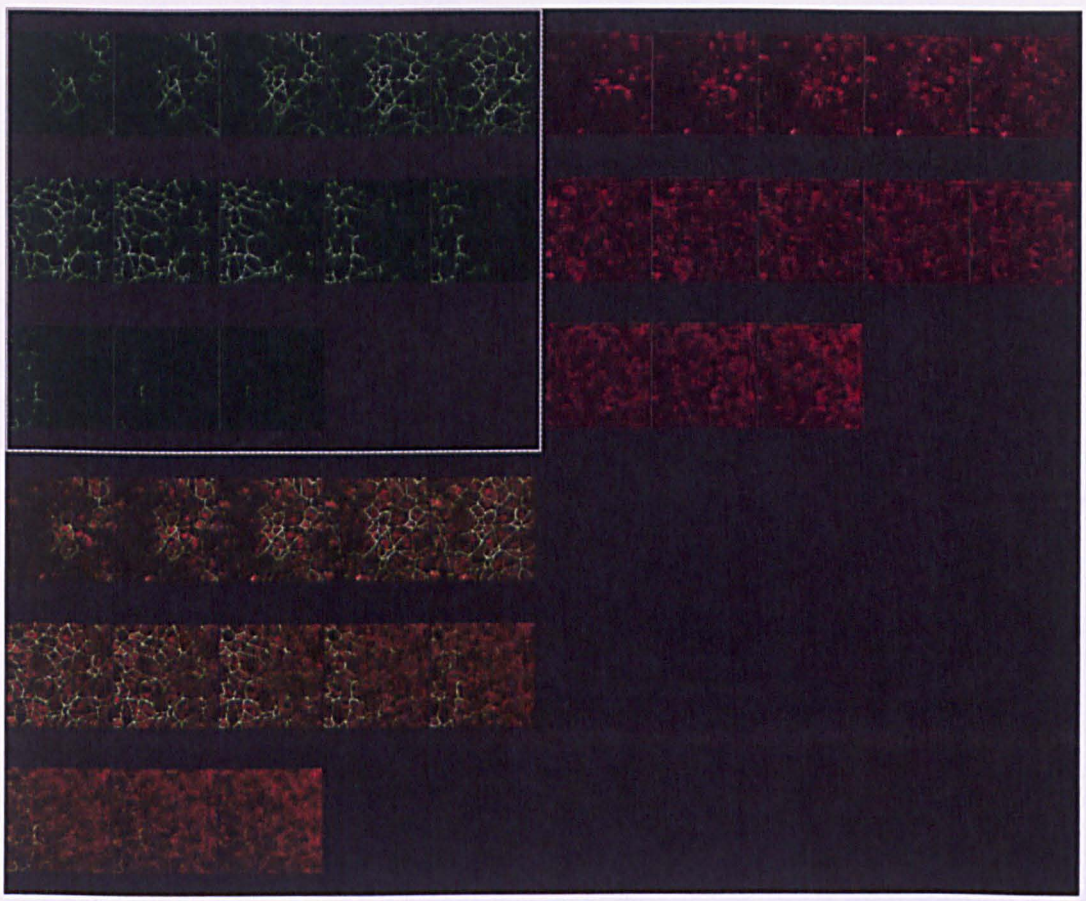

Figure 3.13 *Image represents a gallery of cross sections (from the apical surface to basolateral) of cellular uptake of FA-OVA-TRITC (0.5 mg/ml) in Calu-3 cell layer. Green channel (top left): Zonula Occludens staining, Red channel (top right): TRITC fluorescence and Overlay image (bottom right).*

3.3.7. OVA-FA-FITC transport across cell layers

The transport study was carried out as described in section 3.2.9. Transport of FITC labelled folate and non-folate-conjugate versus time across the cell layers (apical to basolateral direction) is shown in Figure 3.14 and 3.15. The data indicated that transport of the folate conjugate across the cell layer indeed occurred for all tested systems Caco-2, Calu-3, IEC-6 and HBEC. It generally appeared to be higher in cells of cancer than non-cancer origin (Caco-2 and Calu-3 compared to IEC-6 and HBEC).

The rate of folate conjugate transport generally occurred faster in first 2 hours of the 4 hours experiment, except for IEC-6, which showed a slightly different behaviour, with some lag before transport started to increase. It should be noted that TEER of all cell layers were monitored at the end of the experiments in order to ensure that the cell layers integrity was not compromised.

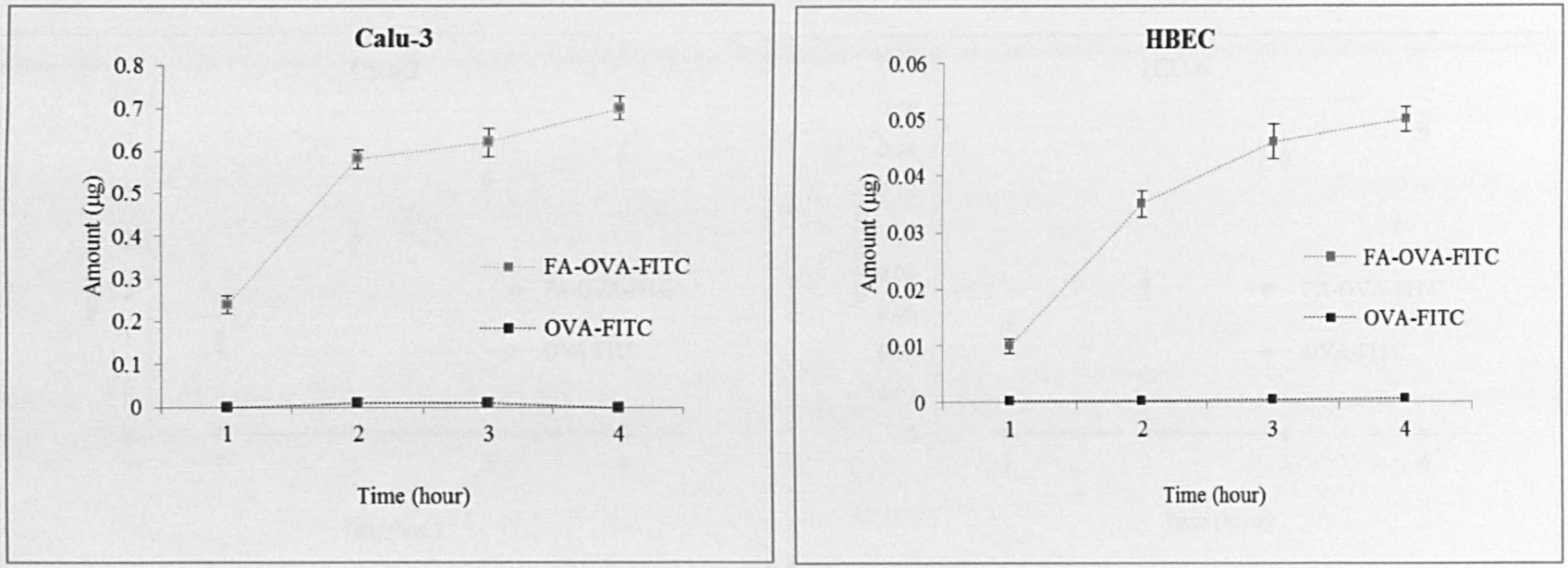

Figure 3.14 *Transport study across Calu-3 and HBE cell layers in apical to basolateral direction showing the cumulative amount of OVA-FA-FITC and OVA-FITC conjugates transported versus time in a four hours experiment. Samples (100µl) were taken every hour from basolateral side of the cell layer. Apical-to-basolateral translocation was assessed by measuring FITC-associated fluorescence present at the basolateral side. One way analysis of variance (ANOVA) with Bonferroni post-hoc test was used. The amount of folate conjugate transported by all cell lines was significantly different from controls ($P<0.001$). Error bar represents mean ± standard deviation (n=3).*

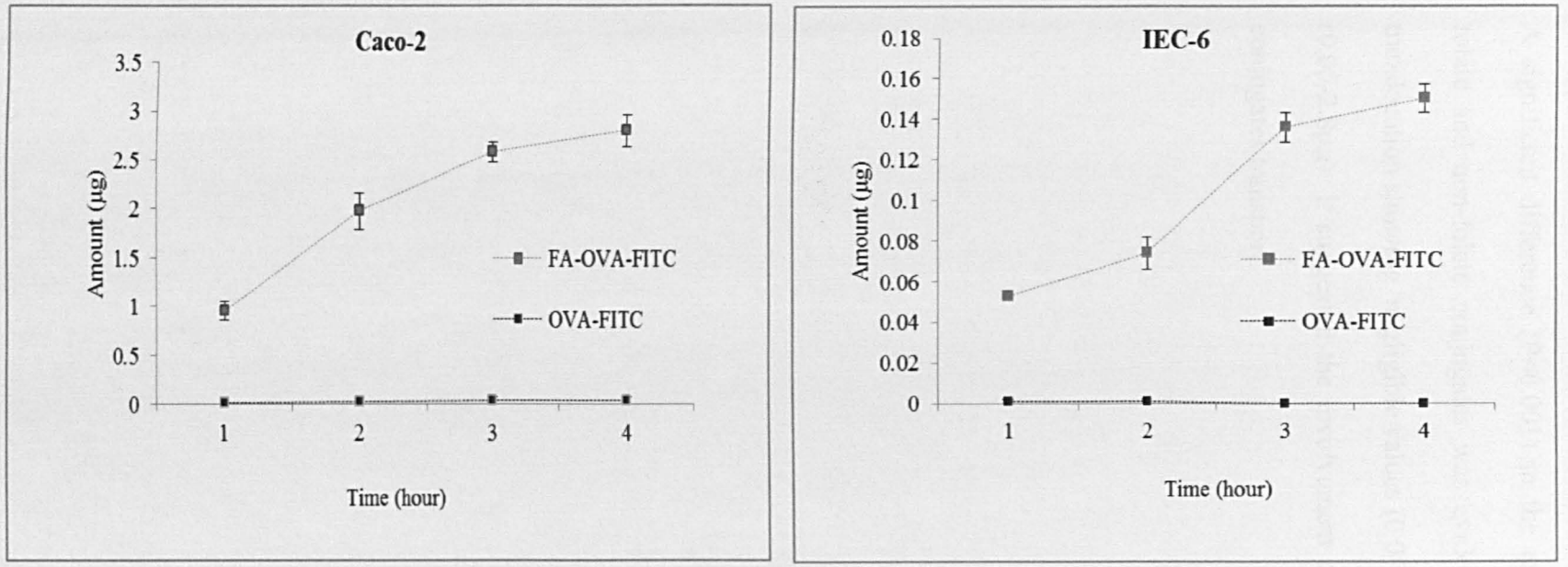

Figure 3.15 *Transport study across Caco-2 and IEC-6 cell layers in apical to basolateral direction showing the cumulative amount of OVA-FA-FITC and OVA-FITC conjugates transported versus time in a four hours experiment. Samples (100µl) were taken every hour from basolateral side of the cell layer. Apical-to-basolateral translocation was assessed by measuring FITC-associated fluorescence present at the basolateral side. One way analysis of variance (ANOVA) with Bonferroni post-hoc test was used. The amount of folate conjugate transported by all cell lines was significantly different from controls ($P<0.001$). Error bar represents mean ± standard deviation (n=3).*

A significant difference ($P<0.001$) in the extent of conjugates transport between folate and non-folate conjugates was evident from the graphs with OVA-FITC translocation showing negligible values (0.0-0.01 μg) compared to folate conjugates (0.05-2.8μg). It suggested the involvement of folate-mediated path way for folate conjugates transport.

3.4 Discussion

Although folate receptor mediated cellular uptake has been exploited in many studies [13-19], to the best of our knowledge, there are no studies reported in the literature that have investigated the transepithelial transport of folate ligand modified cargo across different cell types. It is apparent from the literature discussed in Chapter 1 (section 1.10) that reports on the possible role of folate receptor in transcellular transport in epithelial cells mostly deal with the transport of folate molecule in apical to basolateral direction in proximal tubule cells of kidney [20, 21], basolateral to apical transport of folate in retinal pigment epithelium [22] and folate transport in choroid plexus [23]. Regarding the use of folate as a ligand, majority of studies have investigated folate mediated drug delivery to cancerous cells with the aim of increasing targeting and cellular uptake of the delivery systems. On the contrary, studies on targeted drug delivery via folate receptor to non-cancerous cells or tissues are scarce. This work attempted to address these points.

Work detailed in this chapter hence investigated the potential of the folate ligand to mediate transport into or across four polarised epithelial cell lines for delivery of macromolecules (proteins). To assess this potential, folate-ligand modified OVA, was designed in this study as a model for macromolecular therapeutics.

The model macromolecular therapeutics, fluorescently labelled folate-ovalbumin conjugates used in this work (FA-OVA-TRITC and FA-OVA-FITC) were synthesized by initially reacting isothiocyanate group of FITC or TRITC with the free amino residue (ε-amino group of lysine) in OVA, followed by coupling of the carboxyl group of folic acid with the ε-amino group of lysine residue of OVA, similarly to previous reports [24, 25].

Such an experimental design ensured that the same specific fluorescence is present on both experimental and control preparations. TRITC-labeled conjugates were preferred for cellular uptake studies to avoid FITC fluorescence sensitivity to low pH and to utilize TRITC strong fluorescence in acid conditions [12].

ECDI (a water soluble coupling agent) was used for conjugation of folate in this work, the selection being based on reported 30-40% coupling efficiency [12, 25]. The modification of the procedure to conduct the folate conjugation at pH 6.4-6.6 was based on a previous report that at this pH the efficiency of coupling would be improved, relative to reaction at higher pH [12, 25].

In this study, molar ratio of folate conjugate was 13.1 ± 1.0 mole of folic acid *per* mole OVA which was higher than the ratios utilized by other research groups ranged between of 1-2 mol folate *per* mol of protein (BSA) [26] and 1-10 mol of folate *per* mol of protein (BSA) [27]. A higher molar ratio was chosen as Alsughayer (Drug targeting studies: characterisation and biological interactions of albumin-methotrexate conjugates, 1995) reported that the best MSR of methotrexate (folate analogue) to BSA that was able to work efficiency as a targeting moiety was found to be from 7 to 15 moles of methotrexate *per* mole BSA. Functionality of folate receptor for cellular internalization and transport was assessed by employing protein-folate conjugate based on ovalbumin, as a macromolecule model, rather than human serum albumin. The latter has been reported to have specific transcytosis pathways in epithelial cells *via* gp60 receptor [28-30], which would likely cause an interference in binding and cellular transport results. Ovalbumin is structurally significantly different from serum albumin, and was chosen to avoid the same receptor mediated pathway.

In order to produce polarised cell layers, all cell lines were cultured on permeable membranes applying standard culturing conditions. Data showed that TEER was increasing with time in culture. The observed increase in TEER, which was eventually seen to plateau, suggested formation of polarised, confluent cell layers with restricted permeability. It suggested that cells are interconnected by functional TJs.

Furthermore monitoring of the TEER of cultured cells on permeable membranes provided information regarding the time course needed for cells to form confluent cell layers. This was shown to be different for different cell types used in the study.

Calu-3 and Caco-2 cell are two well-characterised cell lines and are generally considered as a good *in vitro* models for bronchial and intestinal epithelium. They express characteristic features of these epithelia, including expression of TJs, mucus production, expression of relevant transporters and receptors when appropriately cultured *in vitro* [9, 31, 32]. TEER values observed for Calu-3 and Caco-2 in this work were consistent with previous reports from other research laboratories with values ranging between 700 and 2000 $\Omega.cm^2$, respectively [33-37].

Maximal TEER values obtained for HBEC was approximately 560 Ωcm^2, which was in line with literature values ranging 530-790 Ωcm^2 [7, 38].

Highest TEER value obtained in this work for non-cancer derived IEC-6 cell line was 790 Ωcm^2. To the best of our knowledge, the only published report on IEC-6 related to the formation of cell monolayer and tight junctions is an abstract describing an induction of expression of claudin-1 following cell medium supplementation with IL-4. The study reported that addition of IL-4 48 hours prior to

the permeability assay (Dextran-FITC 4400 Da) did not reduce the monolayer permeability (however permeability data were not shown) [39]. On the contrary, in our study IL-4 was present in the cell medium for the duration of IEC-6 culture and this may have facilitated the formation of polarised monolayers. It was noticed that significantly lower TEER values were obtained for the non-cancerous IEC-6 and HBEC cell layers, compared to cancer-derived Caco-2 and Calu-3 cell layers. The reasons behind these differences are not clear at this stage.

Although TEER is an easily measurable parameter and efficient indicator of cell layer integrity and presence of functional TJs, it may not always correlate with the paracellular permeability of hydrophilic molecules which is another parameter typically used in the research area to characterise the formation of the cell layer barrier [40]. Therefore, in addition to monitoring TEER, the paracellular permeability of dextran-FITC (4kDa) was also monitored in this work to complement the TEER and provide more complete information on TJ functionality. Permeability data (Table 3.1) obtained by applying a standard approach using dextran-FITC 4kDa (FD4) demonstrated a low permeability coefficient for the cell layers from all cell types used in the study. The low permeability rate of a modestly sized macromolecule, FD4, across all cell layers (Caco-2, Calu-3, IEC-6 and HBEC) confirmed the barrier properties of the cell layers.

The calculated apparent permeability coefficients (P_{app}) of 4.76×10^{-7} cm/s for Calu-3, 3.91×10^{-7} cm/s for Caco-2, 2.45×10^{-7} cm/s for HBEC and 3.06×10^{-7} cm/s for IEC-6 are similar to those reported in the literature. P_{app} values of 2.36×10^{-6} cm/s for HBE cell layer [41], 1.3×10^{-8}, 5.1×10^{-8} and 9.9×10^{-8} for Calu-3 [42-44] and 3×10^{-9}, 6.2×10^{-6} for Caco-2 [45, 46] have been reported by other groups. Discrepancies in

reported permeability values exist due to inter-laboratory differences in culture conditions, including the type of the filter and its coating to promote cell adherence, cell passage number, media, experimental procedures used to determine the permeability, etc. Therefore, caution must be exercised in comparing these values

The cell culture characterization thus confirms that Calu-3, Caco-2, IEC-6 and HBEC cell lines are all capable of producing electrically-tight monolayers with low permeability to hydrophilic probes, indicating a formation of tight junction structure, when appropriately cultured on permeable membranes. These properties of the cell layers are generally considered to be characteristic of polarised cells in culture, mimicking epithelial tissue properties [47].

The present work clearly demonstrated expression of folate receptor in Calu-3, Caco-2, HBEC and IEC-6 cell layers, as judged from RT-PCR and Western blot analyses. which was in agreement with previously published reports on the existence of FR in normal and cancerous tissue, including lung and intestine [3, 48, 49], however the present study was, to the best of our knowledge, the first demonstration of FR receptor expression in these cell lines in polarised model.

RT-PCR and western blot data revealed expression of folate binding protein in all cell layers at different time points. In more detail, RT-PCR and Western blot data revealed that expression of folate binding protein occurred at different time points in cell culturing on the permeable membrane, this time point being dependent on the cell line. This time point apparently coincides with the occurrence of 'plateau' in TEER resistance (Figure 3.4). This observation would be in line with the previous notion that synthesis and expression of plasma membrane proteins and transporters in epithelial cells depend on their high cell polarization and differentiations [50].

Two reports by Siissalo et al also showed that differentiation and polarization had a major effect on the expression of efflux proteins [51] and enzyme (Glucuronosyltransferases) [52] in Caco-2 cell line.

Although western blot analysis bands appeared to be thicker for cancerous cell lines (Calu-3 and Caco-2), compared to non-caner derived HBEC and IEC-6 cells, indicating the higher expression of FRs in malignant cell lines however, the comparison of the level of FRs expression is not possible because quantitative experiments were not carried out.

Functionality of expressed FR in all cell layers was confirmed by cellular internalization of FA-OVA-TRITC conjugate. Higher uptake of the folate conjugate observed in intestinal cell layers relative to bronchial (cancer derived Caco-2 compared to Calu-3 and non-cancer derived IEC-6 compared to HBEC) could be a consequence of higher levels of folate receptor expression in intestine compared to respiratory epithelium as reported in literature [53, 54].

To make sure that the intracellular delivery of FA-OVA-TRITC conjugate occurred in a folate receptor-mediated specific manner, comparative cellular uptake of OVA-TRITC was monitored which was exceedingly lower than FA-OVA-TRITC conjugate (Figure 3.7). This result suggested that targeted intracellular delivery of FA-OVA-TRITC conjugate took place via a folate receptor-mediated endocytosis mechanism. To further confirm the folate receptor-mediated endocytosis, an excess amount of free folate was added in the medium to see whether it inhibited the cellular uptake within cell layers by competitive binding to folate receptors (inhibitory experiment). As shown in Figure 3.7, the cellular uptake of FA-OVA-TRITC conjugate was effectively suppressed in the presence of 1 mM folate in the medium, supporting the role of folate receptor-mediated endocytosis. Similar

experiment to this work has also performed by Kim et al [17]. They showed 1 mM free folate in the medium inhibited cellular uptake of folate decorated NPs in KB cells.

In an attempt to confirm our aforementioned quantitative observations, confocal microscopy was used to visually monitor the cellular uptake of folate and non-folate conjugates in all cell layers.

Confocal imaging of membrane-cultured cells incubated with folate conjugates showed conjugate distribution throughout the viewed area of the cell layer (Figure 3.8 A, 3.9 A, 3.10 A and 3.11 A). The widespread red fluorescence from apical to basolateral surface (depicted by three dimensional images) of the cell surface indicated a strong internalization of the OVA-FA-TRITC by cell layers. In agreement with the quantitative data of cellular uptake (Figure 3.7), confocal images of cellular uptake of OVA-TRITC (Figure 3.8 B, 3.9 B, 3.10 B and 3.11 B) showed much lower red fluorescence compared to OVA-FA-TRITC confocal images lower conjugate internalization.

The studies on possible role of folate receptor in 'cargo' transport across the epithelial cell layer are scarce. These reports investigated the transport of folate molecule in apical to basolateral direction in proximal tubule cells of kidney [20, 21], basolateral to apical transport of folate in retinal pigment epithelium [22] and folate transport in choroid plexus [23]. To the best of our knowledge, there is no published data investigating folate mediated transport of macromolecules to be compared with the data presented herein.

Periodic measurement of folate conjugate levels in the basolateral solution following its application on the apical surface of the cell layers revealed that only FA-OVA-

FITC traversed the Calu-3 layers. A pattern of an initial increase in basolateral folate conjugate level, followed by a plateau was typically observed in experiments where the basolateral solution was sampled at regular intervals (Figure 3.14 and 3.15). Such behaviour could result from saturation of FR as reported in the literature. FR saturation occurred within the initial 30 min of incubation and continued exposure of the cells to the folate-linked conjugate resulted in continued, but considerably slower, uptake that persisted for the duration of a 6 hour study [55].

The disability of OVA-TRITC conjugate in crossing the cell layers again confirmed the involvement of folate-mediated pathway for folate conjugate transport and also proved that simple attachment of folate is able to change the faith of the cargo.

To end, it is worth emphasising that although the reduced folate carrier is thought to be present in virtually all cells, they cannot facilitate uptake and transport of folate or folate conjugates as they selectively facilitate the uptake of reduced forms of folic acid [56]. On the other hand, Zhao et al [56] demonstrated in HeLa cells that deletion of RFC gene from the genome does not result in any significant alteration of folate uptake and transport activity. Thus, the involvement of RFC in uptake and transport of folate conjugate in this work was omitted.

3.5 Conclusion

This study demonstrated the expression of folate receptor in four epithelial polarised cell layers including Caco-2, Calu-3, IEC-6 and HBEC. TRITC and FITC labelled OVA-FA were synthesised in order to investigate the potential of FR in folate mediated uptake and transport of a model macromolecular conjugate. Data revealed that simple attachment of folate was able to enhance the cellular uptake and transport of OVA.

Worked detailed in this chapter suggested the potential role of folate ligand in endocytosis and transport that can potentially be exploited for delivery of biologics to the epithelium or for non-invasive delivery of biologics to achieve systemic therapeutic effects.

3.6 References

1. Hilgenbrink, A.R. and P.S. Low, *Folate receptor-mediated drug targeting: from therapeutics to diagnostics.* J Pharm Sci, 2005. **94**(10): p. 2135-46.
2. Zhang, K., et al., *Folate-Mediated Cell Uptake of Shell-Crosslinked Spheres and Cylinders.* Journal of Polymer Science Part a-Polymer Chemistry, 2008. **46**(22): p. 7578-7583.
3. Parker, N., et al., *Folate receptor expression in carcinomas and normal tissues determined by a quantitative radioligand binding assay.* Analytical Biochemistry, 2005. **338**(2): p. 284-293.
4. Kelemen, L.E., *The role of folate receptor alpha in cancer development, progression and treatment: cause, consequence or innocent bystander?* Int J Cancer, 2006. **119**(2): p. 243-50.
5. Zhu, Y., A. Chidekel, and T.H. Shaffer, *Cultured human airway epithelial cells (calu-3): a model of human respiratory function, structure, and inflammatory responses.* Crit Care Res Pract. **2010**.
6. Florea, B.I., et al., *Drug transport and metabolism characteristics of the human airway epithelial cell line Calu-3.* J Control Release, 2003. **87**(1-3): p. 131-8.
7. Wan, H., et al., *Tight junction properties of the immortalized human bronchial epithelial cell lines Calu-3 and 16HBE14o.* Eur Respir J, 2000. **15**(6): p. 1058-68.
8. Ehrhardt, C., et al., *16HBE14o- human bronchial epithelial cell layers express P-glycoprotein, lung resistance-related protein, and caveolin-1.* Pharm Res, 2003. **20**(4): p. 545-51.
9. Artursson, P., K. Palm, and K. Luthman, *Caco-2 monolayers in experimental and theoretical predictions of drug transport.* Adv Drug Deliv Rev, 2001. **46**(1-3): p. 27-43.
10. Shah, P., et al., *Role of Caco-2 cell monolayers in prediction of intestinal drug absorption.* Biotechnol Prog, 2006. **22**(1): p. 186-98.
11. Thomas, C. and P.S. Oates, *IEC-6 cells are an appropriate model of intestinal iron absorption in rats.* J Nutr, 2002. **132**(4): p. 680-7.

12. Garnett, M.C. and R.W. Baldwin, *Endocytosis of a monoclonal antibody recognising a cell surface glycoprotein antigen visualised using fluorescent conjugates.* Eur J Cell Biol, 1986. **41**(2): p. 214-21.

13. Sudimack, J. and R.J. Lee, *Targeted drug delivery via the folate receptor.* Adv Drug Deliv Rev, 2000. **41**(2): p. 147-62.

14. Lee, R.J., X.B. Zhao, and H. Li, *Targeted drug delivery via folate receptors.* Expert Opinion on Drug Delivery, 2008. **5**(3): p. 309-319.

15. Schroeder, J.E., et al., *Folate-mediated tumor cell uptake of quantum dots entrapped in lipid nanoparticles.* Journal of Controlled Release, 2007. **124**(1-2): p. 28-34.

16. Leamon, C.P., S.R. Cooper, and G.E. Hardee, *Folate-liposome-mediated antisense oligodeoxynucleotide targeting to cancer cells: Evaluation in vitro and in vivo.* Bioconjug Chem, 2003. **14**(4): p. 738-747.

17. Kim, S.H., et al., *Target-specific cellular uptake of PLGA nanoparticles coated with poly(L-lysine)-poly(ethylene glycol)-folate conjugate.* Langmuir, 2005. **21**(19): p. 8852-8857.

18. Low, P.S. and S.A. Kularatne, *Folate-targeted therapeutic and imaging agents for cancer.* Current Opinion in Chemical Biology, 2009. **13**(3): p. 256-262.

19. Lu, Y.J. and P.S. Low, *Folate-mediated delivery of macromolecular anticancer therapeutic agents.* Advanced Drug Delivery Reviews, 2002. **54**(5): p. 675-693.

20. Sikka, P.K. and K.E. McMartin, *Determination of folate transport pathways in cultured rat proximal tubule cells.* Chemico-Biological Interactions, 1998. **114**(1-2): p. 15-31.

21. Birn, H., J. Selhub, and E.I. Christensen, *Internalization and Intracellular-Transport of Folate-Binding Protein in Rat-Kidney Proximal Tubule.* American Journal of Physiology, 1993. **264**(2): p. C302-C310.

22. Chancy, C.D., et al., *Expression and differential polarization of the reduced-folate transporter-1 and the folate receptor alpha in mammalian retinal pigment epitheliu.* Journal of Biological Chemistry, 2000. **275**(27): p. 20676-20684.

23. Kennedy, M.D., et al., *Evaluation of folate conjugate uptake and transport by the choroid plexus of mice.* Pharm Res, 2003. **20**(5): p. 714-9.

24. Lermo, A., et al., *Immunoassay for folic acid detection in vitamin-fortified milk based on electrochemical magneto sensors.* Biosensors & Bioelectronics, 2009. **24**(7): p. 2057-2063.

25. Garnett, M.C. and R.W. Baldwin, *An improved synthesis of a methotrexate-albumin-791T/36 monoclonal antibody conjugate cytotoxic to human osteogenic sarcoma cell lines.* Cancer Research, 1986. **46**(5): p. 2407-12.

26. Turek, J.J., C.P. Leamon, and P.S. Low, *Endocytosis of folate-protein conjugates: ultrastructural localization in KB cells.* J Cell Sci, 1993. **106 (Pt 1)**: p. 423-30.

27. Leamon, C.P. and P.S. Low, *Delivery of macromolecules into living cells: a method that exploits folate receptor endocytosis.* Proc Natl Acad Sci U S A, 1991. **88**(13): p. 5572-6.

28. Kim, K.J. and A.B. Malik, *Protein transport across the lung epithelial barrier.* Am J Physiol Lung Cell Mol Physiol, 2003. **284**(2): p. L247-59.

29. Swaan, P.W. and L.A. Bareford, *Endocytic mechanisms for targeted drug delivery.* Advanced Drug Delivery Reviews, 2007. **59**(8): p. 748-758.

30. Shin, D.M., et al., *Therapeutic nanoparticles for drug delivery in cancer.* Clinical Cancer Research, 2008. **14**(5): p. 1310-1316.

31. Audus, K.L., et al., *Characterization of the Calu-3 cell line as a tool to screen pulmonary drug delivery.* International Journal of Pharmaceutics, 2000. **208**(1-2): p. 1-11.

32. Borchard, G., et al., *Transfection efficiency and toxicity of polyethylenimine in differentiated Calu-3 and nondifferentiated COS-1 cell cultures.* Aaps Pharmsci, 2002. **4**(3).

33. Foster, K.A., et al., *Characterization of the Calu-3 cell line as a tool to screen pulmonary drug delivery.* International Journal of Pharmaceutics, 2000. **208**(1-2): p. 1-11.

34. Thanou, M.M., et al., *Effect of degree of quaternization of N-trimethyl chitosan chloride for enhanced transport of hydrophilic compounds across intestinal Caco-2 cell monolayers.* Journal of Controlled Release, 2000. **64**(1-3): p. 15-25.

35. Florea, B.I., et al., *Transfection efficiency and toxicity of polyethylenimine in differentiated Calu-3 and nondifferentiated COS-1 cell cultures.* Aaps Pharmsci, 2002. **4**(3): p. -.

36. Shen, R.Q., et al., *Calu-3 - a Human Airway Epithelial-Cell Line That Shows Camp-Dependent Cl- Secretion.* American Journal of Physiology, 1994. **266**(5): p. L493-L501.

37. Cooney, D., M. Kazantseva, and A.J. Hickey, *Development of a size-dependent aerosol deposition model utilising human airway epithelial cells for evaluating aerosol drug delivery.* Atla-Alternatives to Laboratory Animals, 2004. **32**(6): p. 581-590.

38. Forbes, B. and C. Ehrhardt, *Human respiratory epithelial cell culture for drug delivery applications.* Eur J Pharm Biopharm, 2005. **60**(2): p. 193-205.

39. Poritz. L.S , G.K.I., Thompson J, Boyer M, and W. A. Koltun W. A, *Induction of claudin-1 in IEC-6 cells by IL-4* Journal of Surgical Research, 2004. **121**(2): p. 311-312.

40. Balda, M.S., et al., *Functional dissociation of paracellular permeability and transepithelial electrical resistance and disruption of the apical-basolateral intramembrane diffusion barrier by expression of a mutant tight junction membrane protein.* J Cell Biol, 1996. **134**(4): p. 1031-49.

41. Forbes, B., et al., *The human bronchial epithelial cell line 16HBE14o- as a model system of the airways for studying drug transport.* International Journal of Pharmaceutics, 2003. **257**(1-2): p. 161-7.

42. Li, L., et al., *Carbopol-mediated paracellular transport enhancement in Calu-3 cell layers.* J Pharm Sci, 2006. **95**(2): p. 326-35.

43. Chono, S., et al., *Aerosolized liposomes with dipalmitoyl phosphatidylcholine enhance pulmonary insulin delivery.* J Control Release, 2009. **137**(2): p. 104-9.

44. Seki, T., et al., *Effects of a sperminated gelatin on the nasal absorption of insulin.* International Journal of Pharmaceutics, 2007. **338**(1-2): p. 213-8.

45. Yamashita, S., et al., *Optimized conditions for prediction of intestinal drug permeability using Caco-2 cells.* European Journal of Pharmaceutical Sciences, 2000. **10**(3): p. 195-204.

46. Balimane, P.V., Y.H. Han, and S. Chong, *Current industrial practices of assessing permeability and P-glycoprotein interaction.* AAPS J, 2006. **8**(1): p. E1-13.

47. Wakabayashi, Y., et al., *Four-dimensional imaging of filter-grown polarized epithelial cells.* Histochem Cell Biol, 2007. **127**(5): p. 463-72.

48. Salazar, M.D. and M. Ratnam, *The folate receptor: what does it promise in tissue-targeted therapeutics?* Cancer Metastasis Rev, 2007. **26**(1): p. 141-52.

50. Stein, M., A. Wandinger-Ness, and T. Roitbak, *Altered trafficking and epithelial cell polarity in disease.* Trends Cell Biol, 2002. **12**(8): p. 374-81.

51. Siissalo, S., et al., *Effect of cell differentiation and passage number on the expression of efflux proteins in wild type and vinblastine-induced Caco-2 cell lines.* European Journal of Pharmaceutics and Biopharmaceutics, 2007. **67**(2): p. 548-554.

52. Siissalo, S., et al., *The Expression of Most UDP-Glucuronosyltransferases (UGTs) Is Increased Significantly during Caco-2 Cell Differentiation, whereas UGT1A6 Is Highly Expressed Also in Undifferentiated Cells.* Drug Metabolism and Disposition, 2008. **36**(11): p. 2331-2336.

53. Leamon, C.P., et al., *Folate receptor expression in carcinomas and normal tissues determined by a quantitative radioligand binding assay.* Analytical Biochemistry, 2005. **338**(2): p. 284-293.

54. Kamen, B.A. and A.K. Smith, *A review of folate receptor alpha cycling and 5-methyltetrahydrofolate accumulation with an emphasis on cell models in vitro.* Advanced Drug Delivery Reviews, 2004. **56**(8): p. 1085-1097.

55. Paulos, C.M., et al., *Ligand binding and kinetics of folate receptor recycling in vivo: impact on receptor-mediated drug delivery.* Mol Pharmacol, 2004. **66**(6): p. 1406-14.

56. Nakai, Y., et al., *Functional characterization of human proton-coupled folate transporter/heme carrier protein 1 heterologously expressed in mammalian cells as a folate transporter.* J Pharmacol Exp Ther, 2007. **322**(2): p. 469-76.

Chapter 4

Intracellular trafficking study of folate-decorated NPs across epithelium

4.1 Introduction

The possible role of Folate Receptor (FRs) in macromolecule and nanoparticle (NP) transport across mucosal layers has not been investigated in the literature. As mentioned in Chapter 1 (section 1.10), they are only few reports on folate transport in proximal tubule cells of kidney [1, 2], retinal pigment epithelium [3] and in choroid plexus [4].

The mechanism by which folate molecules and folate-ligand modified macromolecules are taken up into the cells is not also clearly understood. Some reports have pointed to internalization of FR by caveolae [5-10] whereas other studies have suggested that FR are endocytosed by clathrin-coated pits [2, 11]. However some recent studies [9, 12, 13] have cautioned that the trafficking pathways taken by a recycling receptor such as FR can be complex and may involve many sorting events in multiple organelles. These reports mostly utilised 5-methyltetrahydrofolate, folate or methotrexate molecules to investigate the endocytosis pathway(s).

Thus, work described in this Chapter investigated the potential of the folate mediated pathway for cellular uptake and transcellular transport of folate decorated NPs, which to the best of our knowledge has not been attempted previously. Furthermore, intracellular trafficking of folate decorated NPs was explored using various endocytic inhibitors with effects on different routes (section 4.1.1) and stages of endocytosis.

The use of Calu-3 cells for the purpose of this work was possible as this cell line has been shown to express FR (3.3.4 and 3.3.5). In addition, confocal microscopy study

was performed to assist the understanding of the route of uptake as well as intracellular trafficking of folate modified NPs.

4.1.1 Endocytosis

As described in chapter one (section 1.5), there are different pathways for endocytosis including pinocytosis, phagocytosis and receptor mediated endocytosis. The latter employs three distinct mechanisms including clathrin-mediated endocytosis, caveolae-mediated endocytosis and clathrin-and caveolae-independent endocytosis. Certain cell treatments can inhibit cellular internalization via these pathways which is useful in determining the uptake pathways of different systems [14].

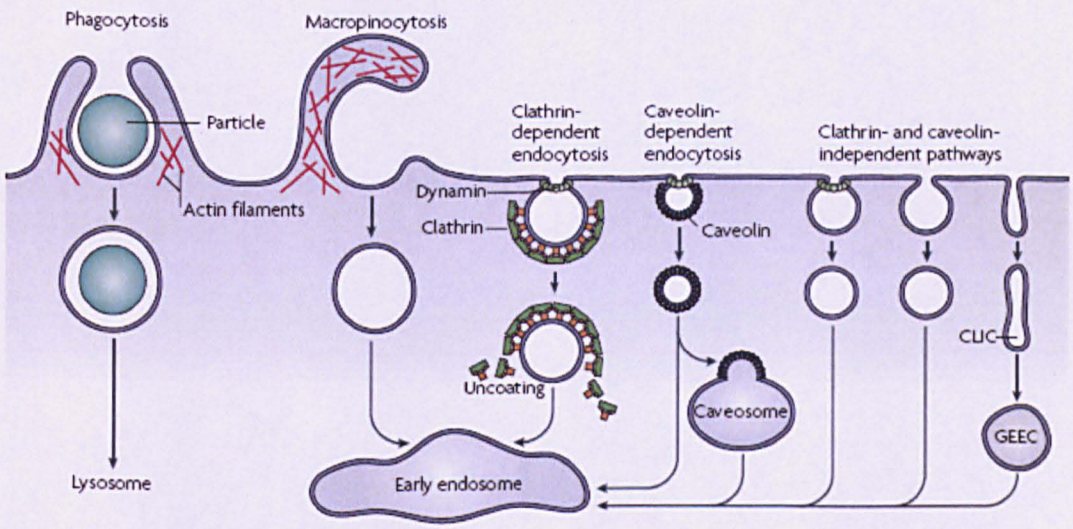

Figure 4.1 *Pathway of entry to the cells, adopted from [15]*

4.1.1.1 Clathrin-mediated endocytosis (CME)

Clathrin-mediated endocytosis is a process by which almost all eukaryotic cells internalize nutrients, antigens, growth factors, pathogens and recycling receptors. Internalization can occur constitutively or in response to certain stimuli. The

constitutive pathway is mainly involved in the uptake of receptors that undergo continuous internalization and recycling. The uptake of macromolecules and some viruses also rely on the constitutive pathway. The signal induced pathway is responsible for the control of signalling potency of the receptor by regulating events that occur at the level of internalisation, which in turn determine the post-endocytic fate such as recycling or degradation of the receptor [16].

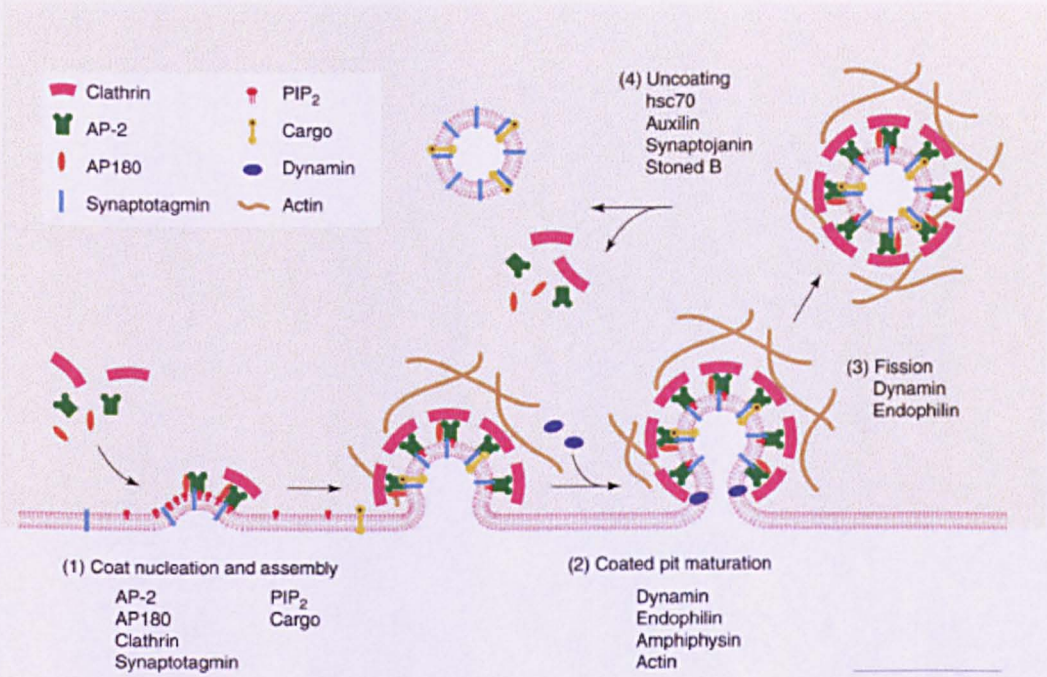

Figure 4.2 *Overview of the steps involved in clathrin-mediated endocytosis. Clathrin is first assembled at the intracellular surface of the plasma membrane. After formation of clathrin coated pit, the invagination occurs. The invaginated coated pits pinch off from the plasma membrane to form clathrin coated vesicle. The vesicle loses its clathrin coat and progresses to endosomes which are acidified. The endosomes are then transported to lysosomes where the internalised material is degraded. Adopted from [16].*

Clathrin coated vesicle formation is a multi-step process: initially clathrin triskelia assemble into hexagonal and pentagonal lattices, then these lattices attach to overlying plasma membrane via AP2 leading to its invagination into coated pit

Dynamin, a multidomain GTPase is then recruited to the neck of coated pits and assembles into spiral to mediate membrane fission and release of clathrin coated vesicles. The vesicles are ~200nm in diameter. Once clathrin coated vesicles have separated, clathrin coats disassemble to leave the naked transport vesicle for their fusion with endosomal compartments. The coat components migrate back to the membrane to participate in another round of endocytosis. [17]. There are a number of ways to inhibit CME such as hypertonic challenge (using sucrose), intracellular potassium depletion and low pH shock to disrupt CME by dissociation of clathrin coats from the plasma membrane. Cationic amphiphilic drugs such as concanavalin A, chlorpromazine and brefeldin act on the clathrin-dependent pathway and inhibit receptor-mediated endocytosis by reducing the number of coated pit–associated receptors at the cell surface and causing the accumulation of clathrin in an endosomal compartment [18, 19].

4.1.1.2 Caveolae-mediated endocytosis

Caveolae are an abundant feature of many mammalian cells including adipocytes, endothelial cells, smooth muscle, and fibroblasts but are not detectable in all mammalian cells. It is a flask-shaped (50-100 nm), cholesterol and sphinogolipid rich invagination of the plasma membrane [20]. Biochemically, caveolae are characterized by their association with a family of cholesterol-binding proteins called caveolins, which function to create and/or maintain these structures. Consistent with this, expressing caveolin in cells that do not normally have caveolae is apparently sufficient to generate these structures [21].

Caveolae are involved in endocytosis, transcytosis, and cell signalling. They directly participate in the internalization of different cargoes such as membrane components

(glycosphingolipids), bacterial toxins (tetanus toxin), extracellular ligands (folic acid) and non-enveloped viruses [22]. Caveolae endocytosis shares many common features with clathrin-dependent pathways, including the same dynamic requirement of molecular machinery in the fission process. However, there are clearly striking differences between the dynamic association of clathrin with the plasma membrane and the stable association of caveolin.

In contrast to CME, internalisation via caveolae is not a constitutive process and only occurs upon cell stimulation in addition, internalisation via caveolae occurs at a much slower rate compared to CME [23]. The caveolae trafficking process involves an initial interaction between the cargo and receptors leading to cargo concentrating within the invaginating caveolar surface formed by caveolin polymerization.This is then followed by membrane budding. Caveolae require GTP hydrolysis to bud directly from the cell surface into a discrete carrier vesicle. Dynamin has been identified as the GTPase mediating this fission at the neck of the invagination resulting in the release of free vesicles and subsequent delivery of molecular cargo to target membrane by docking and fusion mechanisms [23].

One interesting aspect of caveolae mediated endocytosis is that the internalised vesicles bypass the acidic endosome and lysosome. Instead, they are transported to a specific endosomal compartment with neutral internal pH called caveosomes. For this reason, the caveolar internalisation pathway has potential advantages for targeted drug delivery [24].

Several drugs have been reported to inhibit caveolae-mediated endocytosis. Cholesterol is an important component of caveolae and depletion of cholesterol can remove the caveolae from cell membrane. Thus, sterol binding drugs (filipin,

nystatin and methyl-β-cyclodextrin) which remove cholesterol from the cell membrane are able to disrupt caveolae [25]

4.1.2 Involvement of actin filament in endocytosis

Actin is a major component of the cytoskeleton. Growing evidence has suggested a role for the actin cytoskeleton during clathrin-mediated endocytosis. Several works have suggested a close association between the endocytic machinery in mammalian cells and the actin cytoskeleton [17]. First, the GTPase dynamin, a central player in CME, and several dynamin-binding partners (syndapin, mAbp1, intersectin, and profiling) have been shown to directly or indirectly regulate F-actin dynamics [26]. Second, Hip1R, an F-actin-binding protein, also interacts with clathrin and promotes clathrin assembly [27]. Finally, it was recently revealed that actin and regulators of actin polymerization are transiently recruited to clathrin-coated structures coincident with, or shortly after, clathrin-coated vesicle detachment from the plasma membrane [28]. Based on these and other data, F-actin has been postulated to play either a structural role in CME, controlling the localization of endocytic machinery on the plasma membrane, or a mechanical role, driving invagination, the separation of vesicles from the plasma membrane, and/or the translocation of nascent vesicles into the cytoplasm [26]. Commonly used actin filament disrupting drugs include cytochalasin D and latrunculin. Cytochalasin D is a fungal alkaloid and binds to the positive end of actin filaments and prevents elongation [29, 30].

4.1.3 Involvement of microtubules in endocytosis

Microtubules, a component of the cytoskeleton, consist of tubulin and several associated proteins. The protein filaments stretch across cells and provide a mechanical basis for chromosome sorting, cell polarity and organelle localization

among other functions. The transport of endocytic content from early to the late endosomes is dependent on microtubules which also promote fusion and fission of endocytic vesicles. Colchicine, vinblastine and nocodazole are well known microtubules depolymerising agent that binds to tubulin and inhibit its polymerization [31].

4.2 Material and Methods

4.2.1 Preparation of folate and non-folate modified nanoparticles

All chemicals were purchased from Sigma-Aldrich (UK) unless otherwise specified. Ovalbumin-Folic acid (OVA-FA) was prepared by the same method described in 3.2.3 with same molar ratio (13.09 ± 1.04 mole folic acid per mole OVA).

OVA-FA and OVA was adsorbed on the surface of sulfate-modified, polystyrene NPs of 30 nm diameter (green) to create folate and non-folate modified nanoparticles (NPs). To achieve that, 10 µl of NPs suspension (containing 2.5% w/v solid) containing 1.69 x 10^{13} NPs were incubated with 2.02x10^{-9} mole OVA-FA or OVA for at least 3h at room temperature with gentle magnetic stirring. Excess (unbound) OVA-FA or OVA were removed following centrifugation (25,000g) of the nanoparticle suspension for 30 min.

The supernatant was removed and the NP pellet re-suspended in HBSS, the volume of which was equal to the volume of removed supernatant.

The amount of OVA added to the NPs was selected based on the literature (will be discussed in section 4.3.1 and 4.4)

4.2.2 Particle size measurements

Dynamic light-scattering (DLS) (Dynamic Light Scattering, Viscotek, UK) technique was used to measure the hydrodynamic diameter and size distribution of NPs. Folate and non-folate modified NPs were analysed by DLS suspended in Hanks Balanced Salt Solution (HBSS) at pH 7.4 (under the same conditions in which NPs were applied to the cells). The results represent the mean of 10 measurements (± SD).

4.2.3 Calu-3 cell monolayer

Calu-3 cells (used between passages 25-40) were cultured on flasks until confluence. Thereafter cells were detached from the flasks, seeded and cultured on filters (10^5 cells per well) according to the methods detailed previously (section 2.2.1.2 and 2.2.1.4). Cell layers were used at day 24-25 post seeding.

4.2.4 Immunostaining for FRs in Calu-3 monolayer

Folate receptor immunostaining was performed on cultured Calu-3 cell layers in the same fashion as described (2.2.5.2, 2.2.5.3 and 2.2.5.4) using mouse anti-human FOLR1 primary antibody and goat anti-mouse TRITC labelled secondary antibody.

4.2.5 Cellular uptake and transport experiments

These experiments were conducted according to the protocol described in sections 3.2.8 and 3.2.9 with applying folate and non-folate modified NPs.

Cellular uptake of NPs and Cholera toxin B and transferrin in HBSS was determined in the presence and absence of endocytosis inhibitors. Inhibitors (Chlorpromazine (10 μg/ml), Filipin (5 μg/ml), Dynasore (10 μg/ml), Colchicine (5 μg/ml) and Cytochalasin D (10 μg/ml)) were used at concentrations that showed a minimum of 85% cell viability during the 4 h assay period and were applied on cell layers 1 hour prior the application of NPs.

Cellular uptake and transport experiments were performed at 4°C and 37°C. The integrity of the Calu-3 cell monolayer was evaluated by performing TEER measurements (section 2.2.2) every other day post-seeding. As an additional control of cell layers integrity, TEER for each Transwell was checked at the end of experiment. For this purpose, medium was added to the upper and lower chambers.

Significant reduction seldom occurred in <3% of wells; the data from these wells were not included in the final analysis.

4.2.6 Cytotoxicity of endocytosis inhibitors and folate and non-folate modified nanoparticles

Potential short-term cytotoxicity of endocytosis inhibitors and NPs was assessed in Calu-3 cells to ensure cell viability during uptake and transport assays. Solution of chemical inhibitors were prepared and applied to cells at a range of concentrations known to reduce or inhibit clathrin-mediated endocytosis (chlorpramazin, 1-50 μg/ml) caveolae-mediated endocytosis (filipin, 1-50 μg/ml) and dynamin-dependent endocytosis (dynasore, 5-25 μg/ml) in order to find the optimal concentration with minimal cell toxicity. The same toxicity assessment was also performed for cytochalasin D (0.1-25 μg/ml) and colchicine (1-25 μg/ml). Cytotoxicity of the inhibitors and nanoparticles toward Calu-3 cells was assessed by MTS cell metabolic activity assay (section 2.2.4). Cytotoxicity of a certain sample at each concentration was assessed in four replicates. Cell viability of greater than 85% was classified as acceptable for uptake and transport assays. Cytotoxicity expressed as a percentage of cell viability, was calculated from the measured absorbance values normalized to the negative control (HBSS, 100% viability) and taking into account the correction for the positive control (Triton-X, 0% viability).

4.2.7 Basolateral medium analysis: Transmission Electron Microscope (TEM)

After incubation of cell monolayers with folate and non folate-modified NPs solution at 37 °C, basolateral medium was collected. One drop of sample was placed onto the copper grid and allowed to dry in air. The samples were negatively stained

with 3% phosphotungstic acid solution and investigated using transmission electron microscope (Jeol JEM 1010 Electron Microscope, Japan).

4.2.8 Confocal Microscopy

Samples were prepared for confocal microscopy analysis as described in section 2.2.5.2 and visualized using Zeiss LSM 510 confocal system.

4.3 Results

4.3.1 Preparation of NPs systems

Particle size distribution graphs for FA-OVA and OVA decorated nanoparticles as determined by dynamic light scattering (DLS) are shown in Figure 4.3. Data reveals that there is no significant difference in term of particle size between OVA-FA and OVA modified nanoparticles. The mean hydrodynamic particle radius and distribution for all nanoparticles systems, surface decorated with unconjugated (Figure 4.3 B) and those decorated with FA-conjugated OVA (Figure 4.3 C) ranged between 62-66 nm.

For uncoated NPs, the most prominent of the population has radius of approximately 17.9 nm (>98%).

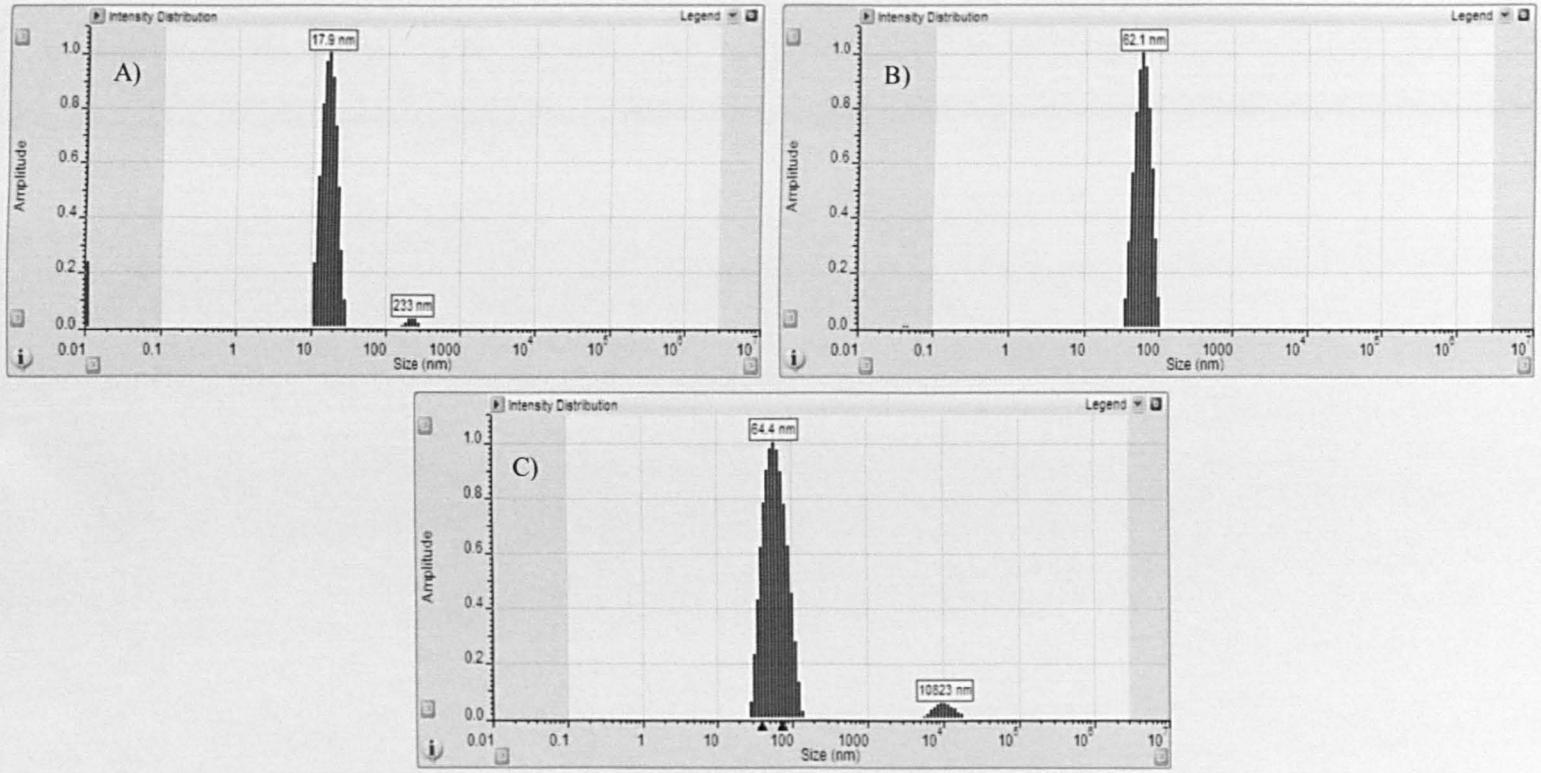

Key	Nanoparticle type	Average hydrodynamic radius (nm) ± SD
A	Unmodified	17.9 ± 4.5
B	OVA modified	62.1 ± 11.7
C	FA-OVA modified	64.4 ±2.1

Figure 4.3 *Particle size distribution for unmodified (A), OVA-FA-modified (b) and OVA-modified NPs (c) by Dynamic Light Scattering (DLS). Table shows information on mean sizes (radii). The result represents the mean of ten measurements, performed in HBSS at 25°C.*

4.3.2 MTS cell toxicity assay

4.3.2.1 Effect of NPs on Calu-3 metabolic activity: MTS Assay

Figure 4.4 demonstrates that the tested NPs and OVA-FA comjugate showed no significant reduction in Calu-3 metabolic activity at tested concentrations, as measured by the MTS assay.

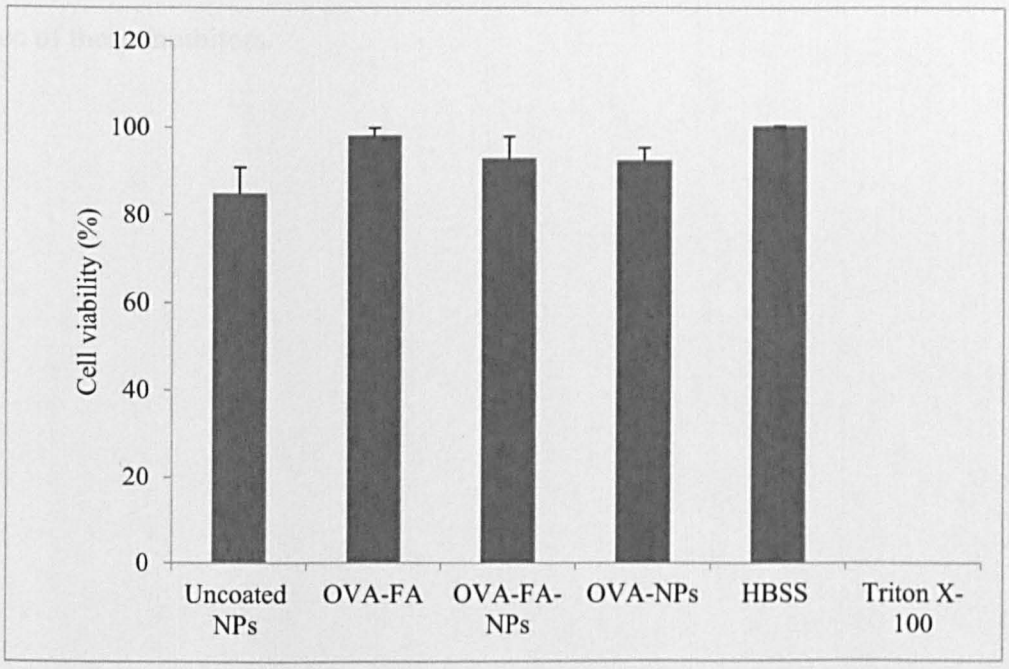

Figure 4.4 *Effect of NPs and OVA-FA conjugate on Calu-3 metabolic activity, as determined by the MTS assay. Uncoated NP, OVA-FA and OVA modified NPs and OVA-FA conjugate were applied to cells at concentrations of 1.69 x 10^{13} and OVA-FA at concentration of 0.5mg/ml. HBSS and Triton-X were used as negative and positive controls respectively. Data expressed as relative cell metabolic activity and presented as the mean ± SD (n=4).*

OVA-FA conjugate (98%) and coated NPs (92%) showed higher cell viability compared to naked particles (85%).

4.3.2.2Effect of endocytic inhibitors on Calu-3 metabolic activity: MTS Assay

Five different inhibitors acting at the different stages of endocytosis were selected to examine the pathways of cellular uptake and transepithelial transport of folate decorated NPs and non-folate decorated NPs (control). Before conducting the uptake and transport studies, viability of Calu-3 cells in the presence of optimized concentration of these inhibitors during the 4-hour assay was confirmed in the presence of these inhibitors.

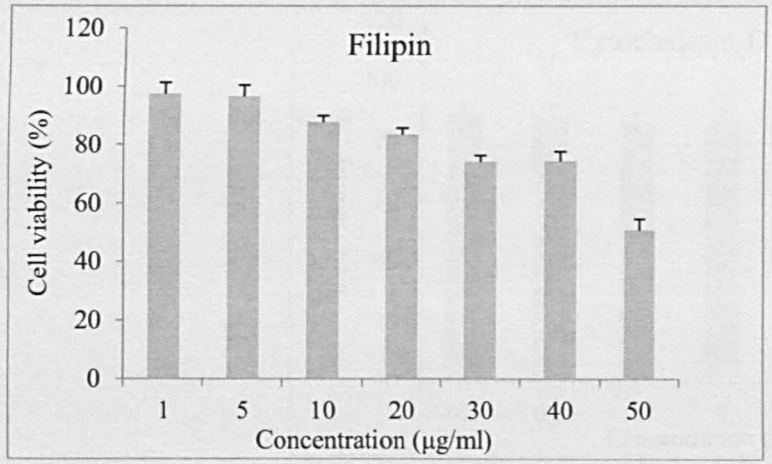
Filipin
Cell viability (%)
120
100
80
60
40
20
0
1
5
10
20
30
40
50
Concentration (µg/ml)

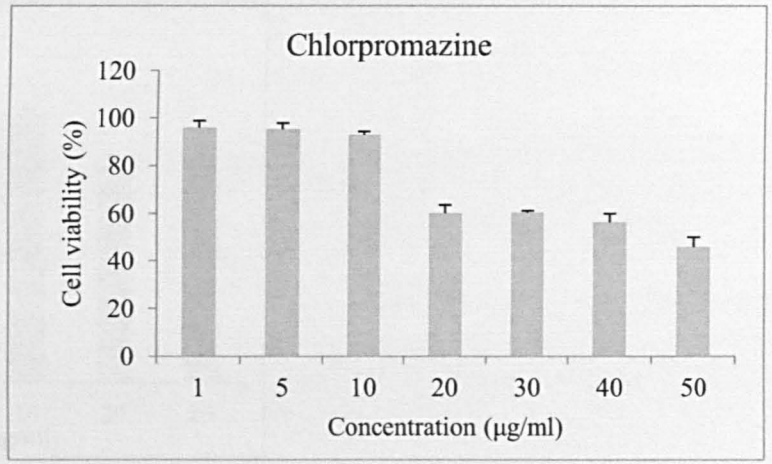
Chlorpromazine
Cell viability (%)
120
100
80
60
40
20
0
1
5
10
20
30
40
50
Concentration (µg/ml)

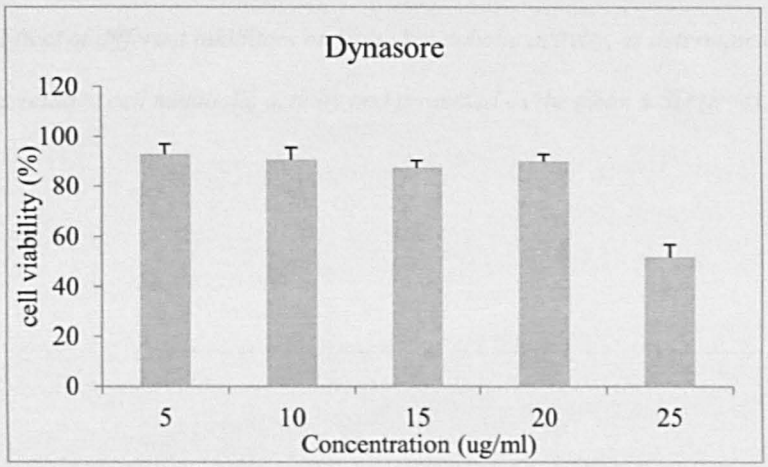
Dynasore
cell viability (%)
120
100
80
60
40
20
0
5
10
15
20
25
Concentration (ug/ml)

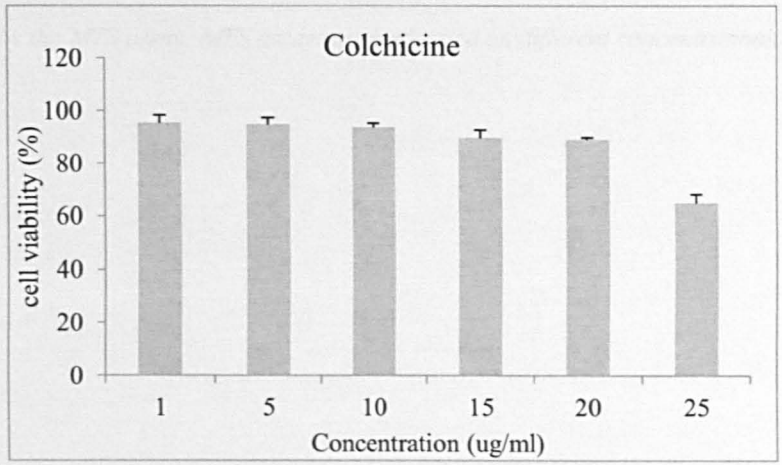
Colchicine
cell viability (%)
120
100
80
60
40
20
0
1
5
10
15
20
25
Concentration (ug/ml)

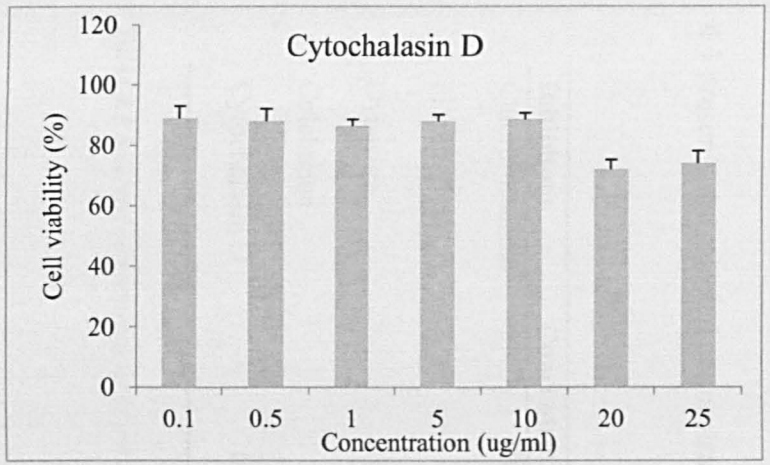

Figure 4.5 *Effect of different inhibitors on Calu-3 metabolic activity, as determined by the MTS assay. MTS assay was performed on different concentrations. Data expressed as relative cell metabolic activity and presented as the mean ± SD (n=4).*

Data in Figure 4.5 showed that chlorpromazine caused cytotoxicity at the concentrations above 20 μg/ml with significant reduction in cell viability (65 %). Calu-3 cells were relatively insensitive to exposure to concentration less than < 20 μg/ml of filipin but decreased viability was seen at higher concentrations and cell viability was reduced to 48 % when 50 μg/ml was applied on cell layers.

Dynasore and colchicine exhibited no cytotoxicity to calu-3 cells in the concentration range tested except at the highest 25 μg/ml point. Cytochalasin D also did not demonstrate considerable toxicity at any of the tested concentrations. Table 4.1 presents the selected concentration of inhibitors for this work.

Inhibitors	Concentration(μg/ml)	Concentration(μM)	%Cell viability
Chlorpromazine	10	28	95
Filipin	5	7	96.45
Dynasore	10	30	90.76
Colchicine	5	12	95
Cytochalasin D	10	20	88.5

Table 4.1 *Selected concentrations of inhibitors.*

4.3.3 Filipin and chlorpromazine effect on Cholera toxin B and transferrin cellular uptake

Cellular uptake of transferrin and cholera toxin B, which are known to selectively enter cells via clathrin [27] and caveolae [28, 29] mediated endocytosis pathways respectively [23], were used as controls to confirm specificity of the inhibitory function of selected concentrations of chlorpromazine and filipin.

As shown in Figure 4.8 treatments with chlorpromazine resulted in a significant inhibition of transferrin uptake (70% decrease, $P<0.001$) in the Calu-3 cells. Treatment with filipin also resulted in 50% reduction of cholera toxin B uptake ($P<0.001$) thus confirming the applied inhibition protocol.

It is noteworthy that a large fraction of cholera toxin B can be endocytosed by clathrin-dependent as well as by caveolae- and clathrin-independent endocytosis in different cell types [28] so inhibition of the caveolae mediated pathway led to only a 50 % decrease in the toxin uptake in Calu-3 cell layer. However lack of specific controls for each of the distinct endocytic pathways leaves no other options.

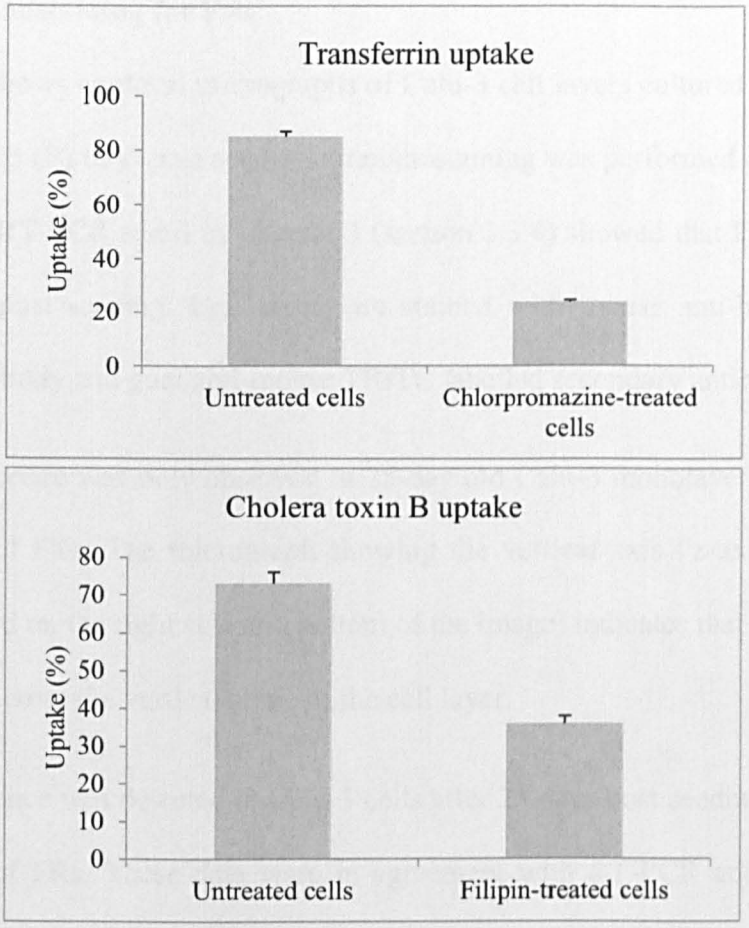

Figure 4.6 *Effect of chlorpromazine and filipin treatment on internalization of transferrin and cholera toxin B into Calu-3 cells. Cells were pre-treated with chlorpromazine and filipin for 1 hour, followed by 3 hours of exposure to Alexa fluor labelled transferrin and cholera toxin B in the presence of inhibitor. Uptake expressed as % of the amount applied apically (5 nM).*

4.3.4 Immunostaining for FRs

Figure 4.7 shows confocal micrographs of Calu-3 cell layers cultured on filters after 25 (A) and 23 (B) days post seeding. Immunostaining was performed on days 23 and 25 because RT-PCR result in Chapter 3 (section 3.3.4) showed that FR is expressed on day 24 post seeding. Cell layers are stained with mouse anti-human FOLR1 primary antibody and goat anti-mouse TRITC labelled secondary antibody.

Red fluorescence was only observed in 25-day old Calu-3 monolayer indicating the expression of FRs. The micrograph showing the vertical axis ('z-axis') of the cell layer (located on the right side and bottom of the image) indicates that the receptor is distributed across the vertical plane of the cell layer.

No fluorescence was detected in Calu-3 cells after 23 days post seeding revealing no expression of FRs. These data were in agreement with RT-PCR and western blot result discussed in chapter 3 (3.3.4 and 3.3.5). In control cells where incubation with the primary antibody was omitted (i.e. cells were exposed to goat anti-mouse TRITC labelled secondary antibody only) no red fluorescence was detected (Figure 4.7 C) indicating that the fluorescence signal in the cell layer in Figure 4.7 A is not present due to non-specific secondary antibody binding.

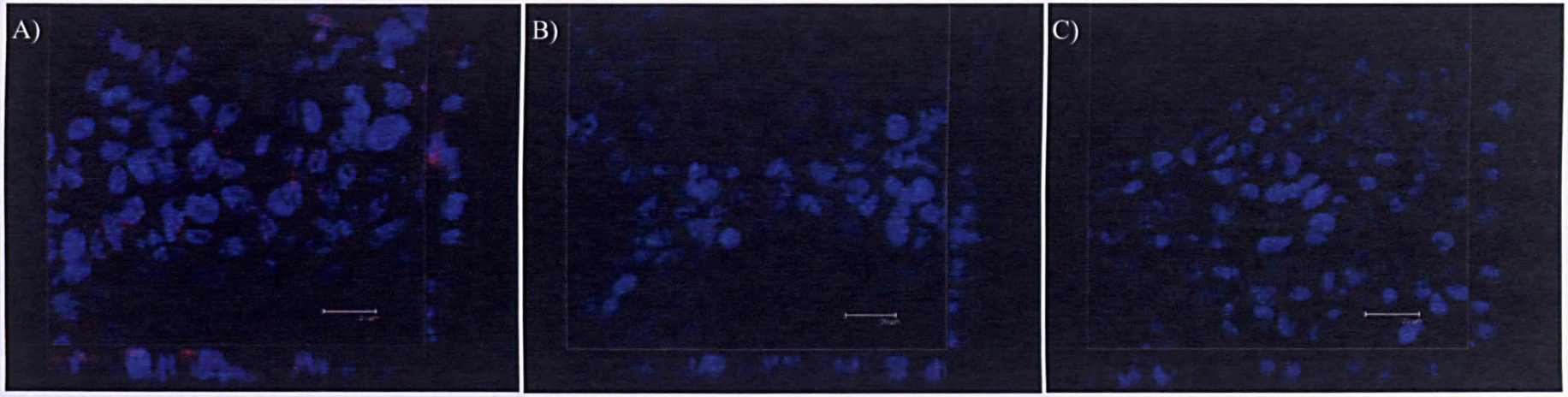

Figure 4.7 *Immunostaining for folate receptor in filter-cultured Calu-3 after A) 25-day old and B) 23-day old cells. Samples were incubated with mouse, anti-human FOLR1 primary antibody and goat, anti-mouse TRITC-labelled secondary antibody. Control cells Calu-3 C) incubated with goat, anti-mouse TRITC-labelled secondary antibody only. Three dimensional image of Calu-3 cell layer is shown vertical ('z-axis') on the bottom and the right hand side. (Scale bar: 20μm).*

4.3.5 Cell uptake of folate and non-folate modified NPs at 37°C and 4°C

In order to determine whether NP uptake was an active or passive process, cell cultures were incubated in parallel at 37°C (normal cell culture conditions) and at 4°C (Figure 4.8). It is known that several proteins and enzymes are sensitive to temperature, thus active processes are mainly inhibited at lowered temperatures [32].

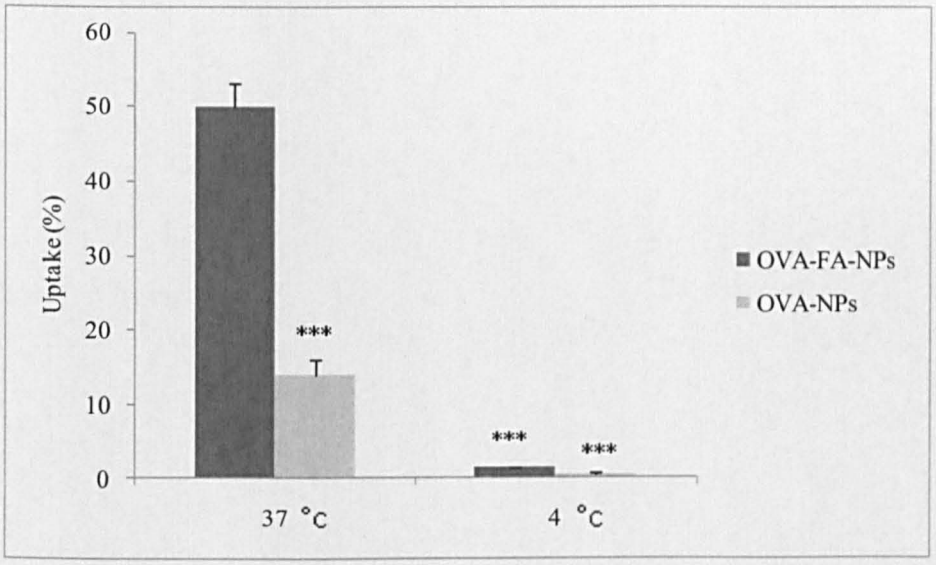

Figure 4.8 *Effect of temperature on cell uptake of OVA-FA-NPs and OVA-NPs. Cells were incubated with samples for 4 hours. Uptake expressed as % of the amount applied apically (1.69x10 ^{13}NPs).One way analysis of variance (ANOVA) with Bonferroni post-hoc test was used. Error bar represents mean ± standard deviation (n=3).*

Data showed that at 37°C experimental conditions, 50% of folate-modified nanoparticles applied on the apical side of the monolayers were internalized by cells and this was reduced to 14% for OVA-modified nanoparticles ($P<0.001$). This strongly suggests an involvement of folate-mediated pathway of nanoparticle uptake.

On the other hand, Exposure to NPs at 4°C resulted, as expected, in a very strong suppression of endocytosis of both nanoparticle systems (FA-OVA-NPs and OVA-

NPs) by approximately 96%; this significant decrease of uptake ($P<0.001$) at 4°C compared to 37 °C suggested a predominantly active endocytic mechanism for internalization of NPs [33]. It should be noted that to discriminate between cell-association and actual internalization, extracellular fluorescence was quenched by addition of Trypan Blue, the non-quenched fraction thus representing internalized beads [34].

4.3.6 Cell uptake of folate and non-folate in the presence of different inhibitors

To investigate the pathway of internalization of folate-modified nanoparticles this section of the project examined the effects of five different inhibitors on the cellular uptake; filipin; caveolae-mediated endocytosis inhibitor, chlorpromazine; clathrin-mediated endocytosis inhibitor [35], colchicine, microtubule inhibitor, cytochalasin D, microfilament inhibitor and dynasore; dynamin inhibitor [36] (Figure 4.9).

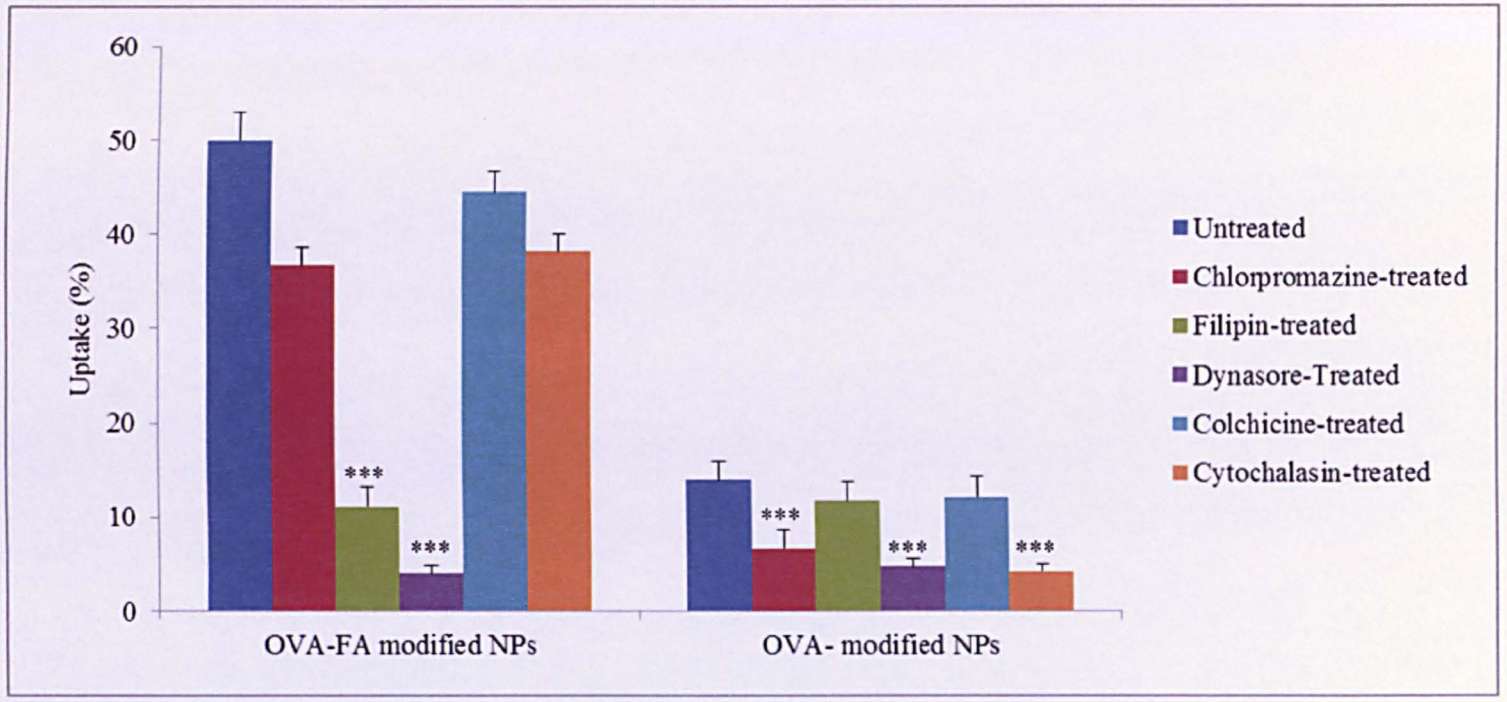

Figure 4.9 *Cellular uptake study of OVA-FA-NPs and OVA-NPs in the presence of different inhibitor of endocytosis. Inhibitors were applied on cell layers 1 hour prior the application of NPs at the optimized concentrations (section 4.3.2.2). Uptake expressed as % of the applied dose apically (1.69x10 ^{13}NPs).One way analysis of variance (ANOVA) with Bonferroni post-hoc test was used. Error bar represents mean ± standard deviation (n=3)*

In the case of folate-modified nanoparticle, in filipin treated cells there was a 75% reduction ($P<0.001$) in the uptake, while in the chlorpromazine treatment resulted in only a 22% reduction, compared with non-inhibited cellular uptake (Figure 4.9). These data hence strongly suggested that the folate-modified nanoparticles are mainly internalized by the caveolar pathway. In parallel, the data showed that uptake of non-folate nanoparticles is mainly mediated by the clathrin pathway, as indicated by a 53% ($P<0.001$) reduction in chlorpromazine treated cells.

The inhibition of dynamin by dynasore (Figure 4.9) reduced the internalization of OVA-FA-NPs to 92% compared with non-inhibited cellular uptake. In contrast, internalization of OVA-NPs was decreased by 66% by dynasore which was significant ($P<0.001$) reduction, but implied the possible involvement of dynamin-independent pathways for uptake of OVA-NPs.

Folate and non folate-modified NPs showed no significant reduction (11 % and 13 % respectively) in uptake in the presence of colchicine, a chemical inhibitor of microtubule (Figure 4.9).

Because exocytosis and endocytosis are controlled by the actin cytoskeleton, actin-disrupting agent cytochalasin D was tested to determine their effect on NPs internalization. Disruption of the actin cytoskeleton resulted in a significant decrease (63%) in OVA-NPs but not OVA-FA-NPs (23%) internalization (Figure 4.9).

4.3.7 Confocal microscopy analysis

The intracellular localizations of nanoparticles in Calu-3 cells were examined by confocal microscopy. It should be noted that extracellular fluorescence was quenched by washing the cell layers with Trypan Blue solution, as described in section 3.2.8

4.3.7.1 Cell uptake of folate-modified NPs at 37°C and 4°C

Figure 4.10 shows confocal micrographs of Calu-3 cells (as confluent filter-cultured layers) incubated with OVA-FA-NPs at 37°C and 4°C. The micrographs reveal the presence of green fluorescence (green channel) resulting from FITC labelled NPs and blue fluorescence (blue channel) from cell nuclei stained with DAPI.

Strong internal cell fluorescence was found for folate decorated NPs at 37°C (A, C) and no fluorescence was observed in cell layer at 4°C (B) indicating the significant internalization at 37°C and no uptake at 4°C.

The gallery of pictures in Figure 4.11 depicts the presence of OVA-FA-NPs in Calu-3 cell layer at 37°C demonstrating the folate-modified uptake is ubiquitous in the cells from apical to basolateral side.

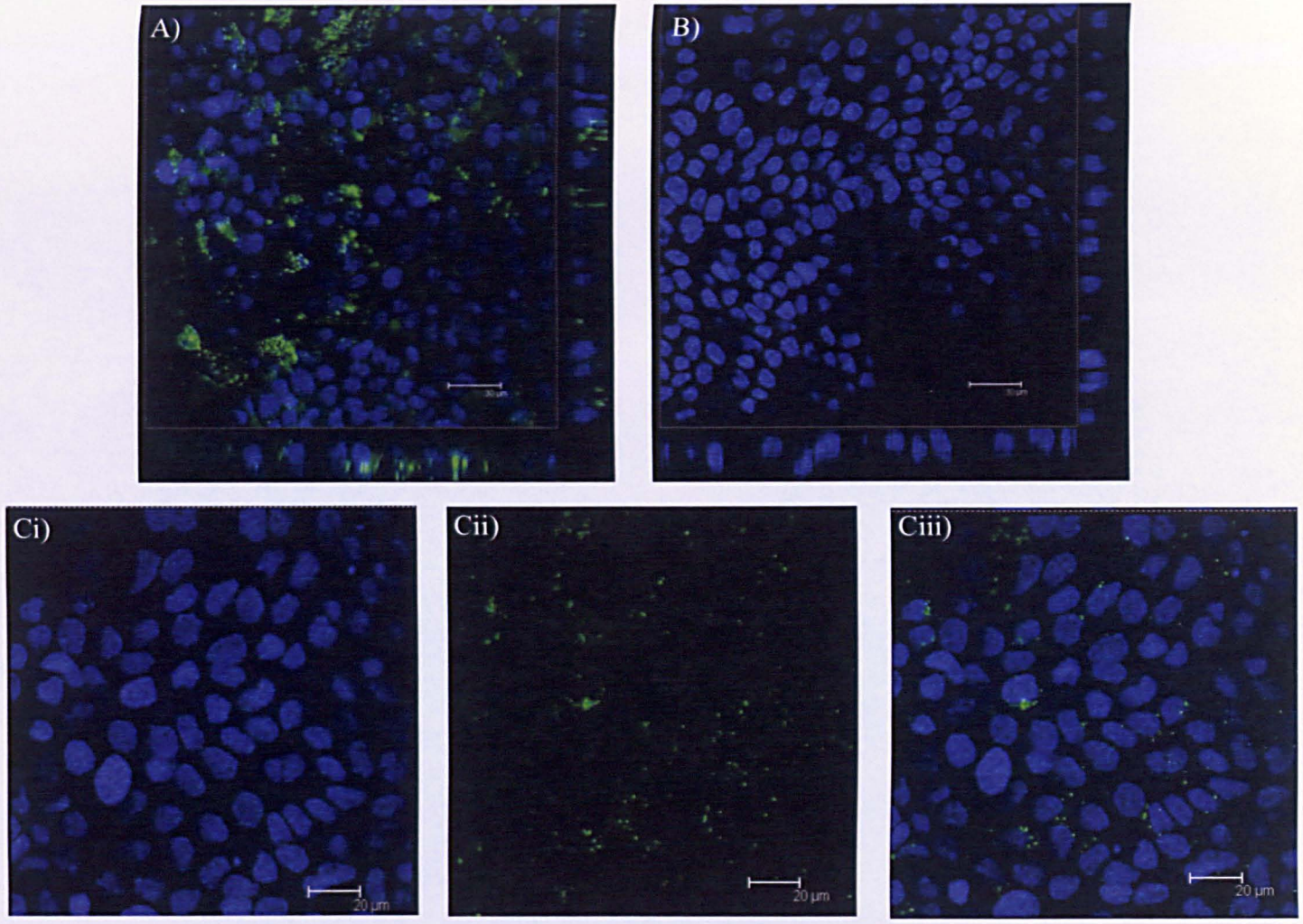

Figure 4.10 *Uptake study of OVA-FA-NPs at 37°C (A &C) and 4°C (B). Three dimensional images (A & B) showing vertical axis ('z-axis') of cell layers (right hand side and bottom of the micrograph). Blue channel (Ci): cell nuclei stained with DAPI, green channel (Cii): FITC labelled folate modified NPs and Overlay image (Ciii).*

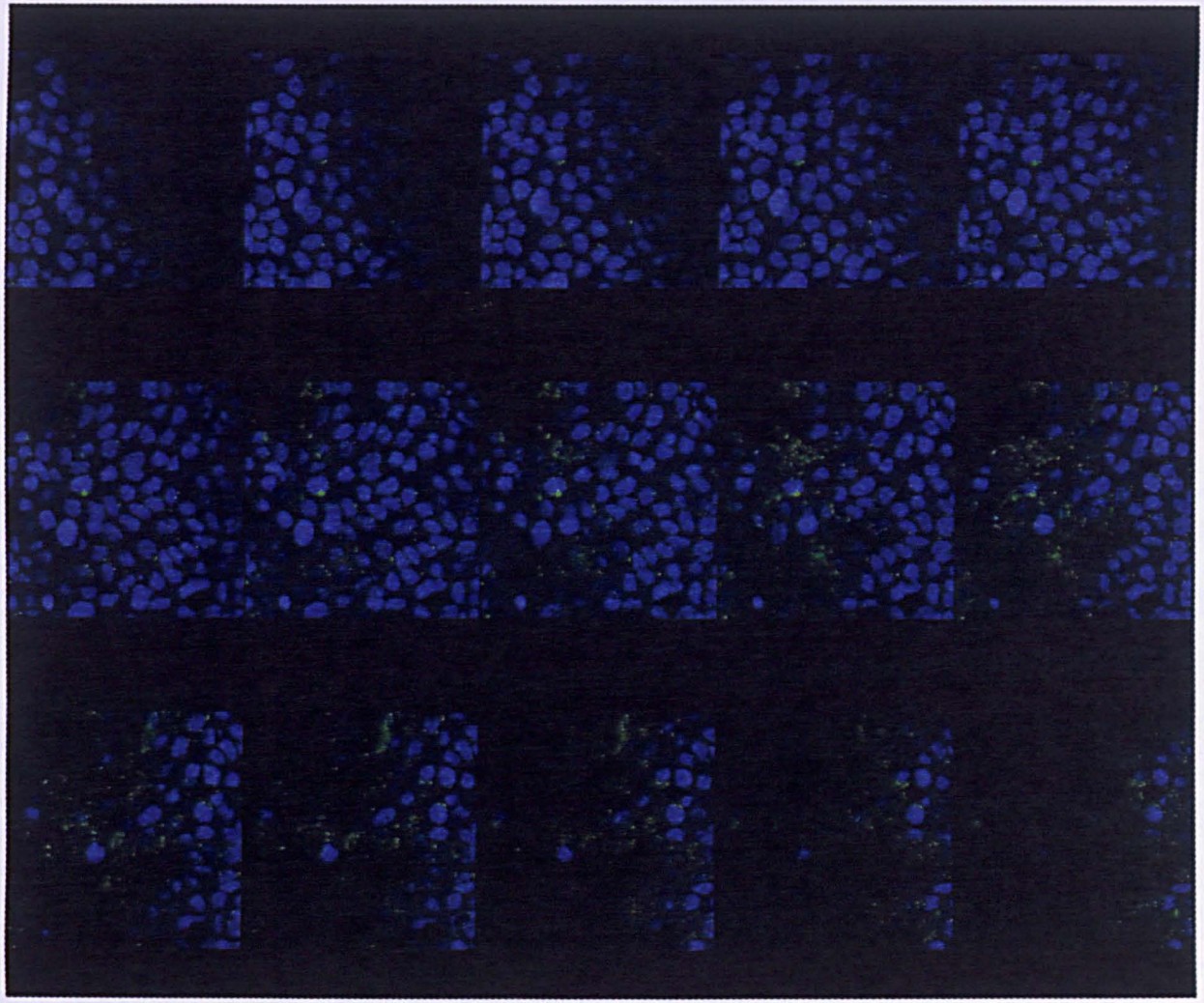

Figure 4.11 *Image represents a gallery of cross sections (from the apical surface to basolateral) of cellular uptake of OVA-FA-NPs in Calu-3 cell layer.*

4.3.7.2 Cell uptake of folate-modified NPs in the presence of inhibitors

Figure 4.12 and 4.13 show uptake of green folate-modified NPs in the absence and presence of inhibitors including filipin (4.12 Bi and Bii), dynamin (4.13 Ai and Aii) and cytochalasin D (4.13 Bi and Bii) in comparison to untreated cell layer (4.12 Ai and Aii).

It is clear from the micrographs that following treatment with filipin (4.12 B), the internalization rate was significantly inhibited; the fluorescence in caveolar inhibited cells was considerably weaker than the fluorescence observed in untreated cells (4.12 A).

Furthermore, folate-modified NPs were only seen in the apical side of the cells (4.13 A, right hand side and bottom of the micrograph) in dynasore-treated cells. It indicated that inhibition of dynamin, which is principally involved in the scission of newly formed vesicles from the cell membrane, resulted in localization of NPs in apical surface and significant inhibition of NPs internalization.

On the other hand, disruption of actin by cytochalasin D (Figure 4.13 B) showed no significant reduction in NPs endocytosis as punctate fluorescence was observed within the cells, at the level above and below the TJs.

Note that findings of the quantitative studies presented in sections 4.3.5 and 4.3.6 were in agreement with the data qualitative data obtained by confocal microscope.

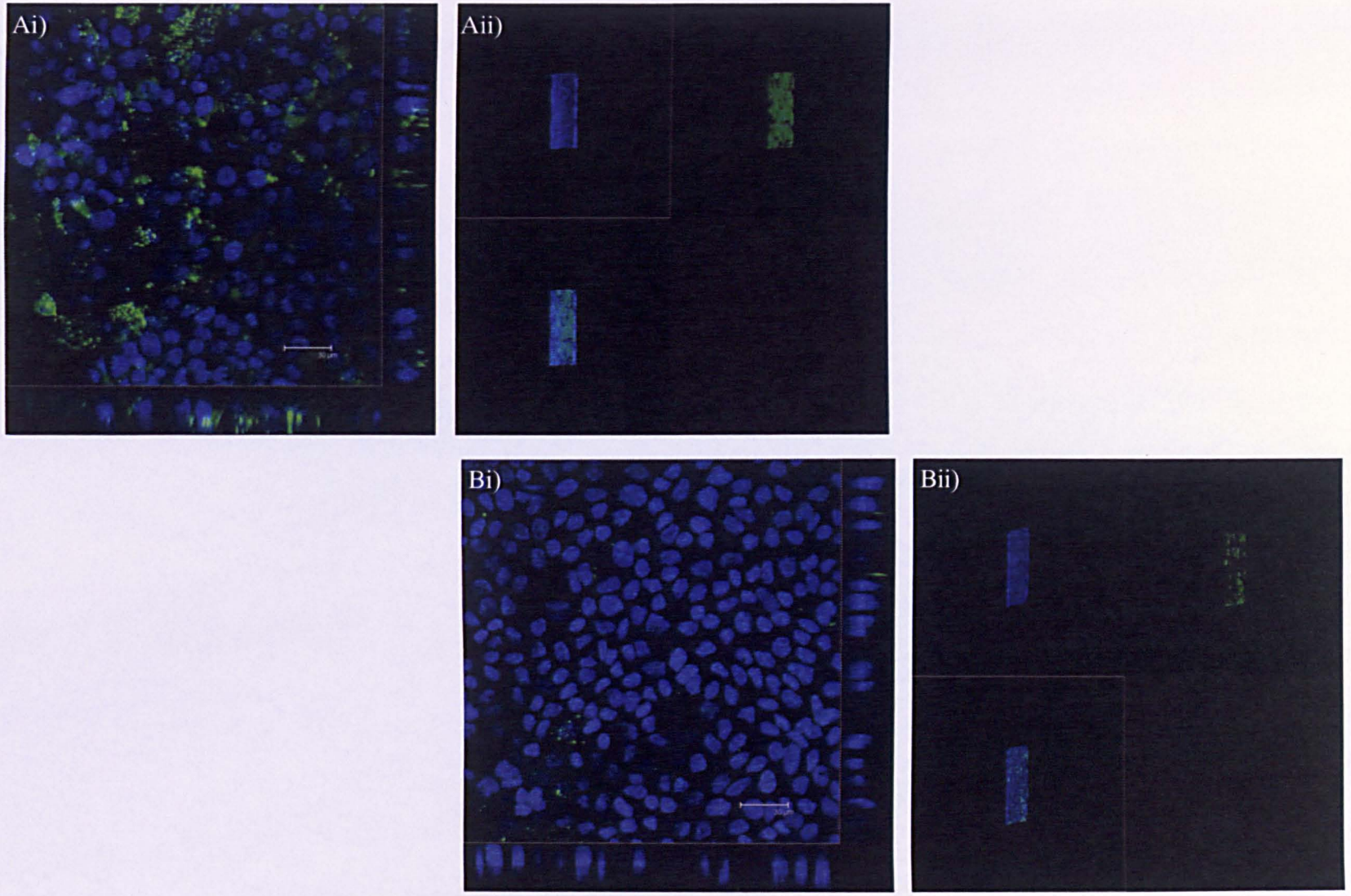

Figure 4.12 *Different three dimensional images of endocytosis of OVA-FA-NPs at 37°C in untreated (Ai & Aii) and filipin-treated (Bi & Bii) Calu-3 cell layers.*

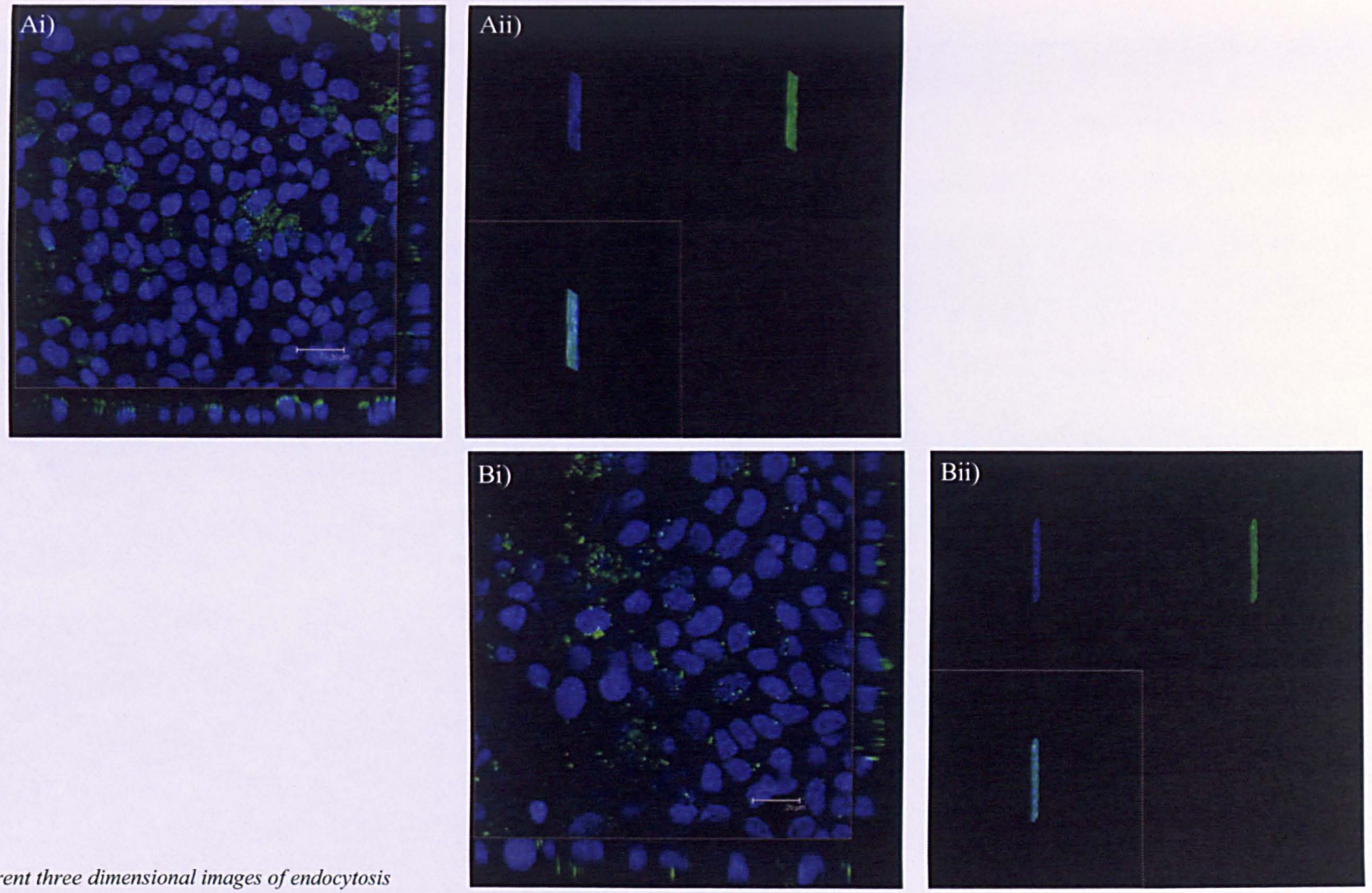

Figure 4.13 *Different three dimensional images of endocytosis of OVA-FA-NPs at 37°C in dynasore-treated (Ai & Aii) and cytochalasin D-treated (Bi & Bii) Calu-3 cell layers.*

4.3.8 Effect of temperature on transcellular transport of folate-modified NPs

Calu-3 layers used in this study had TEER values of 1270-1370 $\Omega.cm^2$ before and 950-1200 $\Omega.cm^2$ after the transport experiments; this indicated no significant changes in the TEER values during these experiments. Cell-culture inserts without cells were not found to be a significant barrier for the permeation of NPs.

Figure 4.14 shows the NPs percentage present in the basolateral solution at different temperature following their addition on the apical surface of the layers ($1.69x10^{13}$ NPs). Data revealed that approximately 4.2 % of applied folate-modified nanoparticles were transported across the monolayer at 37 °C while no transport was observed for OVA-NPs at this temperature ($P<0.001$) suggesting the involvement of folate-mediated path way for NPs transport. Data also proved that simple attachment of folate is able to change the faith of the cargo.

No measurable amount of NP was transported across cell layer for both folate and non-folate systems when the temperature was decreased to 4°C which further confirmed the involvement of predominant active endocytic/exocytic mechanism.

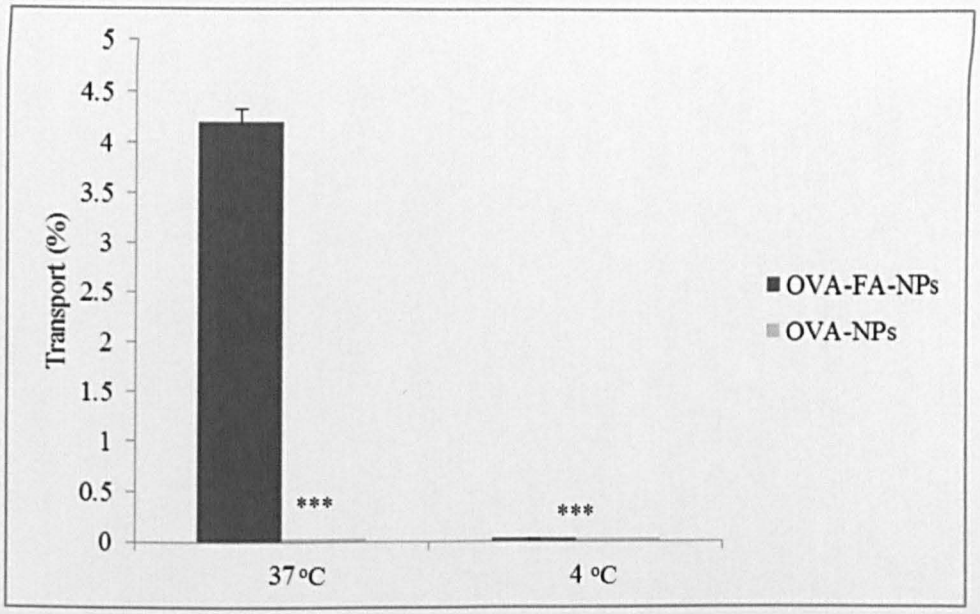

Figure 4.14 *Effect of temperature on cell transport of OVA-FA-NPs and OVA-NPs. Cells were incubated with samples for 4 hours. Transport expressed as % of the amount applied apically (1.69x10 ^{13}NPs).One way analysis of variance (ANOVA) with Bonferroni post-hoc test was used. Error bar represents mean ± standard deviation (n=3).*

4.3.9 Transport study of folate modified NPs in the presence of inhibitors

The transport of folate-modified nanoparticles across Calu-3 layers was examined in the presence of inhibitors as described in section 4.2.5. Cumulative number of folate modified NPs transported across the layers and present in the basolateral solution in the absence and presence of filipin, chlorpromazine and dynasore inhibitors and is depicted in Figure 4.15.

The data indicate that transport of the folate modified NPs indeed occurs (4.2 % of applied dose). Apical-to-basolateral movement occurred faster in the first 2 hours and reached a sustained rate by 4 hours (very similar pattern to FA-OVA-FITC conjugate transport described in Chapter 3).

A significant difference in terms of transport was observed between the untreated and filipin and dynasore-treated cells layers. In fact, the transport was absent in caveolae and dynamin inhibited cells, whilst clathrin inhibition showed no significant decrease in particle transport (1% reduction). It strongly suggested the involvement of caveolae-mediated pathway in the transport of folate-modified NPs and also the important role of dynamin in caveolae-mediated endocytic processes.

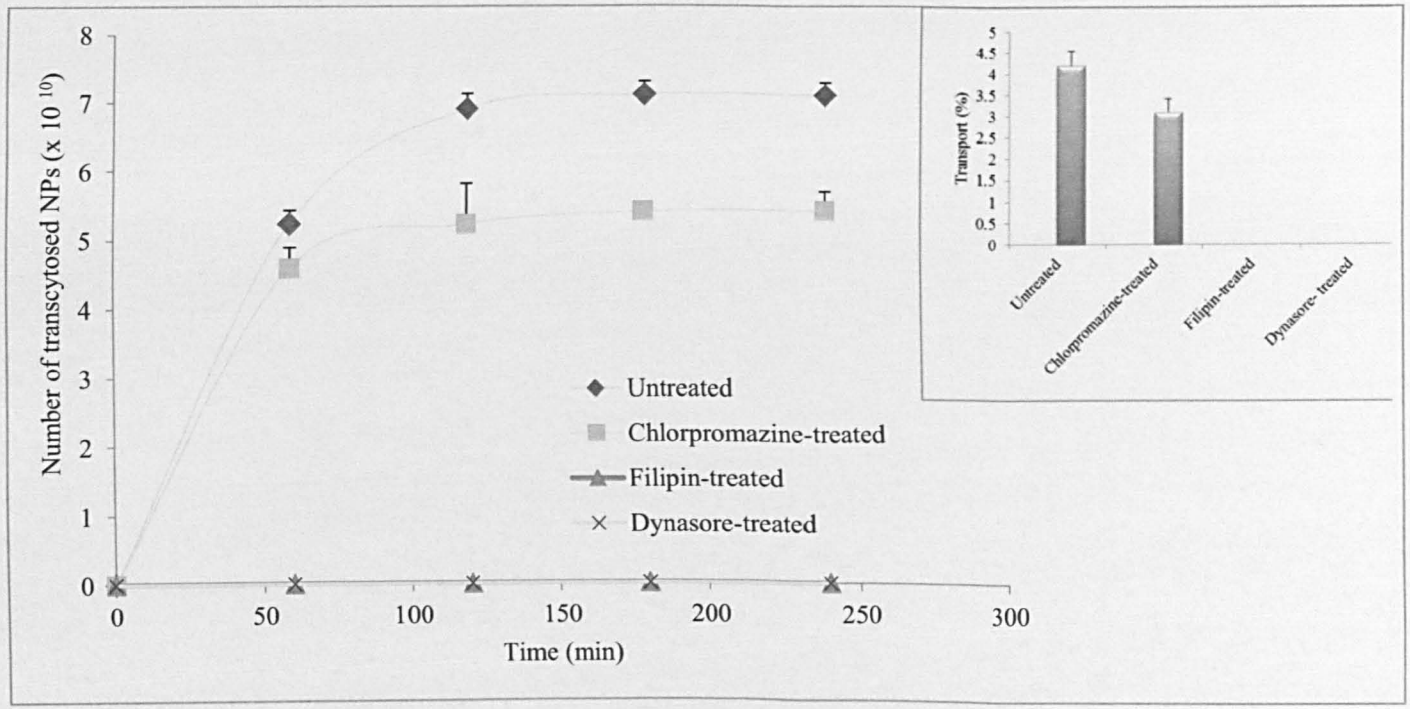

Figure 4.15 *Transport study (in apical to basolateral direction) showing the cumulative number of OVA-FA-NPs transported in four hours experiment in the presence of endocytosis inhibitors. Samples (100µl) were taken every hour from basolateral side and apical-to-basolateral translocation assessed by measuring fluorescence. One way analysis of variance (ANOVA) with Bonferroni post-hoc test was used. Error bar represents mean ± standard deviation (n=3). Small graph (top right) presents the same data expressed as % of apically applied dose.*

Figure 4.16 shows the pattern in basolateral number of folate-modified NPs following their application to the cell layers in the presence of colchicine (tubulin inhibitor) and cytochalasin-D (actin inhibitor).

Data showed that the transport level increased with time in the presence of these two inhibitors (from 7.1 $x10^{10}$ to 12.34 $x10^{10}$ in the presence of colchicine ($P<0.01$) and from 7.1 $x10^{10}$ to10.27 $x10^{10}$ ($P<0.05$) in the presence of cytochalasin D). NP transport in the actin and tubulin inhibited cells showed an initial delay compared to untreated cell layers but at later times, increased transport was observed for treated cell layers relative to untreated ones.

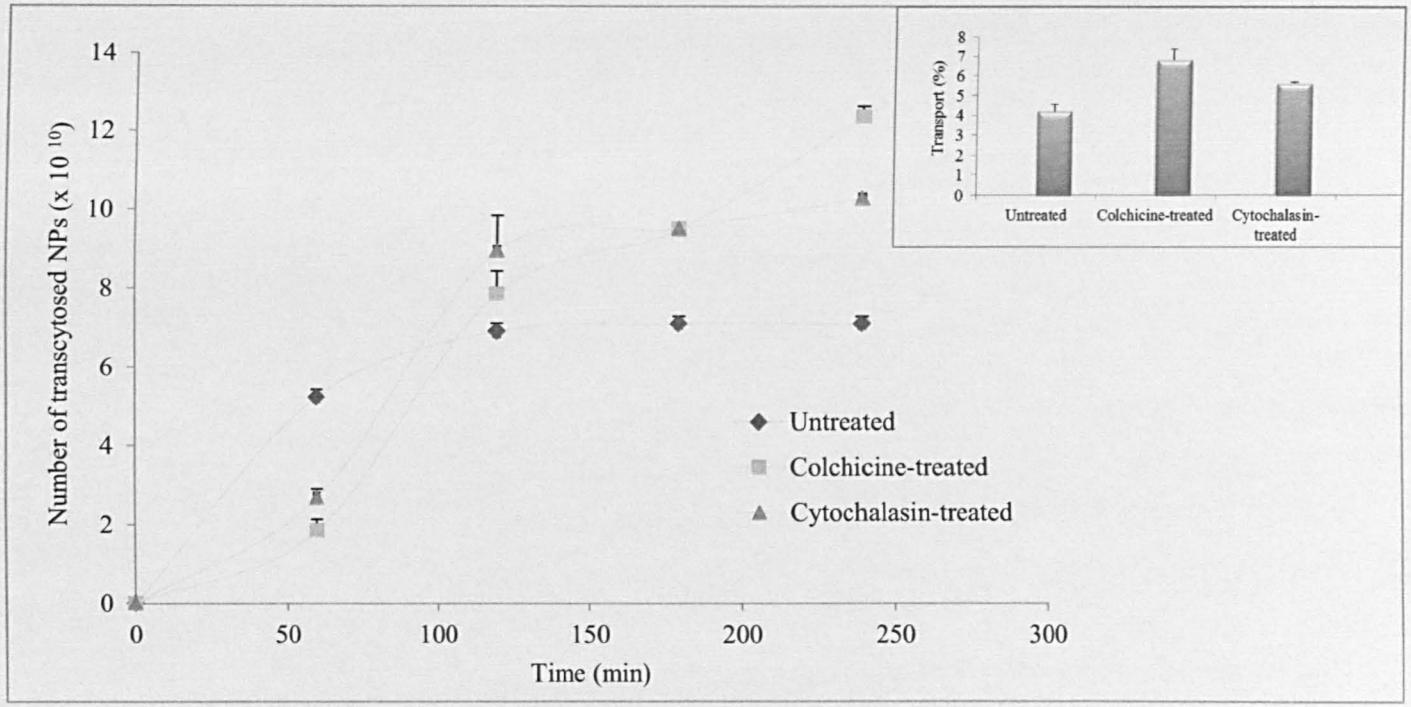

Figure 4.16 *Transport study (in apical to basolateral direction) showing the cumulative number of OVA-FA-NPs transported in four hours experiment in the presence of endocytosis inhibitors. Samples (100µl) were taken every hour from basolateral side and apical-to-basolateral translocation assessed by measuring fluorescence. One way analysis of variance (ANOVA) with Bonferroni post-hoc test was used. Error bar represents mean ± standard deviation (n=3). Small graph (top right) presents the same data expressed as % of apically applied dose.*

4.3.10 Basolateral medium analysis by TEM

The samples from apical and basolateral medium were observed by TEM following a 4h of incubation with OVA-FA-NPs and OVA-NPs (control). As illustrated in Figure 4.17, in apical side, particles with size ~120 nm and some material fragments (more in OVA-FA-NPs solution) were observed. In the basolateral, samples (after transport experiment), species with size and appearance similar to OVA-FA were observed in the OVA-FA-NP experiment, but no such species were found in the control OVA-NP basolateral samples.

This result suggested transcellular transport of NPs only happened for folate modified NPs which would be in agreement with the quantitative data presented in 4.3.8.

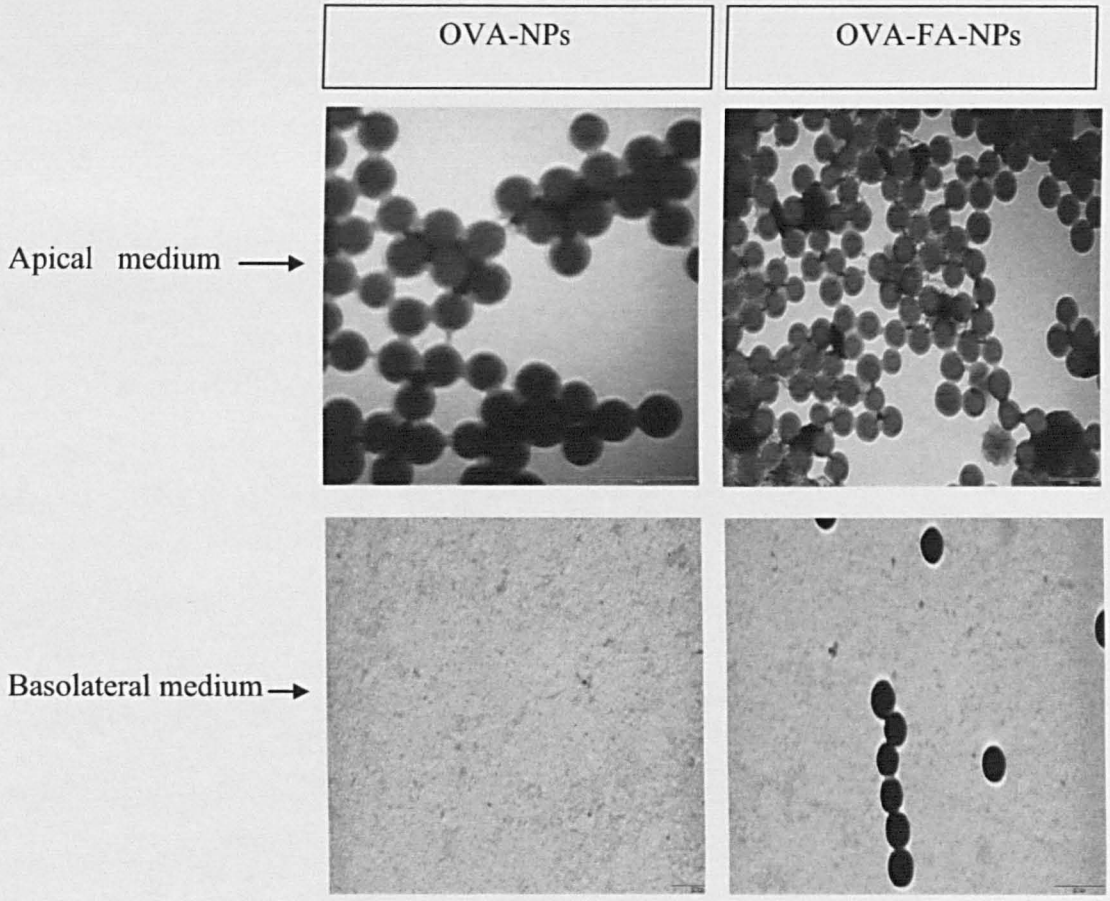

Figure 4.17 *Transmission electronic microscopy images of apical and basolateral media of Calu-3 cells incubated with blank OVA-FA-NPs and OVA-NPs in HBSS for 4 h at 37 °C. (Scale bar: 200nm)*

4.4 Discussion

With interest in nanotechnology rising, it should not be surprising that many studies on uptake of folate-surface modified nanoparticles have been recently undertaken [37-44] but data on folate modified NPs transport across the epithelial cell layers have not yet, to the best of our knowledge, been reported. Work detailed in this chapter hence investigated the potential of the folate-mediated pathway for delivery of folate modified NPs across the epithelium, as a potential drug carrier system for mucosal administration.

To this end, we formulated folate-modified nanoparticles (~120 nm) to investigate the folate mediated endocytosis and transport across polarised Clue-3 cell layer, as an in-vitro epithelial model shown in previous Chapter (Chapter 3) to expresses the FRs in day 24 post seeding.

Polystyrene NPs used in this story, are widely used as a model nano-carrier and reference particles to study cellular uptake [45, 46], in *in-vitro* [47-49] and *in-vivo* studies [50]. They are also commercially available in different sizes, different surface modifications and fluorophores (allowing imaging and quantification).

OVA-FA was not chemically conjugated to the NPs; it was instead physically adsorbed on the NP surface, taking advantage of ovalbumin's ability to adsorb almost irreversibly onto the surface of polystyrene NPs [51].

Characterisation of OVA-FA and OVA-modified NPs for their size by dynamic light scattering (DLS) revealed that the mean hydrodynamic particle radius for both nanoparticle systems, surface modified with OVA (Figure 4.3 B) and those modified with FA-OVA (Figure 4.3 C) ranged between 62-64 nm, indicating no significant

differences in the particle size between OVA-FA modified and OVA modified nanoparticles that could potentially affect their cellular internalization behaviour.

Unmodified nanoparticles displayed a mean hydrodynamic particle radius of 17.9 nm (Figure 4.3 A), indicating the formation of an adsorbed layer in the order of 44-48 nm, considerably larger than that would be expected from adsorption of a monolayer of ovalbumin (molecular dimensions of 7x4.5x5 nm [52]). Such behaviour would be in agreement with previous studies on ovalbumin adsorption onto the latex surface in which ovalbumin adsorption occurs in excess of the quantity required to produce coverage of the surface and where multilayer adsorption behaviour is indicated [53]. In a similar way to hydrophobic sorption of albumin to polystyrene latex, [54, 55] the adsorption of OVA on the surface of polystyrene nanoparticles is expected to be irreversible under the conditions employed, permitting OVA (and hence ligand) association with the nanoparticles during the time course of the experiments.

In the present study the amount of conjugated or unconjugated OVA used *per* surface area of polystyrene nanoparticles (1.7 mg m^{-2}) falls within the higher range of plateau adsorption values reported previously (eg. approximately 1.5 mg m^{-2} [56] and 1.2 mg m^{-2} [57]). It is assumed that molecules immobilized within the surface multilayer would adopt different orientations, including those that permit binding of conjugated folate to the receptor and initiate nanoparticle cellular internalization. By removing excess un-adsorbed ovalbumin (by centrifugation) the possibility that free FA-OVA conjugate in the system compete for the folate receptors with the ligand-bearing nanoparticles is minimised.

Studies on cell toxicity (MTS assay) of OVA-FA, OVA-FA and OVA modified NPs and unmodified NPs towards cells cultured as polarised layers (Figure 4.4) were conducted in addition of assessment of cell layer integrity through measurement of TEER. The tested nanoparticles systems did not show significant reduction in Calu-3 metabolic activity at applied dose ($1.69x10^{13}$ NPs). This result is in agreement with a report by Frohlich [58] showing that polystyrene NPs $\geq$ 40 nm (from 30-500 μm/ml) did not show any indication of cytotoxicity. Another study [59] also confirmed the non-cytotoxicity of polystyrene beads with larger size (0.45 μm, 0.5mg in 100 μl PBS) to murine L929 fibroblasts.

In vitro systems for predicting mucosal drug absorption should ideally be able to model the physiological transport characteristics of the *in vivo* epithelium and provide a reasonable quantitative prediction of drug translocation. The cell culture characterization detailed in chapter 3 (3.3.2 & 3.3.3) confirmed that Calu-3 cell layer cultured on permeable membrane is capable of producing electrically-tight monolayers with low permeability, indicating a formation of tight junction structure. Findings similar to ours [60, 61] have also suggested Calu-3 as an appropriate model for the airway epithelium.

FRs expression in Calu-3 cell layer was shown previously in Chapter 3 (sections 3.3.4 & 3.3.5) and in this chapter; the folate receptor expression was further demonstrated by immunofluorescence which revealed abundant distribution of fluorescence throughout the cell cytoplasm on day 25 post seeding. Interestingly, no fluorescence was apparent in cells cultured on day 23 post seeding indicating the importance of culturing time in expression of FR (as discussed in Chapter 3). Demonstrated expression of folate receptor in investigated Calu-3 cell layer would

be in agreement with previously published reports on its presence in normal and cancerous tissue, including lung [62, 63] (as discussed in Chapter 3).

4.4.1 Uptake study of folate-modified NPs

To assess cellular uptake and transport of folate modified nanoparticles, two different approaches were employed; quantitative analysis of fluorescent-labelled nanoparticles and qualitative assessment using confocal and transmission electron microscopy.

Cellular internalization of 50% of FA-OVA-NPs compared to 14 % of OVA-NPs and significant decrease ($P<0.001$) in uptake of folate-modified NPs at 4°C strongly suggested the involvement of predominantly active folate-mediated endocytosis in cellular internalization of folate-modified nanoparticle. It further confirmed that the attachment of folate promotes cellular uptake of NPs.

There are numerous studies [64-68] confirming that attachment of folate would increase the cellular uptake of NPs *via* folate pathway compared to non-folate NPs. For instance, Zhang [65] visualised the uptake of FITC labelled folate-conjugated bovine serum albumin nanoparticles (BSANPs) (~150n) and BSANPs lacking folate into SKOV3 cell (human ovarian cancer cell line) monolayer by fluorescence microscopy. The absence of FITC fluorescence in the BSANPs lacking folate samples in contrast to the intense fluorescence in the samples containing folate-conjugated BSANPs revealed the dependence of nanoparticle uptake on the conjugation of folate.

Uptake data presented in this work was also in agreement with previous reports that demonstrated particles up to about 100–200 nm could be internalized by a receptor-mediated endocytosis [69, 70].

4.4.2 Transport study of folate-modified NPs

Regarding the potential role of folate-mediated pathway in translocation of material across the polarised cells, there are few reports on transcytosis of folate molecule [1-4] and to the best of our knowledge, there are no studies reported in the literature that investigated potential of the folate mediated transport pathway for cellular uptake and transport of NPs across epithelial cells or mucosal surfaces.

Periodic measurements of NP levels in the basolateral solution (Figure 4.16) following apical administration to Calu-3 cell layers revealed that only folate modified NPs traversed the Calu-3 layers at 37 °C. A pattern of an initial steeper increase in basolateral NPs level, followed by a plateau was typically observed.

Such a trend was also seen for FA-OVA-FITC conjugates (section 3.3.7) and can possibly be attributed to saturation of FR as reported in the literature [71].

The disability of OVA-modified NPs (not containing conjugated folate ligand) in crossing the Calu-3 monolayer again indicated the involvement of folate-mediated path way for NP transport and also proved that simple attachment of folate is able to change the fate of the cargo (will be discussed further).

The basolateral presence of folate-modified NPs was also confirmed by TEM. Only fragments were observed on the basolateral side for OVA-modified NPs (Figure 4.17). This result confirmed the quantitative data and furthermore suggested polystyrene NPs keep their coating after transport as the observed nano-objects in the basolateral and apical chambers have a similar size.

Similar experiments to ours have also been performed by Roger et al [33]. However their analysis revealed that lipid nanocapsules (LNCs) observed at the basolateral side (100-120 nm) were different in size from those observed at the apical side (20-60 nm) after transport across a Caco-2 monolayer.

The nanoparticles translocation across Calu-3 cell layer was also indicated in the confocal microscopy images (Figure 4.11) which show that folate-modified NPs at 37°C were observed uniformly throughout the vertical axis of the cells, including below the level of the TJs and at the level of the Transwell® filter.

4.4.3 Uptake and transport study of folate-modified NPs in the presence of endocytic inhibitors

The internalization and cell trafficking of any cargo can be studied by different methods but all have their limitations. A common method is to use inhibitors that are considered to affect specific cellular uptake mechanisms and also in part this is because they are easy to use [15]. However, there was a big difference in the efficacy and cytotoxicity of the selected inhibitors in the different cell lines. Moreover, they usually lacked specificity for distinct pathways [72]. It is therefore important to fully characterize their effects on any particular cell line before trying to investigate the uptake pathway for any particular nanoparticle that is supposed to enter cells by endocytosis.

To establish a protocol for the use of endocytosis inhibitors for a specific cell type, it is important to assess their *in-vitro* cellular toxicity. This work investigated the viability of Calu-3 cell line after exposure to five frequently used endocytosis inhibitors: chlorpromazine, filipin, dynasore, cytochalasin D and colchicine. All selected concentrations of inhibitors used in this are also frequently selected in the literature for inhibition studies [32, 35, 72-79].

In addition to the cytotoxicity data, this work also evaluated the effect of the inhibitors (filipin and chlorpromazine) on two well-known molecules, transferrin and cholera toxin B which are known to selectively enter cells via clathrin and caveolae mediated endocytosis, respectively. Result presented in section 4.3.3

confirmed the suitability of 10 μg/ml chlorpromazine for inhibition of clathrin mediated endocytosis in Calu-3 cell layer as 70 % reduction in transferrin was observed. Santos *et al* [32] showed inhibition of transferrin endocytosis in HeLa (Human cervix epithelium), A549 (human lung epithelium) and 1321N1 (human glial astrocytoma) for almost 90% by 10 μg/ml chlorpromazine Another study also demonstrated that 10 μg/ml chlorpromazine could supress transferrin internalization for 90-100 % [78].

In this study, cholera toxin B internalization was reduced by 50% in filipin treated cells compared to untreated ones indicating the suitability of 5 μg/ml filipin for inhibition of caveolae mediated endocytosis in Calu-3 cell layer and also the importance of caveolae mediated pathway for cholera toxin B uptake in Calu-3 cell layer. A report by Torgersen [79] has demonstrated that treatment of Caco-2 cells with 5 μg/ml filipin reduced cholera toxin B uptake by less than 20%, suggesting that caveolae do not play a major role in the uptake of cholera toxin B. They concluded that the toxin can be endocytosed by clathrin and caveolae-dependent as well as by clathrin-independent endocytosis in different cell types. On the other hand, findings similar to ours have also been published by Orlandi and Fishman [35, 80] investigating cholera toxin B internalisation pathways in Caco-2 cells. They found that only 33% of surface-bound toxin was internalized by 1 μg/ml filipin-treated cells within 1 h compared with 79% in untreated cells (58% inhibition). They also showed that 10 μg/ml chlorpromazine did not affect toxin internalization. These discrepancies could be the result of different cell lines used in different studies as it has been shown that the effect of endocytosis inhibitors is extremely cell type dependent and treatment with endocytosis inhibitors, which have been applied successfully on one cell line, should not be blindly transferred to other cell lines

without performing the necessary control experiments [72]. Furthermore, it has been shown that expression of caveolae in Calu-3 cells is higher than some tested cell lines such as Caco-2 and Hela [81] which can explain the higher involvement of caveolae in cholera toxin B internalization and also the stronger filipin inhibition in Calu-3 cell layer in this work.

Taking all the aforementioned data together, these results confirmed the suitability and efficiency of selected concentrations of filipin and chlorpromazine for studying the intracellular trafficking of NPs in Calu-3 cell layer.

To investigate the pathway(s) of folate-modified NPs internalization in Calu-3 cells, this work first examined the effect of filipin and chlorpromazine on folate-modified NPs uptake across Calu-3 cell layer.

Data (Figure 4.9) revealed the dominant involvement of caveolae-mediated pathway in internalization of folate-modified nanoparticles which was in line with other reports suggesting FR appears to physically move in and out of the cell using a novel uncoated pit pathway involving caveolae that does not merge with the clathrin-coated pit endocytic machinery [5-9, 82]. It should be noted that all these reports have been undertaken on mostly KB (nasopharyngeal carcinoma), HeLa, MAI04 (monkey kidney epithelial cell line) and Caco2 cell lines and there is no published report on folate internalization pathway on polarised Calu-3 monolayer.

Regarding the folate-modified NPs transport across the calu-3 cell layer, a significant difference was observed in the transport of folate-modified NPs in untreated and filipin treated cell layers. In fact, data presented that transport was absent in caveolae inhibited cells, while clathrin inhibition showed no significant decrease in particle transport (1% reduction). It strongly suggested the involvement of caveolae-mediated pathway in transport of folate-modified NPs.

These observations are explained as follows. Internalised materials are normally transported by the clathrin mediated pathway to endosomes which subsequently fuses with lysosomes where the degradation of the materials takes place [83] so there is no or less chance for transport of NPs in filipin treated cells.

There are some studies [10, 78, 83-85] investigating the caveolar trafficking pathway suggested that materials using caveolae mediated endocytosis avoid the acidic endosomes and lysosomes. After internalization, caveolae-derived vesicles travel to caveosomes, which are distinct from early endosomes in content and pH (neutral pH). In caveosomes, internalized ligands or membrane constituents could reside and would target Golgi apparatus and the endoplasmic reticulum and not lysosomes [86]. Although it is made known that caveolae pathway serve transport functions (including that of the vesicular internalisation of small molecules by the process of potocytosis, and the endocytic and transcytotic movements of macromolecules) by escaping lysosomes but the exact function and interactions of caveolae within the cell are far from fully elucidated [87].

At this point it is worth mentioning that no report was found to investigate the NPs transport and their cell trafficking.

To confirm more the nature of this endocytic route, the present work also assessed the effect of dynamin, a protein that blocks the internalization of both clathrin- and caveolin-coated vesicles [36]. Dynasore was used to block vesicular endocytosis by selectively inhibiting dynamin 1 and dynamin 2 GTPases, which are responsible for vesicle scission during both clathrin- and caveolin-mediated endocytosis [88, 89]. As expected, NPs showed the greatest reduction in uptake (Figure 4.9) in the presence of dynasore. The significant decrease ($P<0.001$) in uptake of folate modified and

control NPs in the presence of dynasore confirmed the endocytosis of NPs by dynamin-dependent pathways. Dynamin inhibition also blocked the folate modified NPs transport across Calu-3 monolayer. It was due to the inhibition of caveolae mediated pathway as discussed above.

Findings similar to ours have also been published by Goldberg [88]. Their work demonstrated that inhibition of dynamin by 50 μM dynasore, strongly reduced the endocytosis and transepithelial transport of Poly (amido amine) dendrimers in Caco-2 polarised monolayer.

The importance of microtubules in the uptake and transport of NPs was investigated in this work. Microtubules are dynamic protein filaments that stretch across cells and provide a mechanical basis for chromosome sorting, cell polarity and organelle localization among other functions. The transport of endocytic contents from early to the late endosomes is dependent on microtubules which also promote fusion and fission of endocytic vesicles [90]. In this study, endocytosis of folate and non folate-modified NPs showed no significant reduction in the presence of colchicine revealing microtubules are not involved in uptake of NPs in Calu-3 cell layer, while transport of folate modified NPs was elevated in colchicine treated cell layer. It is difficult to discuss the reason of these observations at this stage since there are many discrepancies in the literature.

Lin et al [91] synthesised gold NPs with different surface modifications, they noticed that addition of colchicine at 37°C reduced endocytosis of those NPs which were employing the caveolae pathway for their entry in Caco-2 cells. The reduced uptake of NPs resulted in 25–30% increased accumulation of these nanoparticles in the apical layer when compared to the standard 37°C cell assay, indicating strong

contribution of microtubules for the endocytic uptake of NPs under physiological conditions. Their finding was totally in disagreement with ours as endocytosis of FA-OVA-NPs did not decrease in colchicine treated cells in this study.

They [91] also demonstrated that colchicine barely affected the cell uptake and transport behaviour of other coated gold NPs using the clathrin-dependent pathways through Caco-2 cells which were similar to what observed for OVA modified NPs as they were internalized to Calu-3 cell layer through clathrin pathway. Qaddoumi [92] also reported that Nocodazole, a microtubule inhibitor, did not cause any significant reduction in nanoparticle (biodegradable poly (D, L-lactide-co-glycolide) (PLGA)) uptake in Rabbit conjunctival epithelial cells. This is consistent with our study. They concluded that microtubules are involved in vesicle transport and not endocytosis or receptor recycling at the plasma membrane

Kamen [93, 94] also stated similar finding to ours. They confirmed that disrupting microtubules with nocodazole (microtubule inhibitor) had no effect on internalization of 5-methyl [^{3}H] tetrahydrofolate (5-CH3THF) in MA104 cells. They concluded nocodazole could not alter the functional membrane localization of the FR and the initial rate of 5-CH_3THF uptake thus making it unlikely that microtubules are involved in folate-mediated uptake.

Regarding colchicine effect on transport rate, Jevprasesphant [95] showed the effect of colchicine (10 μM) on dendrimer permeation across Caco-2 monolayer. They reported there was no statistically significant difference between apical to basolateral and basolateral to apical transport of dendrimer in the presence or absence of colchicine which was not in line with this work.

One possible explanation for increased transport rate in colchicine treated cells in our study was that since the microtubule is the major contributor to trafficking in the

endosomal / lysosomal pathway, it was logical to suggest that this inhibitor might block the transfer of NPs from the endosomes to the lysosomes, thus preventing degradation of NPs, resulting in an increase in the chance of transport. However, it must be noted that for this hypothesis, further investigation is needed.

Because exocytosis and endocytosis are controlled by filamentous actin, a major component of cytoskeleton, actin disrupting agents cytochalasin D was also tested to determine their effect on FR function and folate mediated endocytosis and transport of NPs in this work.

In this study, disruption of the actin cytoskeleton resulted in a significant decrease of OVA-NPs endocytosis but it did not reduce markedly the internalization of OVA-FA-NPs.

Our observation was not consistent with earlier findings by Qaddoumi [92] and Dausend [96] as they showed treatment of Rabbit conjunctival epithelial cells and HeLa cells with cytochalasin D significantly reduced nanoparticle uptake. Dausend [96] demonstrated that cytochalasin D inhibited the endocytosis of polystyrene nanoparticles (~120 nm) nearly as strongly as cooling to 4 °C, thereby demonstrating that nanoparticle internalization is highly dependent on F-actin.

However, Kamen [93, 94] reported that disruption of the actin cytoskeleton by cytochalasin D and lat B, another actin-disrupting agent, which destroys actin filaments by a different mechanism, reversibly increases the proportion of receptors on the MA104 cell surface and increases the rate of 5-methyl [^{3}H] tetrahydrofolate delivery 2-fold. They reported that increased rate of folate delivery caused by cytochalasin D was not observed in FR-negative cell lines.

So one possible theory for lack of significant reduction of folate modified NPs observed in cytochalasin D treated cell layer in this work is that although

cytochalasin D decreased the endocytosis rate, but at the same time it would increase the number of FRs in the cell membrane and result in higher folate-modified NPs delivery into the cells. On the other hand, significant reduction in OVA-NPs uptake, which was in line with reports mentioned above, confirmed the involvement of actin filament in endocytosis in Calu-3 cell layer.

Our data also presented the transport level increased with time from in the presence of cytochalasin D. Transport in the actin inhibited cells showed the same profile as untreated cell, increasing in first 2 hours and reaching a sustained rate by 4 hours. Unfortunately, there is no report in the literature dealing with the effect of actin disruption on NPs transport. The only possible explanation for increased transport is as mentioned above for colchicine. However, further studies are required to explore the possibility of these strategies.

4.5 Conclusion

Using the Calu-3 epithelial cell model, which is shown to express FR, this work investigated the detailed mechanisms of cellular uptake, intracellular trafficking and transport of folate modified NPs (~120 nm) across Calu-3 cell layer. Various endocytic inhibitors were employed in order to examine the mechanism of cellular uptake and transport of folate modified nanoparticles. The study demonstrated an involvement of the caveolar pathway in internalization of folate modified nanoparticles; as judged from a significant reduction of the internalization in filipin (inhibitor) treated cells. Moreover, the work also showed evidence of transport of folate-modified nanoparticles via caveolar pathway, since translocation of nanoparticles across the cell layer is absent when this path is inhibited. This work therefore showed that the folate mediated transcytotic pathway offers potential for delivery of protein and NP-based therapeutics.

Note that none of the specific chemical inhibitors led to 95% inhibition of internalization. This observation most likely indicates the role of non-clathrin, non-caveolae-mediated pathways for internalization which needs further investigation. Disruption of actin filament and microtubules caused no difference in cellular uptake of NPs but increased the transcytosis of folate modified NPs.

Moreover, data revealed that attachment of folate onto NPs had a key role in their uptake and transport across cell layer and it could change the endocytosis pathway. Furthermore, adsorption of OVA-folate on the surface of NPs was seen to promote their cellular uptake and transport across the cell layers.

4.6 References

1. Sikka, P.K. and K.E. McMartin, *Determination of folate transport pathways in cultured rat proximal tubule cells.* Chemico-Biological Interactions, 1998. **114**(1-2): p. 15-31.
2. Birn, H., J. Selhub, and E.I. Christensen, *Internalization and Intracellular-Transport of Folate-Binding Protein in Rat-Kidney Proximal Tubule.* American Journal of Physiology, 1993. **264**(2): p. C302-C310.
3. Chancy, C.D., et al., *Expression and differential polarization of the reduced-folate transporter-1 and the folate receptor alpha in mammalian retinal pigment epitheliu.* Journal of Biological Chemistry, 2000. **275**(27): p. 20676-20684.
4. Kennedy, M.D., et al., *Evaluation of folate conjugate uptake and transport by the choroid plexus of mice.* Pharm Res, 2003. **20**(5): p. 714-9.
5. Anderson, R.G. and K. Jacobson, *A role for lipid shells in targeting proteins to caveolae, rafts, and other lipid domains.* Science, 2002. **296**(5574): p. 1821-5.
6. Sudimack, J. and R.J. Lee, *Targeted drug delivery via the folate receptor.* Adv Drug Deliv Rev, 2000. **41**(2): p. 147-62.
7. Smart, E.J., C. Mineo, and R.G. Anderson, *Clustered folate receptors deliver 5-methyltetrahydrofolate to cytoplasm of MA104 cells.* Journal of Cell Biology, 1996. **134**(5): p. 1169-77.
8. Gabrielson, N.P. and D.W. Pack, *Efficient polyethylenimine-mediated gene delivery proceeds via a caveolar pathway in HeLa cells.* J Control Release, 2009. **136**(1): p. 54-61.
9. Sabharanjak, S. and S. Mayor, *Folate receptor endocytosis and trafficking.* Adv Drug Deliv Rev, 2004. **56**(8): p. 1099-109.
10. Pelkmans, L. and A. Helenius, *Endocytosis via caveolae.* Traffic, 2002. **3**(5): p. 311-20.
11. Rodman, J.S., L. Seidman, and M.G. Farquhar, *The Membrane-Composition of Coated Pits, Microvilli, Endosomes, and Lysosomes Is Distinctive in the Rat-Kidney Proximal Tubule Cell.* Journal of Cell Biology, 1986. **102**(1): p. 77-87.

12. Kumari, S. and S. Mayor, *ARF1 is directly involved in dynamin-independent endocytosis.* Nature Cell Biology, 2008. **10**(1): p. 30-U22.

13. Maxfield, F.R. and T.E. McGraw, *Endocytic recycling.* Nature Reviews Molecular Cell Biology, 2004. **5**(2): p. 121-132.

14. Doherty, G.J. and H.T. McMahon, *Mechanisms of Endocytosis.* Annual Review of Biochemistry, 2009. **78**: p. 857-902.

15. Mayor, S. and R.E. Pagano, *Pathways of clathrin-independent endocytosis.* Nature Reviews Molecular Cell Biology, 2007. **8**(8): p. 603-612.

16. Takei, K. and V. Haucke, *Clathrin-mediated endocytosis: membrane factors pull the trigger.* Trends in Cell Biology, 2001. **11**(9): p. 385-391.

17. Waterman-Storer, C.M., D. Yarar, and S.L. Schmid, *A dynamic actin cytoskeleton functions at multiple stages of clathrin-mediated endocytosis.* Molecular Biology of the Cell, 2005. **16**(2): p. 964-975.

18. Conese, M., J. Rejman, and A. Bragonzi, *Role of clathrin- and caveolae-mediated endocytosis in gene transfer mediated by lipo- and polyplexes.* Molecular Therapy, 2005. **12**(3): p. 468-474.

19. Brodsky, F.M., et al., *Biological basket weaving: Formation and function of clathrin-coated vesicles.* Annual Review of Cell and Developmental Biology, 2001. **17**: p. 517-568.

20. Parton, R.G. and M. Kirkham, *Clathrin-independent endocytosis: New insights into caveolae and non-caveolar lipid raft carriers (vol 1744, pg 273, 2005).* Biochimica Et Biophysica Acta-Molecular Cell Research, 2005. **1746**(3): p. 349-363.

21. Nichols, B.J. and J. Lippincott-Schwartz, *Endocytosis without clathrin coats.* Trends in Cell Biology, 2001. **11**(10): p. 406-412.

22. Ceresa, B.P. and S.L. Schmid, *Regulation of signal transduction by endocytosis.* Current Opinion in Cell Biology, 2000. **12**(2): p. 204-210.

23. Nabi, I.R. and P.U. Le, *Caveolae/raft-dependent endocytosis.* Journal of Cell Biology, 2003. **161**(4): p. 673-677.

24. Bathori, G., L. Cervenak, and I. Karadi, *Caveolae--an alternative endocytotic pathway for targeted drug delivery.* Crit Rev Ther Drug Carrier Syst, 2004. **21**(2): p. 67-95.

25. Kitchens, K.M., et al., *Endocytosis inhibitors prevent poly(amidoamine) dendrimer internalization and permeability across Caco-2 cells.* Mol Pharm, 2008. **5**(2): p. 364-9.

26. Merrifield, C.J., *Seeing is believing: imaging actin dynamics at single sites of endocytosis.* Trends in Cell Biology, 2004. **14**(7): p. 352-358.

27. Engqvist-Goldstein, A.E.Y. and D.G. Drubin, *Actin assembly and endocytosis: From yeast to mammals.* Annual Review of Cell and Developmental Biology, 2003. **19**: p. 287-332.

28. Almers, W., et al., *Imaging actin and dynamin recruitment during invagination of single clathrin-coated pits.* Nature Cell Biology, 2002. **4**(9): p. 691-698.

29. Cureton, D.K., et al., *Vesicular Stomatitis Virus Enters Cells through Vesicles Incompletely Coated with Clathrin That Depend upon Actin for Internalization.* Plos Pathogens, 2009. **5**(4).

30. Macleanfletcher, S. and T.D. Pollard, *Mechanism of Action of Cytochalasin-B on Actin.* Cell, 1980. **20**(2): p. 329-341.

31. MacDonald, R.C. and L. Wang, *Effects of microtubule-depolymerizing agents on the transfection of cultured vascular smooth muscle cells: Enhanced expression with free drug and especially with drug-gene lipoplexes.* Molecular Therapy, 2004. **9**(5): p. 729-737.

32. dos Santos, T., et al., *Effects of Transport Inhibitors on the Cellular Uptake of Carboxylated Polystyrene Nanoparticles in Different Cell Lines.* Plos One, 2011. **6**(9).

33. Roger, E., et al., *Lipid nanocarriers improve paclitaxel transport throughout human intestinal epithelial cells by using vesicle-mediated transcytosis.* J Control Release, 2009. **140**(2): p. 174-81.

34. Hed, J., et al., *The Use of Fluorescence Quenching in Flow Cytofluorometry to Measure the Attachment and Ingestion Phases in Phagocytosis in Peripheral-Blood without Prior Cell-Separation.* Journal of Immunological Methods, 1987. **101**(1): p. 119-125.

35. Orlandi, P.A. and P.H. Fishman, *Filipin-dependent inhibition of cholera toxin: Evidence for toxin internalization and activation through caveolae-like domains.* Journal of Cell Biology, 1998. **141**(4): p. 905-915.

36. Prieto-Sanchez, R.M., I.M. Berenjeno, and X.R. Bustelo, *Involvement of the Rho/Rac family member RhoG in caveolar endocytosis.* Oncogene, 2006. **25**(21): p. 2961-73.

37. Schroeder, J.E., et al., *Folate-mediated tumor cell uptake of quantum dots entrapped in lipid nanoparticles.* J Control Release, 2007. **124**(1-2): p. 28-34.

38. Alivisatos, P., *The use of nanocrystals in biological detection.* Nature Biotechnology, 2004. **22**(1): p. 47-52.

39. Mansouri, S., et al., *Characterization of folate-chitosan-DNA nanoparticles for gene therapy.* Biomaterials, 2006. **27**(9): p. 2060-2065.

40. Park, E.K., S.B. Lee, and Y.M. Lee, *Preparation and characterization of methoxy poly(ethylene glycol)/poly(epsilon-caprolactone) amphiphilic block copolymeric nanospheres for tumor-specific folate-mediated targeting of anticancer drugs.* Biomaterials, 2005. **26**(9): p. 1053-1061.

41. Choi, H., et al., *Iron oxide nanoparticles as magnetic resonance contrast agent for tumor imaging via folate receptor-targeted delivery.* Academic Radiology, 2004. **11**(9): p. 996-1004.

42. Pan, D., J.L. Turner, and K.L. Wooley, *Folic acid-conjugated nanostructured materials designed for cancer cell targeting.* Chem Commun (Camb), 2003(19): p. 2400-1.

43. Quintana, A., et al., *Design and function of a dendrimer-based therapeutic nanodevice targeted to tumor cells through the folate receptor.* Pharm Res, 2002. **19**(9): p. 1310-1316.

44. Hilgenbrink, A.R. and P.S. Low, *Folate receptor-mediated drug targeting: From therapeutics to diagnostics.* Journal of Pharmaceutical Sciences, 2005. **94**(10): p. 2135-2146.

45. Panyam, J., et al., *Rapid endo-lysosomal escape of poly(DL-lactide-co-glycolide) nanoparticles: implications for drug and gene delivery.* Faseb Journal, 2002. **16**(10).

46. Rejman, J., et al., *Size-dependent internalization of particles via the pathways of clathrin-and caveolae-mediated endocytosis.* Biochemical Journal, 2004. **377**: p. 159-169.

47. Geiser, M., et al., *Ultrafine particles cross cellular membranes by nonphagocytic mechanisms in lungs and in cultured cells.* Environmental Health Perspectives, 2005. **113**(11): p. 1555-1560.

48. Papageorgiou, I., et al., *The effect of nano- and micron-sized particles of cobalt-chromium alloy on human fibroblasts in vitro.* Biomaterials, 2007. **28**(19): p. 2946-2958.

49. Fazlollahi, F., et al., *Polystyrene nanoparticle trafficking across MDCK-II.* Nanomedicine-Nanotechnology Biology and Medicine, 2011. **7**(5): p. 588-594.

50. Yacobi, N.R., et al., *Polystyrene nanoparticle trafficking across alveolar epithelium.* Nanomedicine-Nanotechnology Biology and Medicine, 2008. **4**(2): p. 139-145.

51. Williams, H.B. and A.R. Choppin, *Adsorption Studies in a Synthetic Rubber Latex Ovalbumin System.* Journal of General Physiology, 1950. **34**(2): p. 183-192.

52. Stein, P.E., et al., *Crystal-Structure of Uncleaved Ovalbumin at 1.95 a Resolution.* Journal of Molecular Biology, 1991. **221**(3): p. 941-959.

53. Williams, H.B. and A.R. Choppin, *Adsorption studies in a synthetic rubber latex-ovalbumin system.* J Gen Physiol, 1950. **34**(2): p. 183-92.

54. Elgersma, A.V., et al., *The Adsorption of Bovine Serum Albumin on Positively and Negatively Charged Polystyrene Latices.* Journal of Colloid and Interface Science, 1990. **138**(1): p. 145-156.

55. Fair, B.D. and A.M. Jamieson, *Studies of Protein Adsorption on Polystyrene Latex Surfaces.* Journal of Colloid and Interface Science, 1980. **77**(2): p. 525-534.

56. Kondo, A. and K. Higashitani, *Adsorption of Model Proteins with Wide Variation in Molecular-Properties on Colloidal Particles.* Journal of Colloid and Interface Science, 1992. **150**(2): p. 344-351.

57. Revilla, J., et al., *Adsorption of bovine serum albumin onto polystyrene latex particles bearing saccharidic moieties.* Journal of Colloid and Interface Science, 1996. **180**(2): p. 405-412.

58. Frohlich, E., et al., *Cytotoxicity of nanoparticles independent from oxidative stress.* J Toxicol Sci, 2009. **34**(4): p. 363-75.

59. Olivier, V., et al., *Comparative particle-induced cytotoxicity toward macrophages and fibroblasts.* Cell Biol Toxicol, 2003. **19**(3): p. 145-59.

60. Florea, B.I., et al., *Transfection efficiency and toxicity of polyethylenimine in differentiated Calu-3 and nondifferentiated COS-1 cell cultures.* Aaps Pharmsci, 2002. 4(3).

61. Foster, K.A., et al., *Characterization of the Calu-3 cell line as a tool to screen pulmonary drug delivery.* International Journal of Pharmaceutics, 2000. **208**(1-2): p. 1-11.

62. Parker, N., et al., *Folate receptor expression in carcinomas and normal tissues determined by a quantitative radioligand binding assay.* Analytical Biochemistry, 2005. **338**(2): p. 284-293.

63. Salazar, M.D. and M. Ratnam, *The folate receptor: what does it promise in tissue-targeted therapeutics?* Cancer Metastasis Rev, 2007. **26**(1): p. 141-52.

64. Saeed, A.O., et al., *Modular construction of multifunctional bioresponsive cell-targeted nanoparticles for gene delivery.* Bioconjug Chem, 2011. **22**(2): p. 156-68.

65. Zhang, L., et al., *Uptake of folate-conjugated albumin nanoparticles to the SKOV3 cells.* Int J Pharm, 2004. **287**(1-2): p. 155-62.

66. Oyewumi, M.O., et al., *Comparison of cell uptake, biodistribution and tumor retention of folate-coated and PEG-coated gadolinium nanoparticles in tumor-bearing mice.* J Control Release, 2004. **95**(3): p. 613-26.

67. Dixit, V., et al., *Synthesis and grafting of thioctic acid-PEG-folate conjugates onto Au nanoparticles for selective targeting of folate receptor-positive tumor cells.* Bioconjug Chem, 2006. **17**(3): p. 603-9.

68. Kim, S.H., et al., *Target-specific cellular uptake of PLGA nanoparticles coated with poly(L-lysine)-poly(ethylene glycol)-folate conjugate.* Langmuir, 2005. **21**(19): p. 8852-7.

69. Win, K.Y. and S.S. Feng, *Effects of particle size and surface coating on cellular uptake of polymeric nanoparticles for oral delivery of anticancer drugs.* Biomaterials, 2005. **26**(15): p. 2713-2722.

70. Chen, F., et al., *In vitro and in vivo study of N-trimethyl chitosan nanoparticles for oral protein delivery.* Int J Pharm, 2008. **349**(1-2): p. 226-33.

71. Paulos, C.M., et al., *Ligand binding and kinetics of folate receptor recycling in vivo: impact on receptor-mediated drug delivery.* Mol Pharmacol, 2004. **66**(6): p. 1406-14.

72. Vercauteren, D., et al., *The Use of Inhibitors to Study Endocytic Pathways of Gene Carriers: Optimization and Pitfalls.* Molecular Therapy, 2010. **18**(3): p. 561-569.

73. Hope, H.R. and L.J. Pike, *Phosphoinositides and phosphoinositide-utilizing enzymes in detergent-insoluble lipid domains.* Molecular Biology of the Cell, 1996. **7**(6): p. 843-851.

74. Gupta, G.D., et al., *Analysis of Endocytic Pathways in Drosophila Cells Reveals a Conserved Role for GBF1 in Internalization via GEECs.* Plos One, 2009. **4**(8).

75. Harmon, B., N. Campbell, and L. Ratner, *Role of Abl Kinase and the Wave2 Signaling Complex in HIV-1 Entry at a Post-Hemifusion Step.* Plos Pathogens, 2010. **6**(6).

76. Benzeev, A., S.R. Farmer, and S. Penman, *Mechanisms of Regulating Tubulin Synthesis in Cultured Mammalian-Cells.* Cell, 1979. **17**(2): p. 319-325.

77. Sato, K., et al., *Effects of endocytosis inhibitors on internalization of human IgG by Caco-2 human intestinal epithelial cells.* Life Sciences, 2009. **85**(23-26): p. 800-807.

78. Rejman, J., A. Bragonzi, and M. Conese, *Role of clathrin- and caveolae-mediated endocytosis in gene transfer mediated by lipo- and polyplexes.* Molecular Therapy, 2005. **12**(3): p. 468-74.

79. Torgersen, M.L., et al., *Internalization of cholera toxin by different endocytic mechanisms.* Journal of Cell Science, 2001. **114**(20): p. 3737-3747.

80. Fishman, P.H. and P.A. Orlandi, *Cholera toxin internalization and intoxication.* Journal of Cell Science, 2003. **116**(3): p. 431-432.

81. Bradbury, N.A., et al., *Characterization of the internalization pathways for the cystic fibrosis transmembrane conductance regulator.* American Journal of Physiology-Lung Cellular and Molecular Physiology, 1999. **276**(4): p. L659-L668.

82. Rothberg, K.G., et al., *The Glycophospholipid-Linked Folate Receptor Internalizes Folate without Entering the Clathrin-Coated Pit Endocytic Pathway.* Journal of Cell Biology, 1990. **110**(3): p. 637-649.

83. Kiss, A.L. and E. Botos, *Endocytosis via caveolae: alternative pathway with distinct cellular compartments to avoid lysosomal degradation?* J Cell Mol Med, 2009. **13**(7): p. 1228-37.

84. Pelkmans, L., J. Kartenbeck, and A. Helenius, *Caveolar endocytosis of simian virus 40 reveals a new two-step vesicular-transport pathway to the ER.* Nat Cell Biol, 2001. **3**(5): p. 473-83.

85. Schnitzer, J.E., *Caveolae: from basic trafficking mechanisms to targeting transcytosis for tissue-specific drug and gene delivery in vivo.* Adv Drug Deliv Rev, 2001. **49**(3): p. 265-80.

86. Le, P.U. and I.R. Nabi, *Distinct caveolae-mediated endocytic pathways target the Golgi apparatus and the endoplasmic reticulum.* Journal of Cell Science, 2003. **116**(6): p. 1059-1071.

87. Gumbleton, M., A.G. Abulrob, and L. Campbell, *Caveolae: an alternative membrane transport compartment.* Pharm Res, 2000. **17**(9): p. 1035-48.

88. Goldberg, D.S., H. Ghandehari, and P.W. Swaan, *Cellular Entry of G3.5 Poly (amido amine) Dendrimers by Clathrin- and Dynamin-Dependent Endocytosis Promotes Tight Junctional Opening in Intestinal Epithelia.* Pharm Res, 2010. **27**(8): p. 1547-1557.

89. Macia, E., et al., *Dynasore, a cell-permeable inhibitor of dynamin.* Developmental Cell, 2006. **10**(6): p. 839-850.

90. Bananis, E., et al., *Microtubule-dependent movement of late endocytic vesicles in vitro: requirements for Dynein and Kinesin.* Molecular Biology of the Cell, 2004. **15**(8): p. 3688-97.

91. Lin, I.C., et al., *Cellular Transport Pathways of Polymer Coated Gold Nanoparticles.* Nanomedicine, 2011.

92. Qaddoumi, M.G., et al., *The characteristics and mechanisms of uptake of PLGA nanoparticles in rabbit conjunctival epithelial cell layers.* Pharm Res, 2004. **21**(4): p. 641-8.

93. Kamen, B.A., C.M. Lewis, and A.K. Smith, *Receptor-mediated folate uptake is positively regulated by disruption of the actin cytoskeleton.* Cancer Research, 1998. **58**(14): p. 2952-2956.

94. Kamen, B.A. and A.K. Smith, *A review of folate receptor alpha cycling and 5-methyltetrahydrofolate accumulation with an emphasis on cell models in vitro.* Advanced Drug Delivery Reviews, 2004. **56**(8): p. 1085-1097.

95. Jevprasesphant, R., et al., *Engineering of dendrimer surfaces to enhance transepithelial transport and reduce cytotoxicity.* Pharm Res, 2003. **20**(10): p. 1543-50.

96. Dausend, J., et al., *Uptake mechanism of oppositely charged fluorescent nanoparticles in HeLa cells.* Macromol Biosci, 2008. **8**(12): p. 1135-43.

Chapter 5

Ligand density and clustering effects on endocytosis of folate modified nanoparticles

5.1 Introduction

To achieve intracellular delivery of biologicals (proteins, oligonucleotides or siRNA), the crucial step is to design a delivery system that will protect the incorporated biologic and is efficiently internalized by the cells of interest. The approaches used to formulate delivery systems and achieve cellular targeting and internalization are typically based on sub-micron sized particulate 'carriers', such as liposomes or polymeric nanoparticles which are decorated on their surfaces with targeting ligands, based on either antibodies, polypeptides, fusogenic proteins or hormones. The choice of ligand depends on the type(s) of cells/tissues to be targeted. After attachment, the targeting ligand must be exposed and accessible at the carrier surface to ensure effective interaction with receptor at the targeted cell. For intracellular delivery, it is also important that the ligand-receptor binding interaction leads to internalization of the carrier, followed by an appropriate intracellular transport route, which will eventually deliver a therapeutic biologic to the target intracellular site.

The density of a ligand on the surface of a particulate carrier can have a profound effect on ligand-receptor binding events and the biological processes that follow this binding. Studies on this phenomenon have recently taken momentum with a general aim to enhance prospects of targeting systems by improving their binding and cellular uptake by targeted cells. Surface density of different ligands has been demonstrated to play an important role in cellular uptake of, for instance, PLGA nanoparticles surface modified with wheat germ agglutinin [1] or with a cyclic peptide that specifically binds to ICAM-1 (intercellular cell adhesion molecule-1) [2], composite polymeric micelles surface decorated with RNA A10 aptamer which

specifically binds to the prostate-specific membrane receptor [3], liposomes surface modified with fibronectin-mimetic peptide [4] and caprolactone-polyethylene glycol micellar nanoparticles surface modified with bovine serum albumin as a model ligand [5]. The influence of ligand surface density on cell uptake has also been demonstrated in our recent work with composite polymeric micelles surface decorated with the folate ligand [6].

Typically the surface density of the ligand is controlled by adjusting the composition of the mixture containing ligand-modified and unmodified polymeric molecules that either self-assemble into a micellar-type nanocarrier [3] or adsorb at the surface of the core nanoparticles [2]. However such approaches to achieve surface ligand presentation typically do not allow control over its spatial distribution and consequently, the effect of ligand surface patterning on the binding and cellular uptake remains largely unstudied [7]. Scarce publications on the effect of ligand clustering, using branched materials that afford multi-ligand attachment *per* polymeric molecule, indicate potentially important implication(s) for cell targeting and development of more effective targeting systems [8].

In this chapter, a model nanoparticle system which enables manipulation of the surface density as well as surface clustering of a ligand has been described. This was achieved by controlling the level of ligand (folic acid) conjugation to ovalbumin with multi-ligand linking capacity. Subsequent adsorption of such ligand-OVA conjugate with different conjugation levels onto nanoparticle surface, alone or in the mixture with unconjugated OVA, allows control over surface density and clustering. The system provided a mean to test, not only the impact of surface ligand density, but

also of ligand spatial distribution (clustering) at the carrier surface on its cellular internalization behaviour.

5.2 Material and Methods

5.2.1 Preparation of Folate and non-Folate modified nanoparticles

All chemicals were purchased from Sigma-Aldrich (UK) unless otherwise specified. Ovalbumin-Folic acid (OVA-FA) was prepared by the same method described in 3.2.3. In order to have different Molar Substitution Ratios (MSR), ranging from 1-15 moles of FA per mole of OVA, folic acid was added in 20-40 fold molar excess to OVA in combination with 1-ethyl-3-(3-dimethylaminopropyl)-carbodiimide (ECDI) (in 60 fold molar excess to OVA) to OVA solution (40 mg OVA in 0.1M sodium carbonate buffer (pH 9.5))

As described in chapter 3 (section 3.2.3) the resulting conjugate was desalted and purified with PD10 column (Sephadex G-25 Medium) using PBS (containing 0.14M NaCl and 0.01M phosphate at pH 7.4) as the eluting solution to remove any free unconjugated drug. Molar ratio of FA to OVA was determined by quantifying FA using spectrophotometry at λ_{364} (ε=6.5 x 10^3) and OVA by the Bradford reagent (using UV at 595 nm), using calibration curves of known OVA concentrations.

FA-OVA conjugates and unconjugated OVA were adsorbed on the surface of sulphate-modified, polystyrene latex of 30 nm diameter as described in section 4.2.1.

5.2.2 Light-Scattering Measurements

The hydrodynamic diameter and size distribution of nanoparticles was determined by Dynamic Light Scattering (DLS) (section 4.2.2).

5.2.3 Cell culture

Calu-3 cells were cultured on flasks at 5% CO_2, 37°C until confluence. Thereafter cells were detached from the flasks, seeded and cultured on permeable supports (10^5 cells per well) according to the methods detailed previously (section 2.2.1.2 and 2.2.1.4). The integrity of the cell layers and tight junction formation was assessed by measurement of Transepithelial Electrical Resistance (TEER) as detailed in section 2.2.2.

5.2.4 Cell uptake studies

These experiments were conducted as mentioned in sections 3.2.8. Uptake study was performed for a period of four hours. Cellular internalization of nanoparticles in the presence of inhibitors was studied as described in 4.2.5. Calu-3 cells were pre-treated with either clathrin inhibitor, chlorpromazine (10 μg/ml), or caveolae inhibitor, filipin (5 μg/ml) for 1 hour prior the addition of nanoparticles. Inhibitors were used at concentrations that did not exhibit a prominent effect on cell viability (4.3.2.2).

5.3 Results

5.3.1 Nanoparticle preparation and characterization

Initially, folate ligand (FA) was conjugated to OVA as an 'anchoring' species that served to achieve multi-ligand attachment, as well as to anchor the ligand to the surface of a polymeric carrier, in this case polystyrene latex, via adsorption. FA-OVA conjugates with varying molar substitution ratio (MSR) of 1.5±0.2, 3.3±2.1, 5.5±0.2, 7.8±1.6, 9.0±0.8 and 13.2±1.0 (mean±S.D, n=6) mol FA *per* mol OVA were produced and adsorbed onto 30 nm polystyrene latex (as presented schematically in Figure 5.1).

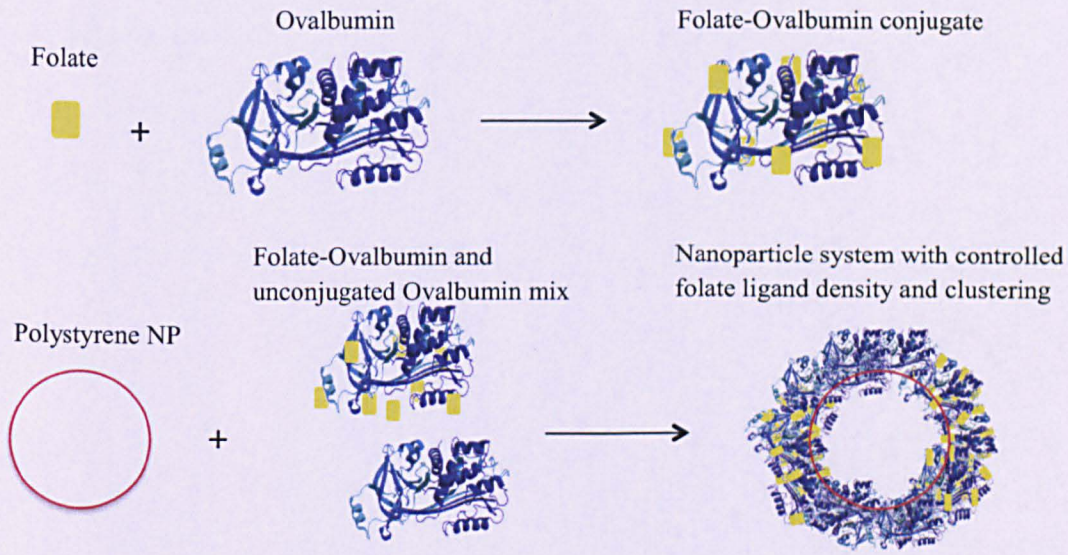

Figure 5.1 *Preparation of folate decorated polystyrene nanoparticles. Each ovalbumin 'anchor' molecule allows covalent linkage of multiple ligands. Co-adsorption of ligand-conjugated (at different molar substitution ratio) and unconjugated anchor molecules achieves ligand clustering on nanoparticle surface.*

5.3.2 Nanoparticle characterization

Particle size determination of a series of FA-OVA decorated nanoparticles by dynamic light scattering (DLS) is shown in Figure 5.2. The systems in the series comprised of nanoparticles with surface adsorbed FA-OVA conjugates produced at different molar substitution ratio of folate to OVA (Figure 5.2 C-F). For the purpose of comparison, the size of unmodified nanoparticles (i.e. prior to surface adsorption of FA-OVA conjugates) and following adsorption of unconjugated OVA are also shown (Figure 5.2 A and B). The particle distribution graphs show that there was no notable aggregation of the nanoparticles following surface modification. The mean hydrodynamic particle radius and distribution for all nanoparticle systems, surface decorated with unconjugated (Figure 5.2 B) and those decorated with FA-conjugated OVA with varying molar substitution ratios (Figure 5.2 C-F), ranged between 62-66 nm, indicating no significant differences in the particle size between modified nanoparticles that could potentially affect their cellular internalization behaviour.

A)

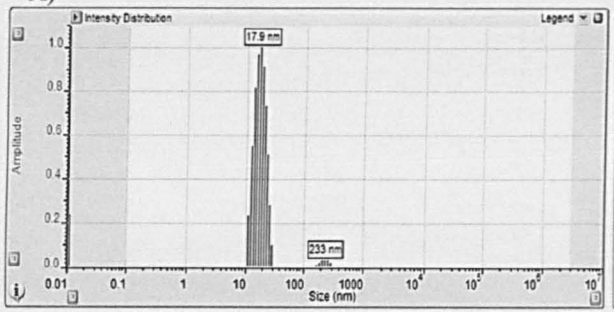
Intensity Distribution
Legend
17.9 nm
233 nm
Amplitude
Size (nm)

B)

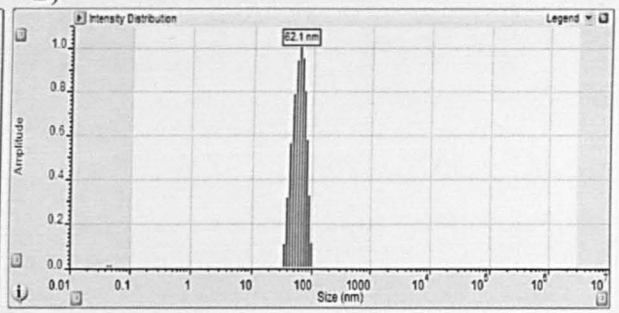
Intensity Distribution
Legend
62.1 nm
Amplitude
Size (nm)

C)

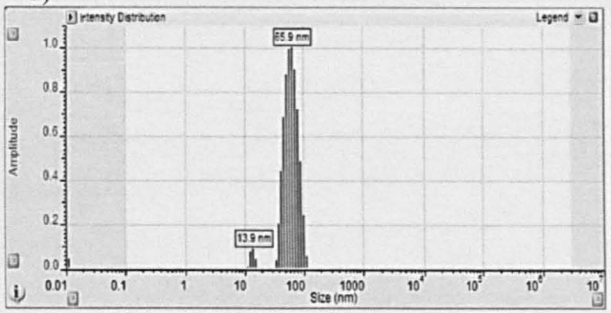
Intensity Distribution
Legend
65.9 nm
13.9 nm
Amplitude
Size (nm)

D)

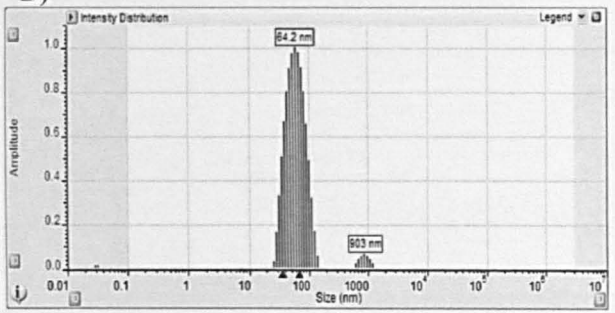
Intensity Distribution
Legend
64.2 nm
903 nm
Amplitude
Size (nm)

E)

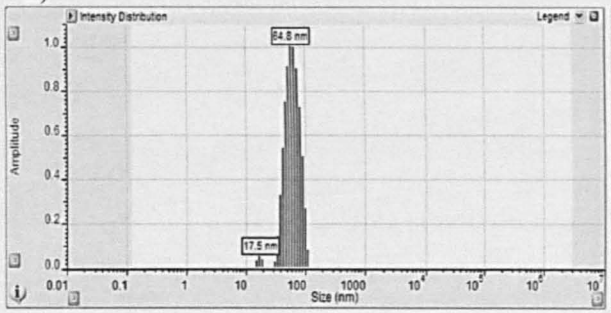
Intensity Distribution
Legend
64.8 nm
17.5 nm
Amplitude
Size (nm)

F)

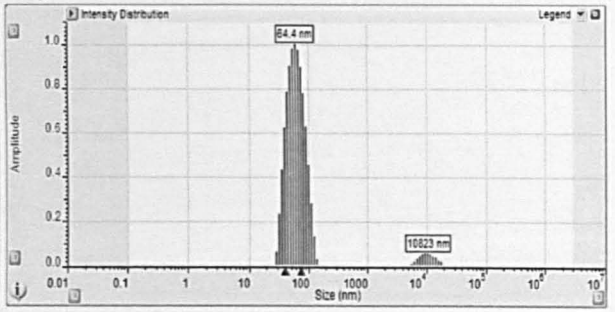
Intensity Distribution
Legend
64.4 nm
10823 nm
Amplitude
Size (nm)

Key	Nanoparticle type (molar substitution ratio FA-OVA)	Hydrodynamic radius (nm) ± SD
A	Unmodified	17.9 ± 4.5
B	OVA modified	62.1 ± 11.7
C	FA-OVA (1/1.5) modified	65.9 ± 1.1
D	FA-OVA (1/5.5) modified	64.2 ± 12.9
E	FA-OVA (1/9.0) modified	64.8 ± 12.4
F	FA-OVA (1/13.2) modified	64.4 ±2.1

Figure 5.2 *Particle size and distribution (hydrodynamic radius) of unmodified (A), and nanoparticles modified with either unconjugated ovalbumin (B) or folate-conjugated ovalbumin (FA-OVA) prepared at different molar substitution ratios (C, D, E and F), as determined by dynamic light scattering. The results in the table represent a mean ± SD of ten measurements performed in Hank's Balanced Salt Solution.*

5.3.3 Effect of ligand density on cellular internalization of nanoparticles

To study the effect of folate ligand density on cellular internalization of nanoparticles, these were surface modified by adsorption of FA-OVA conjugates produced at different molar substitution ratios, ranging from 1.5 to 13.2 moles of folate *per* mole of OVA.

Data in Figure 5.3 clearly demonstrate that cellular uptake of the modified nanoparticles was affected by the surface density of the ligand (i.e. molar substitution ratio), whereby the uptake increased with an increase in folate ligand density and apparently reached a plateau at high ligand densities. In comparison, control nanoparticles surface-modified with unconjugated OVA (therefore lacking in folate ligand) showed a significantly lower cellular internalization ($P < 0.001$).

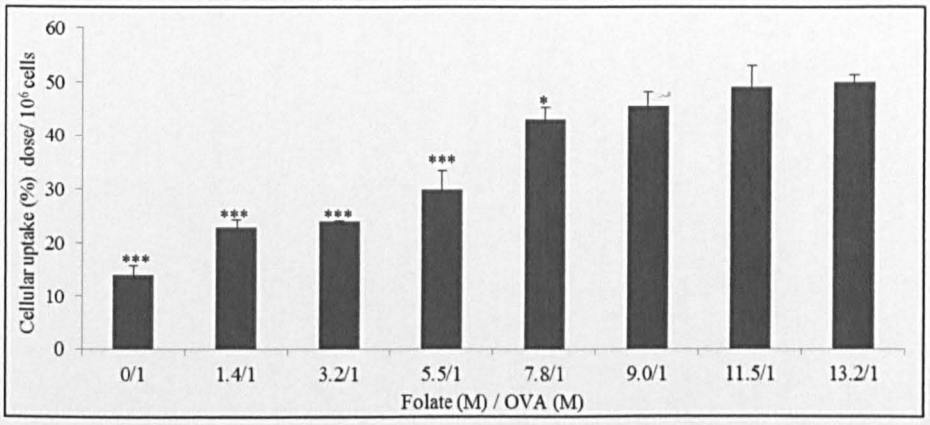

Figure 5.3 *Effect of ligand density on cellular internalization of nanoparticles in Calu-3 layers. Nanoparticles were surface modified with Folate-ovalbumin (FA-OVA) conjugates produced at increasing FA to OVA molar substitution ratios (1.4-13.2/1).) 0/1 represents unmodified OVA nanoparticles (control). Uptake expressed as % of dose applied apically (containing $1.69x10^{13}$ nanoparticles) per one cell layer ($1x10^{6}$ cells). One-way analysis of variance (ANOVA) with Bonferroni post-hoc test was used for statistical analysis. Error bar represents mean ± standard deviation (n=3). *, ** and *** denote $p<0.05$, $p<0.01$ and $p<0.001$, respectively relative to cell uptake of nanoparticles adsorbed with FA-OVA at the highest molar substitution ratio (13.2:1).*

5.3.4 Effect of surface ligand density on cellular internalization pathway (endocytosis)

To investigate the potential effect that surface density of ligand could have on the pathway(s) involved in cellular internalization (endocytosis) of folate-decorated nanoparticles, clathrin and caveolae-mediated pathways were investigated as potential internalization routes suggested for the folate and non-folate NPs [9-11] (also observed in Chapter 4, section 4.3.6). Sterol-binding agent filipin was applied to the Calu-3 cells to disrupt caveolae-mediated endocytosis [12], and cationic amphiphilic agent chlorpromazine to inhibit the clathrin-dependent pathway [13, 14]. Figure 5.4 shows the impact of inhibitors of caveolae- and clathrin-mediated cell uptake pathways on internalisation of nanoparticles surface decorated with FA-OVA of varying substitution ratios. Considering the control system comprising of nanoparticles modified with unconjugated OVA, the cellular internalization was notably reduced ($P<0.001$) with chlorpromazine treatment (i.e. inhibition of clathrin pathway, whilst no significant reduction compared to the untreated cells was seen with filipin treatment (caveolae inhibition), clearly indicating that the cell uptake of folate-free nanoparticles was largely dependent on the clathrin-mediated pathway.

For FA-OVA modified nanoparticles, clathrin inhibition by chlorpromazine significantly ($P<0.01$) influenced cell internalization at the lowest surface density of the folate ligand, indicating that clathrin-mediated pathway was still dominant in the internalisation of this system. On the other hand, chlorpromazine-induced clathrin inhibition showed a moderate effect on systems with intermediate ligand densities (molar substitution ratios of 3.2 and 5.5; $P<0.05$) and displayed no significant effect on the cellular uptake of nanoparticles at higher folate ligand densities (molar substitution ratios >7.8). A mirror trend of statistically significant decrease in

cellular internalization of nanoparticles at higher folate ligand densities (molar substitution ratios >7.8; P<0.001) was apparent when caveolin-mediated endocytosis was inhibited by filipin. The suppression in cell uptake was modest at a lower ligand density (molar substitution ratio of 5.5) and insignificant at lowest two densities (molar substation ratios 3.2 and 1.5).

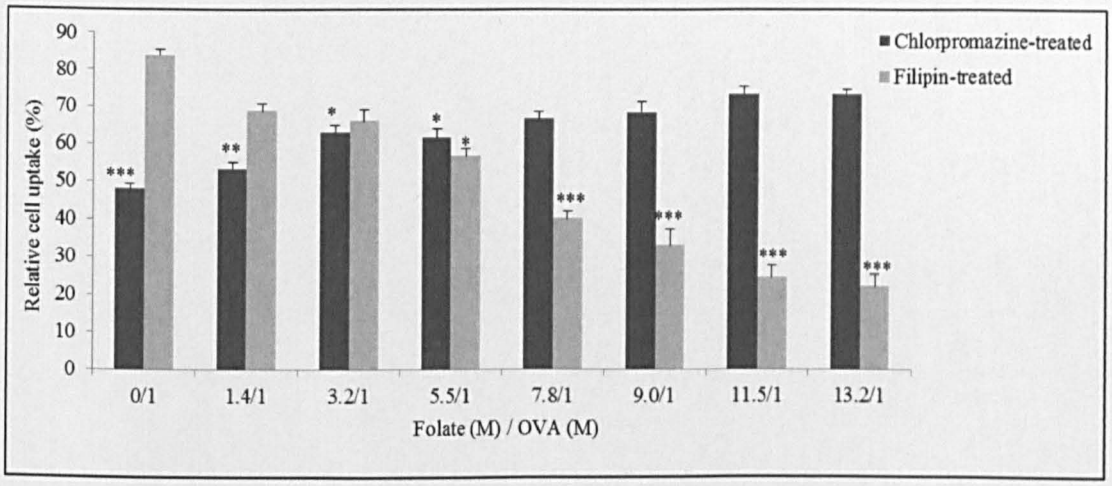

Figure 5.4 *Cellular internalization of folate-modified nanoparticles in the presence of endocytosis inhibitors for clathrin (chlorpromazine) and caveolae (filipin) – mediated pathways. Nanoparticles produced at increasing folate to ovalbumin (OVA) molar substitution ratios (1.5-13.2). 0/1 represents unconjugated OVA modified nanoparticles. Uptake expressed as % relative to uptake in untreated cell layer. One-way analysis of variance (ANOVA) with Bonferroni post-hoc test was used for statistical analysis. Error bar represents mean ± standard deviation (n=3). *p<0.05, ** p<0.01 and *** p<0.001 relative to the respective uptake when untreated with the inhibitors.*

5.3.5 Effect of ligand clustering on cellular internalization

Table 5.1 summarizes the data depicting the effect of ligand clustering on cell uptake of nanoparticles. A matrix of nanoparticle systems with different surface distribution of folate ligand was created by adsorption of different compositions of FA-conjugated OVA, with varying molar substitution ratios (1.5 to 13.2), in combination with unconjugated OVA. Variations in ligand density were largely determined by the folate molar substitution ratio (rows in Table 1), while clustering was largely determined by the composition of FA-conjugated to unconjugated OVA mixtures (columns in Table 5.1).

At first, the table demonstrates dramatic differences in nanoparticle internalization by cells, extending between 60% of the administered dose for the highest surface content of folate ligand (referring to high molar substitution ratio of 13.2 at 100% FA-OVA) and 10% of the dose for the system with low surface content (referring to 1.5 molar substitution ratio and 10% FA-OVA mixture).

Combining this with the data in Figure 5.4, showing that the pathway of the nanoparticles uptake changed with the surface density of the ligand, the high ligand coverage systems would be taken into the cells at high levels (% of applied dose) and primarily by caveolae-mediated pathway, whilst those with the low surface ligand coverage would be internalised in a considerably less efficient manner and primarily by clathrin-mediated pathway. The matrix hence demonstrates how dramatically different outcome, and potentially different drug delivery effect, could be regardless of the fact that the same ligand was employed for nanoparticle surface modification.

Comparing the systems where folate conjugates with the same molar substitution ratio in mixture with unconjugated OVA were used to modify nanoparticles

(columns in the Table 1), the data clearly indicated that decreasing the overall surface density of folate ligand and gradually creating an 'island in the sea' folate pattern at the nanoparticle surface led to a decreased uptake by the cell layer for all the molar substitution ratios.

The matrix in table 5.1 also allows an overall comparison between cell internalization of nanoparticles with relatively clustered ligand pattern with their counterparts prepared at similar content of folate ligand, but in a more dispersed pattern (comparison in diagonal direction of Table 1.5, e.g. nanoparticles surface modified by 75/25 mixture of FA-OVA conjugate at molar substitution ratio of 13.2 with 6.7 nmol FA and nanoparticles with 6.5 nmol FA surface modified with FA-OVA conjugate at molar substitution ratio of 3.3). Such comparisons typically revealed that a statistically higher internalization of the nanoparticles by Calu-3 cell layers was associated with more clustered rather than dispersed surface ligand pattern.

Composition (%) of FA-OVA to OVA	Molar substitution ratio Folate : OVA						
	13.2	11.6	9.0	7.8	5.5	3.3	1.5
	Amount of folate ligand used to modify nanoparticles (nmol) (upper number). Cellular internalization (%) of applied dose (lower number)						
100%	26.7 **60.0**	23.3 **58.2**	18.2 **^1 53.4**	15.8 **49.0**	11.1 ***2 42.3**	6.5 ***1 29.4**	2.9 **24.1**
75%	19.9 **57.2**	17.4 **^1 53.7**	13.6 ***5 45.6**	11.8 ***2 44.6**	8.3 ***6 37.7**	4.9 ***7 25.8**	2.1 ***10 13.2**
50%	13.4 ***5 50.9**	11.6 ***2 50.1**	9.1 ***6 48.4**	7.9 ***6 41.6**	5.5 ***3 30.7**	3.2 ***10 21.5**	1.4 **^3 *9 11.2**
25%	6.7 ***1 38.2**	5.8 ***3 34.6**	4.6 ***7 30.4**	3.9 ***10 26.5**	2.8 ***4 17.6**	1.6 ***8 ^3 11.8**	0.7 **10.8**
10%	2.6 ***4 ^2 24.2**	2.3 **^2 *10 21.1**	1.8 ***8 18.8**	1.5 ***9 18.2**	1.1 **15.3**	0.6 **12.4**	0.2 **10.0**

Table 5.1 *Cellular internalization of folate surface modified nanoparticles. A matrix of nanoparticles surface modified with different folate-OVA substitution ratios (1.5-13.2) and mixtures with unmodified OVA anchor (10-100 %). Systems with similar amount of folate ligand (nmol) are compared. * sign with corresponding number denotes compared systems which are statistically different (p< 0.05 or 0.01), ^ sign with corresponding number denotes compared systems which are not statistically different. One-way analysis of variance (ANOVA) applied as statistical analysis.*

Selected data from Table 5.1 are summarized in figure 5.5, which compares the internalisation of folate-decorated nanoparticles with the similar folate content, distributed at the surface in either more clustered or disperse arrangements. The trends in figure indicated an interesting phenomenon; at higher overall ligand content, cellular internalization of nanoparticles was higher in the clustered ligand, relative to the dispersed series. However at the lower overall ligand content the trends were reversed and the internalization of dispersed ligand nanoparticles was higher with a crossover at the folate content of approximately 2.6-2.9 nmol.

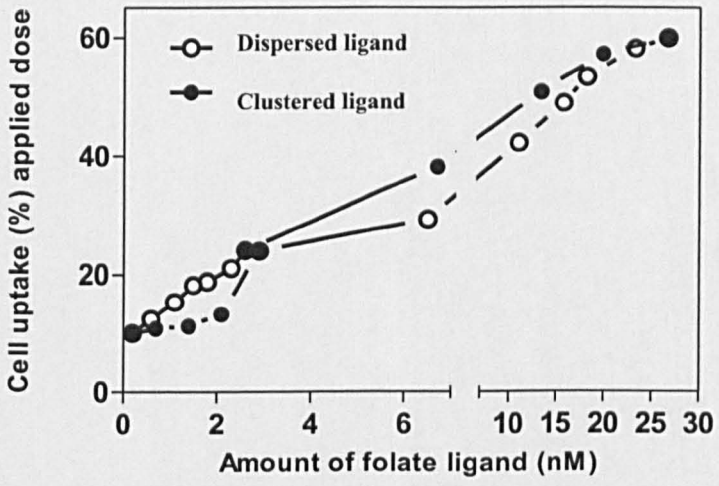

Figure 5.5 *Effect of the surface ligand distribution on cellular internalisation of nanoparticles at corresponding ligand amount (selected data from table 1).*

5.4 Discussion

The interaction of nanomaterials with cells is critical in drug delivery which is mainly dictated by surface properties of nanoparticles. While most studies have reported the effect of surface functional groups/ligands/penetration motifs on the nanoparticle cellular uptake, the impact of ligand density and patterning on the cellular internalization of nanoparticles is seldom examined [7, 8, 15].

Work detailed in this chapter investigated the effects of surface ligand distribution pattern (ligand clustering and density) on the internalization of nanoparticles by bronchial epithelial cells *in vitro* (Calu-3 cells cultured as polarised layers). For this aim, ovalbumin was used as an intermediate species to anchor the folate to the nanoparticle surface. The model system consisted of polystyrene nanoparticles surface-decorated via the adsorption of ovalbumin conjugated to the folate ligand (as discussed in chapter 4). The density of the displayed folate was manipulated by controlling the conjugation level of folate-ovalbumin (3.2.3 & 3.3.1), while ligand clustering was achieved by co-adsorption of varying mixtures of folate-ovalbumin conjugate (at different ligand density levels) and unconjugated ovalbumin.

Characterisation of OVA-FA and OVA coated NPs for their size by dynamic light scattering (DLS) revealed that the mean hydrodynamic particle radius for all nanoparticle systems, surface decorated with OVA (Figure 5.2 B) and those decorated with different density of FA conjugated-OVA (Figure 5.2 C-F) were ranged between 62-64 nm, indicating no significant differences in the particle size between OVA-FA modified and OVA modified nanoparticles that could potentially affect their cellular internalization.

Increasing overall ligand density on the nanoparticle surface resulted in increased internalization of modified nanoparticles by the cells, up to a saturation level.

The trend seen in Figure 5.3 was in close agreement with our previous study where a range of folate decorated micellar-type nanoparticles were produced by progressively increasing the content of folate functionalized copolymer relative to the 'non-functionalized' core polymer [6]. A similar trend of increased folate ligand density resulting in increased internalization by KB cells until an apparent plateau is reached was also reported for solid lipid nanoparticles with folate ligand conjugated to a lipid component incorporated into the formulation [16]. Similar patterns, where cell association reaches a plateau at higher ligand densities was also observed for nanosystems surface-modified with other ligands, for instance bacterial invasion (MBP-Inv479) factor attached at varying surface concentrations to 155-200 nm nanoparticles [17], or for RNA aptamer at the surface of micellar-type PLGA-PEG nanoparticles [3].

The observed plateau in cell internalization at higher ligand densities could arise from saturation of folate receptors at the cell surface [18], whereby increasing ligand density would increase the number of potential receptor interactions until a point at which the maximum number of interactions occurs and the rate of particle internalization approaches the maximum rate allowed by the process, as previously suggested [19].

Data also presented that surface ligand density also affected the cellular uptake pathway; from predominantly clathrin to predominantly caveolae-mediated as the ligand density was increased.

These findings indicated dominant involvement of caveolae-mediated internalization of folate decorated nanoparticles and contributed to our findings discussed in

chapter 4 (section 4.3.6) and also to the body of literature where some studies pointed at caveolae [9-11, 20, 21] and others at clathrin-mediated pathways for folate receptor uptake [22, 23]. The data further indicated a role that ligand density plays in determining internalization pathway of folate-decorated nanoparticles. To the best of our knowledge, no previous studies in the literature had reported such data.

This work further demonstrated that surface clustering of folate ligand enhanced cellular internalization of nanoparticles, relative to its dispersed surface distribution. This finding appears in line with the suggested formation of folate receptor into discrete clusters at the cell membrane associated with caveolae structure [24, 25].

Relating this work with recently published data from other studies illustrated that for liposomes surface modified with either 'individual' or 'clustered' mannosyl ligand those prepared with multi-branched mannosylated lipids also displayed higher binding affinity for the mannose receptor than vesicles containing the mono-mannosylated analogs [26].

Data presented in this chapter were in line with a very recent publication on the effect of folate ligand clustering, where the authors concluded that a particular ligand clustering formation at the surface of mixed micelles had a prominent effect on their association with cells *in vitro* (KB cells) and was reflected in *in vivo* (nude mice bearing KB (FR+) and A375 (FR−) tumors) assessment of the system where optimal clustering was suggested to have higher association with cancer tissue [27].

5.5 Conclusions

This work described a simple approach to the surface modification of nanoparticles systems which, in addition to control of surface density of a ligand, allowed control over ligand clustering. Data also suggested that ligand density not only affects the level of cellular internalization of targeted nanoparticles, but also influences the pathway of nanoparticles internalization by the cells.

Worked detailed in this chapter also showed that ligand presentation in clustered rather than disperse arrangements, affected cellular uptake and that the optimum arrangement was different for different pathways of uptake in an appropriate *in vitro* epithelial model. The systems allowed tuning to a desired ligand density and clustering and could be a useful platform to study targeted delivery of a new generation of nano-scale therapeutics.

5.6 References

1. Shen, Y.H., et al., *Effect of wheat germ agglutinin density on cellular uptake and toxicity of wheat germ agglutinin conjugated PEG-PLA nanoparticles in Calu-3 cells.* International Journal of Pharmaceutics, 2011. **413**(1-2): p. 184-193.
2. Fakhari, A., et al., *Controlling Ligand Surface Density Optimizes Nanoparticle Binding to ICAM-1.* Journal of Pharmaceutical Sciences, 2011. **100**(3): p. 1045-1056.
3. Gu, F., et al., *Precise engineering of targeted nanoparticles by using self-assembled biointegrated block copolymers.* Proceedings of the National Academy of Sciences of the United States of America, 2008. **105**(7): p. 2586-91.
4. Garg, A., et al., *Targeting colon cancer cells using PEGylated liposomes modified with a fibronectin-mimetic peptide.* International Journal of Pharmaceutics, 2009. **366**(1-2): p. 201-210.
5. Gindy, M.E., et al., *Preparation of Poly(ethylene glycol) Protected Nanoparticles with Variable Bioconjugate Ligand Density.* Biomacromolecules, 2008. **9**(10): p. 2705-2711.
6. Saeed, A.O., et al., *Modular construction of multifunctional bioresponsive cell-targeted nanoparticles for gene delivery.* Bioconjug Chem, 2011. **22**(2): p. 156-68.
7. Verma, A. and F. Stellacci, *Effect of surface properties on nanoparticle-cell interactions.* Small, 2010. **6**(1): p. 12-21.
8. Poon, Z., et al., *Ligand-clustered "patchy" nanoparticles for modulated cellular uptake and in vivo tumor targeting.* Angew Chem Int Ed Engl, 2010. **49**(40): p. 7266-70.
9. Sudimack, J. and R.J. Lee, *Targeted drug delivery via the folate receptor.* Adv Drug Deliv Rev, 2000. **41**(2): p. 147-62.
10. Anderson, R.G. and K. Jacobson, *A role for lipid shells in targeting proteins to caveolae, rafts, and other lipid domains.* Science, 2002. **296**(5574): p. 1821-5.

11. Gabrielson, N.P. and D.W. Pack, *Efficient polyethylenimine-mediated gene delivery proceeds via a caveolar pathway in HeLa cells.* J Control Release, 2009. **136**(1): p. 54-61.

12. Kitchens, K.M., et al., *Endocytosis inhibitors prevent poly(amidoamine) dendrimer internalization and permeability across Caco-2 cells.* Mol Pharm, 2008. **5**(2): p. 364-9.

13. Brodsky, F.M., *Biological basketweaving: Formation and function of clathrin-coated vesicles.* Molecular Biology of the Cell, 2001. **12**: p. 1A-1A.

14. Rejman, J., A. Bragonzi, and M. Conese, *Role of clathrin- and caveolae-mediated endocytosis in gene transfer mediated by lipo- and polyplexes.* Molecular Therapy, 2005. **12**(3): p. 468-474.

15. Cairo, C.W., et al., *Control of multivalent interactions by binding epitope density.* Journal of the American Chemical Society, 2002. **124**(8): p. 1615-1619.

16. Oyewumi, M.O. and R.J. Mumper, *Engineering tumor-targeted gadolinium hexanedione nanoparticles for potential application in neutron capture therapy.* Bioconjugate chemistry, 2002. **13**(6): p. 1328-35.

17. Dawson, G.F. and G.W. Halbert, *The in vitro cell association of invasin coated polylactide-co-glycolide nanoparticles.* Pharm Res, 2000. **17**(11): p. 1420-5.

18. Paulos, C.M., et al., *Ligand binding and kinetics of folate receptor recycling in vivo: impact on receptor-mediated drug delivery.* Mol Pharmacol, 2004. **66**(6): p. 1406-14.

19. Dawson, G.F. and G.W. Halbert, *The in vitro cell association of invasin coated polylactide-co-glycolide nanoparticles.* Pharmaceutical research, 2000. **17**(11): p. 1420-5.

20. Smart, E.J., C. Mineo, and R.G. Anderson, *Clustered folate receptors deliver 5-methyltetrahydrofolate to cytoplasm of MA104 cells.* Journal of Cell Biology, 1996. **134**(5): p. 1169-77.

21. Sabharanjak, S. and S. Mayor, *Folate receptor endocytosis and trafficking.* Adv Drug Deliv Rev, 2004. **56**(8): p. 1099-109.

22. Rodman, J.S., L. Seidman, and M.G. Farquhar, *The Membrane-Composition of Coated Pits, Microvilli, Endosomes, and Lysosomes Is Distinctive in the*

Rat-Kidney Proximal Tubule Cell. Journal of Cell Biology, 1986. **102**(1): p. 77-87.

23. Birn, H., J. Selhub, and E.I. Christensen, *Internalization and Intracellular-Transport of Folate-Binding Protein in Rat-Kidney Proximal Tubule.* American Journal of Physiology, 1993. **264**(2): p. C302-C310.

24. Rothberg, K.G., et al., *Cholesterol controls the clustering of the glycophospholipid-anchored membrane receptor for 5-methyltetrahydrofolate.* J Cell Biol, 1990. **111**(6 Pt 2): p. 2931-8.

25. Wu, M., et al., *Clustering of GPI-anchored folate receptor independent of both cross-linking and association with caveolin.* Journal of Membrane Biology, 1997. **159**(2): p. 137-147.

26. Frisch, B., et al., *Influence of Ligand Valency on the Targeting of Immature Human Dendritic Cells by Mannosylated Liposomes.* Bioconjugate Chemistry, 2008. **19**(12): p. 2385-2393.

27. Hammond, P.T., et al., *Ligand-Clustered "Patchy" Nanoparticles for Modulated Cellular Uptake and In Vivo Tumor Targeting.* Angewandte Chemie-International Edition, 2010. **49**(40): p. 7266-7270.

Chapter 6

Applications of Total Internal Reflection Microscopy and Total Internal Reflection Fluorescence Microscopy (TIRM/TIRF) for live cell imaging

6.1 Introduction

Advancement of new microscopic imaging methods and tools, such as advanced imaging instruments, novel methods and new experimental assay, are markedly enhancing assays and tissue models for early drug discovery, as well as more complicated disease models that are used later in drug discovery. Together, these inventions are enabling more sensitive, specific and higher resolution measurements from cells and organisms, and so could have an impact on a wide range of discovery activities ranging from target biology, compound screening and animal models of disease. Many of these innovations are important because they help to improve some of the technical limitations (e.g. low resolution) that are inherent in microscopic optical imaging [1].

Two widely used imaging techniques that can be employed to provide high-resolution information on the interactions of drug delivery systems such as nanoparticles (NPs) with living cells are total internal reflection fluorescence microscopy (TIRF) and total internal reflection microscopy (TIRM) [2].

6.1.1 Total internal reflection microscopy (TIRM)

TIRM is an optical technique which generates contrast from the scattering of a totally internally reflected light beam. It monitors the separation distance between a microscopic sphere and a flat plate. If a refractive object (n_1), is placed in the evanescent field of a light beam undergoing total internal reflection, at the interface between a dense (n_2) and less dense (n_3) e.g. glass and air, and if $n_1 > n_3$, then the object will scatter the evanescent light, resulting in linearly propagating light. By studying the totally internally reflected light beam or the scattered evanescent light, it is possible to build up an image of the object under examination [3].

6.1.2 Total internal reflection fluorescence (TIRF) microscopy

Total internal reflection fluorescence microscopy (TIRF), also known as evanescent wave microscopy, exploits the unique properties of an induced field in a limited region of sample immediately next to the interface between two media having different refractive properties. This surface electromagnetic field, called the 'evanescent wave', can selectively excite fluorescent molecules in the liquid near the interface. In practice, the most commonly utilized interface in the application of TIRF microscopy is the contact area between a sample and a glass coverslip or tissue culture dish. TIRF examination of cell/surface contacts significantly reduces background fluorescence from fluorophores either in the bulk solution or inside the cells (i.e. autofluorescence and debris). On the other hand, as TIRF minimizes the exposure of the cell interior to light, the healthy survival of the culture during imaging time is much enhanced compared to standard epi-illumination. It is highly amenable to live cell imaging due to its low levels of phototoxicity [2, 4] and photobleaching. Additionally, since it is a widefield technique the temporal resolution is outstanding and depends on camera sensitivity, optical setup, illumination intensity and exposure time. The TIRF technique has been used extensively in the imaging of different systems including single molecule detection [5-7] imaging endocytosis and exocytosis [8] and analysis of cell-substrate interactions [9-11].

6.1.3 Combined TIR/TIRF microscope

TIRM offers several advantages over conventional fluorescent techniques such as decreased phototoxicity and tiny photobleaching, but it lacks from the loss of specificity of imaging specific cellular structures stained by fluorescent labelling. A system which combines the label-free high resolution imaging offered by TIRM and

the potential of single molecule imaging offered by TIRF using fluorescently labelled structures is potentially very beneficial in many areas of research. Combining a TIR system into a TIRF microscope provides high-resolution imaging of both the label-free and fluorescence samples either separately or simultaneously (Figure 1). By combination of TIRM and TIRF, high spatial and temporal information on the process of cellular uptake of drug delivery systems will be accessible. For example, selectively labelling certain cell structures could gain information on the cellular processes due to the ability of TIRM to record dynamic events in real time, and the capability of TIRF to image specific structures that are fluorescently labelled [2].

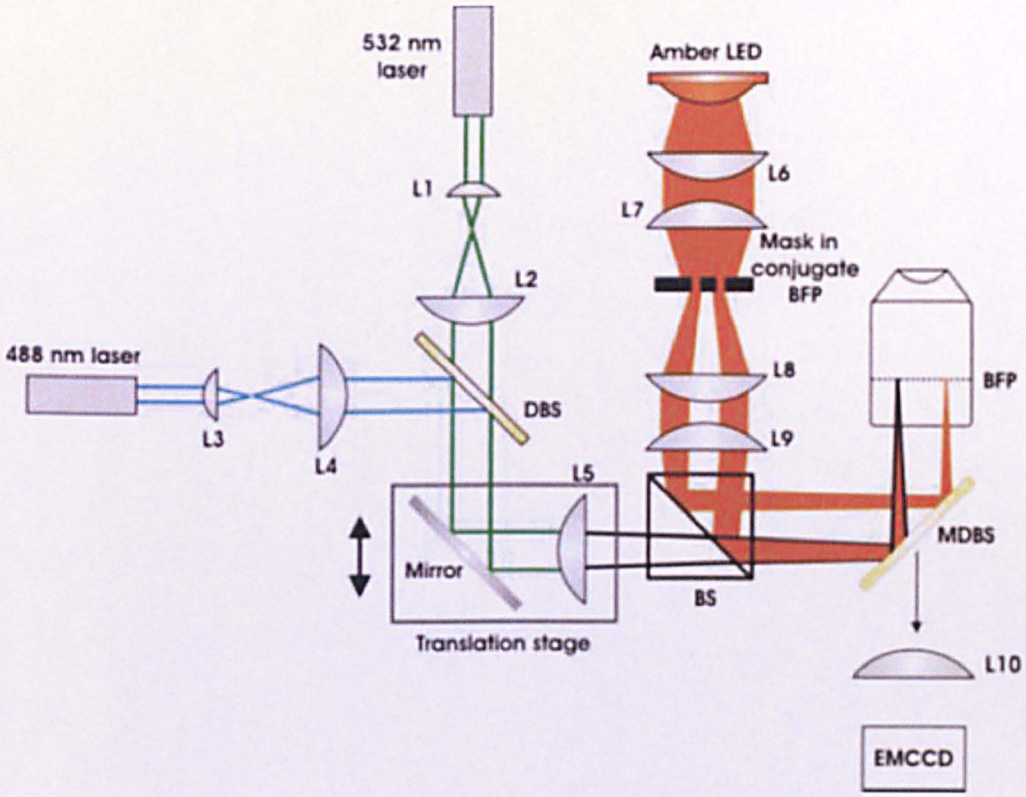

Figure 6.1 *For the two colour TIRF illumination, the laser beams are expanded by lenses L1-4 and combined at a dichroic beamsplitter (DBS). To control the incident illumination angle, the mirror and focusing lens L5 can be translated by the stage to allow positioning of the focal point in the back focal plane (BFP) of the microscope objective lens. For TIRM illumination, the amber LED is imaged by condenser lenses L6 and L7 onto an annular mask that is conjugate to the BFP of the microscope objective. Lenses L8 and L9 image the mask into the BFP to provide illumination above the critical angle. Fluorescent emission and reflected LED illumination pass through the multiband dichroic beamsplitter MDBS, and tube lens L10 forms an image on the electron multiplying charged coupled device (EMCCD). Adopted from [2].*

This Chapter investigates the potential of combined TIRM/TIRF microscopy for real-time imaging of endocytosis and transport of folate modified nanoparticles in an EGFP-clathrin LCa and DsRed-caveolin-1 expressing Calu-3 cell layer.

6.2 Material and methods

Unless otherwise stated, all chemicals were obtained from Sigma, Aldrich (UK).

6.2.1 Plasmids

The plasmids pEGFP-C1 and pDsRed-N1 were purchased from BD Clontech, France.

6.2.2 Oligonucleotide primers

Primers were designed using Primer3 software (version 0.4.0) with default setting. Primers were designed to be intron-spanning to discriminate cDNA from genomic DNA. Gene specificity was confirmed using Primer BLAST on the NCBI website. The following primers were purchased from Sigma-Aldrich:

Hs Caveolin1 DsRed clone Forward

5'GCCCGGGAATTCACCATGTCTGGGGGCAAATACG

Hs Caveolin1 DsRed clone Reverse

5'GCCCGGGTACCCCTATTTCTTTCTGCAAGT

Hs Clathrin Lca EcoRI Forward

5'GCCCGGGAATTCCATGGCTGAGCTGGATCCG

Hs Clathrin Lca EcoRI Reverse

5'GCCCGGGTACCTCAGTGCACCAGCGGGGC

6.2.3 Antibiotics

Ampicillin was used from a 50 mg/ml in 50% (v/v) ethanol stock, kanamycin from 50 mg/ml in dH2O. They were stored in at -20 °C

6.2.4 Luria Bertani medium

All bacterial strains were routinely grown on Luria Bertani broth (LB broth)/ agar (LB agar) media unless otherwise stated. 20 % (w/v) LB broth consisting of 10 g/L tryptone, 5 g/L yeast extract, 10 g/L NaCl and 4 ml/ 1 M NaOH was prepared as described by the manufacturer. LB agar was prepared by addition of 1.5 % (w/v) agar to LB broth prepared as above.

6.2.5 Molecular Biology Techniques

6.2.5.1 cDNA

Human lung first-strand cDNA was obtained from BD Biosciences Clontech, UK.

6.2.5.2 Sample preparation

Standard 2 × PCR ready to use master mix (ReddyMix, Abgene) containing 1.25 units Thermoprime plus DNA polymerase, 75mM Tris-HCl (pH 8.8 at 25°C), 20mM Ammonium sulphate, 1.5mM Magnesium chloride, 0.01% (v/v) Tween 20, 0.2mM Each of dATP, dCTP, dGTP and dTTP, was used to prepare the PCR reaction mixture. The final reaction mix consisted of 7.5 µl PCR Master-Mix, 1 µl each of 10 µM primers (Hs Caveolin1 DsRed clone forward/reverse and Hs Clathrin Lca EcoRI forward/reverse), 1 µl DNA template (lung cDNA) and 4.5 µl nuclease free water (Roche, UK) to a final volume of 15 µl. PCR amplifications were performed according to the protocol of Sakai et al [12] in a final volume of 50 µl. Reactions were carried out in a PTC-200 Peltier Thermal Cycler (MJ Research, UK) for a total of 30-35 cycles. Briefly, the DNA template was denatured at 94 °C for 5 min. This

was followed by 30-35 cycles of denaturation at 94 °C for 30 sec, annealing at 50-55°C for 45 sec and extension at 72 °C for 1-2 min. The last cycle finished with an extension at 72 °C for 8 min to ensure completion of all strands. Reaction mixes were then incubated at 4 °C indefinitely to allow PCR reactions to be carried out overnight.

6.2.5.3 DNA Agarose gel electrophoresis

DNA loading buffer (6 × stock: 1 ml glycerol; 2 ml 10 × TBE; bromophenol blue 0.002 g; sterile dH2O to 10 ml) (New England BioLabs, UK) was added to DNA samples and analysed on 0.8 or 1 % (w/v) agarose gels using a horizontal gel apparatus (Fisher Scientific, UK). The gels were prepared using analytical grade agarose (Promega, UK) in 0.5 × TBE buffer (1 M Tris-HCl; 1M Boric acid; 0.05 M EDTA; pH 8.0) with the addition of ethidium bromide to a final concentration of 10 µg/ml. The gels were run in 0.5 × TBE buffer and electrophoresis was performed at 90-110 V. DNA fragments were visualised on a UV transilluminator with Gene Genius Bio imaging software (UVP, USA).

6.2.5.4 DNA molecular weight markers

To establish the size of DNA fragments, 1 µg of either 100 bp or 1 kb ladder (Invitrogen, UK) in DNA loading buffer were loaded on agarose gels.

6.2.6 DNA manipulation

6.2.6.1 Extraction of PCR amplified DNA from agarose gel

DNA bands were visualized on the agarose gels using a UV transilluminator. The bands were cut from a very small region of gel with a clean razor blade. Insert DNA purification was performed following the manufacturer's instructions using Qiagen gel extraction kit (cat no: 28704).

6.2.6.2 DNA restriction enzymes

The restriction enzymes EcoRI and KpnI were purchased from New England Biolabs (UK) and were used according to the manufacturer's instructions. Reactions generally contained 0.05-1 µg DNA, as determined with a nanodrop spectrophotometer, 0.5-1 µl restriction endonuclease and 1 x restriction buffer made to a final volume of 50 µl with dH2O. The reaction mixture was incubated at 37 °C for a minimum of 1 h or until the digestion was complete. Reactions were analysed on agarose gels and appropriate bands cut out prior to DNA extraction using the Qiagen Gel Extraction Kit (Qiagen, UK).

6.2.6.3 Ligation of insert DNA and plasmid DNA

Concentration of insert DNA was calculated with respect to plasmid concentration using following formula.

(ng of plasmid DNA × kb size of insert DNA / kb size of plasmid DNA) × Molar ratio (insert DNA/plasmid DNA)

Ligation reaction was set up with the concentrations thus obtained in a volume of 6 µl of 10 × ligation buffer (Roche, UK) containing 1 u of T4 DNA ligase (Roche, UK), made up to a final volume of 30 µl with dH2O. The ligation mix was incubated at 4 °C for 16 h.

6.2.7 Introduction of DNA into bacterial cells

Competent E. coli cells were obtained from Invitrogen, UK.

6.2.7.1 Electroporation of electrocompetent E. coli cells

Electroporation was performed in 0.2 cm electrode gap Gene Pulser cuvettes (BioRad, UK) containing 20 µl of competent cells and 0.05-0.1 µg DNA. An

electroporation pulse of 2.5 kV (25 μF, 200 Ω) was delivered using the BioRad Gene Pulsar connected to a BioRad pulse controller (BioRad, UK). A 1 ml aliquot of pre-warmed (37 °C) 480 μl of S.O.C medium was added to the cells and incubated at 37 °C in the absence of antibiotics with shaking at 225 rpm. After 1 h aliquots of cells were plated onto LB agar plates containing kanamycin to select for transformants and grown overnight at 37 °C.

6.2.8 Isolation of plasmid DNA

Plasmid DNA isolation was performed using the Qiagen Miniprep kit (Qiagen Ltd., cat no. 27104) according to the manufacturer's protocol. Briefly, cells pelleted from 1-10 ml of an overnight bacterial culture were subjected to alkaline lysis, then neutralised and centrifuged at 5000 rpm for 10 min to remove denatured and precipitated cellular debris. Lysates were then loaded onto a silica-gel filter, washed and plasmid DNA was eluted into 30-50 μl PCR grade H2O (Roche, UK).

6.2.9 DNA sequence analysis

The DNA sequencing was conducted by comprehensive pharmacogenomics and molecular biology services, cogenics located at Hope End, Takeley, Essex, UK.

6.2.10 Transfection

For transient transfection, Calu-3 cells (used between passages 25-40) were cultured on flasks until confluence. Thereafter, cells were detached from the flasks, seeded on (10^5 cells per well) transwells-Inverted (Underside of transwell, Figure 2.1) as described in section 2.2.1.5.

25 days post seeding, they were transfected with 5 μg EGFP-clathrin LCa and DsRed-caveolin1 using TransFast Transfection Reagent (Promega, UK) in

accordance with the manufacturer's instructions. Firstly, the TransFast reagent and plasmid were added to 2 ml of pre-warmed (37 °C) serum-free DMEM and incubate for 15 minutes at room temperature. The culture medium was removed from the cells grown and the TransFast reagent/DNA mixture was added to the cells. The cells were immediately placed in the incubator for 1 hour at 37 °C and 5 % CO2. Following the incubation period the cells were gently overlayed with pre-warmed complete DMEM (2.1.1). Cells were incubated at 37 °C and 5 % CO2 for 24-48 hours. Cells were then ready to be used for TIRF imaging.

In order to check the transfection efficiency, Calu-3 cells were also seeded into 35 mm glass based dishes (Iwaki, Japan) coated with a 0.01% PLL with the same cell density (10^5 cells per well) (section 2.2.5.1) .

6.2.11 Folate modified Nanoparticles

Ovalbumin-Folic acid (OVA-FA) was prepared by the same method described in 3.2.3 and were adsorbed on the surface of green, sulphate-modified, polystyrene latex of 30 nm diameter as described in section 4.2.1.

6.2.12 Zonula Occludens (ZO-1) TJ staining

Samples for confocal imaging of TJ were immunostained with ZO-1 as described in section 2.2.5.2.

6.2.13 TIRM/TIRF Microscopy

A combination of TIRM and TIRF was performed in the same instrument as previously described in our group [13] utilising illumination through the microscope objective (PlanFluor 100x NA 1.45, Zeiss). All studies were performed using a standard inverted biological microscope (TC 5400, Meiji) with custom built illumination optics. The optical configuration used for TIRF imaging included

excitation with a 488 nm solid state laser (Protera 488-15, Novalux, Sunnyvale, CA) reflected off a polychroic mirror (z488/532). Emitted light was collected through a suitable emission filter (z488/532m). All filters and polychroic and dichroic mirrors were obtained from Chroma Technologies (Brattleboro, VT). TIRM imaging of Calu-3 cells was achieved with illumination using a light emitting diode (LED) with a centre wavelength of 580 nm (LXHL-ML1D Luxeon Star, Lumileds, CA) reflected off the same polychroic mirror.

The camera utilised to acquire images was a 14-bit cooled EMCCD (iXon DV-885 KCS-VP, Andor Technology, Belfast UK). The resolution of the camera was 1004 x 1002 pixels, with each pixel 8 μm x 8μm in size. Sequential TIRM and TIRF images were acquired by the camera under the control of iQ version 1.5 (Andor Technologies, Belfast UK). Mechanical shutters, also under the control of iQ via a break-out box (Andor Technologies, Belfast UK), were placed in the beam path to minimise photobleaching and to switch between TIRM and TIRF illumination. TIRM and TIRF images were acquired with exposure times of 90 and 400 ms respectively. For video imaging, frames were streamed to a kinetic image disc on a PC and then saved to hard disc. Analysis of still images and video sequences was performed with iQ, ImageJ and Excel (Microsoft, Redmond, WA). Digital brightness and contrast was adjusted in Photoshop (Adobe Systems, San Jose, CA).

6.2.14 Image analysis

For overlaying of TIRM and TIRF images, they were first streamed to a kinetic image disc on a PC (Dell, UK). The images from each channel (TIRM and TIRF) were then imported into ImageJ as an image sequence. 16-bit images were converted to RGB images. The RGB images were false coloured using the look-up table (LUT)

function on ImageJ. TIRF images were pseudo-coloured green for EGFP-clathrin and red for DsRed-caveolin1 and TIRM images underwent an inverse LUT prior to a red LUT being applied. The images sequences were overlayed using the image calculator function in ImageJ and adding the images together. The resulting combination image was finally cropped and saved as an Avi file.

6.2.15 Confocal Microscopy

Samples were prepared for confocal microscopy analysis as described in section 2.2.5.2 and visualized using Zeiss LSM 510 confocal system.

6.3 Result

6.3.1 Calu-3 cell layer cultured on the underside of permeable membrane

In order to facilitate the live imaging of filter grown Calu-3, cells were cultured on the underside of permeable membranes (Transwells®) as described in section 2.2.1.5. To test for tight junction formation, Calu-3 cell layer grown in the inverted configuration were subjected to immunostaining of tight junctional proteins, ZO-1. The observed pattern (Figure 6.2 B) of staining was indistinguishable from that observed in Calu-3 cells grown in the conventional configuration (Figure 6.2 A).

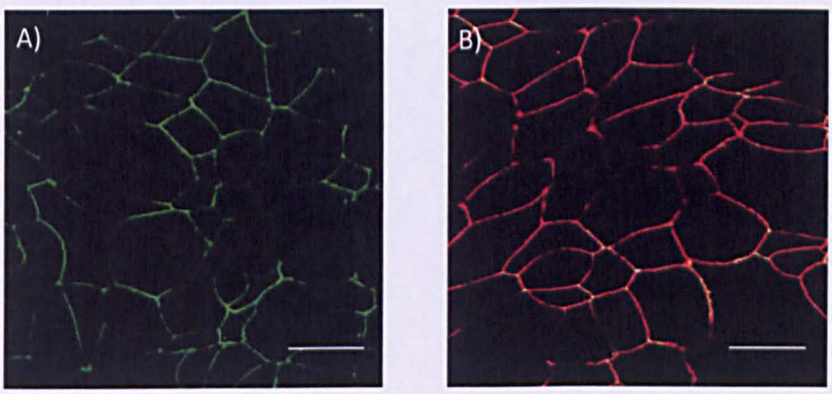

Figure 6.2 *confocal images of ZO-1 of immunostaining of Calu-3 cell layer grown in (A) conventional and (B) inverted configurations. Cell layers were stained with mouse, anti-human ZO-1 (primary) antibody and FITC- (A) or Cy5- (B) labelled goat, anti-mouse (secondary) antibody, Scale bar represents 10 μm.*

Epithelial cells grown in this inverted configuration exhibited a fully polarised architecture, as represented by formation of tight junctions.

6.3.2 TIRM imaging of Calu-3 cells

A typical TIRM image of Calu-3 cell cultured on PLL-coated cover slip is depicted in Figure 6.3. PLL is routinely used in cell culture to aid adherence of cells to a substrate. PLL is known to exert an attractive force on the cell membrane due to an

electrostatic interaction [14]. Figure 6.3 demonstrates the topographical detail achievable with TIRM.

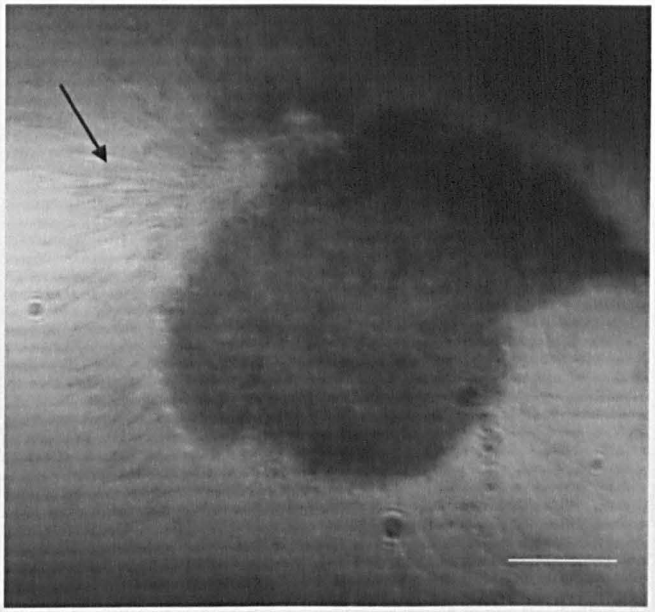

Figure 6.3 *TIRM image of a Calu-3 cell cultured on a PLL coated glass base dish. This image highlights the capability of TIRM to obtain high-resolution topographical information of the adhesion of Calu-3 cell to PLL substrates. Scale bar represents 5 μm.*

Filopodia structures which are attached to the cell surface can be also seen in Figure 6.3 marked by black arrow. TIRM has also been used to image Calu-3 cell layer. Figure 6.4 shows a single frame from a typical time-lapse video of apical membrane of Calu-3 cell layer cultured on the underside of permeable membranes.

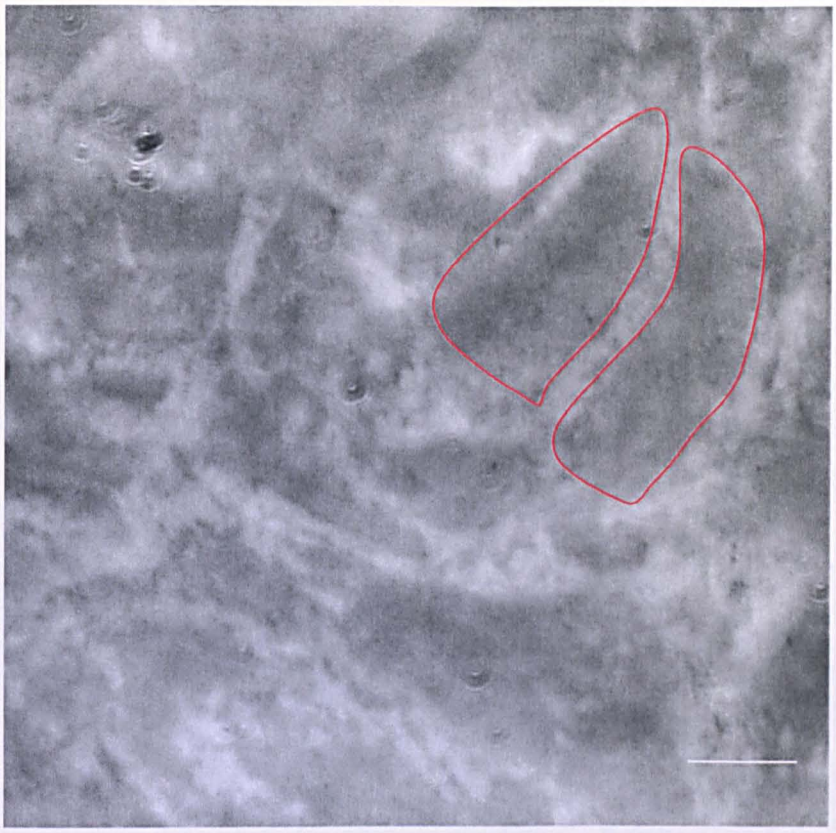

Figure 6.4 *TIRM image of apical surface of Calu-3 cell layer cultured on the underside of permeable membranes for 21 days. Red line denotes two adjacent cells. The image sequence that this image was extracted from is represented in Figure 6.5. Scale bar represents 10 μm.*

This label free TIRM image showed similar structural information about the position of the cell boundaries (and hence tight junctions) as that in the confocal images in Figure 6.2.

Figure 6.5 is demonstrating fifteen sequential images, representing a 75 second time scale, from a TIRM time-lapse video of the cell layer. These images demonstrate that the Calu-3 layer is tightly packed and limited cell movements (red arrows) could be observed.

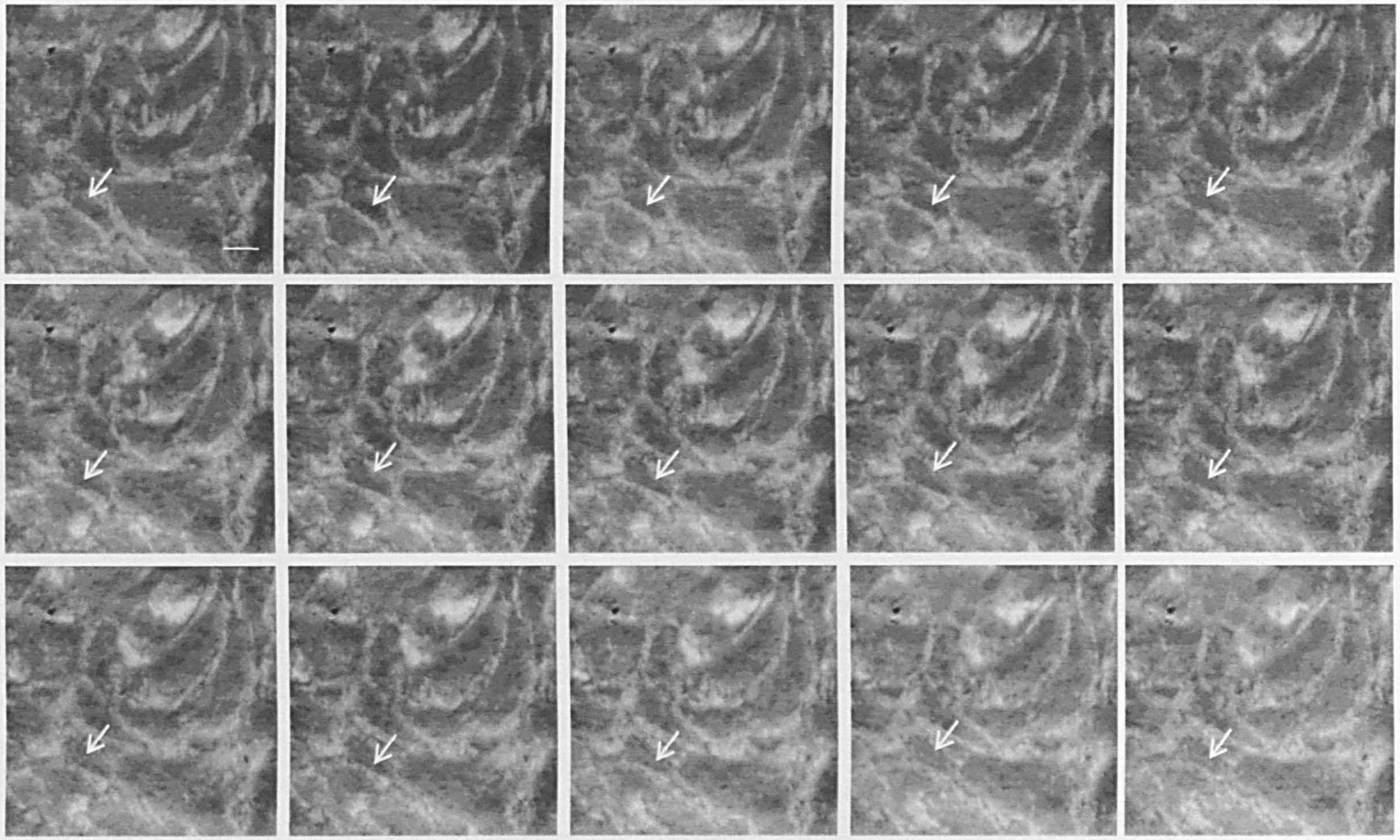

Figure 6.5 *Series of images from a TIRM time-lapse sequence of unlabelled Calu-3 cell layer cultured on permeable filter for 21 days. These 15 sequential TIRM images were taken from a sequence of 160, at 5 seconds per frame. White arrows represent an area where one cell is observed to moving very slowly. Scale bar represents 10 μm.*

6.3.2 Clathrin and caveolin1 expression in Calu-3 cells

Two plasmids encoding DsRed-caveolin1 and EGFP-clathrin LCa were constructed as described in methods (section 6.2.5-6.2.9).

Calu-3 cells were transiently transfected under non-polarised conditions (grown on glass base dish) to visualize and image the expression of these protein fusions. Figure 6.6 and 6.7 shows TIRF/TIRM images of GFP and DsRed positive transfected cells non-polarised cells grown on glass coverslips.

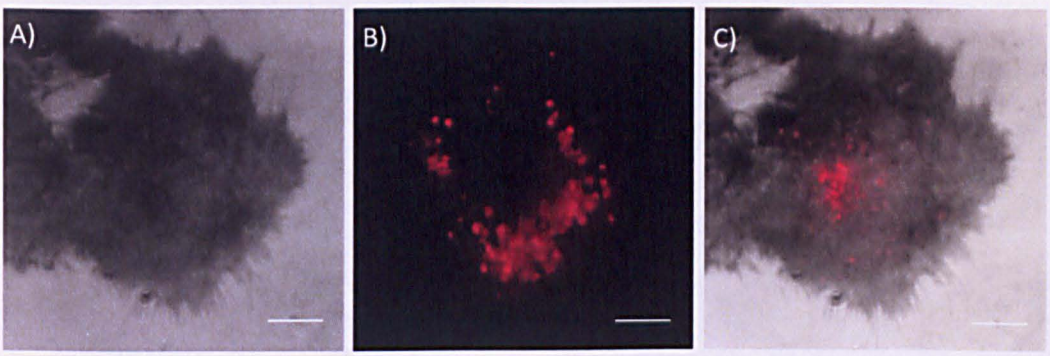

Figure 6.6 *A) TIRM image of a Calu-3 cell B) TIRF image of a Calu-3 cell transfected with DsRed-caveolin 1.C) Combined TIRM/TIRF image highlighting the distribution of caveolae puncta on the basal cell membrane. Scale bar represents 5μm.*

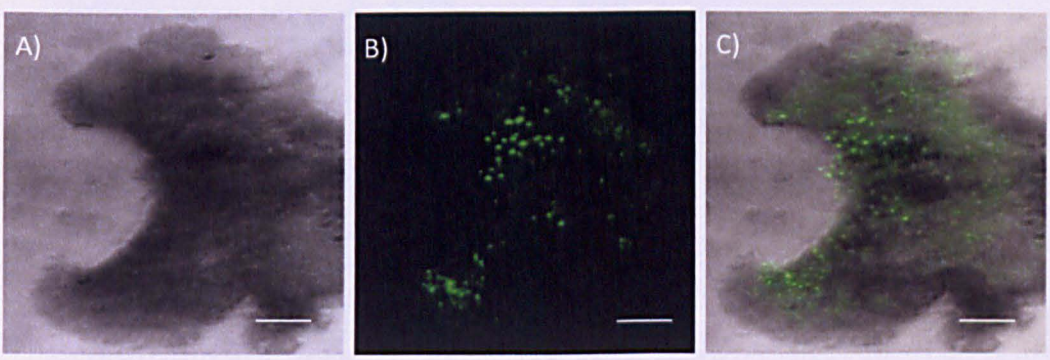

Figure 6.7 *A) TIRM image of a Calu-3 cell B) TIRF image of a Calu-3 cell transfected with EGFP-clathrin. C) Combined TIRM/TIRF image highlighting the distribution of clathrin puncta on the basal cell membrane. Scale bar represents 5 μm.*

The TIRF image in Figure 6.6 (B) and 6.7 (B) show the distribution of DsRed-caveolin1and EGFP-clathrin at the basal cell membrane.

TIRM/TIRF microscopy is an excellent way of studying the dynamics of individually labelled proteins within a living cell whilst simultaneously receiving high resolution topographical information of the basal cell membrane. The TIRM/TIRF microscope enabled high resolution tracking of single clathrin or caveolae vesicle on the basal cell membrane.

Figure 6.8 and 6.9 depicts sequential images from a TIRF time-lapse video of DsRed-caveolin1 and EGFP-clathrin transfected Calu-3 cells. Green arrows in Figure 6.8 and white circles in Figure 6.9 show the potential movement of vesicles from the surface of the cell into the main cell body. Indeed, as the vesicles move away from the cell surface to the main body, their fluorescence intensity will begin to decrease and eventually disappear due to the evanescent nature of the excitation light [15].

It was found that within a population of clathrin and caveolae puncta, the majority were seen to be static (white arrows in Figure 6.8 and 6.9).

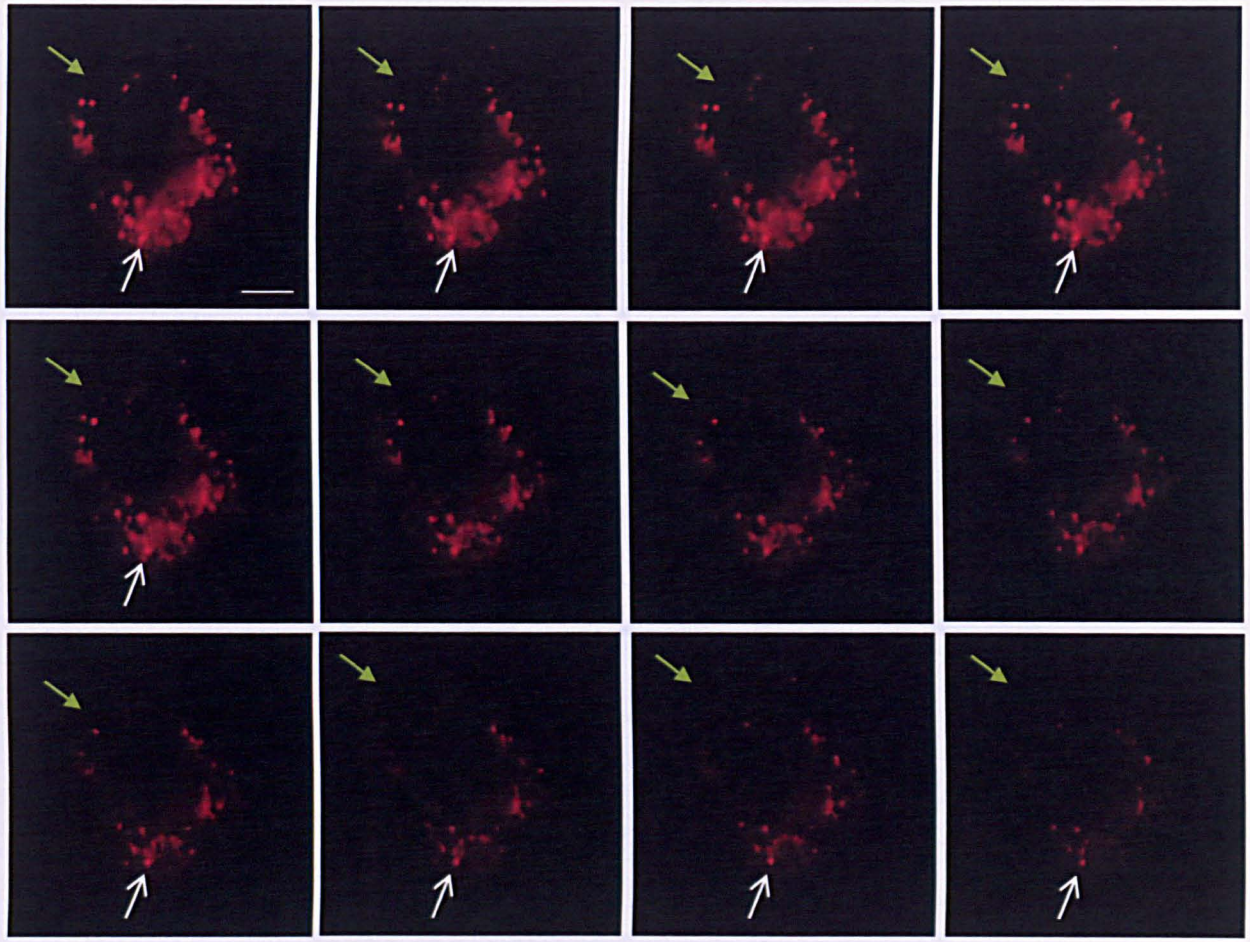

Figure 6.8 *Twelve sequential TIRF images taken from an image sequence of 100, are demonstrating the presence of numerous DsRed-caveolae puncta. The image sequence depicts the disappearance of the caveolae vesicles, marked by green arrows presumably by internalisation and still caveolae vesicles marked by white arrows. Scale bar represents 5 μm.*

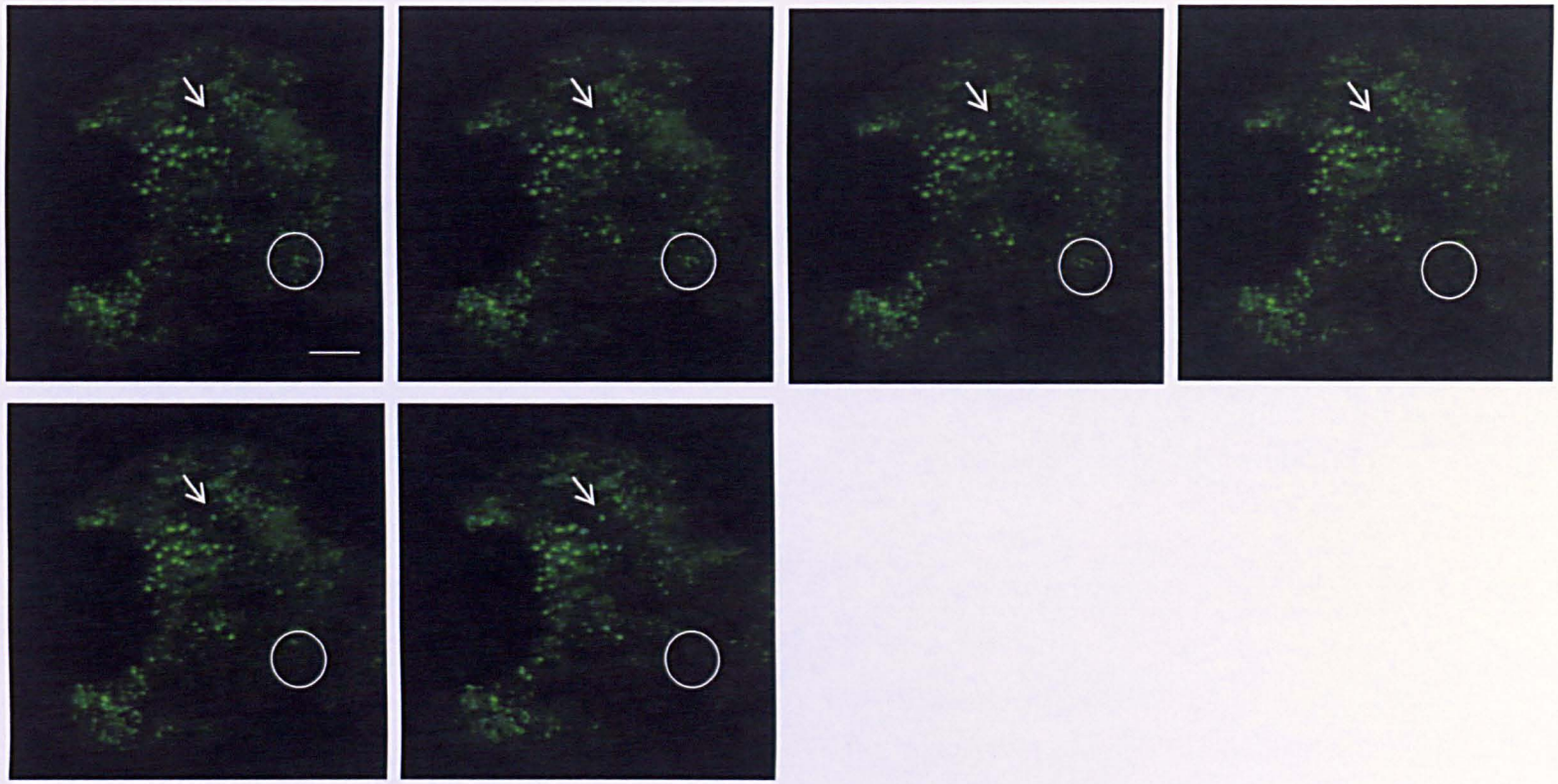

Figure 6.9 *Six sequential TIRF images taken from an image sequence of 60, are demonstrating the presence of numerous EGFP-clathrin puncta. The image sequence depicts the disappearance of the clathrin puncta, marked by circles presumably by internalisation and still EGFP-clathrin punctum marked by white arrows. Scale bar represents 5 μm.*

6.3.4 TIRM/TIRF imaging of clathrin and caveolae mediated endocytosis of folate modified NPs

At the outset of this study, it was planned to image particle uptake in a genetically modified cell line expressing both GFP-clathrin protein and caveolin-1-DsRed protein. This would have greatly benefited the research since it would allow routes of nanoparticle endocytosis to be studied simultaneously and in real time. Unfortunately, live imaging of folate modified NPs internalization in EGFP-clathrin and DsRed-caveolin1 treated Calu-3 layer proved problematic and was not achieved.

6.4 Discussion

Previous studies (Chapter 4) demonstrated that the folate and non-folate modified NPs were internalized predominantly via a caveolar and clathrin pathways respectively into Calu-3 cell layers. Thus, it was of interest to further study the internalization of folate modified NPs by combined TIRF/TIR microscopy to aid visualization of the endocytic pathways.

To this end, DsRed-caveolin1and EGFP-clathrin LCa expression vectors were constructed. Calu-3 cells (in polarised and non-polarised forms) were separately transfected with the plasmids encoding DsRed-caveolin1 and EGFP-clathrin fluorescent proteins, which are subsequently synthesized in the cytosol. Using TIRF it is possible to detect DsRed and GFP constructs which have diffused close to the basal cell membrane and formed vesicles [4, 16]

Gaidarov's seminal work highlighted how a fusion protein consisting of green fluorescent protein and clathrin LCa could be used to visualise the dynamics of endocytic clathrin coated pits and vesicles in mammalian cells [17]. Similar to previous studies, the EGFP-Clathrin developed in this work exhibited a distribution comparable to that of endogenous clathrin. Generally, clathrin is found in an assembled form on the cytoplasmic surface of the plasma membrane in coated pits that are active in endocytosis [18], in the *trans*-Golgi network region [19], in a soluble pool in the cytoplasm [20] and in some endosomal structures [21]. In TIRF, the dynamics of the EGFP-clathrin puncta in Calu-3 cells were similar to those reported previously [8, 17, 22, 23]. The majority of clathrin puncta were relatively stationary throughout the time course of the experiment however, sub-populations of clathrin puncta were seen to move (Figure 6.9) over time.

The caveolin-1-DsRed protein was made through a fusion of the carboxyl terminus of the caveolin-1 gene into the amino terminus of the DsRed plasmid. Pelkmans et al [24] showed that even though both N- and C-terminally GFP-tagged caveolin-1 had the same overall distribution in living canine cells, the C-terminally GFP-tagged caveolin-1 allowed normal simian virus 40 viral infection, whereas N-terminally tagged caveolin served as a dominant negative inhibitor, preventing uptake of simian virus 40 into the cell. This confirmed that the N-terminus of caveolin is crucial for caveolae mediated uptake processes. The distribution and the dynamics of the DsRed-caveolae vesicles in Calu-3 cells were similar to those observed previously [25]. Tagawa et al reported that the majority of Caveolin1-GFP-labeled spots on the plasma membrane (PM) are stationary, whereas some appearing and disappearing caveolar vesicles on the PM are also detected.

The DsRed-caveolin-1 vector constructed in this study to investigate the endocytosis process has also utilised by some other researchers. Singh et al [26] employed DsRed-caveolin1 to study endocytosis of fluorescent glycosphingolipid (GSL) analogs in various cell types (Rat fibroblasts, HeLa, Calu-1, and Calu-6, MDCK etc). Stubbs et al [27] also investigated the association of protein kinase C alpha in DsRed-caveolin1 transfected Chinese hamster ovary (CHO) cells and using expression of two-photon-excitation fluorescence lifetime imaging (2P-FLIM).

Imaging Calu-3 cell layers grown on permeable membrane in a standard configuration was not possible due to the constraints imposed by the microscope optics. The through the lens TIRM/TIRF microscope described in this work relies on the movement of light rays from an optically transparent high refractive medium to a lower refractive index medium in order for evanescent wave generation to occur.

Typically, live cell TIRF imaging is performed at a cell-microscope coverslip interface [28]. The penetration depth of the evanescent field varies with incident angle when the incident beam is 2 deg. above the critical angle the $1/e^2$ penetration depth is approx. 180nm falling to approx. 120nm when the incident angle is increased by a further 5 deg. This means that both the TIRM and TIRF channel are well localised at the basal cell membrane (when the cell is grown directly on glass). However, when the permeable membrane with cell layer are placed into the imaging system, the thickness of the substrate is such that it does not afford evanescent wave penetration through the substrate thus making TIRF/TIRM imaging not possible.

In order to overcome the problems discussed above, this work utilised a new technique for culturing fully polarised Calu-3 cells on the underside of permeable filters in order to enhance live cell imaging (Figure 6.10). Calu-3 cells grown in the inverted configuration displayed similar morphological characteristics as did cells conventionally grown on permeable membrane. Cells formed a confluent polarised monolayer with developed tight junctions.

Unfortunately, imaging polarised layers of cells grown on permeable filter led to other unforeseen difficulties. The process of excising and manipulating the flexible porous membrane film potentially sheared the confluent monolayer, leading to loss of junctional integrity between cells. Cells often appeared distorted under the microscope because it was difficult to place the excised film of cells flat on the glass slide and in intimate contact with the surface, a necessity for TIRF/TIRM imaging. Calu-3 cells grown in the inverted culture system on the filters were used without manipulation except direct transfer to a microscope grade glass chamber for live cell imaging (Figure 6.10).

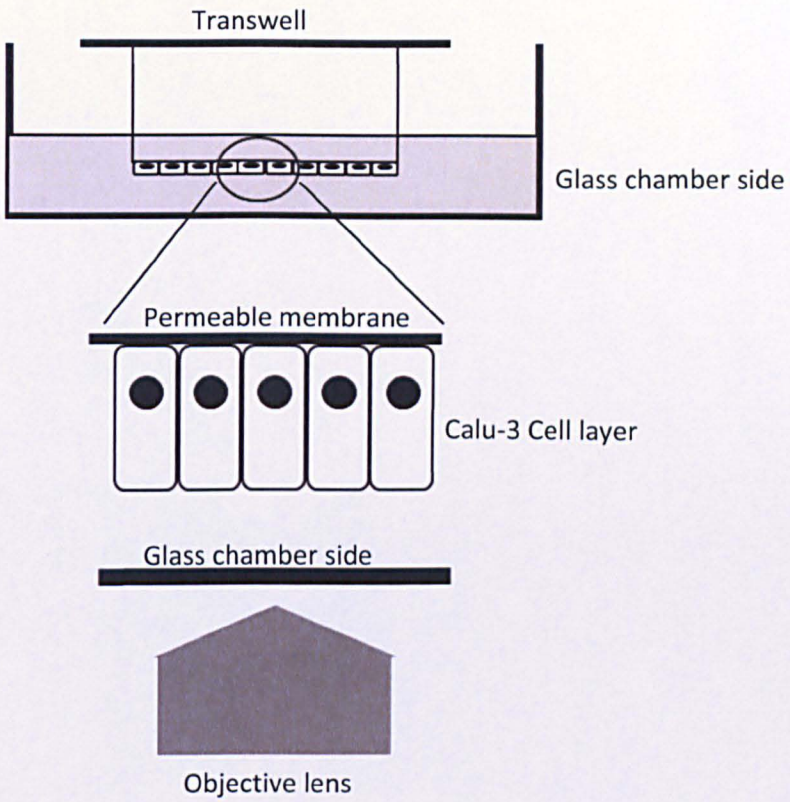

Figure 6.10 *Schematic picture of live cell imaging of Calu-3 cell layer grown on the underside of permeable membrane*

Perhaps the most relevant study investigating the advantages of inverted culture system is that by Wakabayashi [29] which showed that inverted cultured MDCK cells exhibited a fully polarised monolayer, including the presence of functional tight junctions. They also demonstrated that this culturing system permits four-dimensional (three spatial dimension over time) imaging.

Combined TIRF/TIR microscopy was intended to use for live imaging of folate and non-folate modified NPs internalization into DsRed-caveolin1 and EGFP-clathrin expressed Calu-3 cell layers grown in the inverted culture system.

Even though a method for visualising the clathrin and caveolae membrane vesicles in Calu-3 cells grown on glass (non-polarised) was developed (Figure 6.8 and 6.9), the visualisation of these proteins expressed in a Calu-3 polarised layer was not possible as it was difficult to localise the cell layer within the evanescent field for the reasons discussed above. Hence the ultimate aim of visualising the internalisation of folate and non-folate modified NPs and colocalisation with these fusion proteins was not achieved.

6.5 Conclusion

An EGFP-clathrin LCa and DsRed-caveolin1 fusion proteins were successfully developed and expressed in Calu-3 cells grown in the inverted culture. The TIRM/TIRF microscope enabled high resolution tracking of single clathrin or caveolae punctum on the basal cell membrane. It was found that within a population of clathrin and caveolae puncta, the majority were seen to be static whereas some were moving, appearing and disappearing to and from the membrane. It was found that the dynamics of clathrin and caveolae vesicles could also be followed whilst sequentially imaging the basal cell membrane using the TIRM/TIRF microscope.

It was hoped that a combination of the TIRM/TIRF microscope and the EGFP-Clathrin LCa and DsRed-caveolin 1 expressing cell line could also allow the visualisation of endocytosis of folate modified nanoparticles in living Calu-3 cell layer. Several different cell growth methods and microscope set-up were tested but none was successful.

6.6 References

1. Bullen, A., *Microscopic imaging techniques for drug discovery.* Nat Rev Drug Discov, 2008. 7(1): p. 54-67.
2. Byrne, G.D., et al., *Total internal reflection microscopy for live imaging of cellular uptake of sub-micron non-fluorescent particles.* J Microsc, 2008. **231**(1): p. 168-179.
3. Prieve, D.C. and N.A. Frej, *Total Internal-Reflection Microscopy - a Quantitative Tool for the Measurement of Colloidal Forces.* Langmuir, 1990. **6**(2): p. 396-403.
4. Mattheyses, A.L., S.M. Simon, and J.Z. Rappoport, *Imaging with total internal reflection fluorescence microscopy for the cell biologist.* Journal of Cell Science, 2010. **123**(21): p. 3621-3628.
5. Yildiz, A., et al., *Myosin V Walks Hand-Over-Hand: Single Fluorophore Imaging with 1.5 nm Localization.* Science, 2003. **300**(5628): p. 2061-2065.
6. Douglass, A.D. and R.D. Vale, *Single-Molecule Microscopy Reveals Plasma Membrane Microdomains Created by Protein-Protein Networks that Exclude or Trap Signaling Molecules in T Cells.* Cell, 2005. **121**(6): p. 937-950.
7. Reck-Peterson, S.L., et al., *Single-Molecule Analysis of Dynein Processivity and Stepping Behavior.* Cell, 2006. **126**(2): p. 335-348.
8. Rappoport, J.Z. and S.M. Simon, *Real-time analysis of clathrin-mediated endocytosis during cell migration.* Journal of Cell Science, 2003. **116**(5): p. 847-855.
9. Axelrod, D., *Cell-substrate contacts illuminated by total internal reflection fluorescence.* The Journal of Cell Biology, 1981. **89**(1): p. 141-145.
10. Burmeister, J.S., G.A. Truskey, and W.M. Reicher, *Quantitative analysis of variable-angle total internal reflection fluorescence microscopy (VA-TIRFM) of cell/substrate contacts.* Journal of microscopy, 1994. **173**: p. 39-51.
11. Axelrod, D., *Total internal reflection fluorescence microscopy in cell biology.* Methods Enzymol, 2003. **361**: p. 1-33.
12. Saiki, R.K., et al., *Primer-directed enzymatic amplification of DNA with a thermostable DNA polymerase.* Science, 1988. **239**(4839): p. 487-91.

13. Byrne, G.D., et al., *Total internal reflection microscopy for live imaging of cellular uptake of sub-micron non-fluorescent particles.* J Microsc, 2008. **231**(Pt 1): p. 168-79.

14. Lamour, G., et al., *Influence of surface energy distribution on neuritogenesis.* Colloids and Surfaces B-Biointerfaces, 2009. **72**(2): p. 208-218.

15. Rappoport, J., S.M. Simon, and A. Benmerah, *Understanding Living Clathrin-Coated Pits.* Traffic, 2004. **5**(5): p. 327-337.

16. Axelrod, D., *Total Internal Reflection Fluorescence Microscopy.* Biophysical Tools for Biologists, Vol 2: In Vivo Techniques, 2008. **89**: p. 169-221.

17. Gaidarov, I., et al., *Spatial control of coated-pit dynamics in living cells.* Nature Cell Biology, 1999. **1**(1): p. 1-7.

18. Anderson, R.G., et al., *Immunocytochemical visualization of coated pits and vesicles in human fibroblasts: relation to low density lipoprotein receptor distribution.* Cell, 1978. **15**(3): p. 919-33.

19. Keen, J.H., M.C. Willingham, and I. Pastan, *Clathrin and coated vesicle proteins Immunological characterization.* Journal of Biological Chemistry, 1981. **256**(5): p. 2538-2544.

20. Goud, B., C. Huet, and D. Louvard, *Assembled and unassembled pools of clathrin: a quantitative study using an enzyme immunoassay.* Journal of Cell Biology, 1985. **100**(2): p. 521-7.

21. Stoorvogel, W., V. Oorschot, and H.J. Geuze, *A novel class of clathrin-coated vesicles budding from endosomes.* Journal of Cell Biology, 1996. **132**(1): p. 21-33.

22. Merrifield, C.J., et al., *Imaging actin and dynamin recruitment during invagination of single clathrin-coated pits.* Nature Cell Biology, 2002. **4**(9): p. 691-698.

23. Rappoport, J.Z., B.W. Taha, and S.M. Simon, *Movement of Plasma-Membrane-Associated Clathrin Spots Along the Microtubule Cytoskeleton.* Traffic, 2003. **4**(7): p. 460-467.

24. Pelkmans, L., J. Kartenbeck, and A. Helenius, *Caveolar endocytosis of simian virus 40 reveals a new two-step vesicular-transport pathway to the ER.* Nature Cell Biology, 2001. **3**: p. 473-483.

25. Tagawa, A., et al., *Assembly and trafficking of caveolar domains in the cell: caveolae as stable, cargo-triggered, vesicular transporters.* J Cell Biol, 2005. **170**(5): p. 769-79.

26. Singh, R.D., et al., *Selective caveolin-1-dependent endocytosis of glycosphingolipids.* Mol Biol Cell, 2003. **14**(8): p. 3254-65.

27. Stubbs, C.D., et al., *The use of time-resolved fluorescence imaging in the study of protein kinase C localisation in cells.* Bmc Cell Biology, 2005. **6**.

28. Steyer, J.A. and W. Almers, *A real-time view of life within 100 nm of the plasma membrane.* Nature Reviews Molecular Cell Biology, 2001. **2**(4): p. 268-275.

29. Wakabayashi, Y., et al., *Four-dimensional imaging of filter-grown polarized epithelial cells.* Histochem Cell Biol, 2007. **127**(5): p. 463-72.

Chapter 7

Summary and Future Directions

7.1 Overall summary

Receptor-mediated cellular internalizations have received major attention in the field of drug delivery in the past few years. This pathway, which is initiated through endogenous ligands, could be exploited for designing target-oriented delivery systems. The past decade has seen the development of endogenous ligands to selectively deliver drugs to cellular interiors using a wide range of cell surface receptors. Most carrier systems investigated so far can be used as targeting delivery systems for various biomaterials using relevant ligands. Within this growing class of targeted pharmaceuticals, folate-conjugates are a well-studied example of targeted therapeutics [1, 2].

As discussed in chapter 1, the majority of studies on folate mediated drug delivery have focused on folate mediated drug uptake to cancerous cells, whilst data on targeted drug delivery via the folate receptor to non-cancerous cells or the possible role of the folate receptor in transcytosis are still scarce.

Initial work in this thesis focused on establishing and characterising four *in vitro* cell models of the bronchial and intestinal epithelium, namely the cancer-derived intestinal cell line Caco-2 and bronchial cell line Calu-3, as well as the non-cancerous intestinal IEC-6 and bronchial HBEC. Data shown in chapter 3 demonstrated that following their growth on appropriate supports (permeable membranes), these cell lines are all capable of forming polarised layers of closely packed cells exhibiting a TEER >500 Ωcm^2, which also present a barrier to the permeability of FITC-labelled dextran (4400Da). Expression of FR was confirmed by RT-PCR and Western blot analysis for all the tested cell types and shown to be dependent on culturing time.

Fluorescent ovalbumin-folate modified conjugates were synthesised to investigate the functionality of FRs. Data clearly showed that the expressed FRs were capable of mediating the uptake and transport of the macromolecular folate-conjugate across the polarised monolayers of all cell types.

Drug targeting to the lung is attractive as a potential systemic route of delivery and targeting the apical membrane transport proteins in the airways could possibly lead to augmented uptake and transport of delivery systems. This would represent a promising drug delivery strategy for certain drugs and drug candidates [3-5]. And because drug delivery across the airways through folate-mediated pathway had not been previously researched, the Calu-3 cell line was therefore chosen for the rest of the work.

Initial work demonstrated the potential of FRs in transcytosis of folate modified OVA. In order to establish whether the folate-mediated transport pathway could be exploited to deliver nano-sized drug carriers OVA-FA was immobilised on the surface of model polystyrene NPs and their cellular uptake and transport were investigated quantitatively and also by confocal microscopy (chapter 4). Furthermore, the endocytic mechanism(s) involved in folate-mediated NP internalization and translocation across the cell layers was explored by using different endocytic-pathway inhibitors. Data showed that folate modified NPs were taken up and traversed the Calu-3 layers and studies characterizing this uptake and transport strongly indicated folate involvement in the process. The study also demonstrated an involvement of the caveolar pathway in internalization and transport of folate modified nanoparticles, as judged from a significant inhibition of these processes by filipin (inhibitor of caveolae pathway). On the other hand,

disruption of actin filaments and microtubules exhibited no effect in cellular uptake of NPs, but increased the transcytosis of folate modified NPs.

This work therefore showed that the folate mediated transcytotic pathway offers potential for delivery of protein and nanoparticulate therapeutics. However, further studies are required to utilise more specific endocytosis inhibitors and novel biomarkers, which associate specifically with certain endocytic pathways or vesicles for deeper investigation of cell trafficking of NPs which are internalized or transported via the folate pathway.

The interaction of nano-materials with cells and lipid bilayers is critical in drug delivery and is mainly dictated by the surface properties of nanoparticles. Numerous studies have reported the effect of surface functional groups/ligands motifs on the nanoparticle cellular uptake, while the impact of ligand arrangement and ligand density on the nanoparticle surface is seldom examined [6]. Experiments detailed in Chapter 5 investigated the effects of surface ligand clustering and ligand density on the internalization of nanoparticles by polarised Calu-3 layers.

Data indicated that increasing the overall ligand density on the nanoparticle surface resulted in increased internalization of modified nanoparticles by the cells. Surface ligand density also influenced the cellular uptake pathway; directing uptake away from clathrin towards caveolae-mediated uptake as the ligand density was increased. It was further demonstrated that surface clustering of the folate ligand enhanced cellular internalization of nanoparticles, relative to its dispersed surface distribution. This part of the work therefore suggested a simple way to prepare a model system where surface manipulation of ligand density and its distribution are possible and which can be used to study nanoparticle-cellular interaction processes.

For better understanding of cell/NPs interaction, probably the simplest way is to directly visualise it using microscopy techniques [7]. The initial aim of chapter 6 was to utilise combined TIRF/TIR microscopy techniques to enable the visualisation of nanoparticle endocytosis by living cells. To achieve this goal EGFP-Clathrin LCa and DsRed-caveolin1 expressing cell lines were developed and TIRF/TIRM live imaging was performed to visualise the expression of EGFP-Clathrin LCa and DsRed-caveolin1 within the transfected cells. It was hoped that a combination of the TIRM/TIRF microscope and the EGFP-Clathrin LCa and DsRed-caveolin1 expressing cell line could also allow the visualisation of endocytosis of folate modified nanoparticles in living Calu-3 cells. Several different cell growth methods and microscope set-ups were tested, but none was successful. One limitation of the system in its tested configuration was its inability to image fluorescent processes deeper than 100nm within the cell so future work should focus on achieving appropriate configuration of the TIRM/TIRF microscope so as to overcome this limitation and enable live imaging of cells grown on permeable supports rather than coverslips.

7.2 Future view of folate targeted delivery

Based on the recent progress within the area of folate targeted therapy, one can predict a positive future for the field. To date, four distinct FA-drug conjugates have entered human clinical trials for the treatment of various types of cancer:

EC145 represents a novel water soluble FA conjugate of the powerful microtubule destabilizing agent, desacetylvinblastine monohydrazide. EC145 was found to produce a marked anti-tumour effect against well-established, subcutaneous FR-positive tumour [8].

EC0225 represents the "first in class" multi-drug, FR-targeted drug to be reported. It is constructed with a single folic acid moiety and extended by a hydrophilic peptide-based spacer that is, in turn, linked to Vinca alkaloid and mitomycin units via 2 distinct disulfide-containing linkers [9].

BMS-753493 represents a folic acid conjugate that was constructed with a semi-synthetic analogue of Epothilone A (a new class of anti-cancer drugs which prevent cancer cells from dividing by interfering with tubulin) [10].

EC0489 is the latest folate-targeted chemotherapeutic to enter clinical trials. This molecule is a derivative of EC145 that was designed to have limited non-specific clearance properties through the liver. By reducing hepatic clearance, fewer drugs will transit through the biliary excretion route resulted in less side-effect (predicted from preclinical tests on EC145) are expected [11].

Hence, it is hopeful that folate targeting will lead to improvements in the safety and efficacy of clinically-relevant therapeutic agents for both cancer and non-cancer applications. Existing work shows the potential for folate targeting in cancer therapy and the present work demonstrates the future potential of folate targeting in applications for systemic and epithelial delivery of drug and protein NP-based therapeutics.

7.3 References

1. Hilgenbrink, A.R. and P.S. Low, *Folate receptor-mediated drug targeting: From therapeutics to diagnostics.* Journal of Pharmaceutical Sciences, 2005. **94**(10): p. 2135-2146.
2. Vyas, S.P., A. Singh, and V. Sihorkar, *Ligand-receptor-mediated drug delivery: an emerging paradigm in cellular drug targeting.* Crit Rev Ther Drug Carrier Syst, 2001. **18**(1): p. 1-76.
3. Groneberg, D.A., et al., *Fundamentals of pulmonary drug delivery.* Respir Med, 2003. **97**(4): p. 382-7.
4. Patton, J.S., C.S. Fishburn, and J.G. Weers, *The lungs as a portal of entry for systemic drug delivery.* Proc Am Thorac Soc, 2004. **1**(4): p. 338-44.
5. Bansal, S.S., et al., *Advanced drug delivery systems of curcumin for cancer chemoprevention.* Cancer Prev Res (Phila), 2011. **4**(8): p. 1158-71.
6. Verma, A. and F. Stellacci, *Effect of surface properties on nanoparticle-cell interactions.* Small, 2010. **6**(1): p. 12-21.
7. Kam, Z., E. Zamir, and B. Geiger, *Probing molecular processes in live cells by quantitative multidimensional microscopy.* Trends in Cell Biology, 2001. **11**(8): p. 329-334.
8. Reddy, J.A., et al., *Preclinical evaluation of EC145, a folate-Vinca alkaloid conjugate.* Cancer Research, 2007. **67**(9): p. 4434-4442.
9. Leamon, C.P., et al., *Preclinical antitumor activity of a novel folate-targeted dual drug conjugate.* Mol Pharm, 2007. **4**(5): p. 659-667.
10. Kim, S.H., et al., *Synthesis, Chromatographic Purification, and Isolation of Epothilone-Folic Add Conjugate BMS-753493.* Organic Process Research & Development, 2011. **15**(4): p. 797-809.
11. Vlahov, I.R., et al., *Carbohydrate-Based Synthetic Approach to Control Toxicity Profiles of Folate-Drug Conjugates.* Journal of Organic Chemistry, 2010. **75**(11): p. 3685-3691.